# MECHANISTIC INSIGHTS INTO NEURONAL OSCILLATORY ACTIVITY IN THE DOPAMINE-INTACT AND DOPAMINE-DEPLETED PRIMARY MOTOR CORTEX

**Nicholas William Johnson**

**Doctor of Philosophy**

**Aston University**

**September 2016**

**Aston University**

# MECHANISTIC INSIGHTS INTO NEURONAL OSCILLATORY ACTIVITY IN THE DOPAMINE-INTACT AND DOPAMINE-DEPLETED PRIMARY MOTOR CORTEX

**Nicholas William Johnson**

**Doctor of Philosophy 2016**

In Parkinson's disease (PD) the loss of the neurotransmitter dopamine (DA) results in abnormal oscillations of the cortico-basal ganglia network, the emergence of which correlate with symptoms. Increased oscillatory power in the primary motor cortex (M1) is reduced by dopamine replacement therapy and by targeted stimulation, suggesting that M1 plays an important role in the pathology of PD. In this study we have investigated, using pharmacology, the mechanisms by which oscillatory activity in rat M1 is generated and determined the power changes associated with DA depletion and DA receptor modulation.

Extracellular local field potential recordings were made in brain slices of M1 which were prepared using a modified protocol to improve viability. Co-application of carbachol (5 µM) and kainic acid (100 nM) elicited simultaneous theta (4-8 Hz) and gamma (30-40 Hz) oscillations in layer V of M1. These oscillations displayed phase-amplitude coupling; the first report of such findings *in vitro.* These oscillations were found to be pharmacologically distinct with theta oscillations generated by intrinsic non-synaptic mechanisms while gamma oscillations required contributing excitatory and inhibitory networks.

Following successful unilateral lesions using 6-hydroxydopamine (6-OHDA), as determined by the adjusting step test, DA-depleted (ipsilateral) and DA-intact (contralateral) slices were obtained. Although no difference in the oscillatory profile of M1 ipsilateral, contralateral or age-matched control (AMC) slices was found, bath application of DA reduced gamma power only in the ipsilateral slices and amphetamine only decreased gamma power in contralateral slices. Furthermore, D2-like receptor activation consistently increased both theta and gamma power in contralateral and AMC slices, while only theta power was increased in ipsilateral slices. Overall, these data suggest that DA, through action at multiple sites, differentially modulates the power of both theta and gamma oscillations in M1.

Using the 6-OHDA model, the oscillatory activity of M1 *in vivo* was investigated. Successful lesions were determined by using the rotometer, the locomotor activity and the adjusting stepping tests at 2-4 weeks post-surgery. Further testing at 22 weeks post-surgery indicated the long-term stability of the lesions. Using depth electrode and EEG recordings, oscillatory activity in the 2-10 Hz range was found in the ipsilateral and contralateral hemispheres of both lesioned and sham animals. However, only in the ipsilateral hemisphere of DA-depleted animals did we detect a 30-40 Hz oscillatory peak, which was localised to layer V of M1. In EEG recordings this led to a significant increase in the interhemispheric ratio. Using depth electrode recordings, the ipsilateral 30-40 Hz oscillation (but not 2-10 Hz oscillation) was reduced by the administration of L-DOPA (6 mg/kg) with a reduction in interhemispheric ratio. However, administration of zolpidem (0.3 mg/kg), which previously reduced abnormal beta oscillatory activity *in vivo* and *in vitro* resulting in the rebalancing of interhemispheric beta power (Hall et al., 2014; Prokic et al., 2015), was without effect.

Overall, these studies demonstrate that M1 alone can generate multiple, pharmacologically distinct, but interacting oscillations, which contribute to pathological activity in the DA-depleted state.

**Key Words:** Parkinson's disease, motor cortex, oscillations, theta, gamma.

# Acknowledgements

I would first like to thank my supervisors, Prof. Ian Stanford and Prof. Gavin Woodhall for their continued help and support throughout my PhD, and for providing me with the opportunity to work in such a great lab. Additionally, I would also like to thank my industrial supervisors, Dr. Mike O'Neill and Dr. Keith Wafford, at Eli Lilly, for always being available to discuss and help me with my research over these 4 years, as well as providing me with a memorable 9 months during my placement at Erl Wood.

I also would like to thank everyone who's been in the lab throughout my PhD and for being there to share in the fun and frustrations. I would particularly like to thank Dr. Emma Prokic for providing invaluable support when I first started and in teaching me to use and understand MATLAB. Additionally, and perhaps more importantly, I want to thank Mazhar for working with, and putting up with me for almost a year, I could not have completed this thesis without your help.

Furthermore, I want to thank my friends who have put up with my busy schedule these last 4 years (especially the last 6 months!), you've always been there for a drink or a catch up when I have had the time. Likewise, to the other CASE students with me at Eli Lilly, Becky and Christian, you understood being away from friends and colleagues during those 6-9 months and you helped to make that time enjoyable.

I would like to thank my family for their ongoing support throughout and always being a phone call away, even if you still think I'm a neurosurgeon! And finally, I want to thank Jane for sharing this experience with me, for being there during the highs and lows you go through during a PhD and still wanting to see me in the evening! Thanks for all your help and support through these 4 years.

# Table of Contents

# List of Figures

# Abbreviations

µl - Microlitre
µM - Micromolar
5-HT - 5-hydroxytryptamine
6-OHDA - 6-hydroxydopamine
AC - Adenylate Cyclase
aCSF - Artificial Cerebrospinal Fluid
AED - Animal Equivalent Dose
AMC - Age-Matched Control
AMPA - 2-amino-3-(5-methyl-3-oxo-1, 2-oxazol-4-yl) propanoic acid
AMPH - Amphetamine
AP-5 - D-(-)-2-Amino-5-phosphonopentanoic acid
ATR - Atropine
BG - Basal Ganglia
BL - Baseline
$Ca^{2+}$ - Calcium Ion
CA3 - Cornu Ammonis 3
$CaCl_2$ - Calcium Chloride
cAMP - Cyclic Adenosine Monophosphate
CBX - Carbenoxolone
CCh - Carbachol
CCK - Cholecystokinin
CFC - Cross-Frequency Coupling
$Cl^-$ - Chloride Ion
DA - Dopamine
DBS - Deep Brain Stimulation
DHPG - (S)-3,5-Dihydroxyphenylglycine
DYN - Dynorphin
DZP - Diazepam
EEG - Electroencephalogram
ENK - Enkephalin
EPSC - Excitatory Postsynaptic Current
EPSP - Excitatory Postsynaptic Potential
ERD - Event Related Desynchronisation
FFT - Fast Fourier Transform
FIR - Finite Impulse Response

FS - Fast Spiking
g - grams
GABA - Gamma (γ)-Aminobutyric Acid
GBZ - Gabazine
GP - Globus Pallidus
GPCR - G-Protein Coupled Receptor
GPe - External Globus Pallidus
GPi - Internal Globus Pallidus
Hz - Hertz
i/m - Intramuscular
i/p - Intraperitoneal
iCSD - Inverse Current Source Density
iGluR - Ionotropic Glutamate Receptor
iNOS - Inducible Nitric Oxide Synthase
IIR - Infinite Impulse Response
ING - Interneuron Network Gamma
IPSC - Inhibitory Postsynaptic Current
IPSP - Inhibitory Postsynaptic Potential
$K^+$ - Potassium Ion
KA - Kainic Acid
KCl - Potassium Chloride
KET - Ketamine
KO - Knock Out
LI/II/III/V/VI - Layer I, II, III, V, VI
L-DOPA - L-3,4-dihydroxyphenylalanine
LFP - Local Field Potential
LID - Levodopa Induced Dyskinesia
LS - Late Spiking
LTS - Low Threshold Spiking
M1 - Primary Motor Cortex
mAChR - Muscarinic Acetylcholine Receptor
MAO - Monoamine Oxidase
MEG - Magnetoencephalography
mg - milligram
$Mg^{2+}$ - Magnesium Ion
mGluR - Metabotropic Glutamate Receptor
$MgSO_4$ - Magnesium Sulphate

min - Minute
ml - Millilitre
mM - Millimolar
MPTP - 1-methyl-4-phenyl-1,2,3,6-tetrahydropyridine
MSN - Medium Spiny Neuron
MΩ - Megaohm
$Na^+$ - Sodium Ion
NAC - N-Acetylcysteine
NaCl - Sodium Chloride
$NaH_2PO_4$ - Sodium Dihydrogen Orthophosphate
$NaHCO_3$ - Sodium Hydrogen Carbonate
nM - Nanomolar
NMDA - N-Methyl-D-Aspartic Acid
PAC - Phase-Amplitude Coupling
PBS - Phosphate Buffered Saline
PD - Parkinson's disease
PFC - Pre-Frontal Cortex
PIC - Picrotoxin
PING - Pyramidal-Interneuron Network Gamma
PKA - Protein Kinase A
PLC - Phospholipase C
PMBR - Post-Movement Beta Rebound
PV - Parvalbumin
RAS - Rotational Asymmetry Score
RSNP - Regular-Spiking Non-Pyramidal
s - Second
s/c - Sub-Cutaneous
S1 - Somatosensory Cortex
SEM - Standard Error of the Mean
SMA - Supplementary Motor Area
SNc - Substantia Nigra pars compacta
SNr - Substantia Nigra pars reticulata
SP - Substance P
STN - Subthalamic Nucleus
SYM - SYM 2206
TMS - Transcranial Magnetic Stimulation
VTA - Ventral Tegmental Area

# Chapter 1 Introduction

## 1.1 Primary motor cortex (M1)

### 1.1.1 Overview

The primary motor cortex (M1) along with the pre-motor cortex and supplementary motor area (SMA) comprise approximately one third of the frontal lobe. M1, also known as Brodmann area 4, is located adjacent to the central sulcus and is believed to be associated with the control and execution of voluntary movement (Eccles, 1981).

In 1870, Hitzig and Fritsch were the first to show that specific brain areas of dogs, when stimulated, resulted in muscular contractions in the body. The first maps of the human motor cortex were produced by Alfred Campbell in 1905 and these were improved upon by Penfield and Boldrey (1937). They observed that M1 contained a functional map organised somatotopically, with body parts corresponding to specific areas, thus developing the 'motor homunculus'. The motor map of M1 revealed that the greater the necessity for complex or fine movements (such as by the fingers), the more space is given over to this body area in M1. Following these studies, Stoney et al. (1968) performed intra-cortical electrical stimulation of specific body parts in cat sensorimotor cortex to further identify the somatotopic map of M1. More recently, many studies have shown that different body part areas can overlap (Sanes and Donoghue, 1997, 2000). In addition, certain areas (such as those which control individual digits) have been shown to be surrounded by areas controlling spatially adjacent limbs, in a core and circular manner (Kwan et al., 1978). Furthermore, the size and organisation of specific motor areas can vary between subjects depending on preference or movement bias, suggesting a level of dynamic plasticity within M1 (Nudo et al., 1992). The somatotopic assembly of human M1 has been further refined to include the idea that multiple areas of M1 control specific body parts (Binkofski et al., 2002).

### 1.1.2 Laminar organisation

M1 is arranged in cortical columns and consists of five layers; layers I, II, III, V and VI. Traditionally, layers I and II/III comprise the superficial layers and layers V and VI the deep layers. Unlike other brain areas, M1 contains no layer IV and therefore is described as agranular (Donoghue and Wise, 1982). Thus, it lacks what is considered to be a major processing pathway to higher motor areas, such as to the pre-motor cortex (Shipp, 2005). However, recent studies in primates and rodents suggest there are subsets of cells at the

layer III-V boundary in M1 which have the characteristics of layer IV neurons (Garcia-Cabezas and Barbas, 2014; Yamawaki et al., 2014).

#### *1.1.2.1 Layer I*

Layer (L) I of M1 is sparsely populated by pyramidal cell bodies and is predominantly composed of reciprocal axons branching from LII-LVI, as well as input connections from other motor areas (Ueta et al., 2014). The cells which populate this layer have been shown to be approximately 95% inhibitory and can be broadly organised into two main types; those which have dendritic connections confined to LI and those which project to LII-VI (Gabbott and Somogyi, 1986; Zhou and Hablitz, 1996; Chu et al., 2003).

#### *1.1.2.2 Layer II/III*

LII/III contains both pyramidal excitatory cells and non-pyramidal inhibitory cells. The non-pyramidal cell types present within LII/III can be separated into four groups based on their electrophysiological properties. These include fast-spiking (FS), late-spiking (LS), low-threshold spiking (LTS) and regular-spiking non-pyramidal (RSNP) cells. The most common are the FS and RSNP cells, which project mostly local connections within LII/III, with only a few cells projecting or receiving input from other layers (Kawaguchi, 1995). The input to LII/III is provided by LI and reciprocally from LVI, whilst LII/III cells have outputs that either remain in LII/III or output to LV and other brain areas (Shipp, 2007; Ueta et al., 2014).

#### *1.1.2.3 Layer V*

LV in M1 is the largest of the layers present and is often characterised by the presence of large pyramidal cells, known as Betz cells. Smaller pyramidal neurons (cortico-spinal), similar to those seen in previous layers are also present (Cho et al., 2004).

LV can be separated into upper (Va) and lower (Vb) domains, depending on the predominant cell size. In LVa, the majority of neurons, called Betz cells, have a soma volume approximately 20.4x more than the smaller neurons which occupy LVb (Rivara et al., 2003). Furthermore, Betz cells that represent the foot and leg have a greater somatic volume suggesting a relationship between their size and the extent of the body parts which they control (Lassek, 1940; Rivara et al., 2003). Betz cells are further subdivided into two groups based on their morphology, projection areas and electrophysiological properties. Type 1 Betz cells have thick branching apical dendrites, project primarily to the spinal cord, pons and striatum and have a burst firing pattern in response to membrane depolarisation. Type 2 Betz cells have thin apical dendrites that usually terminate in LII/III,

project to the striatum and the contralateral cortical hemisphere and have a regular non-bursting pattern in response to membrane depolarisation (Molnar and Cheung, 2006).

#### *1.1.2.4 Layer VI*

LVI of M1 contains a large population of cortico-thalamic neurons (Yamawaki and Shepherd, 2015) which receive inputs from LVa and LVb (Kim et al., 2014; Yamawaki and Shepherd, 2015).

### 1.1.3 M1-S1 connectivity

M1 and somatosensory cortex (S1) are often grouped together under the name sensorimotor cortex. These areas lie adjacent to each other and are highly interconnected (**Fig 1.1**). The co-ordination between M1, S1 and other brain structures, such as the basal ganglia and the spinal cord, is thought to result in precise control of movement (Wichmann and DeLong, 1999). The connections between M1 and S1 are also organised somatotopically and this may be important for the integration of movement and sensory information (Porter and Sakamoto, 1988). For example, the whiskers of rodents are used to provide sensory feedback, which results in a high level of intercommunication between M1 and S1 which facilitates further movement and exploration (Nguyen and Kleinfeld, 2005; Ferezou et al., 2007). Similarly, primate studies have shown that both M1 and S1 generate synchronous oscillatory activity during movement tasks allowing the integration of movements with environmental stimuli (Murthy and Fetz, 1996; Nguyen and Kleinfeld, 2005). Furthermore, a study by Sakamoto et al. (1989) in cats, demonstrated that destruction of S1 and its connections to M1 resulted in decreased motor learning during complex motor tasks.

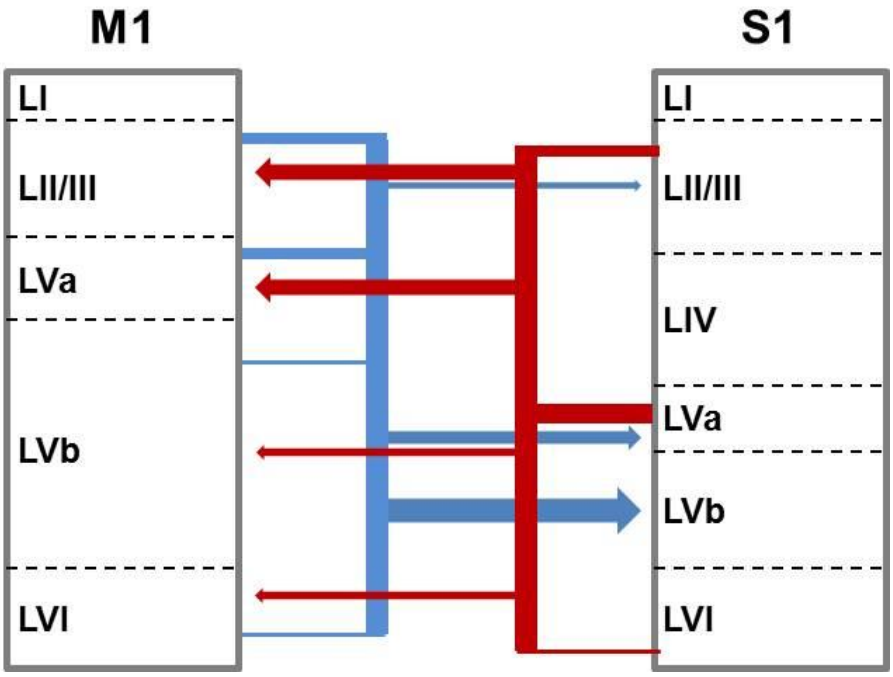


**Figure 1.1 M1-S1 connectivity** Schematic demonstrating the main circuits connecting M1 and S1. Blue lines represent connections from M1 to S1. Red lines represent connections from S1 to M1. Thickness of line represents increasing strength of connection. Adapted from Mao et al. (2011).

### 1.1.4 The basal ganglia

The basal ganglia (BG) are a group of highly interconnected, primarily GABAergic (γ-aminobutyric acid) nuclei (**Fig 1.2**) (Brown and Marsden, 1998). The primary input station of the BG is the striatum (in rodents), which is known as the caudate putamen in primates (McGeorge and Faull, 1989). Cortical information is integrated in the BG before being relayed back to the thalamus and cortex from the internal globus pallidus (GPi) and substantia nigra pars reticulata (SNr). The nuclei of the external globus pallidus (GPe) and the subthalamic nucleus (STN) act as further integration sites. Information flow through the BG is controlled by dopamine (DA) which is released by neurons of the substantia nigra pars compacta (SNc). These neurons primarily project to the striatum although the SNc also projects to other BG nuclei including GPe, GPi, STN and M1 (Lindvall and Bjorklund, 1979; Gaspar et al., 1995; Gauthier et al., 1999; Hosp et al., 2009).

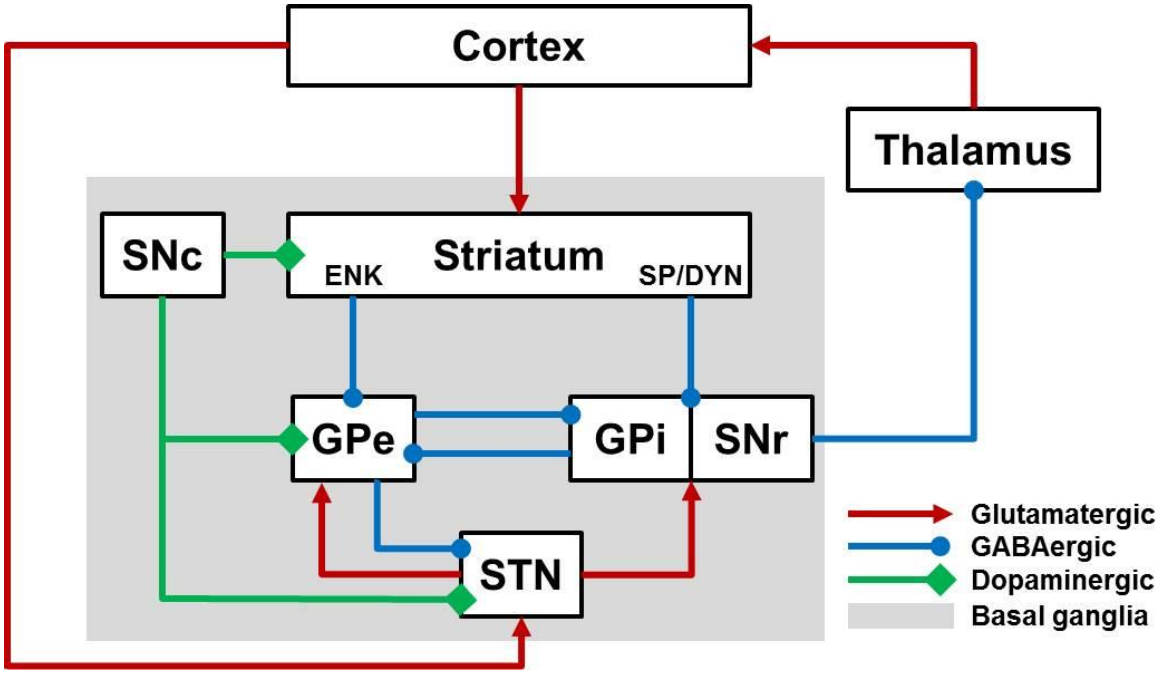


**Figure 1.2 Simplified schematic of BG nuclei** Schematic detailing the synaptic connections and connection types between the BG nuclei, cortex and thalamus. ENK labels the enkephalin group medium-spiny neurons (MSNs) which target the GPe. SP/DYN labels the substance P/dynorphin group MSNs that target the GPi/SNr. Red arrows indicate glutamatergic excitatory connections; blue circles indicate GABAergic inhibitory connections; green diamonds indicate dopaminergic connections. Grey box indicates the nuclei that make up the BG.

Two primary pathways project from the striatum; the 'direct' pathway couples dynorphin (DYN) containing MSN neurons with the GPi/SNr and the 'indirect' pathway couples enkephalin (ENK) containing MSNs and the GPe (see **Fig 1.3**) (Albin et al., 1989; Delong, 1990). The direct pathway's activity is facilitated by DA D1-like receptors and the indirect pathway's activity is inhibited by DA D2-like receptors (Gerfen et al., 1990; Parent et al., 2000; Parent et al., 2001). Though studies have suggested this distinction between the pathways was incorrect, whereby $D_1$ and $D_2$ receptors were observed to co-localise on striatal neurons in rodent brain slices (Aizman et al., 2000). However, these did not take into account specific targets of striatal projection neurons investigated. Thus, recent evidence using transgenic fluorescent proteins in mice has reaffirmed the original hypothesis. Studies demonstrated that in striatal projection neurons that serve either the direct or indirect pathways there is a prominent segregation in receptor expression (Gertler et al., 2008; Valjent et al., 2009; Gerfen and Surmeier, 2011).

From the GPe signals are passed to the STN and then on to the SNr and GPi (Smith and Bolam, 1989; Bolam and Smith, 1992; Kita and Kitai, 1994). The STN is the only glutamatergic nuclei in the BG and receives a direct glutamatergic input from the cortex,

which has been termed the 'hyperdirect' pathway (see **Fig 1.3**) (Monakow et al., 1978; Nambu et al., 2000; Tokuno and Nambu, 2000; Nambu et al., 2002). In addition, reciprocal connections exist between the GPe and the striatum, the striatum and the SNc and the GPe, GPi and STN (Kita et al., 1983; Haber et al., 2000; Sato et al., 2000; Obeso et al., 2006).

The process of movement selection and execution in the BG has been extensively studied. The discovery of the hyperdirect pathway resulted in the suggestion of a 'centre-surround model' of BG function (Nambu et al., 2002), involving the specific selection and inhibition of motor programs (Mink and Thach, 1993; Mink, 1996; Hikosaka et al., 2000). The three pathways (hyperdirect, direct and indirect) work together to specifically select and initiate appropriate movement whilst inhibiting other motor programs (Chevalier and Deniau, 1990). Thus, the hyperdirect cortico-STN pathway provides ultra-fast activation of GPi neurons which then inhibit the thalamus and cortex (Nambu et al., 2000). The direct striatum-GPi pathway is then activated which inhibits neurons specifically related to the selected movement. Subsequently, these neurons are inhibited by the indirect pathway. In this way highly selective movements are executed and terminated appropriately.

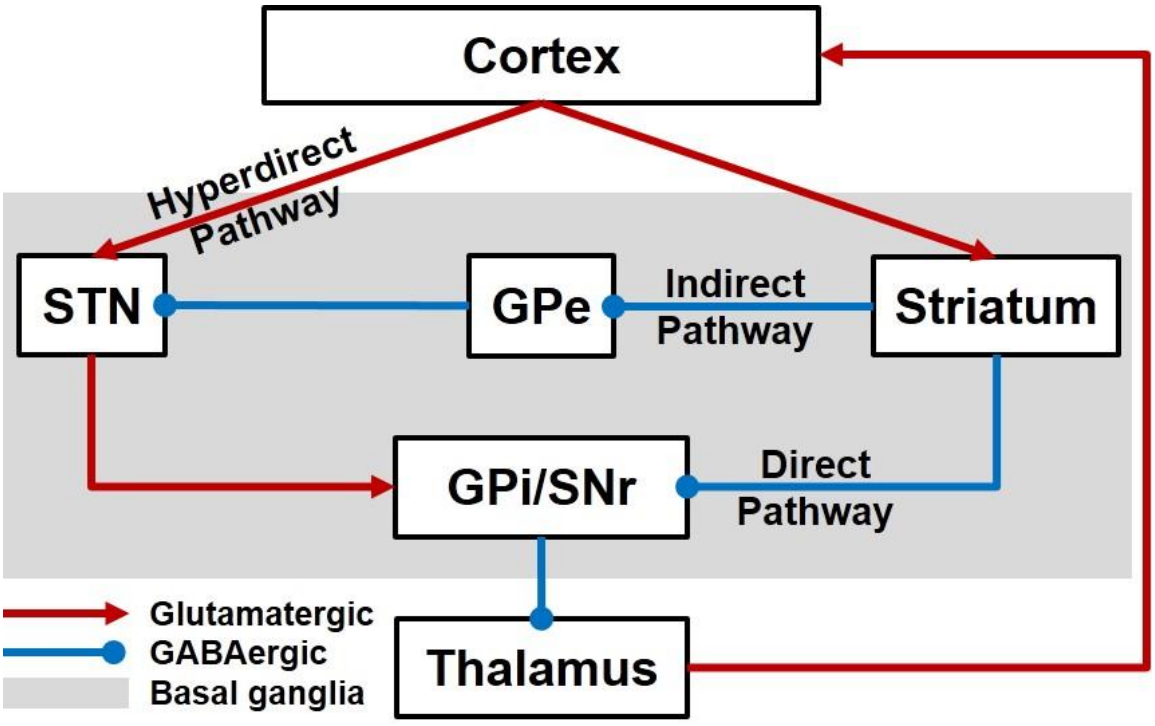


**Figure 1.3 Hyperdirect, direct and indirect pathways involved in movement** Schematic detailing the synaptic connections of the hyperdirect, direct and indirect pathways. Red arrows indicate glutamatergic excitatory connections; blue circles indicate GABAergic inhibitory connections. Grey box indicates the nuclei that make up the BG.

## 1.2 Network oscillatory activity

### 1.2.1 Overview

Groups of neurons arranged in local networks can generate patterns of activity which are termed neuronal oscillations. Hans Berger in 1929 was the first to use electroencephalography (EEG) to observe an oscillation at 10 cycles a second (10 Hz) in a human subject, which he termed the alpha rhythm. A second, faster, oscillation (12-30 Hz) was termed beta. Subsequent studies have observed oscillations in multiple frequency bands, and correlated these to different functional states. However, it is now understood that specific frequency bands are not limited to a single behaviour but that the frequency of activity is dynamic and able to contribute to multiple behavioural states. These frequency bands include delta (1-4 Hz), theta (4-7 Hz), alpha (8-12 Hz), beta (12-30 Hz) and gamma (30-80 Hz). Delta oscillations are observed most commonly during sleep, whilst alpha oscillations are associated with wakefulness when eyes are closed (Buzsaki and Draguhn, 2004). Theta oscillations appear to have many roles including voluntary and non-voluntary (automatic) motor actions (Vanderwolf, 1969; Bland, 1986), whilst gamma oscillations have roles in the processing of movement (Crone et al., 1998; Cheyne et al., 2008; Muthukumaraswamy, 2010), sensory information (Gray et al., 1989), attention and memory (Jensen et al., 2007).

### 1.2.2 Theta oscillations

Theta oscillations (4-8 Hz) were originally defined and studied in the hippocampus (Walter and Dovey, 1944; Green and Arduini, 1954) and have been shown to be associated with spatial navigation and learning (Winson, 1974, 1978; Hasselmo et al., 2002), navigation by place fields (O'Keefe and Recce, 1993; Cacucci et al., 2004), sleep (Cantero et al., 2003) and movement (Vanderwolf, 1969, 1975).

Early studies *in vivo* demonstrated two types of theta oscillations; type 1 or atropine-sensitive (4-9 Hz) and type 2 or atropine-resistant (6-12 Hz) (Vanderwolf, 1969; Kramis et al., 1975; Vanderwolf, 1975; Montoya and Sainsbury, 1985). Type 1 theta was predominantly observed during the complete absence of movement or during periods of automatic instinctive activity such as licking and chewing, while type 2 theta was associated with voluntary behaviours such as walking, running and rearing (Vanderwolf, 1969, 1971; Kramis et al., 1975). Thus distinct theta activity is believed to be associated

with specific motor function (Vanderwolf, 1969; Bland, 1986). However, a review by Bland and Oddie (2001) suggested that theta provided continual feedback between brain areas, such as the hippocampus and motor systems, resulting in the ability to adapt to continuously changing sensory stimuli. Theta oscillations are also thought to play an important role in spatial memory. When a rat enters a set location, place cells in the hippocampus fire in a specific pattern at theta frequency which correspond to visual cues (O'Keefe, 1976). Furthermore the theta activity of the place cells also shifted in phase depending on the location within the place field demonstrating that theta oscillations can be both dynamic and adaptable (O'Keefe and Recce, 1993).

The cholinergic and GABAergic system are believed to be involved in the generation of theta oscillations as the hippocampus receives innervation from the medial septum (Petsche et al., 1962; Konopacki and Golebiewski, 1993; Vinogradova, 1995). Histochemical studies in the hippocampus of rats have shown that the GABAergic fibres from the medial septum terminate on specific populations of GABAergic interneurons, including those containing PV, cholecystokinin (CCK) and calbindin (Freund and Antal, 1988; Gulyas et al., 1991). These interneurons have been termed theta-off cells and have been shown to be active during the troughs and silent during peaks of the theta oscillation. In contrast, septo-hippocampal cholinergic fibres innervate hippocampal pyramidal cells, known as theta-on cells, are active during the peaks of the oscillation. These cells had a co-ordinated pattern of activity that coincided with the troughs and peaks of the theta oscillation, thus were believed to be responsible for its generation (Colom et al., 1991; Smythe et al., 1992). However intracellular experiments in rodent hippocampus and cortex have suggested that the joint cholinergic and GABAergic rhythmic control of networks can generate intrinsic membrane potential oscillations, which are believed to account for *in vitro* theta oscillations (Bland and Colom, 1993; Bland and Oddie, 2001; Bland et al., 2002)

Theta oscillations *in vitro,* elicited by the bath application of carbachol (CCh, an acetylcholine receptor agonist), were first described in the hippocampus by MacIver et al. (1986) and Konopacki et al. (1987). Additional block of $GABA_A$ receptors with bicuculline also produced robust theta oscillations (Konopacki and Golebiewski, 1993). Subsequent studies have demonstrated *in vitro* theta oscillations in other brain areas such as the neocortex (Lukatch and MacIver, 1997; Castro-Alamancos, 2013) and entorhinal cortex (Konopacki and Golebiewski, 1992; Konopacki et al., 1992a; Cunningham et al., 2003). Furthermore, theta oscillations have the ability to entrain faster oscillations (such as gamma oscillations) to their oscillatory phase. This is known as phase-amplitude coupling

and it is believed to play a role in entraining network oscillations between brain areas (Bragin et al., 1995; Chrobak and Buzsaki, 1998; Sirota et al., 2008) (see section 1.2.5).

### 1.2.3 Beta oscillations

Beta oscillations (12-30 Hz) have been observed in many cortical areas including the olfactory bulb, visual cortex, M1 and S1 (Adrian, 1942; Jasper and Penfield, 1949; Freeman, 1978; Gray and Singer, 1989; Murthy and Fetz, 1992; Gray, 1994; Roopun et al., 2006; Yamawaki et al., 2008) during a variety of behavioural states and exploratory activities. The beta oscillations observed in M1 and S1 are some of the most studied, due to their role in movement execution (Pfurtscheller and Berghold, 1989; Pfurtscheller and Neuper, 1992; Baker et al., 1997; Pfurtscheller et al., 2003).

The presence of beta oscillations has been described as a stable or 'idling' state responsible for the maintenance of current state between movement activities (Brown and Marsden, 1998; Brown and Williams, 2005; Engel and Fries, 2010; Brittain and Brown, 2014; Brittain et al., 2014). Such a view suggests that beta oscillations are involved in the maintenance of posture or tonic contraction (Baker et al., 1997; Jenkinson and Brown, 2011). Beta oscillations undergo event-related desynchronisation (ERD) prior to movement execution and post-movement beta rebound (PMBR) is observed once the movement has been completed (Pfurtscheller et al., 1993; Brown et al., 1998; Pfurtscheller et al., 2003; Jurkiewicz et al., 2006; Cheyne et al., 2008).

The degree of synchronous beta oscillations are believed to be important for the level of cortical processing able to be completed by the neuronal network, thus affecting the ability of cortical networks to quickly adjust to new sensory input and movements. Brittain et al. (2014) suggested that there is an precise level of beta oscillation synchrony which allows the computational ability of the network to remain optimal and adaptable during movement, thus allowing appropriate ERD (Kuhn et al., 2004). As such, excessive levels of synchrony throughout the cortico-BG network have been shown to contribute to motor impairments in Parkinson's disease (PD) resulting in bradykinesia and rigidity (Brown and Marsden, 1998; Magill et al., 2000; Brown and Williams, 2005; Brittain et al., 2014) (see section 1.3.2.1 for further details).

### 1.2.4 Gamma oscillations

Gamma oscillations (30-80 Hz) have been thoroughly studied in many cortical regions and the hippocampus and have been associated with many different processes and behaviours, including memory and sensory processing (Gray and Singer, 1989; Traub et al., 1996b; Traub et al., 1999), motor function (Pfurtscheller and Berghold, 1989; Pfurtscheller and Neuper, 1992; Pfurtscheller et al., 1993; Crone et al., 1998; Pfurtscheller et al., 2003), olfactory function (Eeckman and Freeman, 1990) and visual processing (Singer and Gray, 1995).

Gamma oscillations can be generated in several ways involving different networks, mechanisms and temporal scales. For instance, *in vivo* studies have characterised sensory and motor gamma as bursts or waves (Gray et al., 1989; Pfurtscheller et al., 1993), whereas in hippocampal CA3 and dentate gyrus (DG) regions it has been described more as a persistent oscillation (Csicsvari et al., 2003).

A variety of *in vitro* preparations have been developed to provide a pharmacological and mechanistic insight (Whittington et al., 1995; Fisahn et al., 1998; Fisahn et al., 2004). The majority of these have used a combination of carbachol (CCh) and the ionotropic glutamate receptor agonist kainic acid (KA) to elicit oscillations, although metabotropic glutamate receptor (mGluR) agonists and tetanic stimulation have also been used. All of these methods result in gamma oscillations that vary in their frequency, pharmacology and persistence, though the involvement of $GABA_A$ receptors and gap junctions are essential to all. There are two widely accepted models of gamma generation; the interneuron network gamma (ING) and pyramidal-interneuron network gamma (PING) models. It has been suggested that the generation of beta oscillations in M1 are similar to the ING model of oscillations (Yamawaki et al., 2008).

#### *1.2.4.1 Interneuron network gamma (ING)*

The ING model of gamma oscillations was first proposed by Traub et al. (1996b) to describe an oscillatory network sensitive to the block of $GABA_A$ receptors but persisted during the block of α-amino-3-hydroxy-5-methyl-4-isoxazolepropionic acid (AMPA) glutamate receptors with NBQX. Mechanistically, the ING model relies upon the interconnectivity of GABAergic interneurons, resulting in sustained mutual inhibition amongst the interneuronal network (Whittington et al., 2000). The network requires excitatory input to initially bring the interneuronal population to a threshold level of activity. This will increase interneuron activity and promote enhanced synchrony of inhibitory post

synaptic potentials (IPSPs) along with rebound spikes (Wang and Rinzel, 1993). Thus, once the network is activated, the oscillation is generated through the mutual inhibition between the interneurons which will then discharge together and generate synchronous IPSPs (Buzsaki and Wang, 2012). The frequency of the oscillation is primarily determined by the decay time constant of the IPSP, thus the longer the decay time the slower the frequency of the oscillations. This generally produces oscillations in the gamma range and varying the kinetics of $GABA_A$ receptors pharmacologically or in a computer generated model of ING can alter the frequency of the oscillation (Traub et al., 1996b; Wang and Buzsaki, 1996; Bartos et al., 2002). Whilst ING is interneuronal driven they are often connected to excitatory pyramidal neurons. Indeed, pyramidal cell networks can report the oscillation generated in the inhibitory network since they are gated by the same rhythmic IPSPs. This gating means that pyramidal cells have the chance to fire in the periodic intervals when inhibition is low (Whittington et al., 2000).

#### *1.2.4.2 Pyramidal-interneuron network gamma (PING)*

Early studies of gamma oscillations *in vivo* demonstrated networks composed of both excitatory and inhibitory connections (Leung, 1982; Jagadeesh et al., 1992). If the pyramidal neurons also provided a reciprocal driving force to the interneuronal network then another model would begin to appear, known as PING. Thus in this model, excitatory neurons are intimately involved in the generation and regeneration of network oscillatory activity (Whittington et al., 2000).

The excitation delivered to interneurons and the feedback inhibition provided to the excitatory population alternate in the PING model. This improves network stability and coherence (Traub et al., 1996a; Wang and Buzsaki, 1996; White et al., 1998) as shown by the resultant long lasting (persistent) oscillations (Buzsaki and Wang, 2012). AMPA receptor mediated excitatory post-synaptic potentials (EPSPs) provide this excitatory input as PING is sensitive to AMPA receptor block (Whittington et al., 1998; Traub et al., 1999; Fuchs et al., 2007). Thus the EPSPs generated by pyramidal neurons are believed to be the primary drivers of the interneuron population and are also important for the temporal integration of the network (Whittington et al., 1998; McBain et al., 1999). As mentioned previously, the oscillatory frequency of the ING model can be altered by changing the IPSP decay time using $GABA_A$ receptor modulators. In a network involving pyramidal neurons, this can still occur but there degree of change that can be elicited is reduced (Whittington et al., 1996; Faulkner et al., 1998).

In a PING model the excitatory neurons recover from IPSPs before the inhibitory cells. This allows the pyramidal cells to fire EPSPs onto inhibitory cells before they are inhibited by another IPSP. Essentially the activity of the excitatory and inhibitory cells alternates. The pyramidal neurons excite the interneuronal population to threshold through co-ordinated synchronous input. Following this, the interneuronal population inhibits the pyramidal cells involved in the network, whereby the decay time of the IPSP determines the frequency of the oscillation. Therefore, in the intervals when the inhibition in the pyramidal cells has sufficiently decayed, they can generate another EPSP to excite the interneuronal population. This interplay between the populations essentially switces the population in control of the timing of the oscillation from solely the interneurons, to both pyramidal cells and interneurons. However, as in ING networks, not all pyramidal cells involved in a network fire on every cycle of an oscillation. Recordings have shown that pyramidal cells only fired at low frequencies (~3 Hz) but they were always prior to interneurons involved in the network (Fisahn et al., 1998; Hajos et al., 2004).

The involvement of excitatory pyramidal cells in the PING model also results in the ability of the network to synchronise over distances of up to 3.5 mm (Traub et al., 1996a). Using dual site tetanic-stimulation and in computational models, it was shown that spatially distinct regions were able to oscillate together with little phase-lag (Traub et al., 1996a; Whittington et al., 1997; Ermentrout and Kopell, 1998). The basis of long-range oscillation generation by EPSPs relies on the generation of interneuron spike doublets, two EPSPs that arrive onto interneurons within a short space of time gradually resulting in a reduction of the phase-lag between the distant networks. However, this can only occur in two networks that are approximately in phase with each other to begin with (~2 ms), since an interneuron has to have been depolarised by a local EPSP within a few ms prior to a second spike arriving from the distant network (Bibbig et al., 2002). Additionally, the strength of the second EPSP has to be strong enough to overcome any after-hyperpolarisation potentials activated after the initial spike. The doublet on the interneuron can then summate and fire a stronger IPSP onto its local pyramidal and interneuronal populations that it ordinarily would, increasing the length of decay time for the local pyramidal neurons so reducing the phase lag between the two populations (Whittington et al., 1998; McBain et al., 1999).

### 1.2.5 Phase-amplitude coupling

Bragin et al. (1995), was the first to report gamma oscillations in the hippocampus *in vivo* were positively correlated to theta oscillations and the amplitude of the gamma oscillation is dynamically modulated on the phase of a theta oscillatory cycle (Canolty et al., 2006). This phenomenon has become known as phase-amplitude coupling (PAC) or cross-frequency coupling (CFC). Further *in vivo* and computer modelling studies have suggested that one of the roles of theta oscillations in the brain is to activate and entrain large spatially distinct areas, allowing for modulation of local faster oscillations (Chrobak and Buzsaki, 1998; Lakatos et al., 2005; Onslow et al., 2014). This is possible due to the longer temporal window evident in slower oscillations, which enables the entrainment of oscillations over a large area (von Stein and Sarnthein, 2000). Furthermore, gamma oscillations alone do not appear to have the ability to integrate and generate synchronisation over long distances (>8-10 mm), since synchronous activity in this range has been shown to decline with distance (Eckhorn, 1994). This suggests gamma oscillations are primarily involved in higher interactions that take place on a local scale (Kopell et al., 2000).

It may be that hippocampal theta specifically entrains networks of gamma oscillation generating neurons throughout cortical areas as a form of centralised temporal and spatial co-ordination in the brain (Hyman et al., 2005; Jones and Wilson, 2005; Siapas et al., 2005; Sirota et al., 2008). This is supported by evidence that coupling between brain areas is an essential form of neuronal computation and processing (Engel et al., 2001; Fries, 2005; Canolty and Knight, 2010), which is particularly important in the integration of motor and sensory related events (Luo and Poeppel, 2007; Lakatos et al., 2008; Saleh et al., 2010; Schroeder et al., 2010; Onslow et al., 2014). PAC may therefore be used to organise fast oscillations within a single brain structure and/or across multiple cortical layers (Quilichini et al., 2010). For example, in a T-maze task, it has been shown that the power of PAC across different frequency bands is dynamically modulated during distinct behaviours and between brain areas (Tort et al., 2008) and can occur transiently during task related activity, resulting in different patterns of coupling and processing (Canolty et al., 2006). This suggests that PAC may be used to co-ordinate decision making and movement during exploration. PAC can also be observed during motor behaviour, whereby communication between M1 and other cortical areas during specific motor tasks alters the power and frequencies of network activity (Igarashi et al., 2013; von Nicolai et al., 2014).

## 1.3 Parkinson's disease (PD)

### 1.3.1 Overview

Parkinson's disease (PD) is a hypokinetic neurodegenerative disorder, which affects voluntary movement through the destruction of dopaminergic neurons of the substantia nigra in the BG. It was first characterised by Dr. James Parkinson in 1817 in a report titled *"An Essay on the Shaking Palsy",* in which he detailed how the disease progressed over time and outlined the classic symptoms of the disease, which include bradykinesia (slowness in movement execution), akinesia (difficulty executing a movement), rigidity (resistance to passive movement) and resting tremor (rhythmical contraction and relaxation of body parts). With a mean age of onset around 60 years old the lifetime risk of developing PD is 2%, which makes it the second most common neurodegenerative disorder behind Alzheimer's disease (de Lau and Breteler, 2006; Schapira, 2009). The risk rises to 4% in people over 80 years old and is only rarely seen in patients beneath the age of 50 years (de Lau and Breteler, 2006).

Diagnosis of PD is based on clinical assessment, relying on the identification of one or more major symptoms, however approximately 25% of patients are mistakenly misdiagnosed with the disease (Hughes et al., 1992). Unfortunately in many cases, by the time motor symptoms of PD are apparent, more than 70% of the dopaminergic terminals have already been lost (Bernheimer et al., 1973; Yuan et al., 2005; Willard et al., 2015). Whilst this does suggest a level of resilience and redundancy within the motor system, it often means that therapeutic intervention is not initiated until substantial DA loss has already taken place. In fact it has been suggested that the prodromal phase (non-symptomatic phase) of PD can occur up to 20 years before the onset of motor symptoms, affecting multiple areas of the brain and periphery (Braak et al., 2003; Postuma et al., 2012; Kalia and Lang, 2015).

### 1.3.2 Aetiology and pathophysiology

Whilst the majority of patients (approximately 90%) that present with PD are idiopathic (that is, the cause is unknown), there are a rising number of genetic mutations which have been shown to be associated with an inherited form of PD (Weintraub, 2008). The original gene to be associated with inherited PD was *SNCA*, which encodes for the protein α-synuclein, a component of Lewy bodies (Polymeropoulos et al., 1997). Other significant

genetic markers associated with PD include *LRRK2*, *parkin*, *GBA* and *PINK1* (Kalia and Lang, 2015). Studies have also shown that there are several environmental risk factors which contribute to the development of PD. The highest risk is carried by pesticide exposure, followed by head injury, rural living, β-blocker use, agricultural work and well-water drinking (Noyce et al., 2012). Some of these genetic and environmental risk factors have been shown to increase mitochondrial stress and damage, in particular in the SNc of the BG, which is the area of key pathological importance within PD (Bueeler, 2009; Zuo and Motherwell, 2013).

The pathophysiological hallmark of PD is the loss of the dopaminergic neurons of the SNc. Dopaminergic loss progresses from the ventral SNc laterally, which eventually results in the loss of DA innervation of the striatum (Ehringer and Hornykiewicz, 1960; Bernheimer et al., 1973; Hirsch et al., 1988; Goto et al., 1989; Fearnley and Lees, 1991). The loss of D2 receptor mediated inhibition of striatal MSNs is believed to result in increased inhibition and decrease in activity of the GPe (Miller and Delong, 1988; Delong, 1990; Filion and Tremblay, 1991). The decrease in GPe activity has the overall effect of increasing the glutamatergic output of the STN (Wilson and Bevan, 2011). The increased excitation from the STN onto the GPi/SNr, results in an excessive inhibition of the thalamus and therefore a decrease in output to the cortex, which presents as the motor symptoms akinesia and bradykinesia (Wichmann et al., 2011; Wichmann and Dostrovsky, 2011). In addition, studies have shown that there are changes to the firing rates of BG nuclei, from regular tonic activity to a bursting-like pattern of activity which is believed to contribute to the changes in observed neuronal output (Miller and DeLong, 1987; Filion and Tremblay, 1991; Wichmann and Soares, 2006).

#### *1.3.2.1 Pathological oscillatory activity*

Studies involving PD patients have shown that excessive synchronisation occurs within the 12-30 Hz (beta) band in the BG, primarily between the GPi and the STN (Brown et al., 2001; Brown and Williams, 2005). This is also evident in rodent and primate models of PD (Nini et al., 1995; Sharott et al., 2005; Hammond et al., 2007; Mallet et al., 2008a; Mallet et al., 2008b). Coherence between the BG and M1 at this frequency has also been observed (Murthy and Fetz, 1992; Donoghue et al., 1998; Hohlefeld et al., 2015). The exaggerated beta frequency was shown by Brown et al. (2001) and Kuhn et al. (2006) to be correlated to the severity of PD symptoms. Thus, the treatments L-3,4-dihydroxyphenylalanine (L-DOPA) and deep brain stimulation (DBS) reduced the oscillatory power and the severity of the PD symptoms, as well as reducing the synchronisation and coherence of beta oscillations in the cortico-basal ganglia network

(Marceglia et al., 2006; Wilson et al., 2011; Brittain et al., 2014). This suggests that the beta oscillations observed throughout the cortico-BG are not just a symptom of PD but may be causally linked to the hypokinetic symptoms. Furthermore, synchronised theta oscillations (4-10 Hz) have also been observed within the BG in PD and have been shown to be correlated to the emergence of tremor in patients and animal models (Volkmann et al., 1996; Hutchison et al., 1997; Raz et al., 2000; Amtage et al., 2008).

The implications of synchronous activity in the BG have been widely studied in both PD patients and animal models. The main belief is that the intrinsic activity of the BG nuclei are kept tightly controlled by the dopaminergic modulatory input (Wichmann et al., 2011). When this modulation is lost, there are increases in coupling between the nuclei (Brown et al., 2001), which has a negative effect on the ability to initiate voluntary movement. Ordinarily, co-ordinated gamma oscillations throughout the cortico-BG would be present during the movement phase (Crone et al., 1998; Brown et al., 2001; Cassidy et al., 2002; Williams et al., 2002; Pfurtscheller et al., 2003). However in the PD state, synchronisation within the beta oscillatory band results in a difficultly in dynamically switching to a different oscillatory pattern to transfer movement information (Brown and Williams, 2005), as outlined in section 1.2.3.

### 1.3.3 Treatments

#### *1.3.3.1 Pharmacological treatment*

The gold standard treatment for PD is the administration of L-DOPA, a precursor to DA which can cross the blood-brain barrier. Treatment with L-DOPA is still considered the most effective non-invasive treatment, though other treatments include DA agonists (e.g. pramipexole), monoamine oxidase-B (MAO-B) inhibitors (e.g. selegiline) and catechol-o-methyltransferase (COMT) inhibitors (e.g. entacapone), which prevent the breakdown of DA in the synaptic cleft and increase DA's effective time, and DA releasing agents (e.g. amantadine) (Davie, 2008; Schapira, 2009).

In the early stages of PD, L-DOPA is taken up by the remaining nigrostriatal terminals, where it is converted to DA and gradually released. However, as the disease progresses, the remaining nigrostriatal terminals deteriorate, reducing the continuous effect of L-DOPA resulting in fluctuating concentrations leading to detrimental 'on-off' effects (Gancher et al., 1987; Kempster et al., 1989). After being on L-DOPA for several years many patients also develop L-DOPA induced dyskinesia's (LIDs) (Fabbrini et al., 2007, for review see

Jenner, 2008 and Calabresi et al., 2010). LIDs have also been linked to inconsistent levels of L-DOPA which may facilitate the super-sensitivity of the remaining DA receptors (Halje et al., 2012). Recent studies also suggest that the uptake of L-DOPA by serotonergic fibres (which can also convert L-DOPA into DA) can contribute to higher than physiological levels of DA, which result in the generation of LIDs (Keber et al., 2015).

#### *1.3.3.2 Surgical lesioning*

Prior to the development of pharmacological therapies for PD in the 1960s and 1970s surgical interventions were widely used. The first of these was the development of the pallidotomy, involving the electrolytic destruction of the GP (Svennilson et al., 1960). Following this, surgeries were developed which lesioned parts of the thalamus and the STN (Selby, 1967; Narabayashi, 1982; Bergman et al., 1990). Whilst these surgeries often resulted in an alleviation of PD symptoms, they were also prone to side-effects due to inaccurate lesioning. These included post-operative chorea (involuntary movements), hemiballism (flailing movements of limbs), increased chance of stroke and infection, depression, memory impairments and potentially visual deficits (Walter and Vitek, 2004).

#### *1.3.3.3 Deep brain stimulation (DBS)*

In the last 10 years a new surgical treatment for PD has been developed based on the benefits associated with subthalamotomy. Deep brain stimulation (DBS) creates a reversible lesion. The procedure requires the surgical implantation of a stimulating electrode into a BG structure to administer electrically controlled chronic stimulation. The main targets of DBS are the STN and GP (Miller and DeLong, 1987; Bergman et al., 1994). Also, based on *in vivo* studies in rodent models of PD, DBS of the SNr has been shown to be effective in reducing akinesia (Sutton et al., 2012).

DBS is reserved for patients who have advanced PD, with disabling LIDs or tremor, as previous to this point the symptoms of the disease can be managed pharmacologically. For clinical benefit it is necessary for stimulation protocols to be above 50 Hz (common clinical stimulation is 130 Hz); while low-frequency stimulation either has no effect or results in enhanced PD symptoms (Moro et al., 2002; Garcia et al., 2005; Kuhn et al., 2006; Hammond et al., 2007; Eusebio et al., 2008; Timmermann and Florin, 2012). The treatment of PD using DBS has time-related effects on different symptoms, with tremor and rigidity being alleviated within a minute, and bradykinesia and akinesia taking a few minutes to days (Krack et al., 2002).

How DBS reduces pathological activity in the BG is still being debated. One study compared the effects of L-DOPA and DBS on pathological oscillations in the STN. They found that L-DOPA completely abolished the excessive beta activity, whilst DBS stimulation only reduced the beta activity and that combining the treatments provided no additional benefits (Giannicola et al., 2010). This suggests that the presence of beta oscillations themselves is not pathological, but rather the excessive power and synchronisation of them in the network that contributes to or is the result of the movement deficits observed in PD. Other studies have suggested that DBS acts to inhibit the output of the targeted structure, similar to permanent lesioning studies (Bergman et al., 1990; Aziz et al., 1991; Hamada and Delong, 1992). However, studies *in vitro* using high frequency stimulation protocols resulted in the synaptic depression of cortico-STN synapses in DA-depleted tissue, suggesting that part of the clinical effect of DBS could be mediated by the reduction in glutamatergic inputs from the cortex to the STN (Yamawaki et al., 2012) (also see Gradinaru et al., 2009).

Recent studies have also begun to look at stimulation of M1 as a less invasive option to STN/GP DBS. M1 input to the STN has been suggested to play a role in the pathological oscillations generated during PD (Magill et al., 2001; Bevan et al., 2002). Pagni et al. (2003) and Drouot et al. (2004) both demonstrated that stimulation of M1 resulted in a reduction in PD symptoms, producing immediate improvements in tremor and rigidity, as well as long-term improvements in bradykinesia and akinesia. It was also found that M1 stimulation restored normal firing rates in GPi and STN structures, similar to that seen in DBS (Drouot et al., 2004). Further studies have begun to investigate the use of transcranial magnetic simulation (TMS). Stimulation at 5 Hz or greater produced an excitatory effect in the cortex that, with repeated sessions, could last several months, effects which correlated with a reduction in symptoms in PD patients (Khedr et al., 2003; Lefaucheur et al., 2004; Fitzgerald et al., 2006; Wu et al., 2008).

## 1.4 Final summation

Overall, the involvement of M1 in PD is suggested to be important for future studies of the disease. This is particularly relevant when considering the pathophysiological involvement of excessive beta oscillations in the cortico-BG and the benefits of M1 stimulation in the alleviation of Parkinsonian symptoms. The study of oscillatory activity in M1 *in vitro* and the elucidation of mechanisms underlying physiological and pathological activity could identify potential targets for pharmacological or surgical interventions in PD. Furthermore, the use of *in vivo* animal studies and PD models of the disease affords the opportunity to identify the involvement of M1 in global network activity and observe changes that occur upon DA-depletion.

## 1.5 Aims and Objectives

To investigate the role of DA in M1 neuronal network oscillations *in vitro* and *in vivo.*

- Using LFP recordings *in vitro* to pharmacologically investigate the basis of theta and gamma oscillations in M1.
- To assess the evidence for or against phase-amplitude coupling *in vitro*.
- To investigate the power, frequency and pharmacology of M1 oscillations *in vitro* using the 6-OHDA model of PD.
- Using depth electrode and EEG recordings *in vivo* to investigate the neuronal networks and interhemispheric power of M1 in a DA-depleted animal.

# Chapter 2 Methods

## 2.1 *In vitro* recordings

### 2.1.1 Cortical Slice Preparation

Sagittal slices were prepared from male Wistar rats (weight 50-150 g). Each rat was anaesthetised with 4% isoflurane in $N_2/O_2$, and injected with pentobarbital (~600 mg/kg s/c) and xylazine (10 mg/kg i/m) until no paw pinch or corneal response reflex was detected (following the Animals Scientific Procedures Act 1986, U.K.). The rat was then transcardially perfused via the left ventricle with ice-cold sucrose-based artificial cerebrospinal fluid (aCSF), which contained (in mM): 180 sucrose, 2.5 KCl, 10 $MgSO_4$, 1.25 $NaH_2PO_4$, 25 $NaHCO_3$, 0.5 $CaCl_2$, 10 glucose, 20 ethyl pyruvate, 1 L-ascorbic acid (Rice, 2000), 2 N-acetyl-L-cysteine (Tian et al., 2003), 1 taurine (Ellren and Lehmann, 1989), saturated with carbogen (95% $O_2$/5% $CO_2$) and with an osmolarity 300-310 mOsm. To improve cell viability indomethacin (22.5 µM), a cyclo-oxygenase inhibitor (Pakhotin et al., 1997), uric acid (400 µM), an anti-oxidant (Proctor, 2008), and aminoguanidine (40 µM), an inducible nitric oxide synthase (iNOS) inhibitor (Griffiths et al., 1993; Sun et al., 2010), were also added to the solution. After transcardial perfusion was complete, using a loss of colour in the extremities as an indicator, the brain was rapidly extracted and incubated in the same sucrose-based aCSF. For extracellular recordings, 450 µm thick sagittal slices were cut at room temperature using a HM 650 V microslicer (Microm GMBH, Germany). Slices containing M1, S1 and striatum (**Fig 2.1**) were then transferred to an interface chamber of glucose-based aCSF which contained (in mM): 126 NaCl, 3 KCl, 1.6 $MgSO_4$, 1.25 $NaH_2PO_4$, 26 $NaHCO_3$, 2 $CaCl_2$, 10 glucose, saturated with carbogen (95% $O_2$/5% $CO_2$) and with an osmolarity 300-310 mOsm. The glucose-based aCSF also contained indomethacin (22.5 µM) and uric acid (400 µM). Slices were stored at room temperature (20-25$^{\circ}$C) for at least an hour before use. Slices were then transferred to a recording chamber (Scientific System Design Inc., Canada, **Fig 2.2**) where they were perfused with glucose-based aCSF (not containing indomethacin or uric acid) at 1-2 ml/min. Slices were kept in a humid atmosphere and solutions were saturated with carbogen (95% $O_2$/5% $CO_2$) and maintained at 32-34$^{\circ}$C by a PTC03 proportional temperature controller (Scientific System Design Inc., Canada).


**Figure 2.1 M1-S1 sagittal slice** Nissl stained slides showing the locations of the primary motor cortex (M1), somatosensory cortex (S1) and striatum (Str) in the sagittal section of a rat brain slice. The thick black dashed line denotes the approximate locations where cuts were made.
Adapted from The Rat Brain Atlas (Paxinos and Watson, 1998)

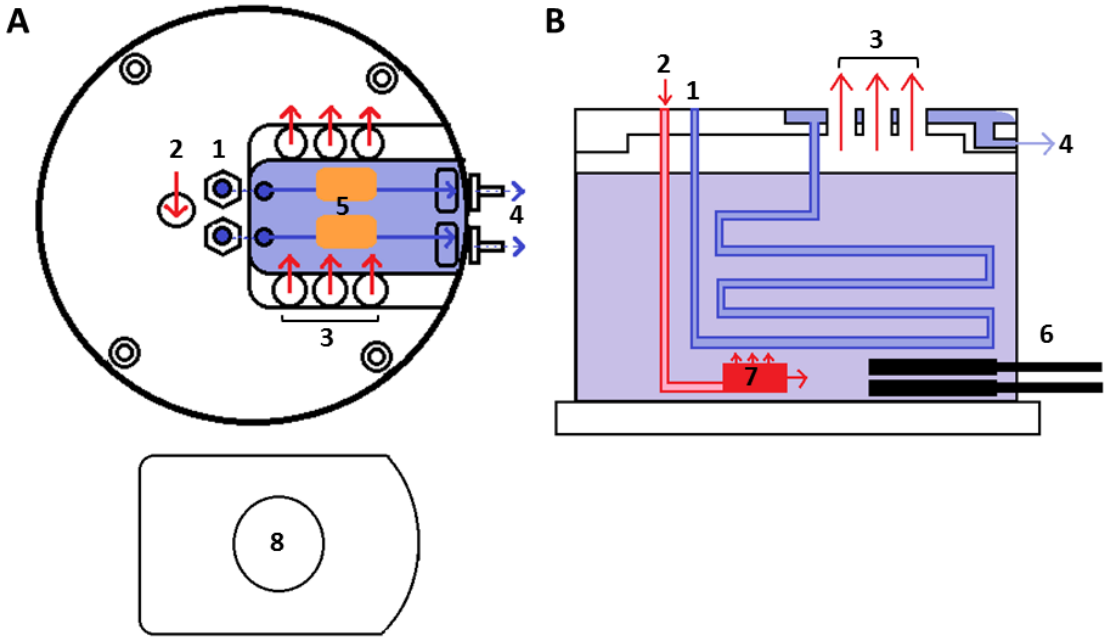


**Figure 2.2 A schematic diagram of an interface extracellular recording tissue bath.** The tissue bath consists of two chambers. Brain slices were placed in the upper chamber and perfused with glucose-based aCSF and humidified carbogen (95% $O_2$/5% $CO_2$). The lower chamber was filled with distilled water, heated to 32-34°C and continually bubbled with carbogen. **A)** Top view. **B)** Side view. Red arrows indicate direction of gas flow. Blue arrows indicate direction of aCSF flow. 1. aCSF solution entry point, 2. gas entry point, 3. Port holes for humidified gas, 4. waste aCSF outflow, 5. slices, 6. temperature controller/heater, 7. air stone, 8. acrylic lid to maintain high humidity environment.

### 2.1.2 Electrophysiological Recordings

#### *2.1.2.1 Local field potential (LFP)*

The local field potential (LFP), is the summation of the electrical activity of nearby neuronal networks (for review see Buzsaki et al. 2012). When current enters or leaves a cell it must be balanced by current flow in the opposite direction at a spatially distinct site (Leung, 2011). Thus, the movement of positive current across a membrane can result in either a current source (current flow entering the extracellular medium) or a current sink (current flow exiting the extracellular medium), which is reversed for negative current. Therefore, LFPs result from synchronous dendro-somatic dipole activity which can be recorded within 0.5-3 mm of the electrode tip (Mitzdorf, 1985; Logothetis, 2003). Most commonly these changes arise through synchronous IPSP and EPSP activity which can be recorded as oscillatory changes (Buzsaki et al., 2012). Changes in power and frequency in response to drug application can then be analysed to provide mechanistic insight (Elul, 1971; Logothetis, 2003). However, using LFP recordings alone, it is not possible to determine whether the positive or negative potentials results from EPSPs and/or IPSPs. Furthermore, it is not possible to determine the exact origin of the activity recorded. The changes in the LFP may result from activity generated away from the recording site as extracellular changes can spread through a conductive medium (such as the brain) from their source. This spread of the field potential is known as volume conduction (Lorente de No, 1947).

#### *2.1.2.2 Extracellular Recordings*

Borosilicate glass microelectrodes were pulled using a Flaming/Brown micropipette puller (P-97, Sutter instrument Co. U.S.A.) with an open tip resistance of 1-3 MΩ. Microelectrodes were filled with glucose-based aCSF and inserted into electrode holders containing a silver chloride coated wire. Using manually-operated micromanipulators (Kanetec, Japan) and a stereomicroscope (Leica Wild M3Z, U.K.), microelectrodes were inserted into layer V of M1, located using the rat brain atlas of Paxinos and Watson (1998) as a reference guide (**Fig 2.1**). The recorded potential was passed through an EXT amplifier headstage (NPI, Germany). The signal was then amplified x100 through an EXT10-2F amplifier (NPI, Germany) and then further amplified x10, high-pass filtered at 0.5 Hz and low-pass filtered at 700 Hz through a LHBF-48X amplifier/filter (NPI, Germany). Environmental line noise (50 Hz) was reduced by passing the signal through a HumBug 50/60 Hz noise eliminator (Quest Scientific Instruments Inc., Canada). Signals were digitized at 10 kHz using a CED micro-1401 mkII and recorded using Spike2

software (version 7.0, Cambridge Electronic Design, U.K., **Fig 2.3**). Data was saved to disk and analysed using Spike2 (version 7.0, Cambridge Electronic Design, U.K.), GraphPad Prism 5 (GraphPad software Inc., U.S.A.) and MATLAB R2015b software (MathWorks, U.S.A.).

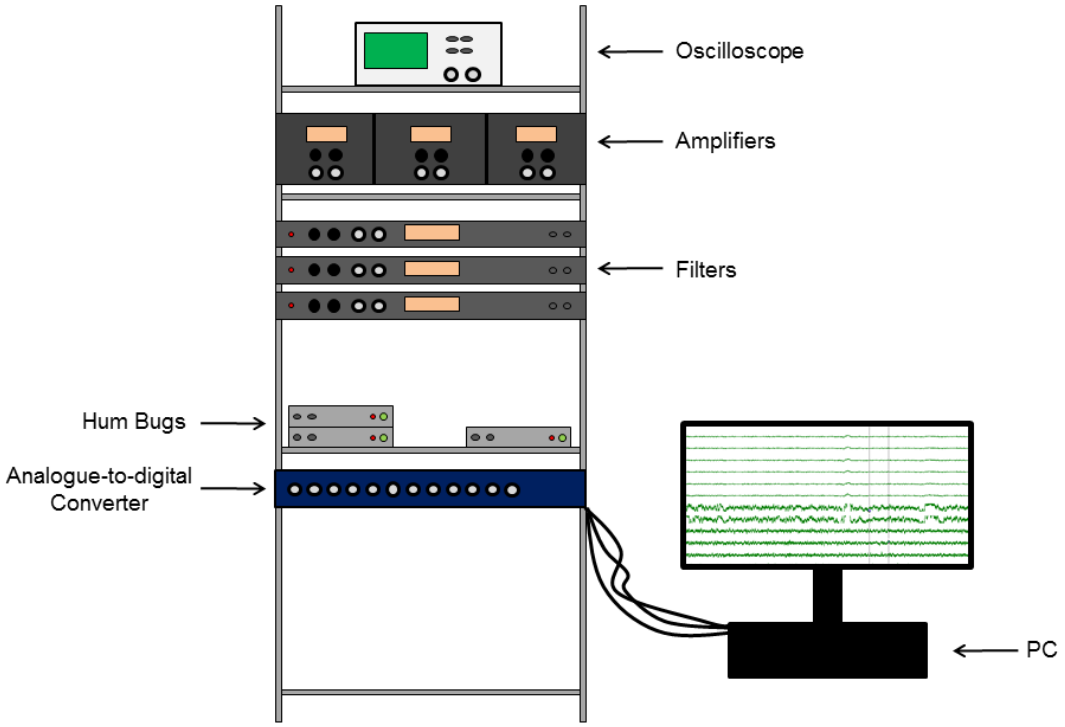


**Figure 2.3 Extracellular rig hardware set up.** Electrophysiology rig setup for LFP recording.

### 2.1.3 Noise concerns

Electrical interference (noise) and physical interference are important concerns when undertaking any electrophysiological recordings. However, there are multiple methods which can minimise the impact of noise. Physical interference mainly comes from vibrations which reduce electrode stability. These were negated through the use of an anti-vibration isolation table (TMC, U.S.A.) and strong magnets on the bases of micromanipulators to prevent any movement. Electrical interference is primarily derived from external sources, such as lights/power sockets (which provide 50 Hz noise) or electromagnets in pieces of equipment. This form of interference was negated by shielding the electrophysiological recording equipment with a Faraday cage (TMC, U.S.A.) and connecting this to a common ground. In addition recording signals are passed through HumBugs (Quest Scientific, Canada), which are filters that provide immediate 50

Hz noise cancellation without affecting the phase and amplitude of the recording which would occur if standard filtering systems were used.

### 2.1.4 Drug preparation

All drugs were purchased from Sigma, Tocris or Abcam. Stock solutions were prepared at a known concentration and stored at -20°C. Stock solutions were bath applied directly to the circulating aCSF to achieve desired concentrations. Drugs were applied after a stable period of recording which was used as a baseline (usually 30-40 mins). Subsequent neuronal oscillatory activity was then recorded for at least 40 mins.

### 2.1.5 Data collection and analysis

#### *2.1.5.1 Data analysis*

All extracellular data was converted from analogue to digital waveform and then visualised and recorded in Spike2. The sampling rate used was 10 kHz, which provides ample bandwidth for the original input signal to be digitally reconstructed without errors. This is determined from the Nyquist-Shannon sampling theorem, whereby in order to adequately reconstruct the signal the sampling rate must be at least twice the frequency of the frequency of interest in the signal (though greater than 10x is often utilised) (Shannon, 1949). Data was analysed in Spike 2 to produce the frequency power spectra, which uses a fast Fourier transform (FFT) algorithm. This algorithm splits the waveform into frequency components and the spectral resolution of the power spectrum can be modified by altering the FFT size. An FFT size of 8192 was selected to provide a spectral resolution of 0.6104 Hz per bin, using a Hanning window. This size was selected in order to provide adequate frequency resolution to observe the oscillations in our slices, without averaging the power spectra (from too small FFT size) or loss of specificity (from too large FFT size). 40 s epochs of data were analysed unless otherwise stated. In GraphPad Prism 5 peak power changes and pooled data were normalised (using control value as 100%) and presented as mean ± standard error of the mean (SEM). All statistical analyses were performed using normalised peak power changes. For figures, raw data was filtered in Spike2, using Bessel band pass IIR digital filters (3-10 Hz for theta oscillations and 30-45 Hz for gamma oscillations).

*2.1.5.2 Waveform correlations*

Correlation analysis reveals the temporal relationship between two waveforms. This analysis was used determine the temporal lag between simultaneous recordings made in layers II/III, Va, Vb of M1. To isolate theta and gamma frequency oscillations, 60s of raw data was zero-phase filtered using equiripple FIR filtering between 3-10 Hz (for theta) and 30-45 Hz (for gamma), using MATLAB (filtfilt). This data was then re-imported into Spike2 and cross-correlations produced, the results being expressed in terms of cross-correlation coefficient.

*2.1.5.3 Spectrogram analysis*

MATLAB was used to conduct further time-frequency analysis using a Morlet-Wavelet approach to create spectrograms from 0.5 Hz to 60 Hz, with a frequency bin width of 0.5 Hz, and a wavelet width of 5. This provides a time-frequency representation of the waveform. Spectrograms utilise a “hot” (red/orange/yellow) or “cold” (blue/green/purple) colour representation to denote the power of the activity. 10 s of data recorded at the end of the epochs as used in FFT analysis were selected and stored as a text file from Spike2. These data were then converted and analysed in MATLAB (MathWorks) using a script (‘invitrospec.m’, written by Dr. S.D. Hall, Plymouth University) to create a Morelet-Wavelet spectrogram.

*2.1.5.4 Phase-amplitude coupling*

PAC analysis of concurrent theta and gamma oscillatory activity utilised a custom-made MATLAB script (CallerRoutine.m) provided by Dr. A.B.L. Tort (Brain Institute, UFRN, Brazil). This analysis determines the modulation index (MI) which is a measure of the intensity of the coupling. We used 40 s epochs of control data for this analysis, exported to a text file with a sampling rate of 1000 Hz. A detailed outline of the mathematical processes that are used in the script can be found in Tort et al. (2010). In brief, the data was zero-phase filtered between 3-10 Hz; for phase, and 30-45 Hz; for amplitude. The time-series of the phase angles and amplitude envelope was then obtained using separate Hilbert transforms. These data were then used to produce a normalised phase-amplitude plot, providing the mean amplitude of the 30-45 Hz oscillation across the phase (0-360$^{o}$) of the 3-10 Hz rhythm. MI was then calculated by identifying deviations of the phase-amplitude from a uniform distribution. Therefore, the greater the variation of the amplitude distribution from the uniform result, the greater the MI.

The MI values were sorted numerically and a split was observed between the groups with an order of magnitude difference in numerical value. According to the original paper by

Tort et al. (2010), with a perfectly coupled model dataset an MI value in the range of $10^{-2}$ could be obtained. However the highest MI we observed with our data was $10^{-4}$, an order of magnitude lower than the mode data. Therefore, while it was not within the same range of the sample data, it was upon this basis that the groups MI+ ($10^{-4}$) and MI- ($10^{-5}$) were determined.

#### *2.1.5.5 Statistical analysis*

In order to determine the correct statistical tests to use when analysing our data, we utilised the Kolmogorov-Smirnov and Shapiro-Wilk normality tests. These determine whether our data can be matched to a Gaussian distribution (or was normally distributed). We determined that while some data sets were normally distributed, they did not all display this property. As such, in order to maintain fewer differences between interpreting our data as possible, we performed only non-parametric tests to determine statistical significance ($p<0.05$). Furthermore, as all our data concerns a control value, followed by a drug condition change in power, our data is considered paired, in the context of statistical analyses.

Thus, when analysing experiments concerning only control and a single drug concentration (e.g. SYM 2206 or quinpirole) we used the Wilcoxon matched-pairs signed rank test, as this takes into account the paired and non-parametric nature of the recordings. Accordingly, when analysing the effects of experiments with control and multiple drug concentrations (e.g. diazepam), we used the Friedman test with Dunn's multiple comparison post-hoc analysis, as this concerns the repeated and non-parametric nature of our recordings. However, in the gabazine and zolpidem experiments (in chapter 3), the pooled data for each drug condition resulted in unequal sample sizes as some experiments were only run on a smaller selection of doses than the total pooled experiment. As a result, in order to analyse the data we performed the Kruskal-Wallis test with Dunn's multiple comparisons, which does not take into account repeated measures, and this should be taken into account when interpreting this data.

Power analysis was performed on already completed experiments using GraphPad StatMate (v 2.00). This utilises the number of samples in the desired experiment and the standard deviation of the differences to produce a table of power for the experiment.

All data is shown normalised to control (using control as 100%) and presented as mean ± SEM unless otherwise stated. Statistical significance of $p < 0.05$ is denoted by *, $p < 0.01$ is denoted by ** and $p < 0.001$ is denoted by ***.

## 2.2 *In vivo* recordings

### 2.2.1 6-OHDA Lesions

#### *2.2.1.1 The 6-hydroxydopamine (6-OHDA) model of PD*

The 6-OHDA rat model of PD was developed by Ungerstedt (1968). In this model 6-OHDA is injected directly into a targeted brain structure (since it cannot cross the blood-brain-barrier). Injection can be made bilaterally but for our purposes we made unilateral lesions so that the contralateral hemisphere could serve as a control for the ipsilateral (lesioned) hemisphere. To test for adequate lesioning, animals can be dosed with either amphetamine (to enhance DA release in the intact hemisphere) or apomorphine (an agonist of DA receptors, acting on the depleted hemisphere) to induce ipsiversive (turning towards lesioned hemisphere) and contraversive (turning towards control hemisphere) rotations, respectively (Ungerstedt and Arbuthnott, 1970; Ungerstedt, 1971; Perese et al., 1989). The 6-OHDA lesion can be targeted to the SNc itself, the medial forebrain bundle (MFB) or the striatum to induce the degeneration of the dopaminergic neurons (Sauer and Oertel, 1994; Blum et al., 2001).

The 6-OHDA model of PD has several advantages for our experiments over other established models, such as the 1-methyl-4-phenyl-1,2,3,6-tetrahydropyridine (MPTP) model. Primarily, we can target the 6-OHDA toxin to a particular brain area, through intra-cerebral injection, which also allows us to lesion only a single brain hemisphere to create a unilateral lesion. Whereas, the MPTP model is injected peripherally into the animal, creating a non-targeted bilateral lesion, resulting in widespread dopaminergic neuron damage (Forno et al., 1986; German et al., 1988; Seniuk et al., 1990). Furthermore, rodents have been shown to be resistant to the dopaminergic neuron damage resulting from MPTP administration (Boyce et al., 1984; Chiueh et al., 1984; Sahgal et al., 1984) and considering that our control work has focused on rodent M1, switching species is not a viable or sensible option.

6-OHDA acts specifically upon catecholaminergic neurons via dopamine transporters and noradrenaline transporters (Porter et al., 1963; Porter et al., 1965). To increase specificity 6-OHDA was co-administered with injections of desipramine (a noradrenaline and serotonin reuptake inhibitor) to prevent reuptake of the 6-OHDA into non-dopaminergic neurons and pargyline (a MAO inhibitor) to prevent catabolism of the 6-OHDA. 6-OHDA has been suggested to cause cell death via oxidative stress, through the generation of

hydrogen peroxide ($H_2O_2$) and hydroxyl group free radicals ($OH^{\bullet}$) (Breese and Traylor, 1971; Heikkila and Cohen, 1971, 1972a; Heikkila and Cohen, 1972b; Karoum et al., 1993).

*2.2.1.2 Surgical Procedures*

5 mg of 6-OHDA HBr powder containing 0.1% ascorbic acid (Sigma Aldrich, UK) was dissolved in 0.676 ml 0.9% saline to a final concentration of 5 mg/ml. Six aliquots of 100 µl were then stored in at -20°C in foil covered vials. On the day of surgery, one aliquot was stored in a +2°C fridge until needed. When required, 25 µl of 6-OHDA solution was drawn into a 700 series Hamilton syringe (Hamilton, Switzerland) and covered with tin foil to prevent exposure to light. The colour of the solution was regularly monitored and replaced if oxidation (pink/brown discolouration) occurred. Desipramine was prepared to a final concentration of 12.5 mg/kg dissolved in saline, and pargyline, dissolved in saline to a final concentration of 75 mg/kg. Animals received intraperitoneal (i/p) injections of desipramine (2 ml/kg) and pargyline (1 ml/kg) 30 mins prior to 6-OHDA infusion.

Wistar (in house breeding at Aston University for chapter 4 experiments) and Sprague-Dawley (from Harlan (Italy) for chapter 5 experiments completed at Lilly U.K.) rats (290-310 g) were anaesthetised using 4% isoflurane with 1.5 L/min $O_2$. Once fully unconscious the rats heads were shaved, cleaned with iodine and mounted in a stereotaxic frame (Kopf Instruments, U.S.A.), secured with blunt ear bars and a toothbar set to -3.3 mm. Anaesthesia was maintained by isoflurane (2%).

Co-ordinates for injection of 6-OHDA were calculated from bregma (0, 0). The medial forebrain bundle (MFB) was identified at AP -2.8 mm, ML +2.0 mm and marked. At this location a small hole was drilled in the skull and a 28 gauge steel cannula, attached to the Hamilton syringe via FEP tubing, was lowered to a depth of 9.0 mm (from skull surface). The Hamilton syringe was attached to a syringe infusion pump (WPI, U.S.A.) and 6-OHDA was infused at a rate of 0.5 µl/min over 5 min to a total volume of 2.5 µl. After infusion, the cannula was left in place for a further 5 minutes before retraction to allow full diffusion of the toxin. Skull incisions were sutured using vicryl sutures (Ethicon) and to aid rehydration animals received a subcutaneous (s/c) injection of 5 ml 0.9% saline. Rats were placed in heated recovery cages for a minimum of 2 hours, and were checked at least four times during this period. Following this, rats were moved into recovery cages with food, treats and hydrogel available *ad libitum* and their weights were monitored daily for 2 weeks. Analgesia was not provided post-surgery, since it can act as a protectant from the 6-

OHDA toxin and prevent the formation of a stable lesion. Animals were allowed 2 weeks recovery time post-surgery before lesion testing.

For chapter 5 experiments similar procedures were conducted on 10 sham-control animals. In these animals phosphate buffered saline (PBS) was infused instead of 6-OHDA. All other manipulations, injections and surgical procedures were identical.

### 2.2.2 Motor Behavioural Tests

#### *2.2.2.1 The Adjusting Step Test*

The adjusting step test was first outlined by Olsson et al. (1995) to measure akinesia in the forelimbs of a hemi-parkinsonian rat model. This test was used in the experiments outlined in chapter 4 and 5.

The adjusting step tests were performed over three consecutive days. Rats were left to acclimatise to the testing room for at least 5 min prior to the start of each test in order to reduce the impact of stress. Rats were restrained by the experimenter so that only a single forelimb could be used. Rats were then moved across a level surface for a distance of 1 m in both the forehand and backhand direction to assess the motor ability of each forelimb. On each of the three days, the tests were completed twice. The total number of adjusting steps made by each forelimb in each direction was counted and the average determined.

Each animal was considered individually in order to determine the success of the lesion. For a successful lesion a drastic reduction in adjustment steps for the contralateral (opposite to the lesioned hemisphere) limb was observed. All data was averaged and presented as mean ± SEM. 2-way ANOVA was used to determine statistical significance between groups, with Bonferroni post-hoc test to correct for multiple comparisons. Statistical significance was denoted by *, $p < 0.05$; **, $p < 0.01$; ***, $p < 0.001$.

#### *2.2.2.2 The Rotometer test*

Rotometers, manufactured by Med Assosciates Inc., (U.S.A), use spherical bowls which are designed to promote rotational activity (**Fig 2.4**). Prior to testing rats were left to habituate to the experiment room in home cages for 5 min. Rats were then secured to the elastic tethers allowing them free use of both their fore and hind limbs. Rats were then placed within the bowl and the lights in the room were dimmed to promote activity. The

elastic tethers were attached to a freely moving rotational sensor and movement recorded in real-time.

Basal 'spontaneous' rotations were recorded over a 40 min period. Contraversive and ipsiversive rotations were recorded and the data was divided into 5 min bins. For our analysis only full rotations (360°) were taken into account. The system also takes into account jitters or other movements when counting less than full rotations, which may or may not be the result of lesions, so using only the full rotations as a measure keeps this test specific to our data. Data was presented as a rotational asymmetry score (RAS), which was calculated by subtracting the contraversive from the ipsiversive rotations. Thus, a successful lesion was demonstrated by a strongly negative score, whilst sham or failed animals had a score closer to zero. Results were averaged per bin (mean ± SEM) in each rotational direction. Statistical significance between lesioned and sham animals was verified using 2-way ANOVA (repeated measures), with Bonferroni post-hoc test used to correct for multiple comparisons. Statistical significance was denoted by *, $p < 0.05$; **, $p < 0.01$; ***, $p < 0.001$.

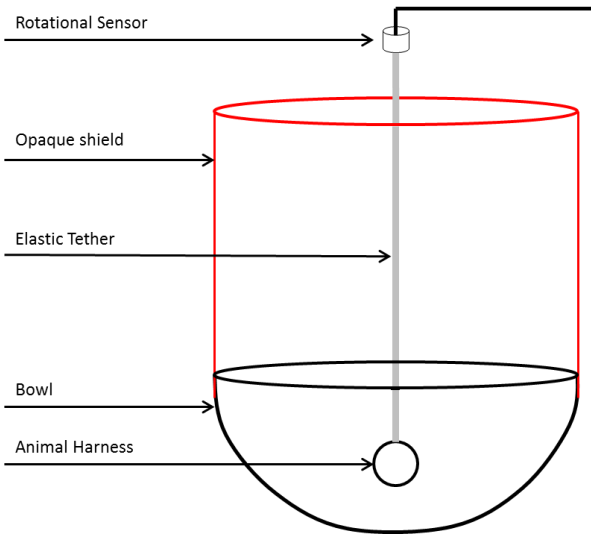


**Figure 2.4 Schematic representation of a rotometer chamber.**

*2.2.2.3 Locomotor activity (LMA) test*

Ethovision XT video tracking software (Noldus Information Technology, Netherlands) was used to measure basal rotations in an open field environment. This software utilises an infrared camera to record the locomotor activity of rats in a dark or light environment. A single camera recorded the activity within four transparent chambers, positioned in a 2 x 2 design; each chamber being 40 x 40 cm in size (**Fig 2.5**).

Animals were left in home cages in the recording room for 5 min prior to the experiment. This is especially crucial for these experiments, as they are performed in a dark room, so that the animals can adjust to the change in light to produce the best potential activity. Movements were tracked via a 2-point system (using head-centre axis) in order to determine frequency of rotational behaviour. As this system uses more tracking software to determine rotations, rather than a mechanical tether (as in the rotometer recordings), we were able to use turns greater than $90^{o}$ to determine rotational frequency as there is greater recording accuracy. Each recording lasted for 40 min and 5 min bins of activity were used to determine contraversive and ipsiversive rotations.

The success or failure of the lesion for each animal was once again determined by calculating the RAS obtained by subtracting the number of contraversive from ipsiversive turns. Statistical significance between lesioned and sham animals was calculated using 2-way ANOVA (repeated measures), with Bonferroni post-hoc test used to correct for multiple comparisons. Statistical significance was denoted by *, $p < 0.05$; **, $p < 0.01$; ***, $p < 0.001$.

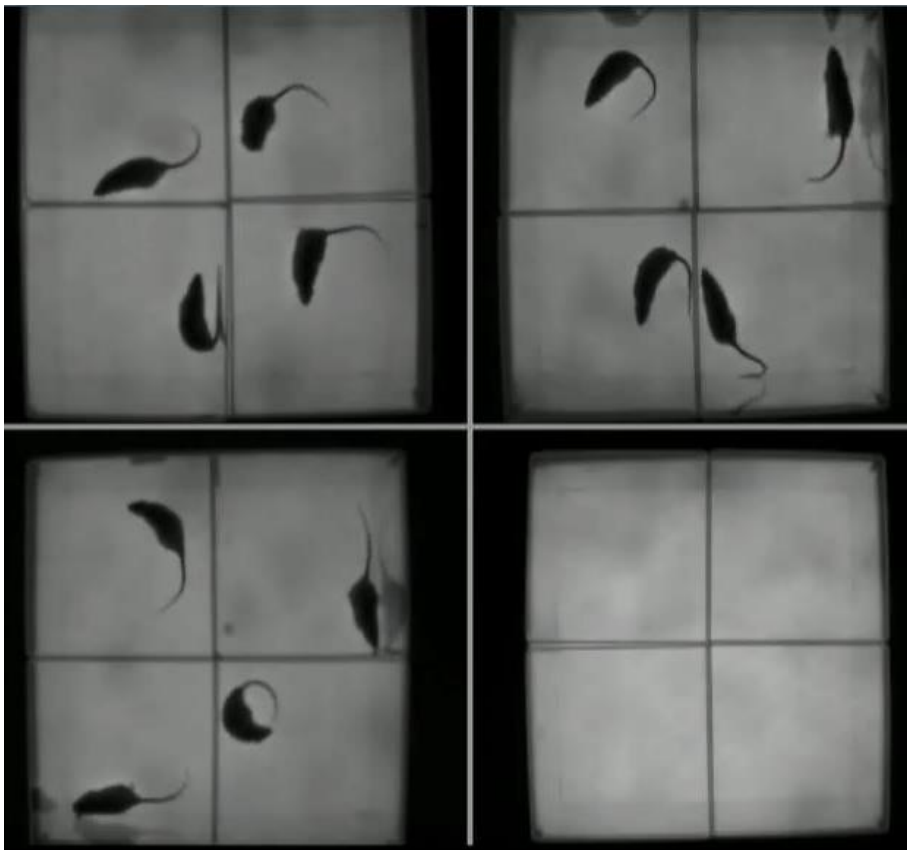

**Figure 2.5 The LMA test.** Picture showing twelve experiments running concurrently, the movement of each rat was tracked within a separate chamber. Experiments were run in the dark using an infrared camera, therefore white Sprague-Dawley rats showed up as black against the light background.

### 2.2.3 Depth Electrode Recording

*2.2.3.1 Surgical Procedures*

Following two weeks recovery from surgery, 6-OHDA-lesioned and sham animals were prepared to receive 2x depth electrodes which were implanted bilaterally (schematic shown in **Fig 2.6**). Depth electrodes were purchased from Neuronexus (U.S.A) and were a CM16 electrode package connected to an A1x16-3mm-100-703 electrode array (16-channel electrode array 3 mm in length with 703 $\mu m^2$ probe areas spaced 100 µm apart).

Animals were anaesthetised with 4% isoflurane and their heads subsequently shaved and cleaned. Animals were secured in a stereotaxic frame using blunt ears and fixed to a teeth bar. A single incision was made and the skull and bregma (0, 0) located and marked using a cauteriser, along with the two locations above each M1 to determine the site for the implantation of the depth electrodes (AP +1.5 mm, ML ±2.5 mm) in each hemisphere. Prior to depth electrode implantation, a hand operated manual drill bit was used to make three holes for skull screws, which acted as anchor points for the head cap. Three screws were also implanted above the cerebellum, one at the midline-point and one either side used for grounding and reference (**Fig 2.6**). Once all screws were secured, a high-speed hand-drill was used to make holes at each point previously marked above each M1. Depth probes were inserted to a depth of 2.1 mm from the surface of the brain and secured in place using hybrid resin composite which was hardened using a UV light source (Kerr Revolution Formula 2 - A2, Kerr Corporation, U.S.A.). To the cerebellum screws the two reference wires (screws either side of midline) and the two ground wires (both to the central midline screw) were attached, one wire of each was provided from each depth probe. The skull, implants and wires were fully covered by the hybrid resin composite to form a solid head cap. Once secure, the surrounding skin was sutured using vicryl dissolvable thread in a simple interrupted stitch.

Post-surgery, animals were administered an analgesic, carprofen (5 mg/kg - brand name Rimadyl), and an antibiotic, cefovecin (8 mg/kg - brand name Convenia). Animals were moved to a heated recovery cage and monitored at least four times for 2 hours before being returned to clean home cages. Animals were given another dose of carprofen the day following surgery, as well as daily administration of meloxicam (0.15 mg/kg) for 7 days post-surgery to help with pain relief. Animals were allowed two weeks to recover prior to the commencement of experimental testing.

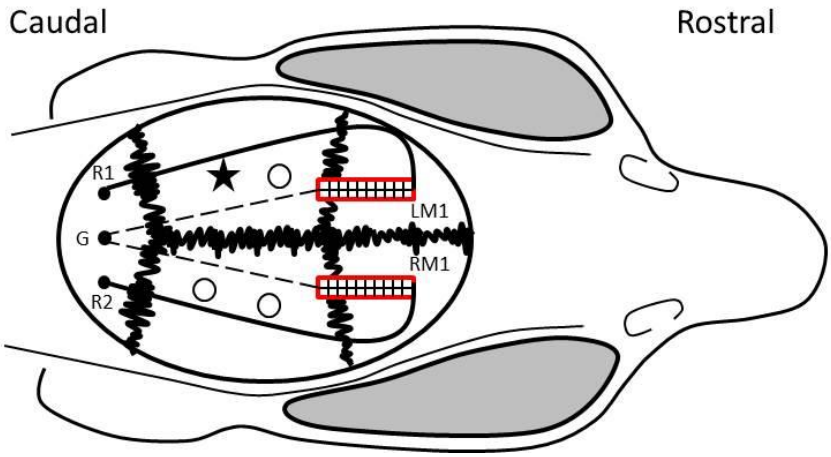


**Figure 2.6 Schematic of depth electrode placement.** A diagram showing the placement of the depth electrodes in a top down schematic of a rat skull. LM1 and RM1 show the locations of the left and right probes in M1 (outlined in red). Open circles denote locations of anchor screws in the skull. The star symbol shows the location of the 6-OHDA injection site. R1, R2 and solid lines, denote reference screw locations in the cerebellum. G and dotted lines denote the shared ground screw in the cerebellum.

#### *2.2.3.2 Open field depth-electrode recording*

Following the two week recovery period from surgery, animals were placed onto a food deprivation regimen. Water was available *ad libitum*. Animal's pre-food deprivation weights were recorded and used to calculate a deprivation weight loss. Weights were monitored on a daily basis and animals were fed accordingly to keep them within the limits of 5-10% of their pre-deprivation weight.

The open field environment consisted of a circular transparent chamber (80 cm diameter) located in a dimmed room. Prior to an experiment, animals were moved to the testing room in home cages and allowed to habituate for 5 min. Subsequently animals were tethered to the recording probes, placed within the open field space and recording was initiated. A 30 min control period was allowed before drug administration, followed by a 1 hr drug period. In order to promote movement and exploratory behaviour from the animal during the experiment, sugar pellets (~0.5 g in weight each) were dropped into the recording environment every 20 s.

LFP signals from each channel were digitised using a Neuralynx Digital Lynx 16SX and recorded using Neuralynx Cheetah5 software (Neuralynx Inc., Montana, U.S.A.). Activity recorded in channels 1-16 corresponded to the probe situated in the lesioned hemisphere and activity recorded in channels 17-32 corresponded to the probe situated in the non-lesioned hemisphere. Signal data was saved to individual Neuralynx files and was imported to Spike2 and MATLAB for further analysis.

#### *2.2.3.3 Data analysis*

FFTs were generated from 60 s of uninterrupted data selected every 10 min. In some cases, this period coincided with a high amount of movement artefacts, affecting the FFTs generated. As such, the period of time closest to the 10 min target containing uninterrupted data was selected to generate the next FFT. An FFT size of 8192 was selected to provide a spectral resolution of 0.1436 Hz per bin, using a Hanning window. Again this FFT size was selected to provide optimum resolution for the power spectra without subjecting the signal to averaging (with too small FFT) or loss of specificity (with too large FFT) related issues.

CSD analysis was carried out based on inverse CSD (iCSD) scripts outlined in Pettersen et al. (2006) and the *CSDplotter* toolbox (http://software.incf.org), which allows for the prediction of CSD at the boundary electrodes and has greater flexibility when using different probe sizes and geometries. After the data was imported into MATLAB, it was zero-phase (forward and backwards) filtered between 20 and 45 Hz, in order to isolate the specific frequency of the observed oscillations. Following this a 1 min section from the end of the recording, from when the animal would have adjusted to being attached to the tether and resumed normal behaviour, was isolated for each channel. This data was split into epochs of 235 ms (based on epochs of 0.2 s x sampling rate of 1176) and the peak maxima of the oscillatory events categorised. These peaks were sorted and aligned for each epoch and subsequently averaged across the 1 min recording. The array of the peaks in the recording formed the basis of the CSD analysis. The final CSD is determined by taking into account the position of each electrode and cortical conductivity of the extracellular medium (standard is set to 0.3). The analysis uses polynomial equations to map the electrode positions in relation to the oscillatory peaks determined previously to generate the pattern current sources and sinks across the probe. This generates the CSD graph, which demonstrates a pattern of sources (in red) and sinks (in blue) across the averaged 235 ms epoch.

### 2.2.4 EEG experiments

*2.2.4.1 Surgical procedures*

After recovery from 6-OHDA surgery, a cohort of animals were prepared to receive a custom made cranial implant (**Fig 2.7**) that allowed for chronic electroencephalogram (EEG) recordings. At least 24 hours pre-surgery and immediately prior to surgery animals were given oral antibiotics (Septrin$^{TM}$ – Sulfamethoxazole (40 mg/ml) and Trimethoprim (8 mg/ml)). Animals were anaesthetised in an induction chamber (4% isoflurane) and once unconscious their head and abdomen were shaved. The isoflurane concentration was reduced (2%) at this point, and the hind limb pinch was used to test for the absence of reflexes before surgery began.

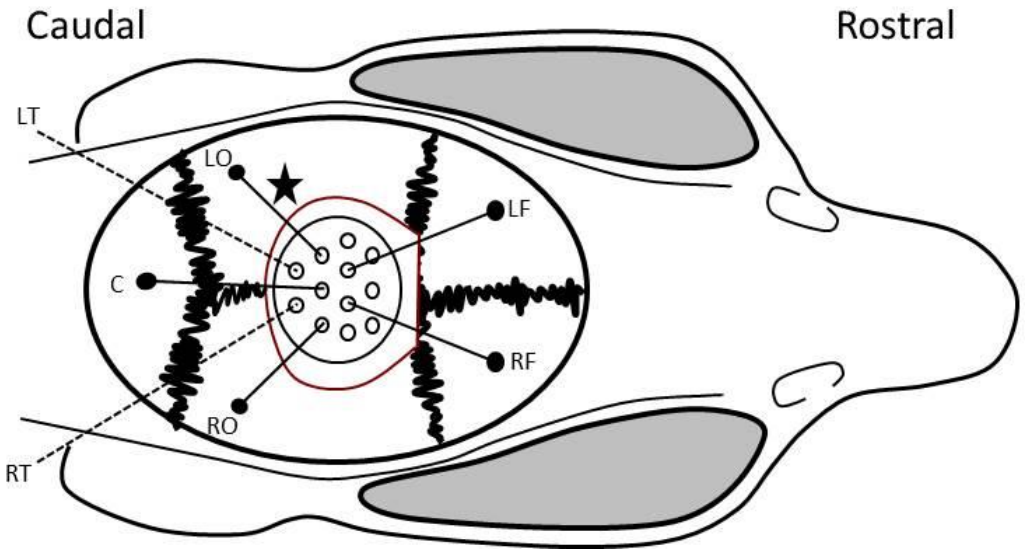


**Figure 2.7 SCORE EEG implant** Schematic showing placement of the SCORE EEG recording implant on the skull of a rat. LF, left frontal EEG; RF, right frontal EEG; LO, left occipital EEG; RO, right frontal EEG; C, cerebellum ground screw; LT, left trapezoid EMG; RT, right trapezoid EMG; Star symbol shows the location of the 6-OHDA injection site.

Initial preparations for the head implant surgery were the same as in section 2.2.3.1. Once the skull was exposed, bregma (0, 0) was located and marked using the tip of a cauteriser. Locations for the EEG screws were determined (two frontal [AP +3.5 mm, ML ±2.0 mm] and two occipital [AP -6.4 mm, ML ±5.2 mm]; see **Fig 2.7**), marked and subsequently holes were made using a hand-held high-speed micro-drill. Five screws were inserted; one for each EEG recording wire and the SCORE EEG implant was secured to the skull using cyanoacrylate. One screw was also implanted above the cerebellum at the midline-point to act as a ground. The entire assembly was then secured in place and covered by the application of dental acrylic (1 g acrylic powder to 1 ml resin),

to form a complete cap. The skin was then sutured loosely over the acrylic head cap using simple interrupted stitches.

Following surgery animals were given 5 ml 0.9% saline s/c to aid re-hydration and transferred to a heated recovery cage. Animals were monitored at least four times over the course of 2 hours before being placed in clean home cages. The animals were administered an analgesic (buprenorphine 0.05 mg/kg) s/c at the end of the surgical day and the first morning post-operatively. For 6 days post-surgery, animals were given 0.15 mg/kg meloxicam orally twice daily and further doses of antibiotic (Septrin) were also provided twice daily for 7 days. Animals were given 2 weeks to fully recover from surgery before any experiments or further tests took place.

*2.2.4.2 Recording environment*

Upon completion of the two week recovery period animals were transferred from the post-surgery recovery room to a light-reversed holding room (lights on: 7 pm, lights off: 7 am, GMT). Since our experiments were analysing the pharmacological effect of drugs on the movement deficits of the 6-OHDA lesion, animals were light reversed so experiments would take place during the dark phase. This ensured that the point of drug administration would be at their peak awake period. Following 2 weeks habituation to light reversal animals were moved to the SCORE chamber. Each SCORE chamber was a modified Ancare$^{TM}$ microisolator cage (Ancare, U.S.A.), complete with a custom polycarbonate filter-top riser which dispended food and drink. The riser also contained infrared sensors to determine when exactly animals were eating or drinking. Each chamber was housed in separately ventilated, square stainless-steel compartments (**Fig 2.8**). Each chamber had an infrared light source and digital camera, which allowed for 24 hour monitoring of the animal, with at least two remote checks carried out every day. Food and water were available *ad libitum* and the ambient temperature was maintained at 23 ± 2$^{\circ}$C. Throughout the study individual strip lighting within each chamber was used to maintain equal lighting per cage and a 12/12 hour light/dark cycle (7pm/7am, respectively).

EEG head implants were connected using a custom-engineered flexible tether and ultra-low torque slip-ring commutator (Hypnion, U.S.A) giving the animals free movement. In order to prepare animals for treatments that would involve an oral gavage (i.e. zolpidem), a control vehicle solution (methylcellulose 0.25%, 1 ml/kg) adaption dose was initially administered.

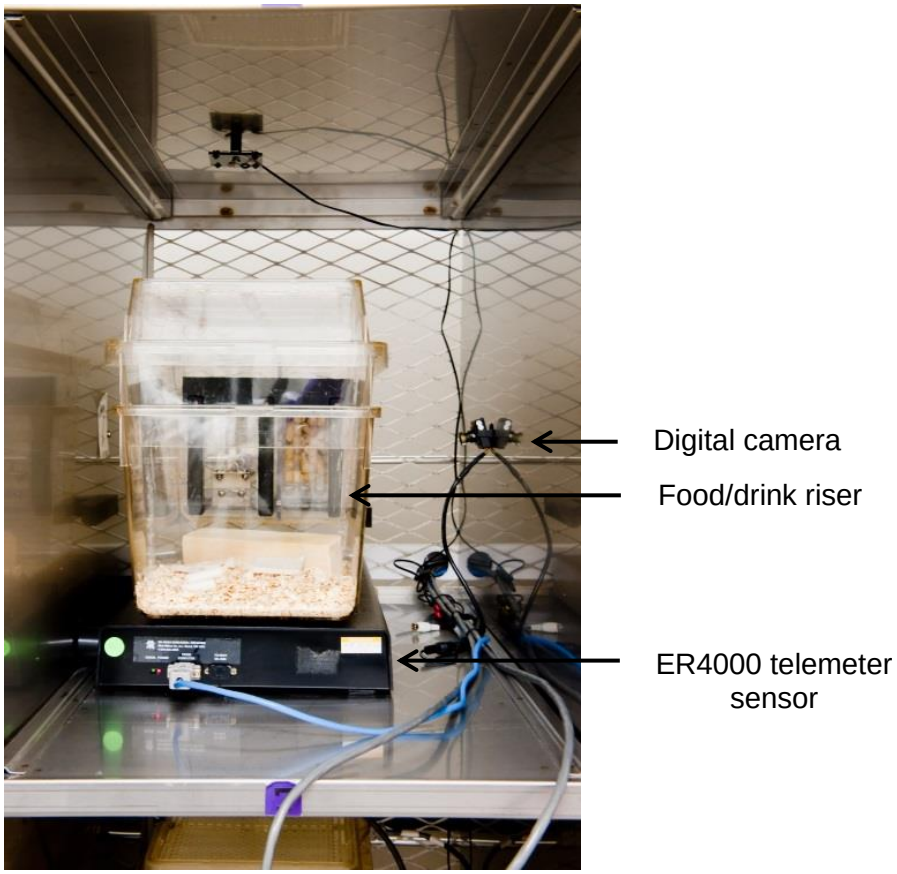


**Figure 2.8 Standard SCORE chamber set-up.** Photograph of a standard SCORE cage for an individually housed rat. Showing food and drink riser at the back of the cage

*2.2.4.3 Treatment and study design*

Each drug to be administered was pre-weighed by the Sample and Reagent Management team at Lilly U.K. Each drug was formulated to a stock solution and diluted to required doses from the stock using a designated vehicle. Before each treatment, animals were left undisturbed for 48 hours to provide a baseline set of data. Animals were removed from recording cages for 60-90 s, weighed and dosed before being returned to cages and monitored undisturbed for at least 48 hours post-treatment time. Studies were run using a full-crossover protocol. All drugs studied were given at 6 hours after the lights off time.

*2.2.4.4 EEG Data Collection and Analysis*

EEG signals were amplified (x10,000), bandpass filtered (between 1-100 Hz) and digitised (at 400 Hz) (Grass Corp, Quincy, MA, USA). Using EEG and EMG amplitude features to form templates, the scoring system classified 10 s epochs of data as different states of arousal, NREM sleep, REM sleep, wake and theta-dominated wake. Data was digitised and written to CD-R before being exported as required into Spike2 for further analysis.

Initial data analysis was performed both on-line, during daily inspections of animal welfare, and off-line by expert analysts (DSR team, Lilly, U.K.) using a specialised suite of programs (ScoreView$^{TM}$, Eli Lilly proprietary software). This suite of programs allows for the visual examination of raw EEG data files, construction of hourly mean time series and use of graphical and statistical assessments to provide group mean time series data. This provided an assessment as to the quality of the data recorded for each treatment and helped to guide future studies.

Exported data was organised into different dosing and experimental groups (ipsilateral vs contralateral and 6-OHDA lesioned vs sham). Data was analysed in MATLAB using a custom-made cumulative power script (CumPower.m), written by Dr. E. J. Prokic (University of Helsinki, Finland). Based upon pre-defined time information, the disrupted dosing period was removed to provide a continuous (pre- and post-dosing) signal. The data was zero-phase filtered (using MATLAB function filtfilt) to the target frequency band (25-40 Hz) and a Hilbert transform applied. This was used to determine the absolute power and generate the power envelope of the signal over time. Data was separated into pre- and post-drug epochs of 30 mins each and the cumulative power change of the amplitude over each epoch determined from the envelope. Cumulative changes in amplitude over each 30 min epoch were then displayed graphically for each individual file recording in a treatment group (an example of which is shown in **Fig 2.9**). This allowed for the removal of outlier recordings, which did not demonstrate a stable accumulation of power over time and differed substantially from the rest of the treatment group. These were removed after visual inspection, specifically looking for those which clearly deviated from the trend of the data set. Visual inspection of the raw data traces of these removed data sets, usually showed clear signal artefacts or sudden shifts in the power of the data which would not normally be representative of a biological recording. The mean of the remaining data was determined for each epoch and condition and presented as changes to cumulative power values in bar graphs using GraphPad Prism 5.

These results were analysed using 2-way repeated measures ANOVAs, as we wanted to discover the statistical significance of not only the changing drug concentration, but also if this changed over time. Therefore, we could not perform a 1-way ANOVA, which only compares the statistical effect of a single factor. Statistical significance of $p < 0.05$ is denoted by *, $p < 0.01$ is denoted by ** and $p < 0.001$ is denoted by ***.

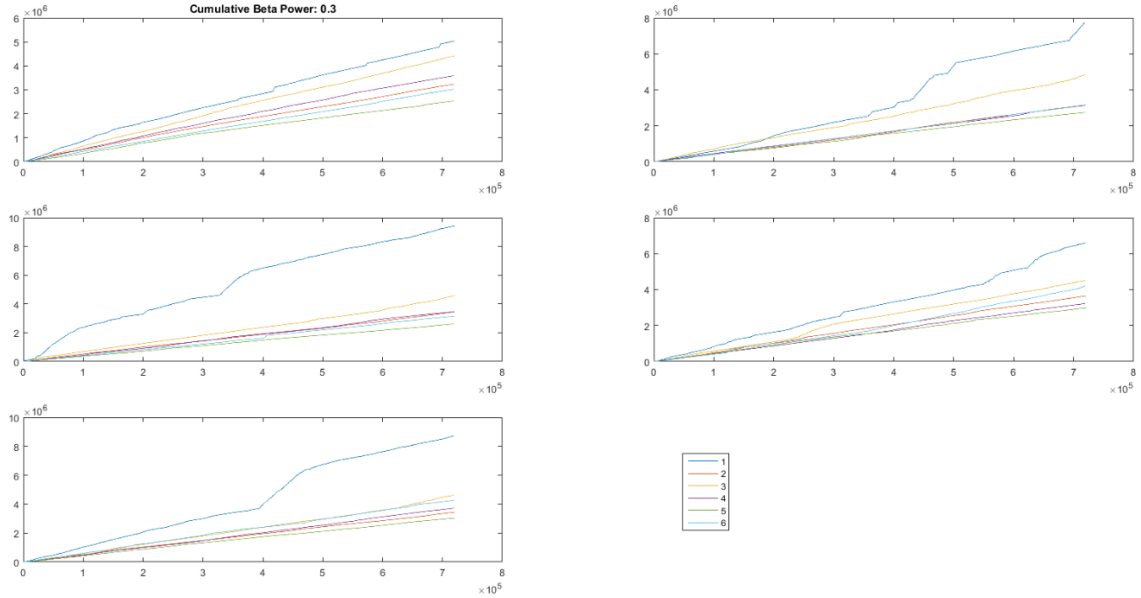


**Figure 2.9 Example graphs demonstrating outliers in cumulative power.** Visual display of each 30 min epoch in a data set which demonstrates an individual cumulative power value for each animals recording. This allows for the visual examination and removal of outlier data prior to the generation of the mean cumulative power value. For example, the blue (1) trace in these graphs shows clear aberrant deviations from the trend of the rest of the data in each epoch and was removed from the average.

# Chapter 3 Theta-Gamma Pharmacology *in vitro*

## 3.1 Introduction

Neuronal network oscillations have been studied *in vivo* (whole animal) and *in vitro* (brain slices). The advantage of studying oscillations *in vivo* is the ability to observe them physiologically and provide an insight into their functional relevance. However, using *in vitro* techniques the recording environment can be directly controlled allowing mechanistic and pharmacological investigation, thus allowing a thorough analysis of the cells and receptors which contribute to the network activity.

*In vitro* studies of gamma oscillations (30-80 Hz) have taken place in many areas of the brain, including hippocampal CA1 and CA3 (Whittington et al., 1995; Fisahn et al., 1998), dentate gyrus (Towers et al., 2002), entorhinal cortex (Cunningham et al., 2003), somatosensory cortex (Buhl et al., 1998; Roopun et al., 2006) and auditory cortex (Cunningham et al., 2004; Traub et al., 2005). Early work established protocols for the induction of oscillatory activity which involved the addition of the mGluR agonists (such as DHPG) or tetanic electrical stimulation (Whittington et al., 1995; Whittington et al., 1997), to elicit transient (~200-800 ms) gamma oscillations. The induction of persistent gamma oscillations was found to be elicited through the bath application of CCh and KA (Buhl et al., 1998). However, persistent oscillations have also been induced by application of either CCh or KA (Fisahn et al., 1998; Hajos et al., 2000; Fisahn et al., 2004; Modebadze, 2014).

First described in the hippocampus by MacIver et al. (1986) and Konopacki et al. (1987), theta oscillations *in vitro* were elicited by the bath application of CCh (50 µM). More recent studies in the hippocampus (MacIver et al., 1986; Konopacki et al., 1987; Konopacki et al., 1997; Cobb et al., 2000; Scanziani, 2000), entorhinal cortex (Cunningham et al., 2003) and neocortex (Lukatch and MacIver, 1997; Castro-Alamancos, 2013) have focused on the mechanism and pharmacology of theta oscillations.

Previously, application of CCh and KA to brain slices of M1 has been shown to elicit beta frequency oscillations (Yamawaki et al., 2008). These investigations used CCh and KA at concentrations of 50 µM and 400 nM respectively, which produced high power, narrow band oscillations around 28 Hz. Due to the uncertainty of DA concentrations in slice preparations, this was presumed to be analogous to the pathological beta frequency (12-30 Hz) oscillations observed in patients and *in vivo* animal models of PD (Magill et al., 2000; Kuhn et al., 2006; Chen et al., 2007; Mallet et al., 2008b).

However, the development of modified slice preparation protocols using neuroprotectants in a sucrose-based aCSF (see methods section 2.1.1) has allowed for lower doses of CCh (5 µM) and KA (100 nM) to be used in order to promote gamma range activity (~37 Hz). This is presumably due to the improved slice viability of network elements. The network activity observed in these slices was found to be broad band (complex) and include both theta and gamma peaks. This allowed for the simultaneous pharmacological investigation of both oscillations and also the determination of PAC which has previously only been observed *in vivo* during motor or waking behaviours (Bragin et al., 1995; Canolty et al., 2006; Sirota et al., 2008; Quilichini et al., 2010; Igarashi et al., 2013; von Nicolai et al., 2014).

## 3.2 Results

### 3.2.1 Induction of network oscillations in M1

Previous studies demonstrated that LV was the source of beta oscillations in M1 (Yamawaki et al., 2008). Application of 5-10 µM CCh and 100-150 nM KA resulted in the generation of two distinct, persistent rhythms at 6.61 ± 0.12 Hz and 36.55 ± 0.37 Hz (**Fig 3.1**, n=169 slices), which we have termed theta and gamma oscillations respectively. These oscillations appeared within 30 minutes following drug application with the oscillatory power peaking after approximately 1-2 hours.

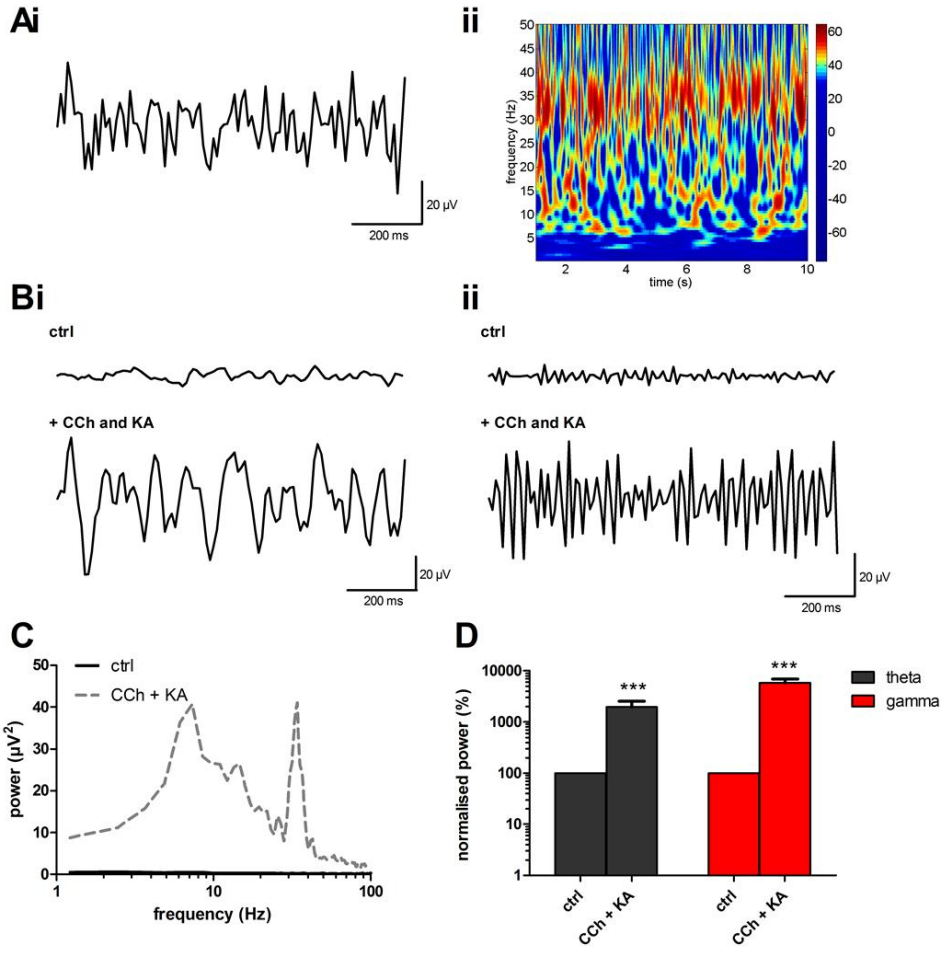


**Figure 3.1 Co-application of CCh and KA produces simultaneous theta and gamma oscillations in layer V of M1 (A)** Raw data after application of CCh and KA (i) low-pass filtered at 60 Hz and (ii) presented as a Morlet-wavelet time-frequency spectrogram. **(B)** Band-passed raw data of (i) theta (3-10 Hz) and (ii) gamma (30-45 Hz) oscillations before (ctrl) and after the application of CCh (5 µM) and KA (100 nM). **(C)** Typical power-spectra demonstrating emergence of theta and gamma peaks before drug application (ctrl - solid line) and after application of CCh and KA (dashed line). **(D)** Peak power changes of theta (grey bars) and gamma (red bars) oscillations normalised to control. ***, p<0.001.

CCh and KA were first applied alone and then in combination (**Fig 3.2**). Initial application of CCh (5-10 µM) resulted in a significant increase in the baseline power of both theta and gamma oscillations (theta: 586 ± 152% of control, n=11 slices, p<0.05. gamma: 448 ± 92% of control, n=11 slices, p<0.05, **Fig 3.2A**), however this did not result in the emergence of coherence peaks in the FFT. Subsequent addition of KA (100-150 nM) resulted in the appearance of robust, coherent and simultaneous theta, to 1970 ± 591% of control (n=11 slices, p<0.001, **Fig 3.2A**), and gamma, to 5784 ± 1124% of control (n=11 slices, p<0.001, **Fig 3.2A**) oscillations. The initial application of KA (100 nM) to baseline resulted in a significant increase in the power of theta oscillations to 162.2 ± 31.1% of control (n=12 slices, p<0.05, **Fig 3.2B**), without a significant increase in the power of gamma oscillations (to 134.9 ± 14.3% of control, n=12 slices, ns, **Fig 3.2B**), again however these were not coherent oscillatory peaks. Subsequent addition of CCh (5 µM), resulted in a substantial increase in both theta and gamma oscillations, to 2384 ± 825% of control (n=12 slices, p<0.001, **Fig 3.2B**) and to 3348 ± 897% of control (n=12 slices, p<0.001, **Fig 3.2B**) respectively. Hence, co-application of both KA and CCh was found to be required for the reliable induction of both theta and gamma oscillations. Such induction protocols were used for all further experiments.

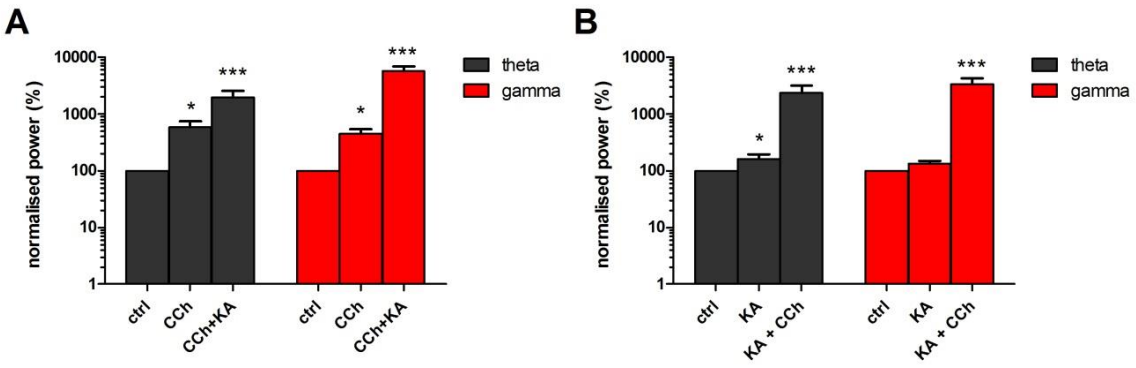


**Figure 3.2 Application of CCh or KA alone does not produce coherent theta and gamma oscillatory peaks.** Peak power changes of theta (grey bars) and gamma (red bars) oscillations normalised to control after initial application of **(A)** CCh followed by subsequent addition of KA and **(B)** KA followed by subsequent addition of CCh.

Three recording electrodes were placed into superficial (LII/III) and deep (LVa and LVb) layers of M1. The greatest oscillatory power of theta (61.49 ± 3.01% of total theta power, n=6 slices, p<0.001; **Fig 3.3Aii**) and gamma (51.52 ± 3.59% of total gamma power, n=6 slices, p<0.05; **Fig 3.3Bii**) oscillations was recorded in LVa. Furthermore, using the electrode in LVa as a reference, we observed that theta oscillations in LII/III and LVb were led by those in LVa (LII/III: 6 ms lag, 0.22 ± 0.07 cross-correlation coefficient; LVb: 5 ms lag, 0.12 ± 0.04 cross-correlation coefficient; n=6 slices; **Fig 3.3Aiii**), however this

distinction is only individually present in 4/6 slices. In contrast, in the case of gamma oscillations, the waveform in both LVa and LII/III lagged LVb by an average of 3 ms and 7 ms respectively and correlation was much stronger across layers (LII/III versus LVa - 0.38 ± 0.05; LVb versus LVa - 0.29 ± 0.07; n=6 slices; **Fig 3.3Biii**), and this distinction is individually present in all (6/6) slices recorded.

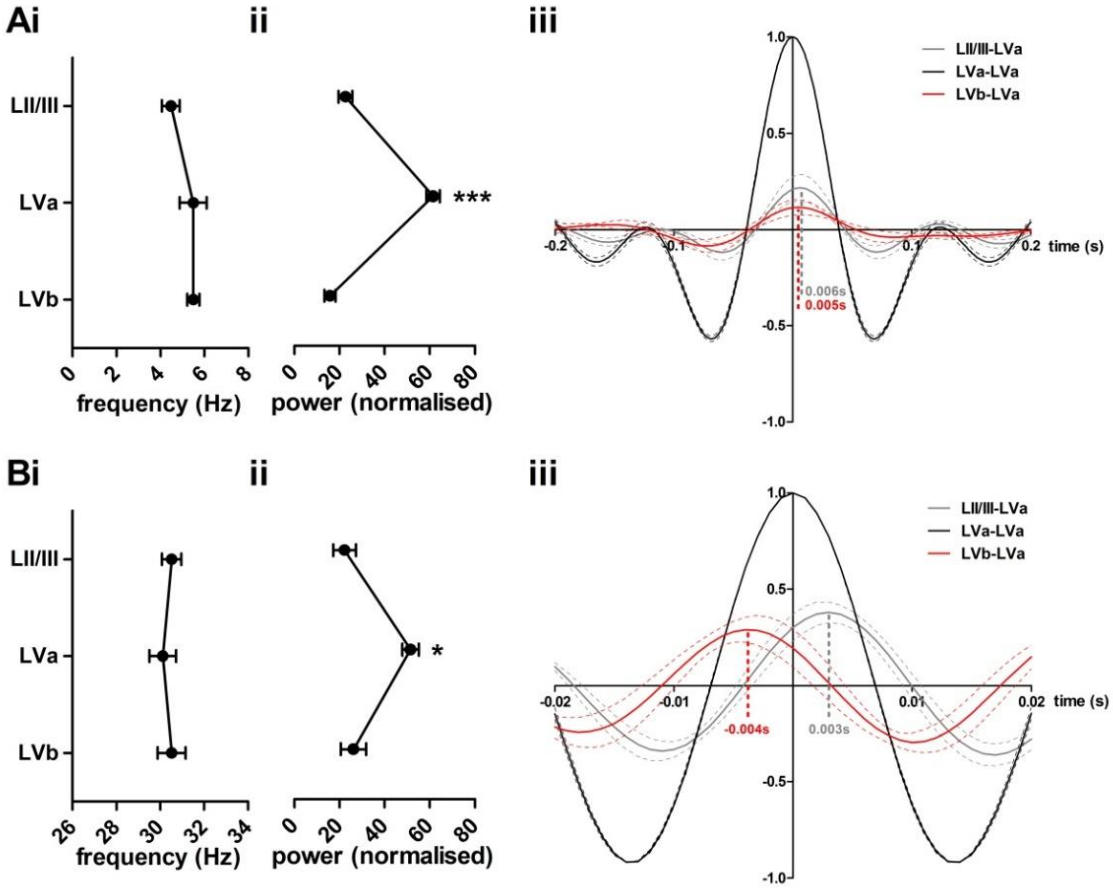


**Figure 3.3 Layer specific frequency and power changes in M1 with cross-correlations of oscillatory timing (A)** Theta and **(B)** gamma laminar specific oscillatory changes in M1 demonstrating (i) frequency changes, (ii) power changes and (iii) cross-correlations between LII/III, LVa and LVb. ***, p<0.001. *, p<0.05.

### 3.2.2 Phase-amplitude coupling (PAC) of M1 network activity

Using scripts generated and published by Tort et al. (2010), we analysed the emergent simultaneously recorded theta and gamma oscillations, in order to determine whether any PAC existed. PAC analysis was conducted on 40 s epochs of control data. We organised our results based on those which demonstrated a modulation index (MI) within the same order of magnitude. Thus, in the majority of cases we believe that theta (3-10 Hz) and gamma (30-45 Hz) oscillations in M1 were coupled ($2.9 \times 10^{-4} \pm 0.3 \times 10^{-4}$, n=6 slices, **Fig 3.4Ai, B, C**), although three recordings demonstrated less coupling in the chosen frequency bands by an order of magnitude ($5.0 \times 10^{-5} \pm 0.1 \times 10^{-4}$, n=3 slices, **Fig 3.4Aii, C**).

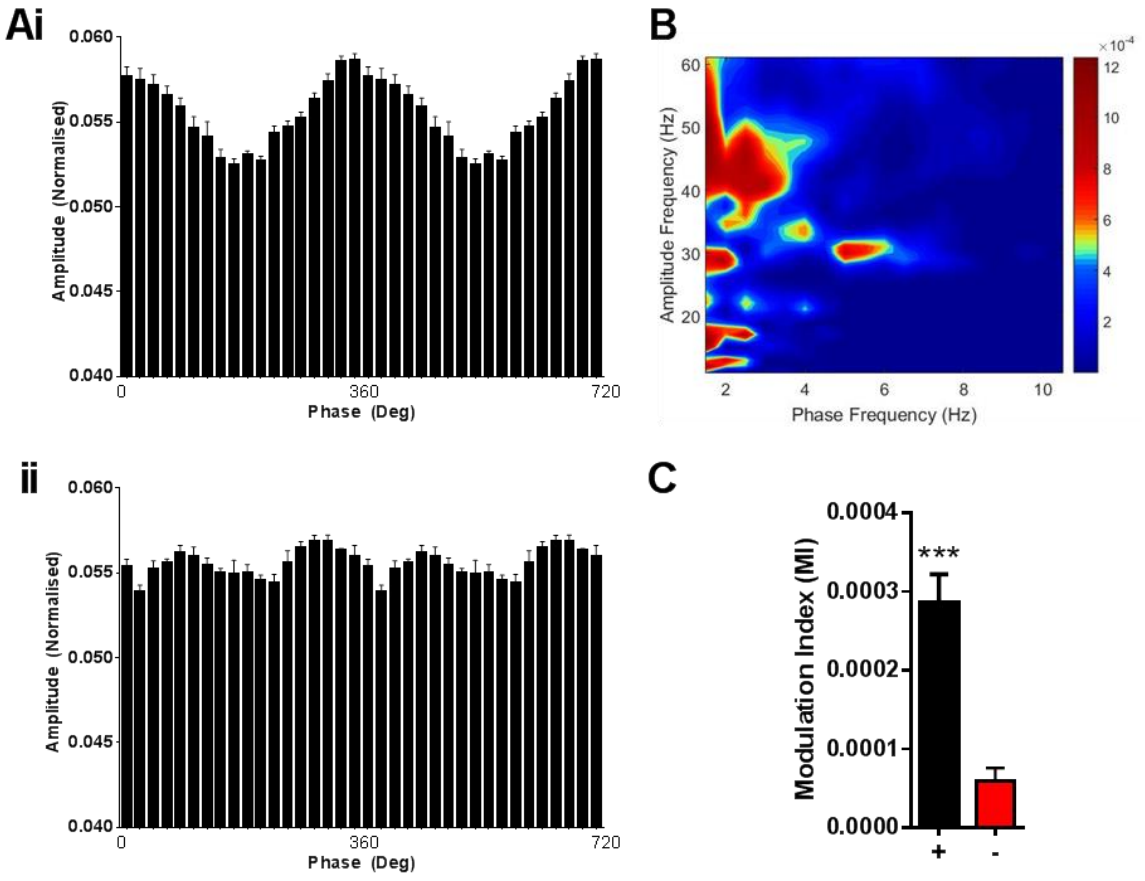


**Figure 3.4 Local phase-amplitude coupling is present between theta-gamma oscillations in the majority of cases (A)** (i) Phase-amplitude relationships in (i) modulated and (ii) unmodulated recordings. **(B)** Example co-modulogram showing areas of high modulation index (MI) and coupling in red. **(C)** Bar graph showing the average modulation index (MI) score for recordings showing phase-amplitude coupling (black bar) and those showing no coupling (red bar).

### 3.2.3 Pharmacological profile of oscillations

#### *3.2.3.1 GABAergic pharmacology*

We initially investigated the involvement of $GABA_A$ receptors using the competitive-antagonist gabazine (GBZ) at two concentrations (250 nM and 2 µM), in order to differentiate between both the synaptic (phasic) and extrasynaptic (tonic) GABAergic inhibition (Farrant and Nusser, 2005; Roopun et al., 2006).

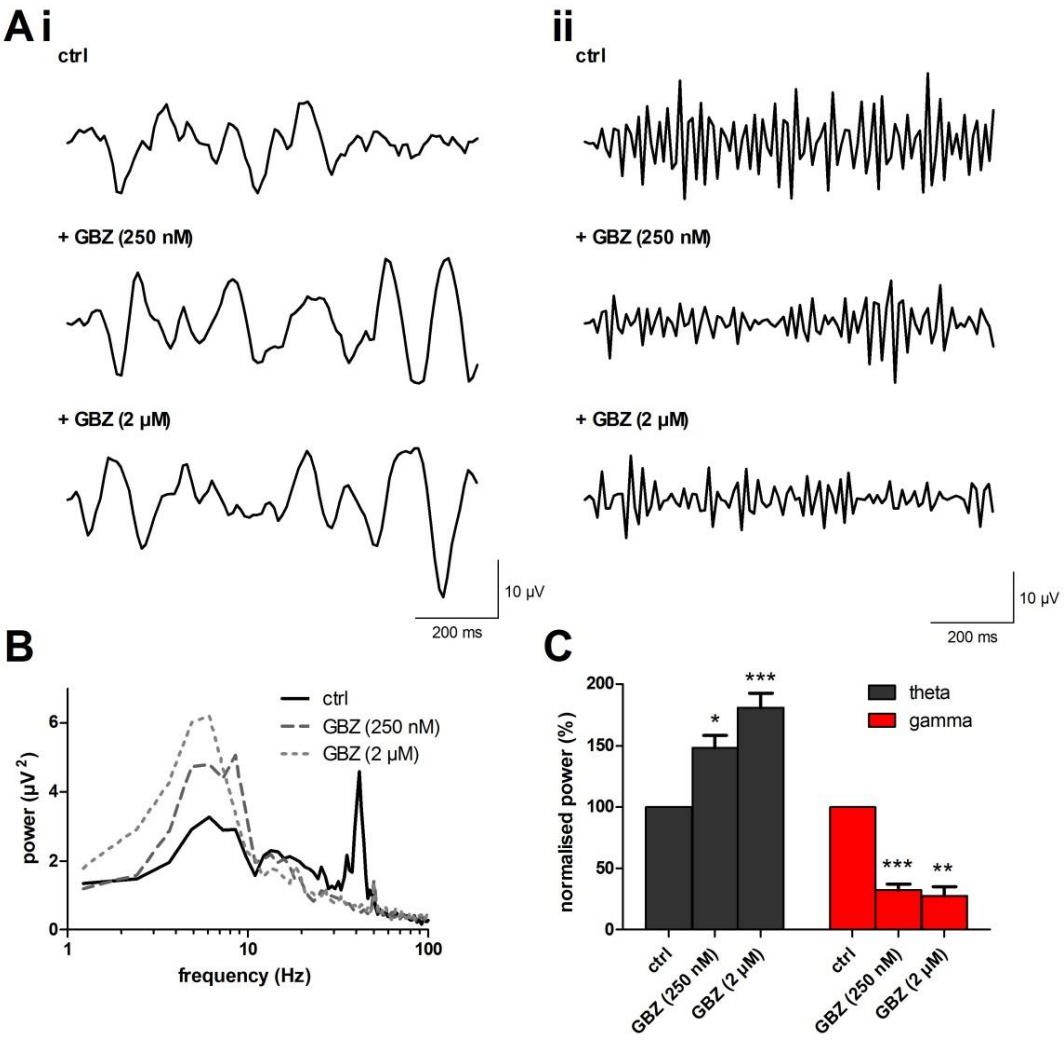


**Figure 3.5 Gabazine increases the power of theta and decreases the power of gamma oscillations in LV of M1. (A)** Band-passed raw data of (i) theta and (ii) gamma oscillations after induction with CCh and KA (ctrl) and after drug application. **(B)** Typical power spectra demonstrating peak responses before (solid line) and after 250 nM (dashed line) and 2 µM (dotted line) GBZ application. **(C)** Peak power changes of theta (grey bars) and gamma (red bars) oscillations normalised to control. ***, p<0.001, **, p<0.01, *, p<0.05.

Theta power was significantly increased by the application of 250 nM GBZ (to 147.9 ± 10.2% of control, n=7 slices, p<0.05, **Fig 3.5Ai, B, C**) and further increased by consecutive application of 2 µM GBZ (to 181.0 ± 11.6% of control, n=7 slices, p<0.001, **Fig 3.5Ai, B, C**). In contrast, gamma power was significantly reduced by both 250 nM GBZ (32.3 ± 4.9% of control, n=16 slices, p<0.001, **Fig 3.5Aii, B, C**) and by 2 µM GBZ (27.5 ± 7.5% of control, n=7 slices, p<0.01, **Fig 3.5Aii, B, C**). To support this result, we used picrotoxin (PIC), also a $GABA_A$ receptor antagonist, which binds within the channel itself. Application of 50 µM PIC mimicked the changes in power of the oscillations produced by GBZ, resulting in an increase in theta power (to 239.8 ± 61.5% of control, n=8 slices, p<0.01, **Fig 3.6Ai, B, C**) and decrease in gamma power (28.3 ± 7.4% of control, n=8 slices, p<0.01, **Fig 3.6Aii, B, C**).

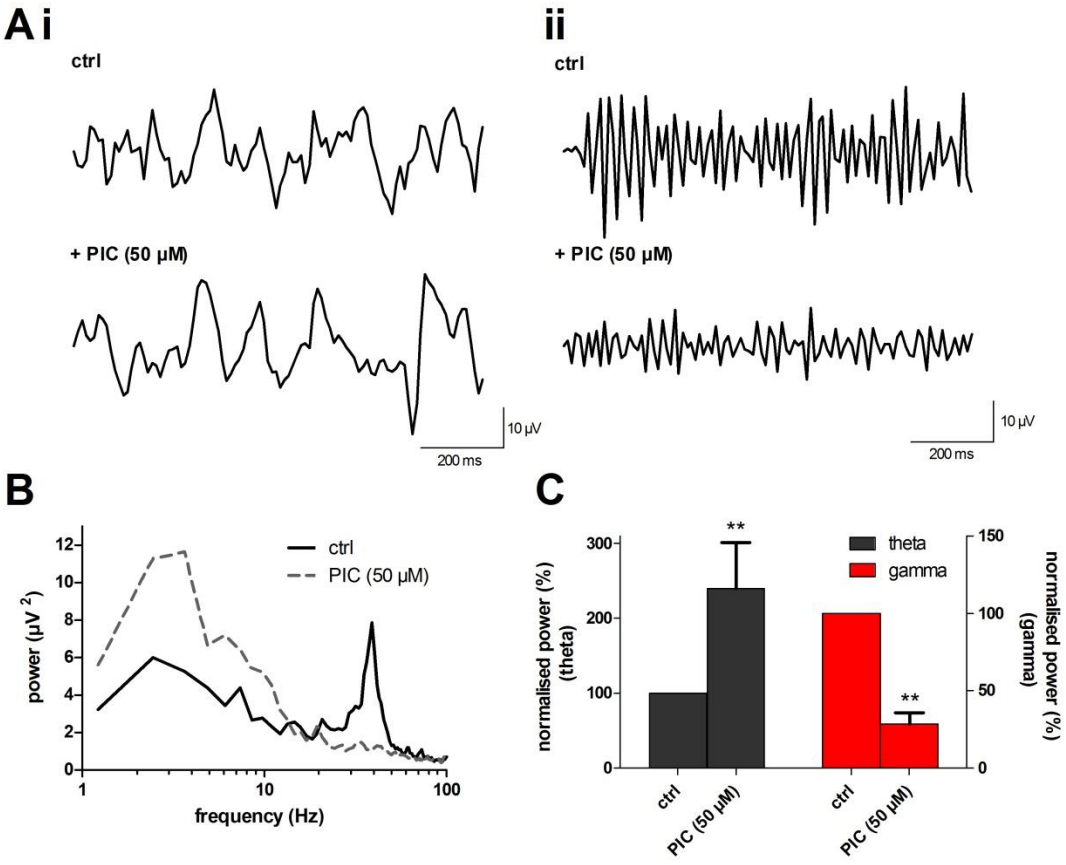


**Figure 3.6 Picrotoxin increases the power of theta and decreases the power of gamma oscillations in LV of M1. (A)** Band-passed raw data of (i) theta and (ii) gamma oscillations after induction with CCh and KA (ctrl) and after drug application. **(B)** Typical power spectra demonstrating peak responses before (solid line) and after 50 µM (dashed line) PIC application. **(C)** Peak power changes of theta (grey bars - left y-axis) and gamma (red bars - right y-axis) oscillations normalised to control. **, p<0.01.

To investigate the effects of $GABA_A$ receptor positive modulation on the oscillatory network we applied modulators of the benzodiazepine binding site. We used diazepam (DZP), a non-specific benzodiazepine, which acts at $\alpha_{1\text{-}3,5}$ subunit-containing $GABA_A$ receptors. The binding of DZP results in increased frequency of channel opening when GABA binds (Rogers et al., 1994; Eghbali et al., 1997; Barnard et al., 1998). Application of 30 nM DZP resulted in no significant changes in the power of either theta or gamma oscillations (theta: to 174.0 ± 43.9% of control, n=8 slices, ns; gamma: to 121.9 ± 12.9% of control, n=8 slices, ns; **Fig 3.7**). However application of 100 nM DZP resulted in a significant increase in the power of both theta (to 188.8 ± 26.1% of control, n=8 slices, p<0.05, **Fig 3.7Aii, B, C**) and gamma (to 142.2 ± 22.3% of control, n=8 slices, p<0.05, **Fig 3.7Aii, B, C**) oscillations.

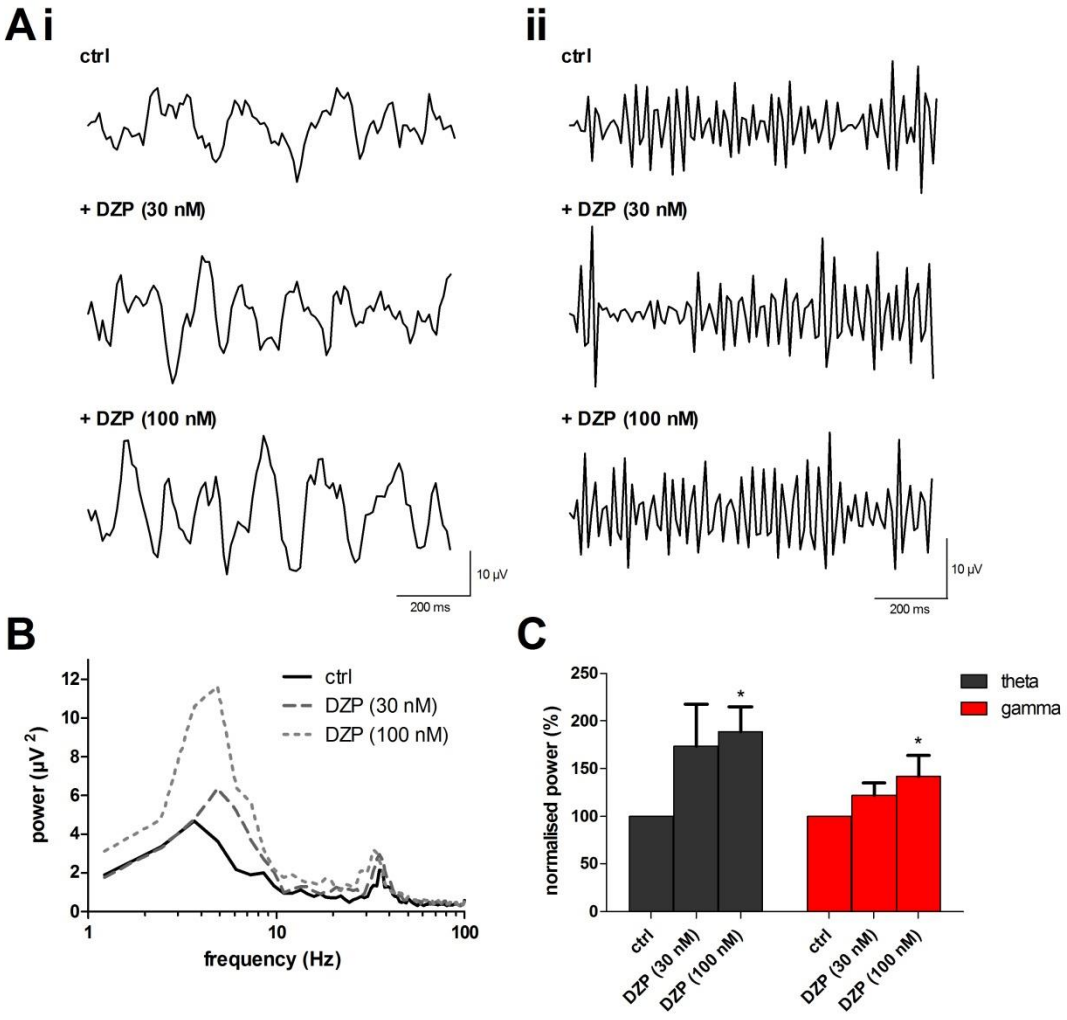


**Figure 3.7 Diazepam increases the power of theta and gamma oscillations in LV of M1 (A)** Band-passed raw data of (i) theta and ii) gamma oscillations after induction with CCh and KA (ctrl) and after drug application. **(B)** Typical power spectra demonstrating peak responses before (solid line) and after application of 30 nM (dashed line) and 100 nM (dotted line) DZP. **(C)** Peak power changes of theta (grey bars) and gamma (red bars) oscillations normalised to control. *, p<0.05.

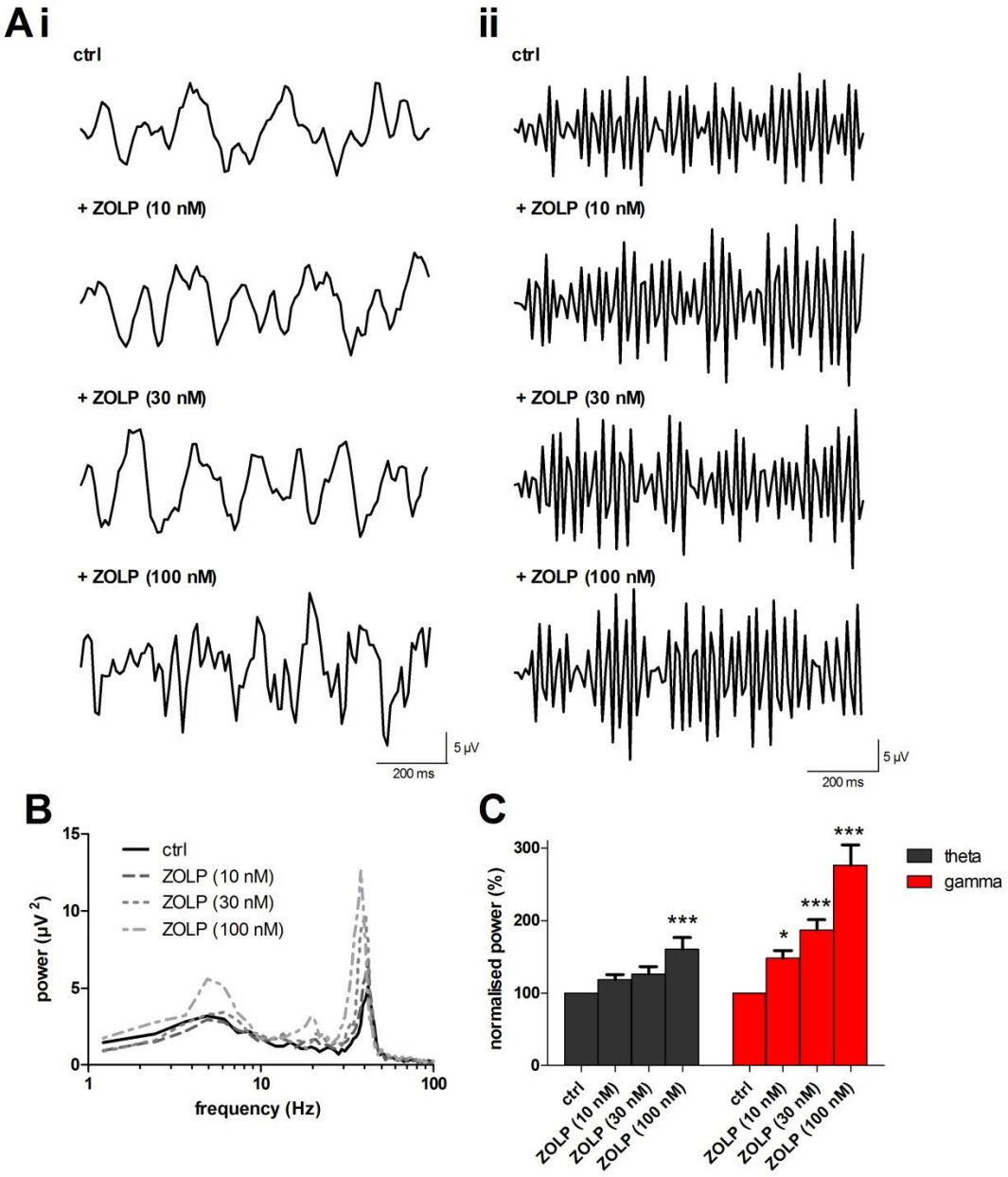


**Figure 3.8 Zolpidem increases the power of theta and gamma oscillations in LV of M1. (A)** Band-passed raw data of (i) theta and (ii) gamma oscillations after induction with CCh and KA (ctrl) and after drug application. **(B)** Typical power spectra demonstrating peak responses before (solid line) and after application of 10 nM (dashed line), 30 nM (dotted line) and 100 nM (hybrid line) ZOLP. **(C)** Peak power changes of theta (grey bars) and gamma (red bars) oscillations normalised to control. ***, $p<0.001$, *, $p<0.05$.

Zolpidem (ZOLP) is a $\alpha_1$-subunit specific positive modulator of $GABA_A$ receptors. Previous work has shown that a low-dose of ZOLP (10 nM) resulted in a desynchronisation of pathological beta oscillations in M1, observed in stroke (Hall et al., 2010) and PD (Hall et al., 2011; Hall et al., 2014) patients. In addition, ZOLP (10 nM) resulted in decreased beta oscillations *in vitro* (Prokic et al., 2015).

Here we investigated the effect of 10, 30 and 100 nM ZOLP on our oscillations. A significant effect of ZOLP on the power of theta oscillations was only seen in 100 nM (to 160.7 ± 16.0% of control, n=8 slices, p<0.001, **Fig 3.8Ai, B, C**), no change was observed at 10 or 30 nM. However gamma oscillations showed significant increases in power at all doses (10 nM: to 148.5 ± 10.1% of control, n=14 slices, p<0.05; 30 nM: to 187.1 ± 14.4% of control, n=14 slices, p<0.001; 100 nM: to 276.3 ± 28.0% of control, n=8 slices, p<0.001; **Fig 3.8Aii, B, C**). The application of flumazenil (FLU; 500 nM and 1 µM), an antagonist at the benzodiazepine binding site, resulted in no significant effect on theta oscillations. However, we did observe a significant increase in gamma oscillations at both concentrations (500 nM: to 176.4 ± 14.4% of control, n=15 slices, p<0.001; 1 µM: to 243.4 ± 40.0% of control, n=15 slices, p<0.001; **Fig 3.9Aii, B, C**).

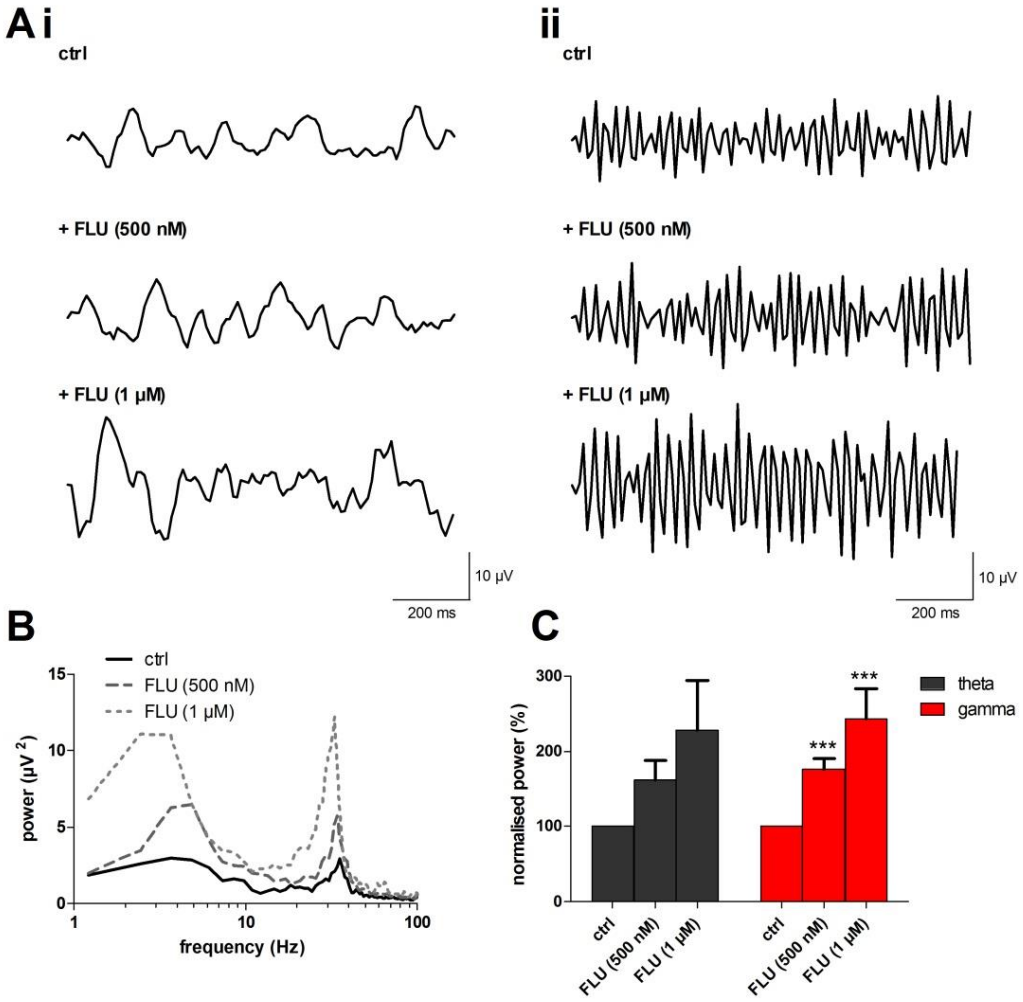


**Figure 3.9 Flumazenil increases the power of gamma oscillations in LV of M1. (A)** Band-passed raw data of (i) theta and (ii) gamma oscillations after induction with CCh and KA (ctrl) and after drug application. **(B)** Typical power spectra demonstrating peak responses before (solid line) and after application of 500 nM (dashed line) and 1 µM (dotted line) FLU. **(C)** Peak power changes of theta (grey bars) and gamma (red bars) oscillations normalised to control. ***, p<0.001.

We also investigated the effects of the $GABA_A$ receptor allosteric modulator pentobarbital (PENTO; 10 µM), which binds at the β-subunit increasing the duration of channel opening (Macdonald and Barker, 1979). Application of 10 µM PENTO had no significant effect on the power of theta oscillations. However, we observed a significant decrease in gamma oscillatory power (77.7 ± 7.2% of control, n=7 slices, p<0.05, **Fig 3.10Aii, B, C**). There was also a significant reduction in frequency of the gamma oscillations (to 88.0 ± 1.6% of control, n=7 slices, p<0.05, data not shown).

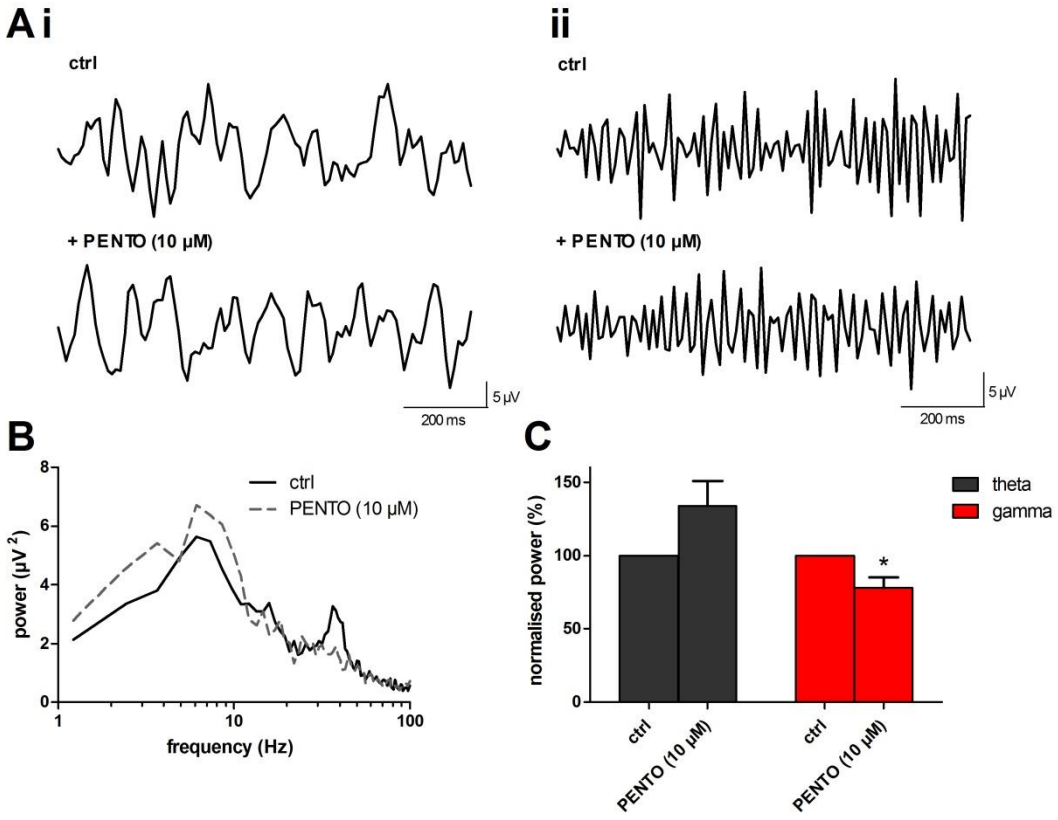


**Figure 3.10 Pentobarbital decreases gamma oscillatory power in LV of M1 (A)** Band-passed raw data of (i) theta and (ii) gamma oscillations after induction with CCh and KA (ctrl) and after drug application. **(B)** Typical power spectra demonstrating peak responses before (solid line) and after application of 10 µM (dashed line) PENTO. **(C)** Peak power changes of theta (grey bars) and gamma (red bars) oscillations normalised to control. *, p<0.05.

LSN3074113 (LSN307), a specific $GABA_A$ receptor $\alpha_3$-subunit agonist was applied in five consecutive doses ranging from 100 nM to 10 µM. Theta oscillatory power was significantly increased by 3 µM LSN307 (to 266.9 ± 30.6% of control, n=7 slices, p<0.05, **Fig 3.11Ai, B, C**) and 10 µM LSN307 (to 455.7 ± 96.0% of control, n=7 slices, p<0.001, **Fig 3.11D**). Though no specific dose effect on gamma oscillatory power was observed, there was a trend towards an increase at 1 µM before decreasing in power at subsequent doses.

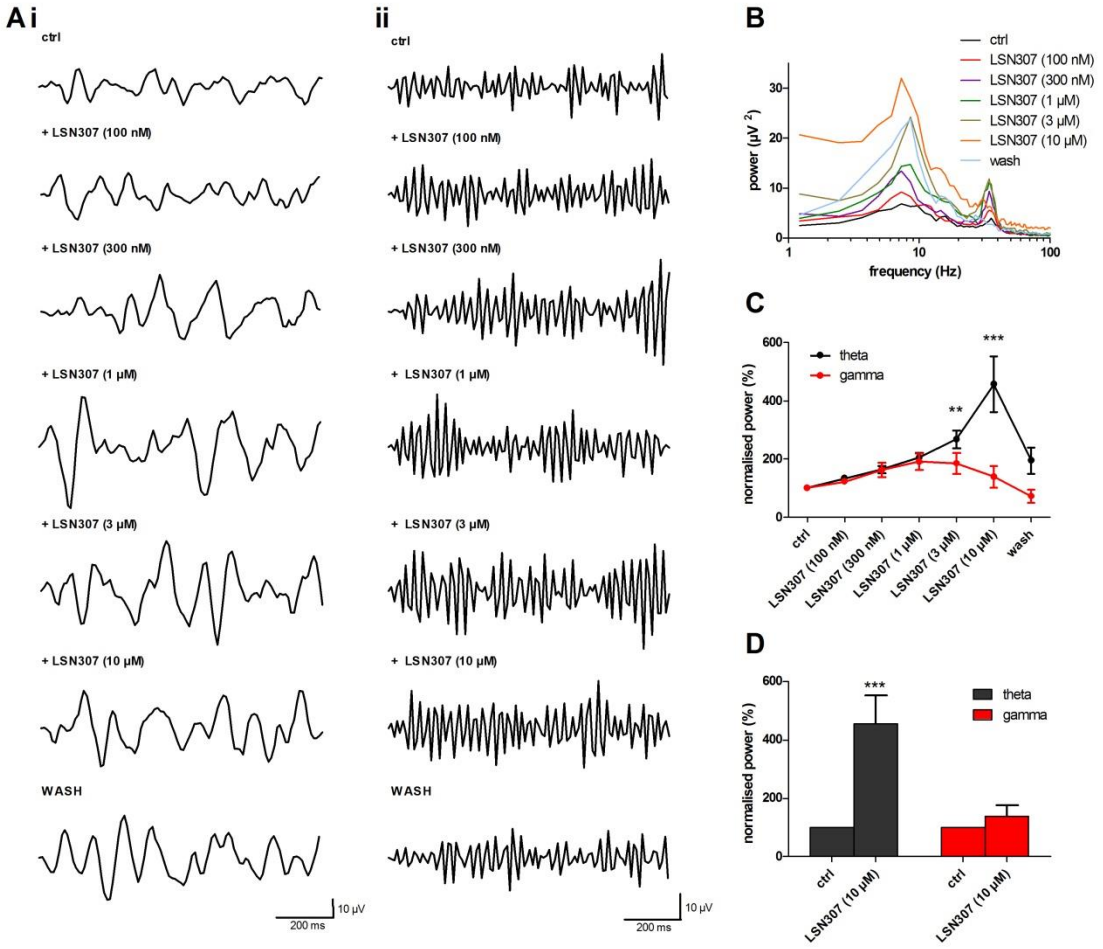


**Figure 3.11 LSN3074113 increases theta oscillatory power in LV of M1 (A)** Band-passed raw data of (i) theta and (ii) gamma oscillations after induction with CCh and KA (ctrl) and after drug application. **(B)** Typical power spectra demonstrating peak responses before (black line) and after application of 100 nM - 10 µM LSN307. **(C)** Normalised power change (%) of theta (black line) and gamma (red line) oscillations across all doses given. **(D)** Peak power changes at 10 µM of theta (grey bars) and gamma (red bars) oscillations normalised to control. ***, p<0.001, *, p<0.05.

To test the involvement of $GABA_B$ receptor inhibition, we used 5 µM CGP55845 (CGP), a competitive antagonist. Unlike the differing effects observed when blocking $GABA_A$ receptors, both theta and gamma oscillations showed significant increases in power after 5 µM CGP application. Theta oscillations increased in power to 131.8 ± 10.6% of control (n=17 slices, p<0.01, **Fig 3.12Ai, B, C**) and gamma oscillations increased in power to 149.4 ± 10.9% of control (n=17 slices, p<0.001, **Fig 3.12Aii, B, C**).

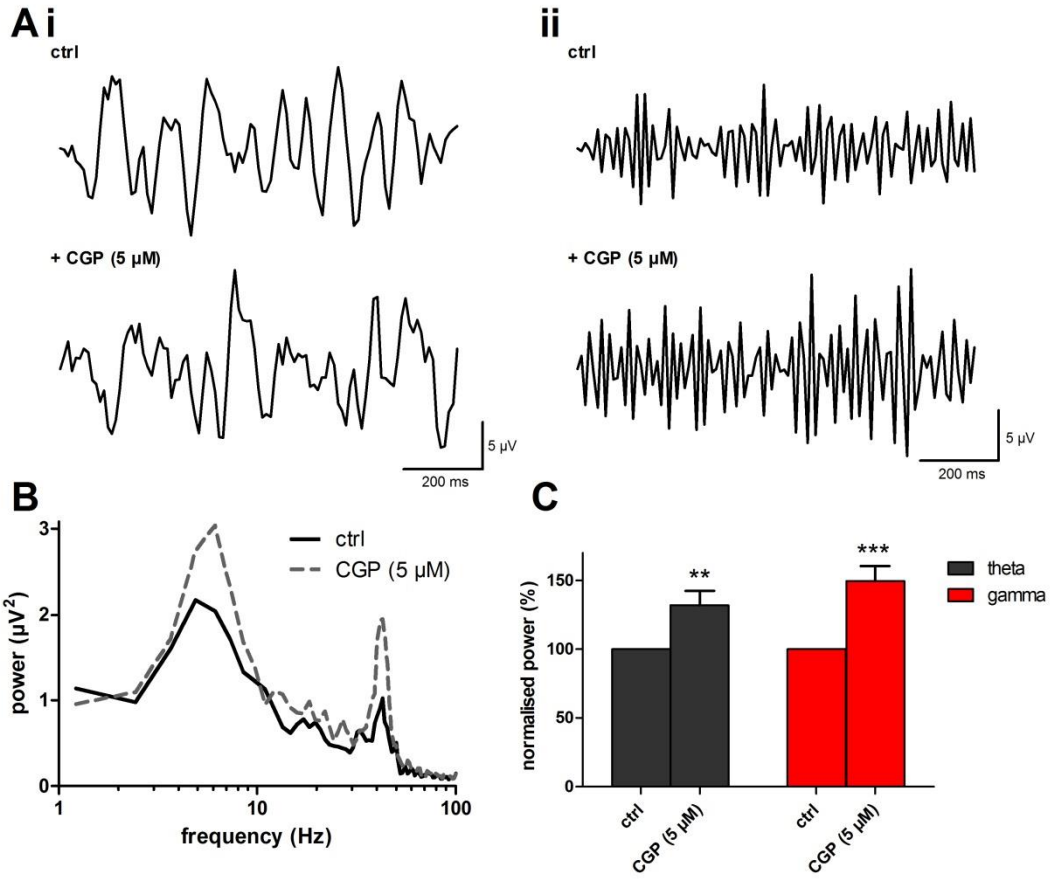


**Figure 3.12 CGP55845 increases the power of both theta and gamma oscillations in LV of M1. (A)** Band-passed raw data of (i) theta and (ii) gamma oscillations after induction with CCh and KA (ctrl) and after drug application. **(B)** Typical power spectra demonstrating peak responses before (solid line) and after 5 µM (dashed line) CGP application. **(C)** Peak power changes of theta (grey bars) and gamma (red bars) oscillations normalised to control. ***, p<0.001, **, p<0.01.

### *3.2.3.2 Ionotropic glutamate receptors (iGluRs)*

The importance of ionotropic excitatory transmission in oscillations has been firmly established in previous studies of oscillations in other brain areas (Buhl et al., 1998; Fisahn et al., 1998; Traub et al., 2000). Even though the involvement of KA receptors is important for inducing oscillations, the majority of the ionotropic excitatory communication between neurons is via AMPA and N-methyl-D-aspartate (NMDA) receptors.

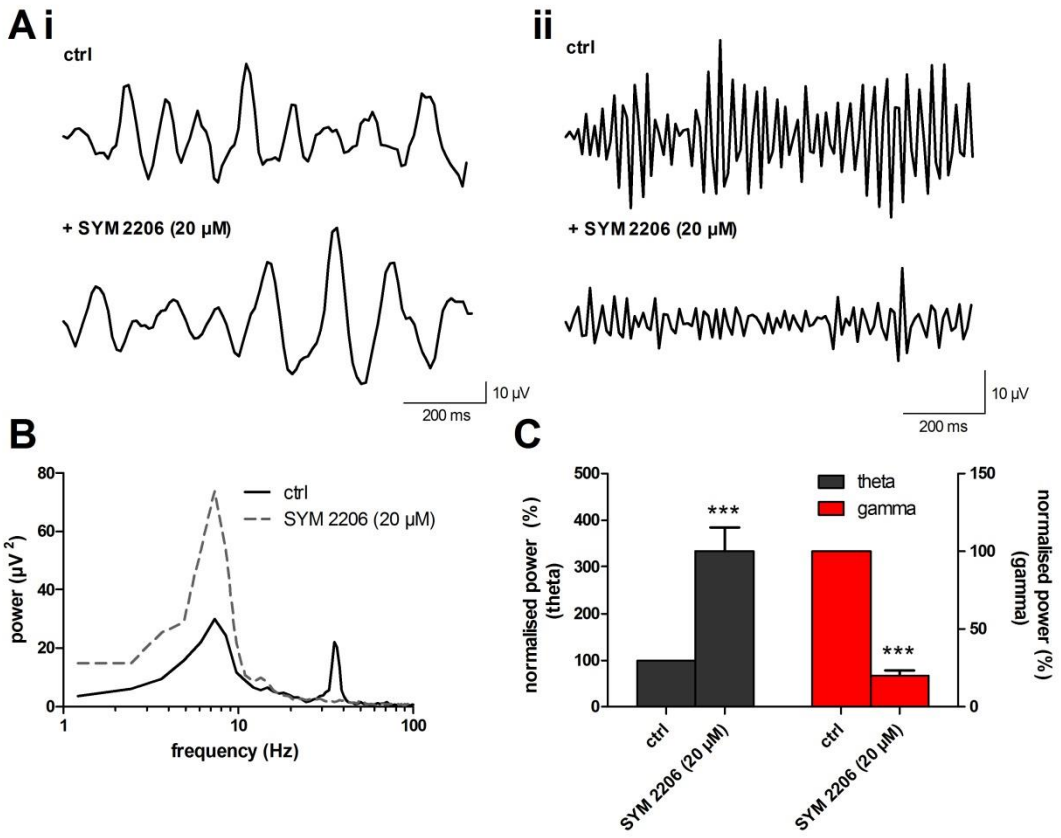


**Figure 3.13 SYM 2206 increases the power of theta and abolishes gamma oscillations in LV of M1. (A)** Band-passed raw data of (i) theta and (ii) gamma oscillations after induction with CCh and KA (ctrl) and after drug application. **(B)** Typical power spectra demonstrating peak responses before (solid line) and after 20 µM (dashed line) SYM 2206 application. **(C)** Peak power changes of theta (grey bars) and gamma (red bars) oscillations normalised to control. ***, p<0.001.

To explore the involvement of AMPA receptors in theta and gamma oscillations, the specific antagonist, SYM 2206 (SYM) was applied. 20 µM SYM resulted in a significant increase in the power of theta oscillations (to 333.8 ± 51.6% of control, n=20 slices, p<0.001, **Fig 3.13Aii, B, C**) and the significant block of gamma oscillations (20.2 ± 3.2% of control, n=20 slices, p<0.001, **Fig 3.13Aii, B, C**). We also used NBQX at an AMPA specific concentration (2.5 µM), which resulted in a significant increase in theta oscillations (to 131.6 ± 15.1% of control, n=9 slices, p<0.05, **Fig 3.14Ai, B, C**) and a significant reduction of gamma oscillations (24.9 ± 5.3% of control, n=9 slices, p<0.01, **Fig 3.14Aii, B, C**).

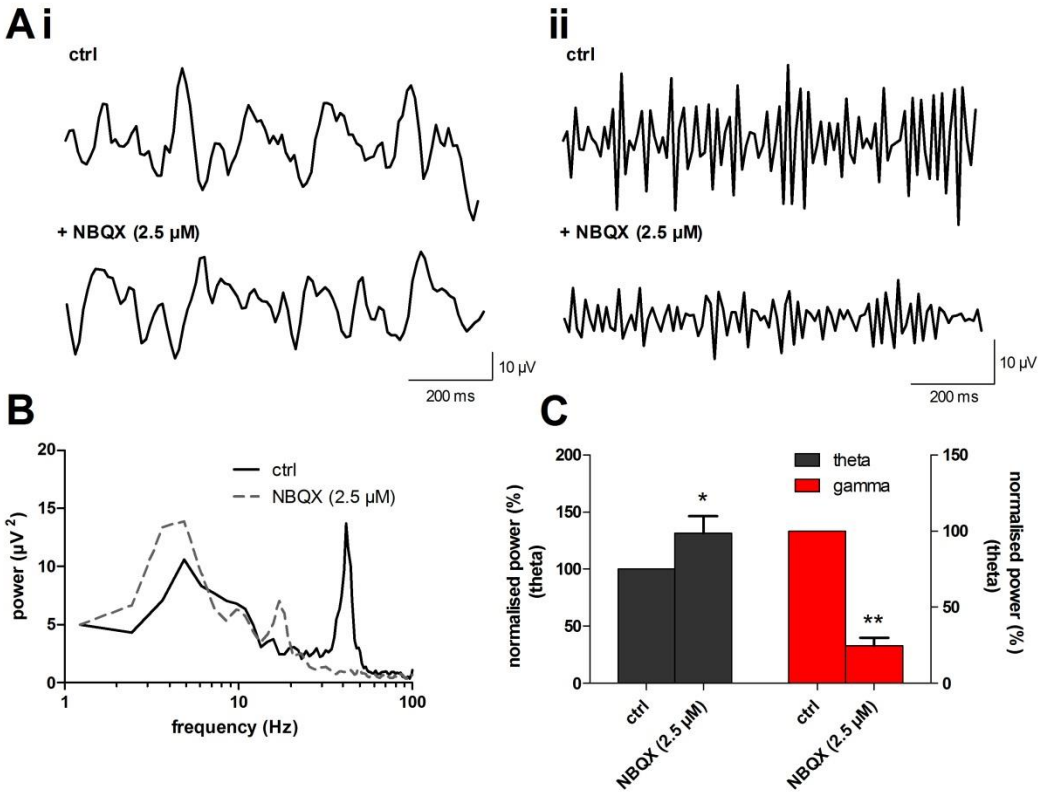


**Figure 3.14 NBQX increases the power of theta and abolishes gamma oscillations in LV of M1. (A)** Band-passed raw data of (i) theta and (ii) gamma oscillations after induction with CCh and KA (ctrl) and after drug application. **(B)** Typical power spectra demonstrating peak responses before (solid line) and after 2.5 µM (dashed line) NBQX application. **(C)** Peak power changes of theta (grey bars) and gamma (red bars) oscillations normalised to control. **, p<0.01, *, p<0.05.

We also investigated the role of NMDA receptors, which have slower receptor activation kinetics than AMPA receptors and allows the passage of $Ca^{2+}$ ions across the membrane. Our initial investigation used DL-AP5 (AP5), a competitive antagonist of NMDA receptors. Application of 50 µM AP5 had no effect on theta oscillations but resulted in a significant increase in gamma oscillatory power (to 166.3 ± 13.6% of control, n=15 slices, p<0.001, **Fig 3.15Aii, B, C**). We also used another competitive and selective NMDA receptor antagonist in order to confirm this result, (R)-CPP (CPP; 5 µM). This produced the same result with no significant change in theta oscillation power and a significant increase in the power of gamma oscillations (to 179.5 ± 15.2% of control, n=11 slices, p<0.01, **Fig 3.16Aii, B, C**).

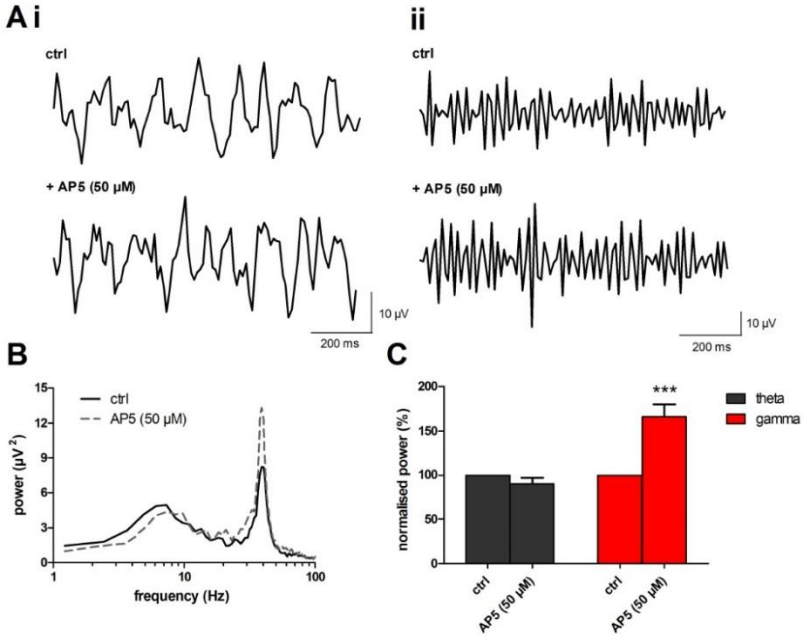


**Figure 3.15 AP5 increases the power of gamma oscillations in LV of M1. (A)** Band-passed raw data of (i) theta and (ii) gamma oscillations after induction with CCh and KA (ctrl) and after drug application. **(B)** Typical power spectra demonstrating peak responses before (solid line) and after 50 µM (dashed line) AP5 application. **(C)** Peak power changes of theta (grey bars) and gamma (red bars) oscillations normalised to control. ***, p<0.001.

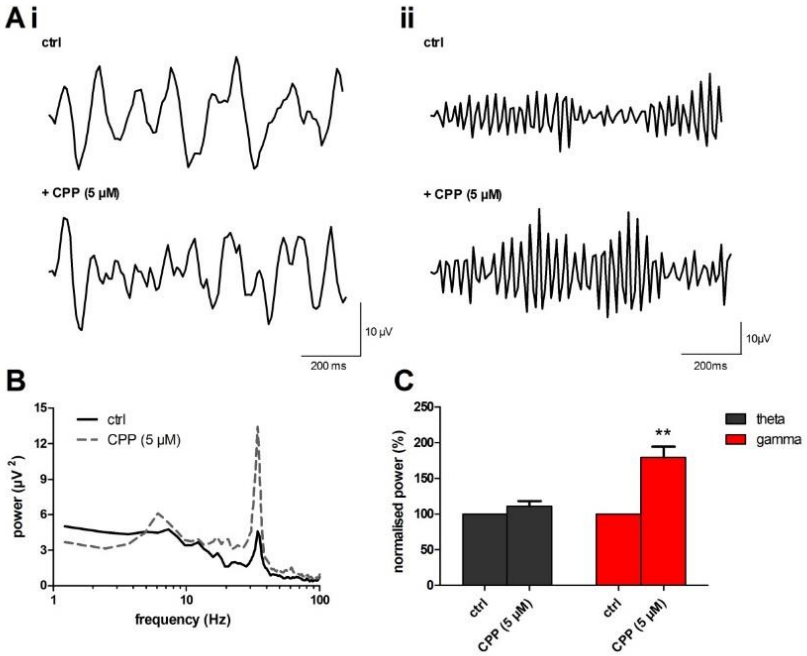


**Figure 3.16 CPP increases the power of gamma oscillations in LV of M1. (A)** Band-passed raw data of (i) theta and (ii) gamma oscillations after induction with CCh and KA (ctrl) and after drug application. **(B)** Typical power spectra demonstrating peak responses before (solid line) and after 5 µM (dashed line) CPP application. **(C)** Peak power changes of theta (grey bars) and gamma (red bars) oscillations normalised to control. **, p<0.01.

As a high glutamate concentration resulting from the increased activity of the excitatory neuronal network could out-compete a competitive antagonist, we tested the effect of NMDA receptor channel blockers, MK-801 and ketamine. These experiments were run over the course of 40 mins, allowing the drug effect time and for the effect to stabilise, the same as is seen and used in other experiments. This is important to note, since channel blockers require the activation and opening of the channel in order to access their binding site. The addition of 20 µM MK-801 resulted in increases in the power of both theta (to 201.3 ± 22.5% of control, n=12 slices, p<0.001, **Fig 3.17Ai, B, C**) and gamma (to 254.7 ± 36.5% of control, n=12 slices, p<0.001, **Fig 3.17Aii, B, C**) oscillations. Application of 20 µM KET resulted in similar significant power increases seen in MK-801 in both theta (to 146.6 ± 9.2% of control, n=7 slices, p<0.05, **Fig 3.18Ai, B, C**) and gamma (to 201.2 ± 23.6% of control, n=7 slices, p<0.05, **Fig 3.18Aii, B, C**) oscillations.

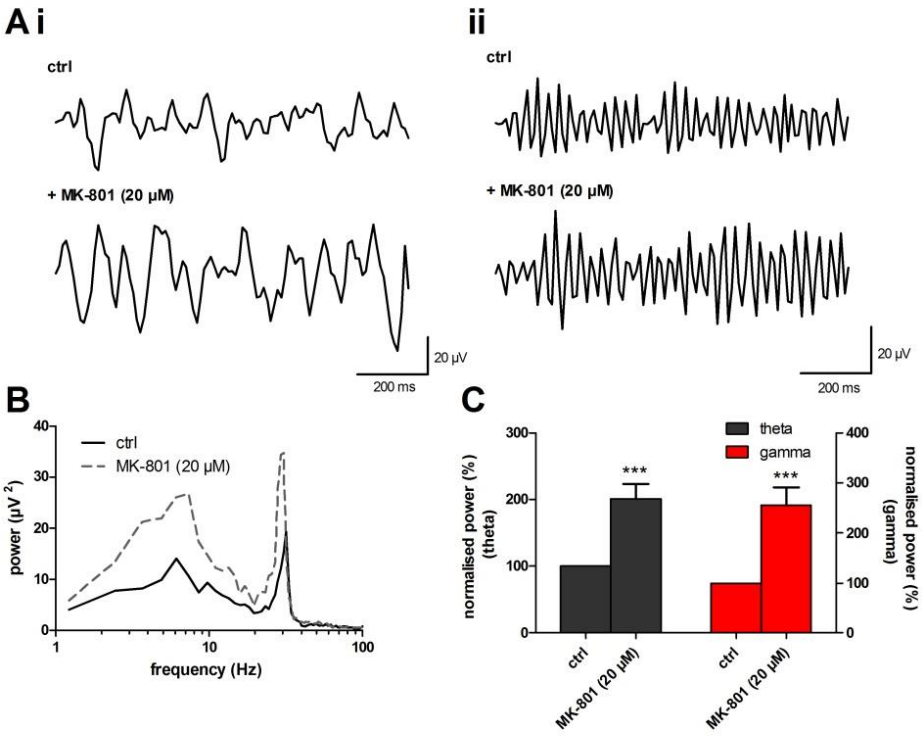


**Figure 3.17 MK-801 increases the power of both theta and gamma oscillations in LV of M1.** **(A)** Band-passed raw data of (i) theta and (ii) gamma oscillations after induction with CCh and KA (ctrl) and after drug application. **(B)** Typical power spectra demonstrating peak responses before (solid line) and after 20 µM (dashed line) MK-801 application. **(C)** Peak power changes of theta (grey bars) and gamma (red bars) oscillations normalised to control. ***, p<0.001.

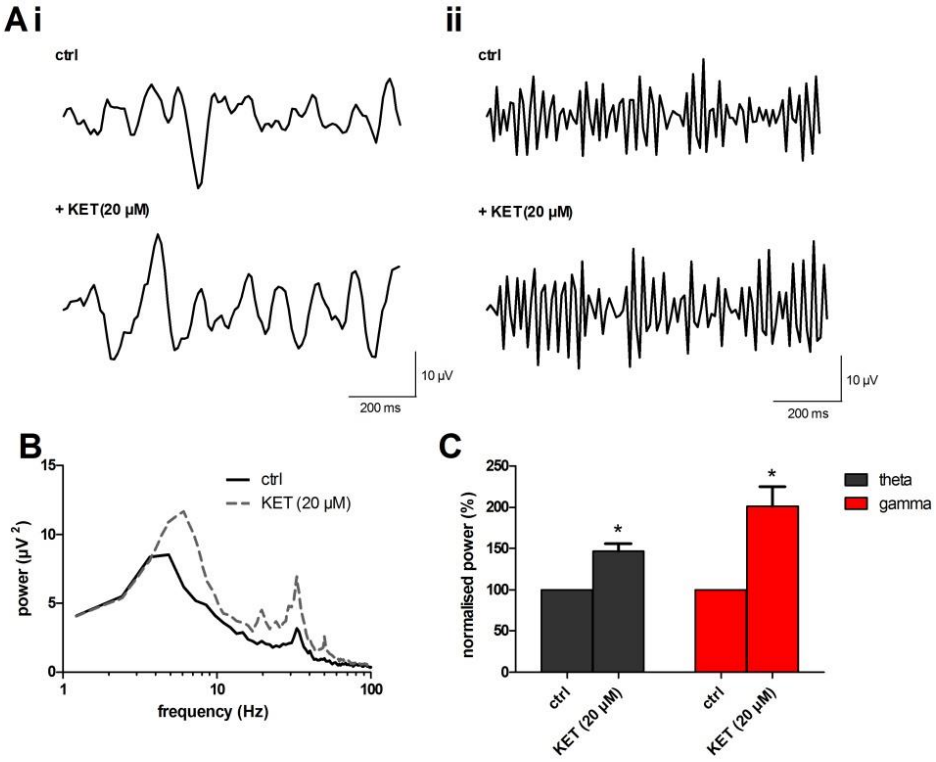


**Figure 3.18 Ketamine increases the power of both theta and gamma oscillations in LV of M1.** **(A)** Band-passed raw data of (i) theta and (ii) gamma oscillations after induction with CCh and KA (ctrl) and after drug application. **(B)** Typical power spectra demonstrating peak responses before (solid line) and after 20 µM (dashed line) KET application. **(C)** Peak power changes of theta (grey bars) and gamma (red bars) oscillations normalised to control. *, p<0.05.

### *3.2.3.3 Metabotropic glutamate receptors (mGluRs)*

The three groups of mGluRs, groups I, II and III, each have distinct localisation and receptor effects. As such, activation of each type of receptor group could have very different effects on the neuronal networks generated in the brain. We initially investigated the role of $mGluR_1$ using CPCCOEt (20 µM), a non-competitive antagonist. Application of CPCCOEt resulted in an increase in power of both theta and gamma oscillations (theta: to 184.3 ± 22.5% of control, n=7 slices, p<0.05; gamma: to 216.1 ± 22.4% of control, n=7 slices, p<0.05; **Fig 3.19A**). Application of 20 µM MPEP or 100 nM MTEP, both non-competitive antagonists of $mGluR_5$ also resulted in the significant increase in the power of both theta (MPEP: to 138.4 ± 8.9% of control, n=10 slices, p<0.01, **Fig 3.19B**; MTEP: to 168.4 ± 18.5% of control, n=8 slices, p<0.01, **Fig 3.19C**) and gamma (MPEP: to 154.0 ± 7.5% of control, n=10 slices, p<0.01, **Fig 3.19B**; MTEP: to 163.7 ± 10.8% of control, n=8 slices, p<0.01, **Fig 3.19C**) oscillations. To test the non-specific effect of mGluR group I activation, we applied the agonist DHPG (10 µM), which produced a significant decrease of theta oscillatory power to 79.9 ± 4.0% of control (n=10 slices, p<0.01, **Fig 3.19D**), with no effect on gamma oscillatory power.

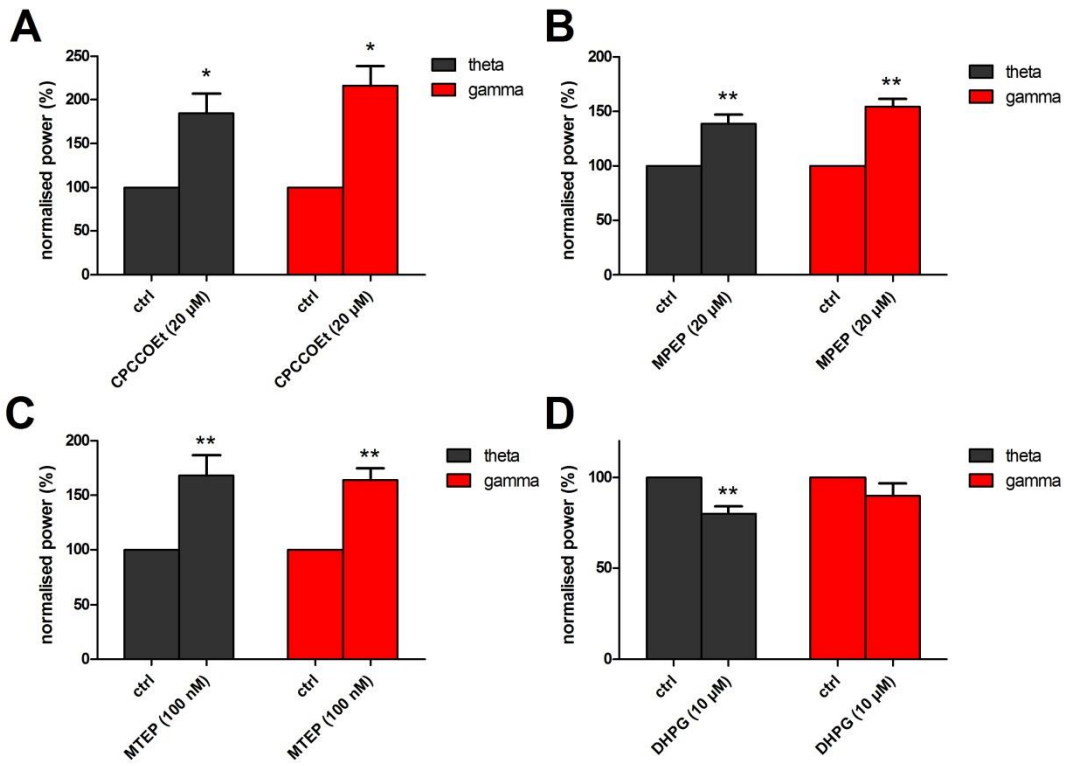


**Figure 3.19 Effect of group I mGluR agonists and antagonists on theta and gamma oscillations in LV of M1.** Peak power changes of theta (grey bars) and gamma (red bars) oscillations normalised to control. **(A)** Application of 20 µM $mGluR_1$ antagonist CPCCOEt significantly increased both theta and gamma oscillations. **(B)** Application of 20 µM $mGluR_5$ antagonist MPEP significantly increased theta and gamma oscillations. **(C)** Application of 100 nM $mGluR_5$ antagonist MTEP significantly increased theta and gamma oscillations. **(D)** Application of 10 µM $mGluR_{1/5}$ agonist DHPG significantly reduced theta oscillations without an effect on gamma oscillations. **, $p<0.01$, *, $p<0.05$.

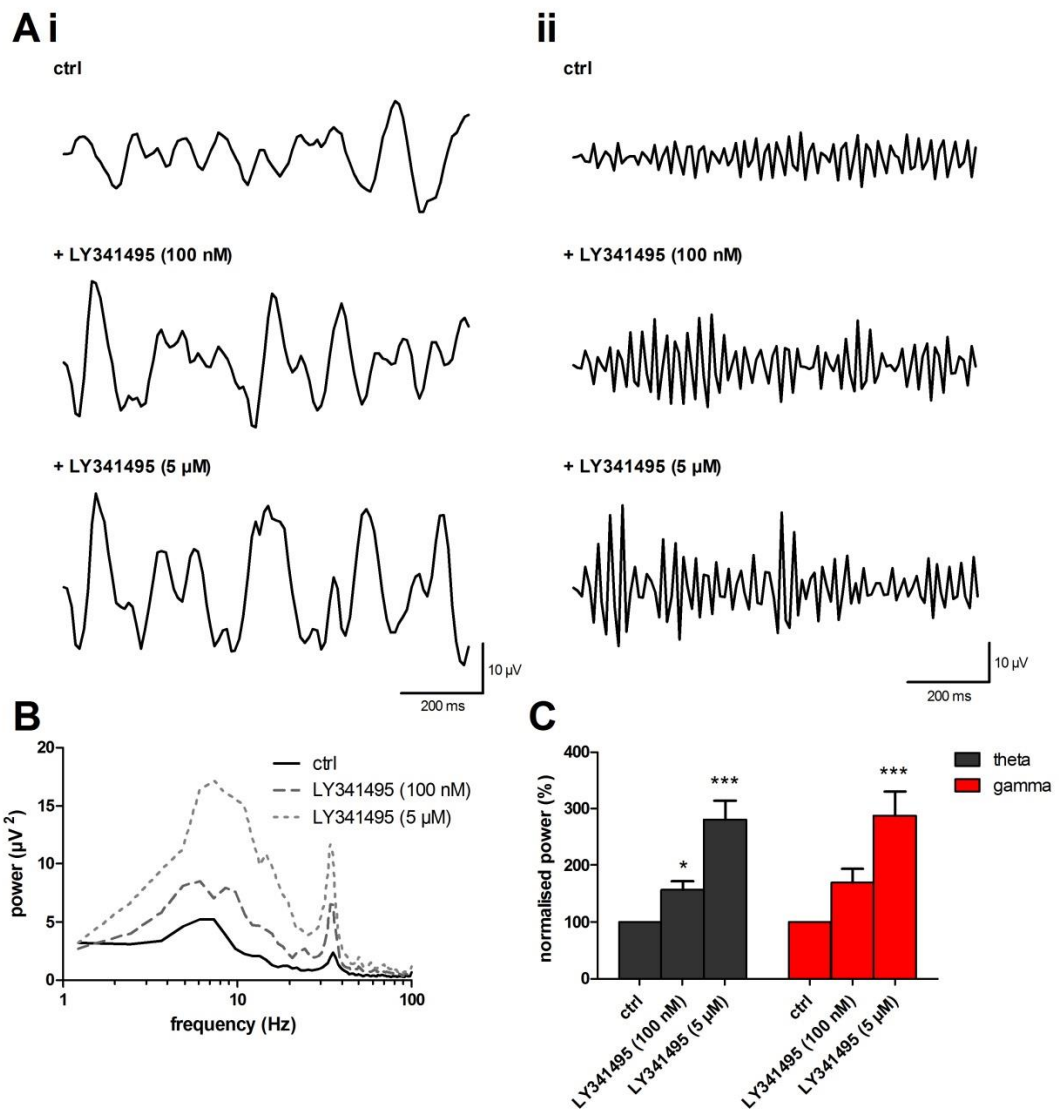


**Figure 3.20 LY341495 increases the power of theta and gamma oscillations in LV of M1. (A)** Band-passed raw data of (i) theta and (ii) gamma oscillations after induction with CCh and KA (ctrl) and after drug application. **(B)** Typical power spectra demonstrating peak responses before (solid line) and after application of 100 nM (dashed line) and 5 µM (dotted line) LY341495. **(C)** Peak power changes of theta (grey bars) and gamma (red bars) oscillations normalised to control. ***, p<0.001, **, p<0.01.

Following this we applied LY341495, an antagonist of group II and III receptors at nanomolar and micromolar concentrations respectively (Wright et al., 2000; Lavreysen and Dautzenberg, 2008). At 100 nM (specific for group II receptors) an increase in the power of theta oscillations was observed (to 156.9 ± 15.3% of control, n=9 slices, p<0.05, **Fig 3.20Ai, B, C**), with no significant change to gamma oscillations. Increasing the dose to 5 µM (to include group III receptors) resulted in further significant increases in power to both theta and gamma oscillations (theta: to 280.3 ± 34.1% of control, n=9 slices,

p<0.001; gamma: to 287.3 ± 43.3% of control, n=9 slices, p<0.001; **Fig 3.20**). To complete our investigation of the role that mGluRs play in the neuronal network oscillations of M1, we applied LY379268 (an agonist of group II receptors) and L-AP4 (AP4, an agonist at group III receptors). Application of 1 µM LY379268 resulted in a significant decrease in power of both theta and gamma oscillations (theta: 72.2 ± 5.3% of control, n=8 slices, p<0.01; gamma: 67.6 ± 5.5% of control, n=8 slices, p<0.01; **Fig 3.21A**). Application of 50 µM AP4 resulted in an increase in both theta (to 164.8 ± 15.4% of control, n=8 slices, p<0.01, **Fig 3.21B**) and gamma (to 139.2 ± 11.4% of control, n=8 slices, p<0.01, **Fig 3.21B**) oscillatory power.

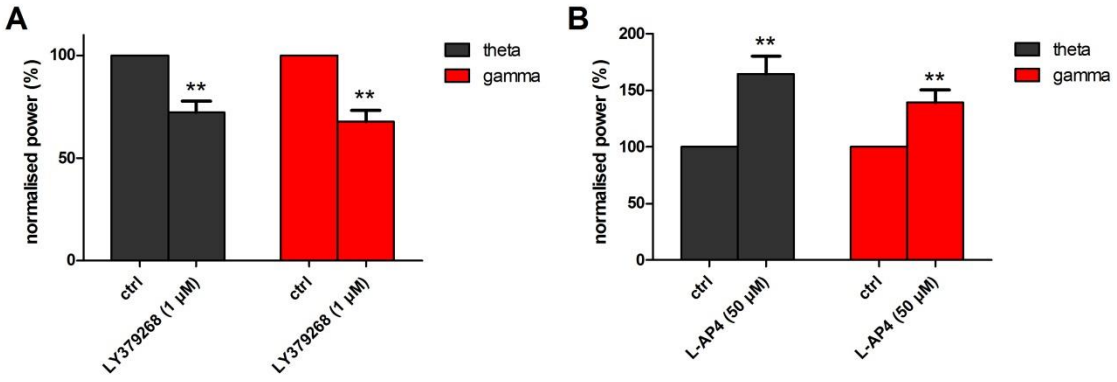


**Figure 3.21 Effect of group II and III mGluR agonists on theta and gamma oscillations in LV of M1.** Peak power changes of theta (grey bars) and gamma (red bars) oscillations normalised to control. **(A)** Application of 1 µM mGluR group II agonist LY379268 significantly decreased both theta and gamma oscillations. **(B)** Application of 50 µM mGluR group III agonist L-AP4 significantly increased theta and gamma oscillations. **, p<0.01.

*3.2.3.4 Cholinergic pharmacology*

Since these oscillations rely on CCh for their generation it would stand to reason that they are dependent on cholinergic networks. Application of the non-specific cholinergic antagonist atropine (5 µM), resulted in near complete abolition of both the theta and gamma oscillatory power (theta: 24.9 ± 9.0% of control, n=7 slices, p<0.05; gamma: 9.1 ± 3.3% of control, n=7 slices, p<0.05; **Fig 3.22**).

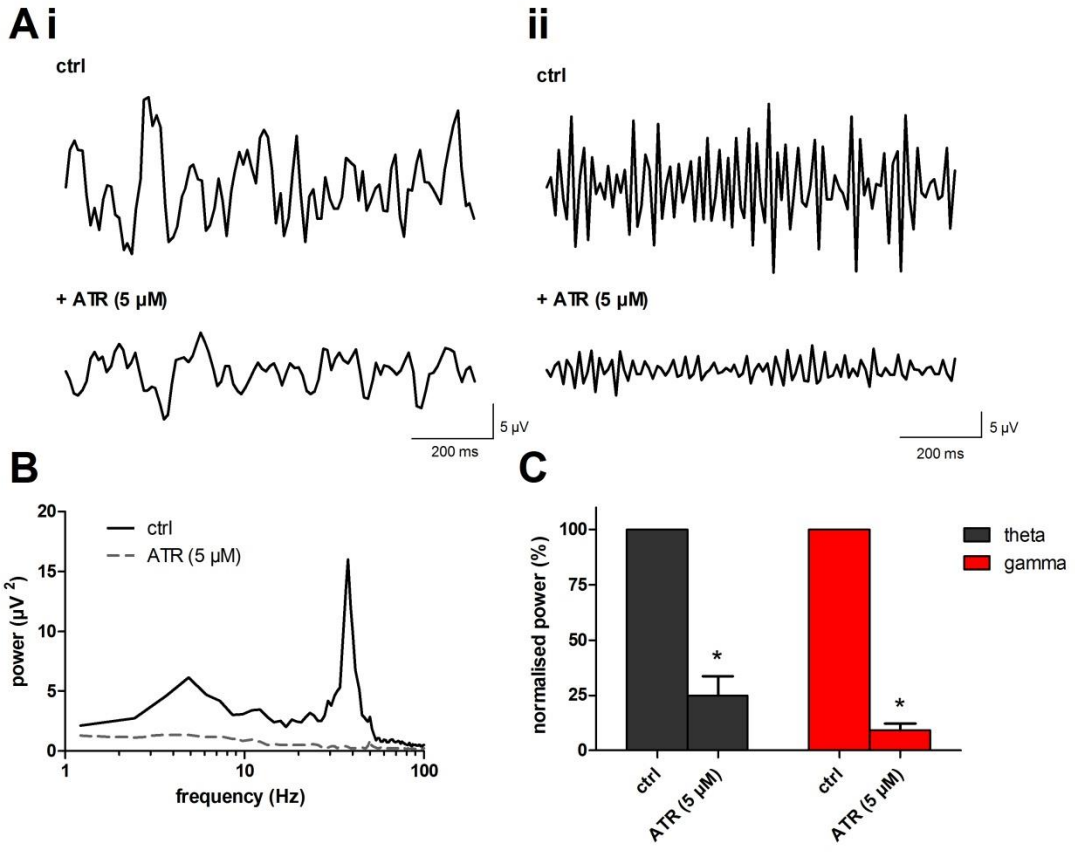


**Figure 3.22 Atropine abolishes both theta and gamma oscillations in LV of M1. (A)** Band-passed raw data of (i) theta and (ii) gamma oscillations after induction with CCh and KA (ctrl) and after drug application. **(B)** Typical power spectra demonstrating peak responses before (solid line) and after application of 5 µM (dashed line) ATR. **(C)** Peak power changes of theta (grey bars) and gamma (red bars) oscillations normalised to control.*, p<0.05.

*3.2.3.5 Gap junction pharmacology*

In order to assess the importance of gap junctions in the generation of M1 neuronal network oscillations, carbenoxolone (CBX) was added at 200 µM. Due to the known slow response of gap junction block (Konopacki et al., 2004), oscillations were recorded for a period in excess of 1.5 hrs following CBX application and a significant reduction in theta (40.6 ± 5.1% of control, n=13 slices, p<0.001, **Fig 3.23Ai, B, C**) and gamma (28.7 ± 5.7% of control, n=13 slices, p<0.001, **Fig 3.23Aii, B, C**) oscillatory power was observed.

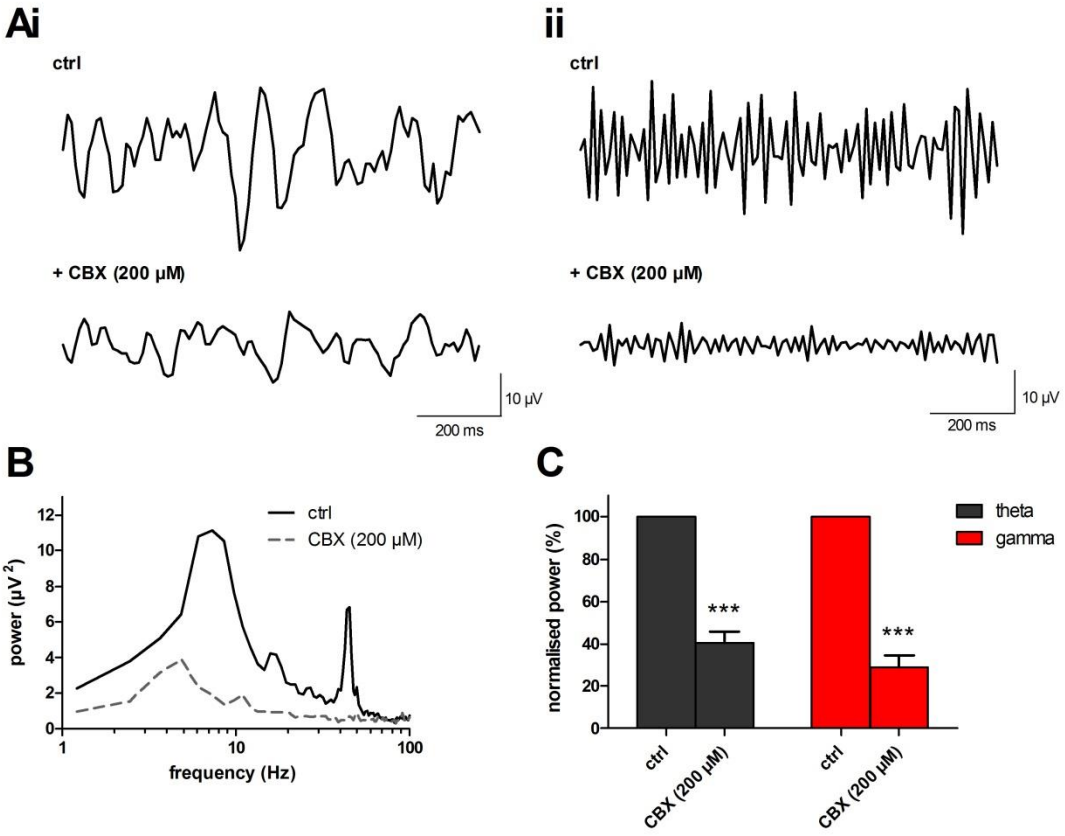


**Figure 3.23 Carbenoxolone decreases both theta and gamma oscillations in LV of M1. (A)** Band-passed raw data of (i) theta and (ii) gamma oscillations after induction with CCh and KA (ctrl) and after drug application. **(B)** Typical power spectra demonstrating peak responses before (solid line) and after application of 200 µM CBX (dashed line). **(C)** Peak power changes of theta (grey bars) and gamma (red bars) oscillations normalised to control. ***, p<0.001.

## 3.3 Discussion

In this chapter we have shown that simultaneous theta (4-8 Hz) and gamma (30-45 Hz) oscillations can be elicited in LV of M1. We found that application of both KA and CCh was required to induce these oscillations, which exhibit phase-amplitude coupling (PAC). Pharmacologically, both oscillations were sensitive to the block of cholinergic receptors and gap junctions. However, only gamma oscillations were reduced by block of synaptic $GABA_A$ and AMPA receptors, while theta oscillatory power was augmented. Both oscillations were amplified by increased $GABA_A$ receptor modulation, with the exception of pentobarbital, which reduced gamma oscillatory power, and LSN3074113, which solely increased theta oscillatory power. Theta oscillations were also largely unresponsive to NMDA receptor block, unlike gamma oscillations which were consistently increased in power. Agonists of group I and II mGluRs depressed theta and gamma oscillations, whilst block of mGluRs resulted in increases to oscillatory power. Overall, we demonstrate the presence of coexistent but pharmacologically distinct theta and gamma oscillations in LV of M1.

### 3.3.1 Generation of theta and gamma oscillations in M1

Previous research in our laboratory investigated beta oscillations (12-25 Hz), produced in M1 using 400 nM KA and 50 µM CCh (Yamawaki et al., 2008). Since then a modified sucrose-based cutting solution was developed, which incorporated neuroprotectants (to prevent excitotoxicity and cell death) and anti-oxidants (to prevent damage from reactive oxygen species and free radicals), such as indomethacin, uric acid, ascorbic acid, N-acetyl cysteine (NAC), taurine and amino-guanidine (Griffiths et al., 1993; Pakhotin et al., 1997; Rice, 2000; Kreisman and Olson, 2003; Tian et al., 2003; Tutak et al., 2005; Proctor, 2008; Prokic, 2011). We believe that this enhanced slice preparation protocol presumably resulted in increased slice viability and allowed the use of reduced concentrations of KA (100-150 nM) and CCh (5-10 µM) to be used to elicit oscillatory activity in M1. Oscillations could be elicited through the use of the lower ranges of both KA and CCh, however these concentrations were increased in some experiments to the higher end of the ranges to facilitate the emergence of oscillations. We observed that the range of KA and CCh concentrations produced oscillations with the same frequency, power and pharmacology. It is important to note that drug groups were not split by use of a single concentration of KA and CCh over another and that use of the whole range was used on average throughout all experiments. This suggests that there were no adverse

differences in pharmacology or frequency in our oscillations, as a result of the different concentrations used.

Furthermore care should be taken when interpreting these results as there may be unknown effects from the use of the various neuroprotective drugs in the generation of more physiological activity in the brain slice. Even though the protocol used does provide time between slicing and recording to wash out the neuroprotectants, it is possible that the action of specific pathways and oxidising compounds is important for the natural function of certain cells and the neuronal network as a whole. Further histological studies, using cell counts or staining for specific cellular markers should be completed to ascertain what (if any) changes in cells and network components are being altered between slicing protocols. This may help to inform on the changes that are taking place and allow us to create a more controlled recording environment and slice preparation that is more akin to an *in vivo* recording.

Previous work by Prokic et al. (2015), as referenced several times throughout this chapter, has demonstrated the emergence of 25-30 Hz beta oscillations in M1, which were sensitive to both $GABA_A$ receptor block and the application of a low-dose (10 nM) of zolpidem. Both the study by Prokic et al. and the work presented here use lower concentrations of KA and CCh to elicit oscillatory activity, than previously used by Yamawaki et al. (2008), as well as a similar slice preparation protocol. Therefore, it should be noted that the distinction between what this paper noted as a “beta” oscillation and what we call a “gamma” oscillation is only a difference of ~6 Hz. However, aside from the differences we observe in the response of our “gamma” oscillations to low-dose zolpidem, the slice preparation protocol we utilise here includes aminoguanidine, which is an iNOS inhibitor included in the sucrose-based aCSF. Nitric oxide is a short-lived free radical that has roles in apoptosis and swelling, which results from ischemia, results which have been shown to be reduced by the inhibition of iNOS by aminoguanidine (Griffiths et al., 1993; Sun et al., 2010). It is our belief that in the slice preparation used by Prokic et al. there was a subset of cells or network connections which were being damaged during the slicing protocol, which resulted in the altered frequency and pharmacology observed during these studies. Thus the use of aminoguanidine in our slice preparation may result in the prevention of this damage and contribute towards the generation of theta and gamma oscillations in our slices.

Application of both CCh and KA were required for high power, persistent oscillations. Previous work has demonstrated that the application of KA results in increased axonal

excitability in both interneurons and pyramidal cells, inducing a depolarised state that can produce spontaneous action potentials (Cossart et al., 1998; Semyanov and Kullmann, 2001). CCh is an agonist of the muscarinic acetylcholine (mACh) receptor, a GPCR coupled to several $K^+$- and $Ca^{2+}$-currents (Lucas-Meunier et al., 2003), which also increases glutamate and GABA release in interneurons and pyramidal cells. One $K^+$-current is the M-current ($I_M$), which is inhibited when the mACh receptor is activated. The $I_M$ channel is usually open at rest and generates an outward hyperpolarising current (Halliwell and Adams, 1982). Furthermore, the mACh receptor also increases certain non-specific cation currents, such as the $I_h$ current (hyperpolarisation activated current), which have been demonstrated to be important for oscillatory activity (Traub et al., 2000; Fisahn et al., 2002; Neymotin et al., 2013). Thus, increased activation of the mACh receptor, results in an overall membrane depolarisation and as a result the network is more excitable (Halliwell and Adams, 1982; Wang and McKinnon, 1995). This increased excitability in the interneuronal and pyramidal cell network results in neuronal network oscillations (Whittington et al., 1997).

Two distinct but simultaneous oscillations, at theta (6.6 Hz) and gamma (36.6 Hz) frequency were observed. Since application of CCh is required for the generation of both theta and gamma oscillations in M1, it is possible that the neuronal networks required to generate each oscillation are similar or overlap. Consistent with this hypothesis, we observed that blocking of mAChRs with atropine, results in the abolition of both oscillations. This also suggests that the theta oscillations induced in M1 are pharmacologically similar to previously studied atropine-sensitive theta oscillations observed in the hippocampus (Konopacki and Golebiewski, 1993; Gillies et al., 2002).

### 3.3.2 Phase-amplitude coupling

Oscillations in neuronal networks are known to interact between brain areas and are theorised to be required for spatial and temporal co-ordination between different regions (Gray and Singer, 1989; Jensen and Colgin, 2007). Early research in the hippocampus and entorhinal cortex focused on the interaction of the theta oscillation phase with the gamma oscillatory power (Bragin et al., 1995; Chrobak and Buzsaki, 1998; Csicsvari et al., 2003; Mormann et al., 2005; Tort et al., 2008; Quilichini et al., 2010). Igarashi et al. (2013) also demonstrated the involvement of theta-gamma coupling in the sensorimotor area *in vivo* during different behavioural and movement phases. Recent advances in computer processing power have allowed for complex and rapid analysis of data to determine coupling between theta and gamma oscillations, including *in silico* modelling

(Neymotin et al., 2013) and a measure of coupling called the 'modulation index' (Canolty et al., 2006; Canolty and Knight, 2010; Tort et al., 2010; Kramer and Eden, 2013). This compares the mean amplitude of a higher frequency oscillation and where it falls on the phase of a lower frequency oscillation, then calculates what is known as the modulation index as a measure of the deviation of the mean phase-amplitude distribution from a uniform distribution. Additionally, studies have begun to determine the underlying mechanisms that allow the facilitation of coupling between networks. Fast spiking (FS) inhibitory interneurons, known to be important in gamma and theta oscillations (Bragin et al., 1995; Bartos et al., 2002; Buzsaki, 2002; Tort et al., 2007), are believed to be involved in phase-amplitude coupling. Using mice with a genetic KO of these interneurons, studies have shown that this attenuated theta oscillatory power *in vivo* and reduced coupling with gamma oscillations (Wulff et al., 2009).

Interestingly however, not all of our recordings demonstrated the same intensity of phase-amplitude coupling, there was an order of magnitude difference between groups. Furthermore, the level of coupling in our slices was 2 orders of magnitude smaller than the MI value obtained by perfectly coupled model data used in the Tort et al. (2010) paper. It is therefore important to consider the potential differences between our data and theirs. One important consideration is that in modelled data using a computer there would be no noise or other biological variation within the recording, this could interfere with the MI calculation resulting in lower MI values. Additionally the paper by Tort et al. (2008), which observed PAC in *in vivo* recordings of rat hippocampus and striatum during a T-maze task, found that they only obtained MI values at $10^{-3}$; an order of magnitude lower than the perfect data used in the 2010 paper. Therefore, it is possible that the results we obtained are actually a product of looking at PAC in an *in vitro* setting. After all, experiments performed *in vivo* are conducted on networks and oscillations in a fully intact brain, with specific cues and behaviours which are directing these oscillations together. Thus it would make sense that successfully coupled oscillations in an *in vitro* setting, whereby the networks between brain areas are often severed and the slice is being artificially driven pharmacologically, would be less modulated than those observed in a physiological setting. It is possible that as *in vitro* slice preparations improve in the future and we are able to preserve physiological networks closer to those observed *in vivo*, we would be able to see a higher level of modulation during *in vitro* recordings.

In our recordings, the differences in MI values between those we considered to be positively coupled (MI+) and those negatively coupled (MI-) could be attributed to differences in slice viability, resulting in the production of some brain slices that do not

have adequate circuitry to produce coupled rhythms. Additionally, the variation in the MI between slices could also be due to differences in the time since slicing throughout the day or the strength of the initial oscillations to begin with. Though when checked, it was observed that 50% of the slices with higher MI were slices used earlier in the day and 50% were slices used later in the day, suggesting this was not a participating factor. However this caveat notwithstanding, the presence of a higher level of coupling in a significant number of slices is still important as a demonstration of the ability to generate phase-amplitude coupling in M1 *in vitro*. Further analysis could look at whether significant differences in the MI are the result of other factors, such as the initial power of theta and gamma oscillations in the slices, which may provide insight into the necessary machinery in the slices that allows for coupling between different frequencies to occur.

### 3.3.3 Pharmacological profile

In order to gain mechanistic insight into the neuronal networks involved in theta and gamma oscillations in M1, we pharmacologically investigated the different inhibitory and excitatory networks present. This demonstrated that the oscillations generated are pharmacologically distinct, not only from each other, but also from previously presented *in vitro* beta oscillations in M1 (Yamawaki et al., 2008).

#### *3.3.3.1 GABAergic pharmacology*

We have shown that blockade of $GABA_A$ receptors with gabazine and picrotoxin results in reduced gamma oscillatory power and the potentiation of theta oscillatory power in M1. The sensitivity of gamma oscillations to $GABA_A$ receptor block is consistent with previous reports in the hippocampus and other cortical areas (Whittington et al., 1995; Traub et al., 1996b; Traub et al., 1996a; Buhl et al., 1998; Fisahn et al., 1998; Dickson et al., 2000; Cunningham et al., 2003; Roopun et al., 2008; Cardin et al., 2009).

The involvement of the GABAergic system in the generation of theta oscillations has been shown previously (Golebiewski et al., 1993; Konopacki and Golebiewski, 1993; Konopacki et al., 1997; Lukatch and MacIver, 1997). In the hippocampus, theta-on pyramidal neurons and theta-off GABAergic interneurons have been observed. In these studies pyramidal neurons were tonically excited by a cholinergic drive (via CCh), whilst the inhibitory activity of the interneurons was inhibited by the application of a $GABA_A$ receptor antagonist (such as bicuculline). This was believed to result in a reduction of the inhibition produced by the theta-off neurons and release of subsequent excitation from theta-on neurons, producing

a robust theta oscillation in rodent recordings of hippocampus (Colom et al., 1991; Smythe et al., 1992) and cortex (Lukatch and MacIver, 1997). This is consistent with increases in theta oscillatory power in our recordings of M1, observed when applying $GABA_A$ receptor antagonists, such as gabazine or picrotoxin. Additionally, we applied a higher dose of gabazine (2 µM), which blocks extra-synaptic $GABA_A$ receptors that regulate tonic inhibitory currents (Farrant and Nusser, 2005). We found that the higher concentration of gabazine further increased theta oscillatory power, suggesting that the loss of tonic inhibition results in increased excitation of interneurons in the neuronal network. Furthermore, persistence of the theta oscillation in synaptic $GABA_A$ receptor block, suggests a non-synaptically coupled network of intrinsic oscillators, potentially similar to a non-synaptic beta2 rhythm generated in S2 *in vitro* (Roopun et al., 2006).

Activation of the benzodiazepine site of the $GABA_A$ receptor with diazepam and zolpidem application resulted in increases in power of both theta and gamma oscillations, although the effect on theta oscillations were only observed at the highest concentrations of either drug. These data are consistent with the known synaptic inhibitory components of gamma oscillations, and indicate that the theta network may have a synaptic component as well as the previously discussed non-synaptic element. The effects of benzodiazepine site agonists are suggestive of an increase in oscillatory power following recruitment and synchronous activation of pyramidal neurons, and may be related to the enhanced beta activity or ‘beta buzz’ seen *in vivo* (Glaze, 1990).

Zolpidem is a specific modulator of $GABA_A$ receptors containing the $\alpha_1$-subunit (Crestani et al., 2000) and at low concentrations (10 nM) has been shown to desynchronise beta oscillations *in vitro* (Prokic et al., 2015) and *in vivo* (Hall et al., 2010; Hall et al., 2014). However, we observed significant increases in the power of our gamma oscillations with increasing concentrations of zolpidem similar to gamma oscillations in the hippocampus (Heistek et al., 2010; Modebadze, 2014) indicating a distinct difference between previously observed beta and the gamma oscillatory activity observed here in M1. Additionally flumazenil, an antagonist of the benzodiazepine site, resulted in an increase in both theta and gamma oscillatory power. It has previously been suggested that flumazenil increases the power of beta oscillations in M1 (Prokic et al., 2015) through a decrease in a tonic inhibitory current, which is constitutively active in FS interneurons. Therefore, this result could be attributed to the presence of endogenous benzodiazepines or ‘endozepines’ (Costa and Guidotti, 1985; Farzampour et al., 2015). Alternatively, flumazenil may also act as an agonist at $\alpha_4$-subunit containing $GABA_A$ receptors, which could produce effects similar to diazepam (Whittemore et al., 1996).

The $GABA_A$ receptor modulator pentobarbital decreased gamma oscillatory frequency and power in M1. This is similar to responses observed previously in other cortical areas (Buhl et al., 1998; Cunningham et al., 2003). Pentobarbital increases $GABA_A$ receptor opening time and prolongs the decay time of GABAergic IPSCs (Segal and Barker, 1984). These results confirm the roles of IPSP/Cs in the pacing of these oscillations. The decrease in oscillatory power could alternatively be due to a non-specific antagonistic effect that barbiturates have on AMPA receptors containing GluR2 subunit (Martin et al., 1993; Taverna et al., 1994).

Block of metabotropic $GABA_B$ receptors increased the power of both our theta and gamma oscillations. These receptors are located synaptically and extrasynaptically on pre- and post-synaptic elements of both interneurons and pyramidal cells (Vanbrederode and Spain, 1995; Gonchar and Burkhalter, 1999; Lopez-Bendito et al., 2002; Bettler et al., 2004; Lopez-Bendito et al., 2004; Bettler and Tiao, 2006). $GABA_B$ receptors activate inwardly-rectifying $K^+$-channels, and inhibit voltage-sensitive $Ca^{2+}$-channels (Newberry and Nicoll, 1984; Gage, 1992; Bettler et al., 2004; Couve et al., 2004; Bettler and Tiao, 2006; Pérez-Garci et al., 2006; Palmer et al., 2012). Therefore, activation of $GABA_B$ receptors would result in both a postsynaptic membrane hyperpolarisation resulting in a reduction of action potential dependent glutamate and GABA release and a presynaptic reduction in the probability of release (Luscher et al., 1997; Bettler and Tiao, 2006). With regard to theta oscillations, Konopacki et al. (1997) reported that using a combination of $GABA_A$ and $GABA_B$ receptor antagonists in hippocampal slices could elicit such activity. Thus, in our studies CGP55845 may be acting to disinhibit a theta-on/theta-off network, increasing the oscillatory power of our theta oscillations.

Briefly, studies in the hippocampus of anaesthetised rodents have shown that multiple interneuronal types (including those that express PV and CCK) fire at different stages of a theta rhythm and are believed to innervate a range of sites across pyramidal neurons, from the apical to the distal dendrites, as well as the somatic region (Klausberger et al., 2003; Somogyi et al., 2014). Therefore, whilst the involvement of $GABA_A$ receptors in modulating the power of both theta and gamma oscillations is evident, we cannot be certain which population of interneurons may be responsible for our observations. Additionally, while the involvement of FS interneurons are believed to be important in gamma oscillation generation (Cardin et al., 2009), whether the same population is involved in coupling of theta to these oscillations or contribute equally to the generation of both is unknown from these data alone.

*3.3.3.2 Ionotropic glutamate receptor (iGluR) pharmacology*

The generation of EPSPs by AMPA receptors in neuronal networks are believed to be important in maintaining and increasing the synchrony of gamma oscillations (Whittington et al., 1997). Furthermore, gamma oscillations can synchronise over long-distances, which has been shown to be reliant on the generation of EPSPs by AMPA receptors onto cortical interneurons (Traub et al., 1996a; Fisahn et al., 1998; Traub et al., 2000; Fuchs et al., 2001; Traub et al., 2004). In our studies, block of AMPA receptors resulted in a reduction in the power of our gamma oscillations, suggesting a similarity to previously recorded gamma oscillations from the hippocampus and other cortical areas (Buhl et al., 1998; Fisahn et al., 1998; Dickson et al., 2000; Cunningham et al., 2003; Roopun et al., 2008; Cardin et al., 2009). These results suggest that there are clear differences between gamma oscillations observed here and the previously generated beta oscillations, which were insensitive to AMPA receptor block (Roopun et al., 2006; Yamawaki et al., 2008).

In contrast, block of AMPA receptors increased theta oscillatory power consistent with a non-synaptically coupled network of intrinsic oscillators in which synaptic blockade augments an intrinsically generated rhythm (e.g. the beta2 rhythm in somatosensory cortex *in vitro* as shown by Roopun et al., 2006). Furthermore, application of AMPA receptor antagonists to gamma oscillations has been shown to result in the emergence of theta oscillations (Gillies et al., 2002; Cunningham et al., 2003; Modebadze, 2014). One hypothesis suggests that theta-on cells within hippocampal networks generate a sub-threshold rhythm of intrinsic membrane properties, which emerge as theta frequency oscillations (Bland et al., 1988). These intrinsic membrane generators of theta appear to be reliant on the depolarisation by carbachol and subsequent hyperpolarisation by a GABAergic network (MacVicar and Tse, 1989). However, it is also possible that gamma oscillations, dependent on synaptic communication, are not abolished by antagonists at AMPA receptors but are merely slowed into the theta range, thereby augmenting apparent theta power. Though having measured the relative time-courses of gamma decline and theta augmentation, such a hypothesis was not supported.

Blockade of NMDA receptors with NMDAR antagonists significantly increased power in both the theta and gamma band in M1, consistent with other reports of such NMDAR antagonist effects in the literature (Pinault, 2008; Hakami et al., 2009; McNally et al., 2011). It has been reported that GABA interneurons and the generation of IPSPs in hippocampal CA1 are sensitive to NMDAR antagonism (Grunze et al., 1996) and selective genetic ablation of NMDAR on parvalbumin-positive (PV+, FS) interneurons has been reported to augment gamma activity (Korotkova et al., 2010). Therefore, disinhibition of

GABA interneurons has been suggested as a mechanism for augmented excitability in pyramidal neurons, leading to increased oscillatory power. In the same report Korotkova et al. (2010) showed that selective NMDAR ablation on interneurons reduced theta power in CA1, an effect not seen in M1. This may reflect different local circuit organisation between hippocampus and neocortex, or simply be due to the acute versus chronic effects of ablation as compared to pharmacological intervention.

In contrast, our studies of M1 theta oscillations were unaffected by NMDA receptor block by AP5 and CPP. It is certainly possible that the increased activity of the gamma oscillations could be increasing the ambient glutamate concentration around synapses, which could affect the competitive action of AP5 and CPP, resulting in only a partial antagonistic effect on NMDA receptors. On the other hand the non-competitive antagonists MK-801 and ketamine increased the power of theta oscillations. These drugs also have a variety of non-specific targets which may be affecting the neuronal network oscillations (for a review see Kohrs and Durieux, 1998). In particular, ketamine has been shown to have active properties on opioid receptors (Smith et al., 1987), cholinergic receptors (Aronstam et al., 1982) and on 5-HT/dopamine reuptake (Martin et al., 1988), while MK-801 has been reported to inhibit nicotinic acetylcholine receptors (Amador and Dani, 1991), potentiate the release of 5-HT (Iravani et al., 1999) and interact with DA release and reuptake (Clarke and Reuben, 1995). Overall, the difference in the response of theta oscillations to ketamine and MK-801 could be due to non-specific effects on other neuronal receptors within the network, rather than through a specific block of NMDA receptors.

#### *3.3.3.3 Metabotropic glutamate receptor (mGluR) pharmacology*

Whittington et al. (1995) demonstrated that the activation of $mGluR_1$ and $mGluR_5$ results in the generation of interneuronal network gamma oscillations in the hippocampus. Furthermore, activation of $mGluR_{1/5}$ has been shown to result in increased IPSC frequency (Kerner et al., 1997) via a block of $K^+$-channel induced hyperpolarisation and an increase in GABA release onto interneurons (Desai et al., 1994; Deng et al., 2010; Errington et al., 2011) resulting in an increase in gamma power. However, in our studies, block of group I mGluRs increased the oscillatory power of both theta and gamma while agonists decreased the power of theta alone. Previous studies have reported that activation of group I mGluRs decreased synaptic inhibition (Desai and Conn, 1991; Varma et al., 2001) and it seems likely that blockade of mGluRs may result in increased synaptic inhibition, either through reduction in constitutive activity at the receptor or through reduction of glutamate driven activation of mGluRs in the CCh/KA activated network. In

such a scenario, increased action-potential dependent GABA release may lead to increased oscillatory power in the same manner that positive modulation of $GABA_A$ receptors with benzodiazepines or barbiturates are known to do.

Typically mGluR group II and III receptors are present on both excitatory-inhibitory and inhibitory-inhibitory terminals and their activation results in a decrease in neurotransmitter release (Iserhot et al., 2004; Cosgrove et al., 2011; Liu et al., 2014). We found that the power of both theta and gamma oscillations increased in block of group II and III mGluRs. However, whilst we observed a decrease in theta and gamma oscillatory power using an agonist of group II mGluRs, activation of group III mGluRs increased oscillatory power. A study in hippocampus demonstrated that agonists of group II mGluRs resulted in a reduction of gamma oscillatory power, through the reduction of EPSCs onto interneurons (Price et al., 2005). Furthermore, studies using LY341495, a group II and III mGluR antagonist, in sensorimotor cortex demonstrated a pyramidal neuron specific increase in EPSCs, independent of GABA receptor disinhibition (Bandrowski et al., 2003). Activation of $mGluR_{2/3}$ can also initiate a PKC-dependent mechanism, which has been shown to increase NMDA receptor currents on interneurons (Tyszkiewicz et al., 2004). This supports our observations that an application of $mGluR_{2/3}$ agonists result in a decrease in the power of our oscillations, potentially also due to secondary effects on NMDA receptors.

Application of the group III mGluR agonist L-AP4 resulted in an increase in the power of our theta and gamma oscillations. Group III mGluRs are believed to be localised pre-synaptically on interneurons to reduce recurrent GABAergic inhibition in an interneuronal network. Group III mGluR activation could therefore result in inhibition of interneuron-pyramidal neuron activity, increasing the power of both our theta and gamma oscillations (Semyanov and Kullmann, 2000).

#### *3.3.3.4 Gap junction pharmacology*

Gap-junctions and electrical coupling between cells allows the free flow of ions between interneurons, which facilitates the generation of large, synchronous IPSPs and increased oscillatory power (Galarreta and Hestrin, 1999; Gibson et al., 1999; Deans et al., 2001). In line with previous studies, blocking gap-junction communication resulted in the abolition of our gamma oscillations (Fisahn et al., 1998; Traub et al., 2000; Hormuzdi et al., 2001; Traub et al., 2003). Theta oscillations were also acutely sensitive to blocking of gap-junctions as shown previously *in vivo* (Golebiewski et al., 2006; Bocian et al., 2009) and *in vitro* (Konopacki et al., 2004).

However, we must be aware of the complications associated with the use of carbenoxolone. While carbenoxolone is a potent gap junction antagonist, there are also reports that it acts at multiple different receptors and supresses neuronal activity in the brain, which makes it a very non-specific and dirty drug to use in pharmacological investigations. These include 11β-hydroxysteroid dehydrogenase, post synaptic NMDA receptors, $GABA_A$ receptors, $Ca^{2+}$ channels and the suppression of action potentials and input resistance (Connors, 2012). Therefore we cannot say for certain that the effect we've observed on our oscillations after carbenoxolone application is completely due to its role on gap junctions. Further investigations using knock-out models of different gap junction subunits would allow us to investigate the actual role of gap junctions in our oscillations. Furthermore, we could utilise electron microscopy to actually identify the presence of gap junctions between different neuronal cells. This would allow us to formulate an idea of their role through their location on different pyramidal and interneuronal subtypes, as well as extrapolate how their knock-out or loss from these locations affects our recorded oscillations. This is especially important, given the role that axo-axonal gap junctions are believed to play in the generation and propagation of theta and gamma oscillations in the hippocampus and M1.

## 3.4 Conclusion

In this chapter we have shown that M1 can generate co-existent theta and gamma oscillations with distinct pharmacological profiles. We believe that improvements in slice preparation and neuronal viability have contributed to the protection of neuronal elements essential for generation of theta and gamma oscillations. Importantly, the protection of a population of cells or neuronal process sensitive to nitric oxide damage during slicing by aminoguanidine may be key in the generation of the oscillations we observe here. The pharmacology of our gamma oscillations appear consistent with gamma oscillations observed in the hippocampus, somatosensory cortex (S1) and entorhinal cortex. These oscillations appear to be generated through the combined action of KA and CCh, and involve both excitatory and inhibitory synaptic transmission, as well as non-synaptic communication through gap junctions. However, based on the pharmacology of our theta oscillations, we would suggest that they result from a non-synaptic network involving the intrinsic properties of neurons themselves. A summary of the pharmacological characterisation of these oscillations is provided in **Table 3.1**. Additionally, evidence of phase-amplitude coupling between the two networks underlies an important physiological

aspect of theta-gamma rhythms. Overall, this presents a new model of oscillations in M1 and the first evidence for theta-gamma coupling *in vitro.* Though ultimately, further studies are required to determine the relative involvement of different neuronal populations to each oscillation generated in M1 (see chapter 6). Additionally, more slices to improve N numbers throughout this study would improve the certainty for the effect each drug condition has on the different theta and gamma oscillations. In order to determine the amount needed to remain statistically relevant and to prevent unwanted statistical errors, power analysis could be performed, which would prevent us wasting animals and slices on experiments that are already adequately powered.

| Drug | | N (slice) | Theta power | Gamma power |
|---|---|---|---|---|
| **GABAergic receptors** | | | | |
| **Gabazine** | **250 nM** | 7 | ↑ | ↓↓↓ |
| | **2 µM** | 7 | ↑↑↑ | ↓↓ |
| **Picrotoxin** | **50 µM** | 8 | ↑↑ | ↓↓ |
| **Diazepam** | **30 nM** | 8 | - | - |
| | **100 nM** | 8 | ↑ | ↑ |
| **Zolpidem** | **10 nM** | 14 | - | ↑ |
| | **30 nM** | 14 | - | ↑↑↑ |
| | **100 nM** | 8 | ↑↑↑ | ↑↑↑ |
| **Flumazenil** | **500 nM** | 15 | - | ↑↑↑ |
| | **1 µM** | 15 | - | ↑↑↑ |
| **Pentobarbital** | **10 µM** | 7 | - | ↓ |
| **LSN3074113** | **10 µM** | 7 | ↑↑↑ | - |
| **CGP55845** | **5 µM** | 17 | ↑↑ | ↑↑↑ |
| **Ionotropic glutamate receptors** | | | | |
| **SYM 2206** | **20 µM** | 20 | ↑↑↑ | ↓↓↓ |
| **NBQX** | **2.5 µM** | 9 | ↑ | ↓↓ |
| **D,L-AP5** | **50 µM** | 15 | - | ↑↑↑ |
| **(R)-CPP** | **5 µM** | 11 | - | ↑↑ |
| **MK-801** | **20 µM** | 12 | ↑↑↑ | ↑↑↑ |
| **Ketamine** | **20 µM** | 7 | ↑ | ↑ |
| **Metabotropic glutamate receptors** | | | | |
| **CPCCOEt** | **20 µM** | 7 | ↑ | ↑ |
| **MPEP** | **20 µM** | 10 | ↑↑ | ↑↑ |
| **MTEP** | **100 nM** | 8 | ↑↑ | ↑↑ |
| **DHPG** | **10 µM** | 10 | ↓↓ | - |
| **LY341495** | **100 nM** | 9 | ↑ | - |
| | **5 µM** | 9 | ↑↑ | ↑↑↑ |
| **LY379268** | **1 µM** | 8 | ↓↓ | ↓↓ |
| **L-AP4** | **50 µM** | 8 | ↑↑ | ↑↑ |
| **Cholinergic receptors** | | | | |
| **Atropine** | **5 µM** | 7 | ↓ | ↓ |
| **Gap junctions** | | | | |
| **Carbenoxolone** | **200 µM** | 13 | ↓↓↓ | ↓↓↓ |

**Table 3.1 Summary table of drugs used to pharmacologically characterise theta and gamma oscillations.** Listed are names of individual drugs, the N's per experiment, the changes to oscillatory power for theta and gamma oscillations.

# Chapter 4 Dopamine Pharmacology of M1 Oscillations

## 4.1 Introduction

Dopamine (DA) neurons of the substantia nigra pars compacta (SNc) and ventral tegmental area (VTA) project to large areas of the frontal cortex and basal ganglia (BG) and as such DA signalling has been shown to be functionally involved in the regulation of motor execution, behaviour (including motivation, reward learning, prediction and pain) and working memory (Schultz, 1998; Lisman and Otmakhova, 2001; Mallet et al., 2008b; Mitsi and Zachariou, 2016). Therefore it is not surprising that dysfunction of the dopaminergic system has been implicated in a number of neurological disorders, including schizophrenia, attention deficit hyperactivity disorder (ADHD), Tourette's syndrome, Huntington's disease and PD (Ehringer and Hornykiewicz, 1960; Snyder et al., 1970; Creese et al., 1976; Jakel and Maragos, 2000; Mink, 2006; Swanson et al., 2007; Borroto-Escuela et al., 2016).

### 4.1.1 Dopamine Receptors

DA activates a group of G-protein coupled receptors (GPCRs), namely D1 to D5. These are separated into two groups, the D1-like receptors, which include D1 and D5, and the D2-like receptors, which include D2, D3 and D4. These groups are based on their ability to modulate adenylate cyclase (AC) activity (Kebabian and Greengard, 1971; Spano et al., 1978; Seeman and Vantol, 1994). Thus, D1-like receptors increase AC activity and stimulate the production of cyclic adenosine monophosphate (cAMP), while D2-like receptors decrease AC activity and inhibit the production of cAMP (Kebabian and Calne, 1979; Enjalbert and Bockaert, 1983). These differences were later found to result from specific Gα–proteins linked to the receptors, D1-like are linked to $G\alpha_{s/olf}$, and D2-like to $G\alpha_{o/i}$. (Missale et al., 1998; Tritsch and Sabatini, 2012). The activation of cAMP by D1-like receptors has a major role in the regulation of protein kinase A (PKA), which has many downstream phosphorylation targets (Greengard, 2001). In contrast, activation of D2-like receptors activates phosphatases that result in the inhibition of PKA activity (Tritsch and Sabatini, 2012). DA also stimulates phospholipase C (PLC) production, primarily by D2-like receptors, via the Gβγ-protein which can directly increase intracellular $Ca^{2+}$ levels and regulate the activity of $Ca^{2+}$ and $K^{+}$ channels (Friedman et al., 1997; Beckstead et al., 2004).

Within the M1 of monkeys, D1-like and D2-like receptors are distributed across all cortical layers, though both groups of receptors demonstrated a greater localisation to the

superficial layers (LI and LIII) (Lidow et al., 1989; Lidow et al., 1991; Huntley et al., 1992). This is in contrast to rodents where D1-like receptors were found to be localised to the deep layers V and VI (Dawson et al., 1986; Vitrac et al., 2014). Furthermore, D1 receptors in M1 have been shown to be localised to the soma of pyramidal neurons, whilst D5 receptors extend more to their apical dendrites (Awenowicz and Porter, 2002). Additionally, both D1-like and D2-like receptors are localised on PV+ interneurons, preferentially in deep layers V and VI (Gaspar et al., 1995; LeMoine and Gaspar, 1998).

### 4.1.2 Dopamine and neuronal activity

DA plays a major role in locomotor activity, whereby the degeneration of the dopaminergic neurons of the SNc results in PD and the symptoms of akinesia, bradykinesia and rigidity. The loss of DA coincidently results in the emergence of highly synchronous and coherent beta oscillations (12-30 Hz), which are indicative of PD (Magill et al., 2001; Bevan et al., 2002; Brown, 2003). The role of DA in modulating the activity of the cortico-BG network is therefore important for our understanding of this disease.

In this chapter, we investigated the modulation of network oscillations by DA in brain slices of M1 and pharmacologically explore the receptors involved. The chronic loss of DA and the consequences of modulatory loss were investigated by using the 6-OHDA model of PD (Ungerstedt, 1968). Thus, using the previously established protocol for the generation of oscillations in M1 slices *in vitro* using CCh and KA (see chapter 3); we investigated the importance of dopaminergic modulation on M1 theta and gamma oscillations in DA-intact and DA-depleted slices.

Experiments were performed in collaboration with Mazhar Ozkan (Marmara University, Turkey).

## 4.2 Results

### 4.2.1 Basic dopaminergic pharmacology

*4.2.1.1 General DA receptor activation*

DA can become readily oxidised which may affect the intended applied concentration and potentially produce unreliable and varied results. Furthermore, DA oxidation may result in the production of reactive oxygen species (ROS) and free radicals. These can be reduced by the application of the neuro-protectant ascorbic acid (Hastings and Zigmond, 1994; Hastings et al., 1996). Oxidised DA resulted in the aCSF turning a blue colour. We found that 500 µM ascorbic acid successfully prevented the oxidation of DA for the duration of our experiments.

Our initial experiments were conducted on brain slices obtained from rats 50-100 g. In this cohort of animals, application of DA (30 µM) caused no significant change in the power of both theta (to 110.5 ± 13.1% of control, n=9 slices, ns, **Fig 4.1Ai, B, C**) and gamma (to 92.5 ± 9.7 % of control, n=9 slices, ns, **Fig 4.1Aii, B, C**) oscillations.

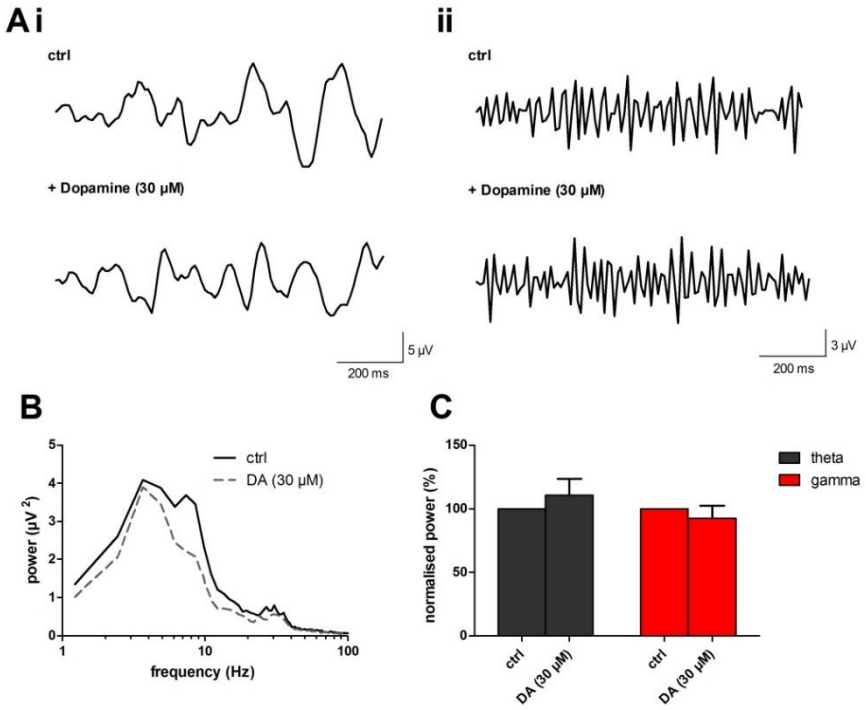


**Figure 4.1 Dopamine application has no effect on oscillations in layer V of M1 (A)** Band-passed raw data of (i) theta and (ii) gamma oscillations after induction with CCh and KA (ctrl) and after drug application. **(B)** Typical power spectra demonstrating peak responses before (solid line) and after application of 30 µM dopamine (DA, dashed line). **(C)** Peak power changes of theta (grey bars) and gamma (red bars) oscillations normalised to control.

However, application of the non-specific DA receptor agonist, apomorphine (20 µM), caused a significant increase to theta oscillatory power (to 149.7 ± 11.8% of control, n=15 slices, p<0.001, **Fig 4.2Ai, B, C**) but was without effect on the power of gamma oscillations (108.4 ± 14.9% of control, n=15 slices, ns, **Fig 4.2Aii, B, C**).

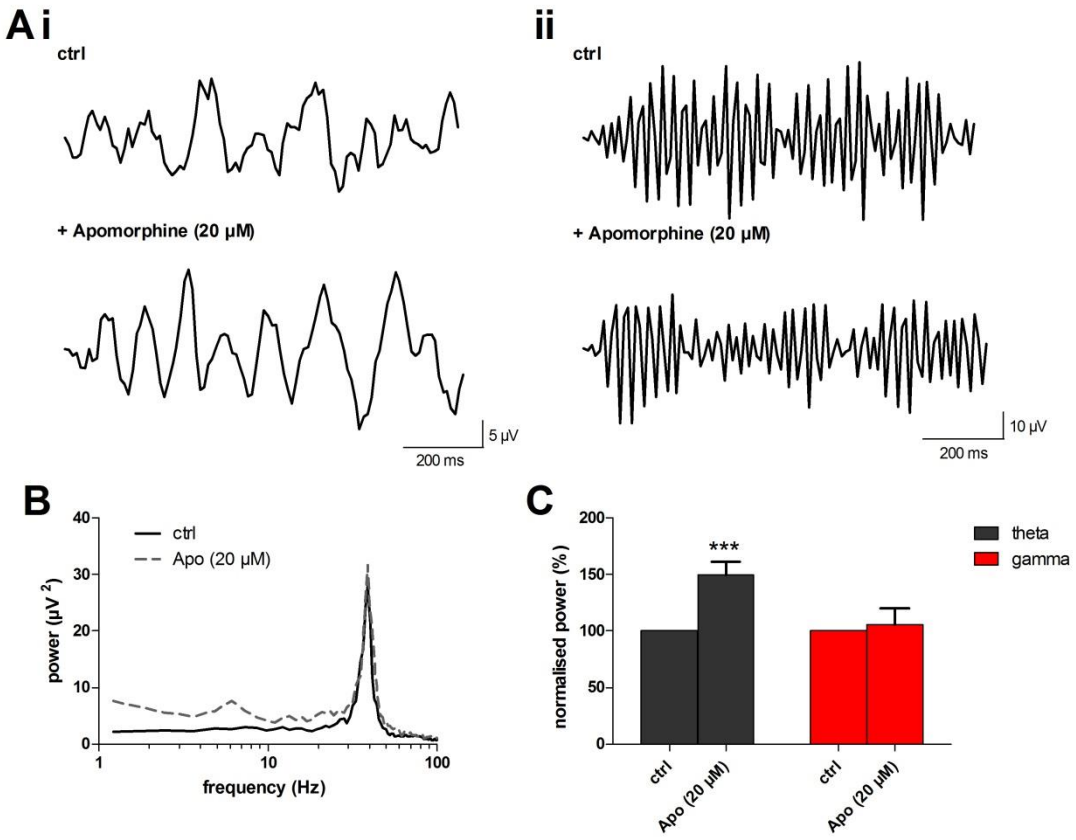


**Figure 4.2 Apomorphine significantly increases theta oscillations in LV of M1 (A)** Band-passed raw data of (i) theta and (ii) gamma oscillations after induction with CCh and KA (ctrl) and after drug application. **(B)** Typical power spectra demonstrating peak responses before (solid line) and after application of 20 µM Apomorphine (Apo; dashed line). **(C)** Peak power changes of theta (grey bars) and gamma (red bars) oscillations normalised to control. ***, p<0.001

*4.2.1.2 D1-like receptor pharmacology*

Although DA has no effect on the power of theta and gamma oscillations, action at D1-like and D2-like receptors could be in opposition and directly cancelling each other out. Therefore, to determine the possible contribution of D1-like receptors in modulation of network oscillations in M1, we applied the D1-like receptor agonist SKF 38393 (SKF; 10 µM). This resulted in the significant increase in the power of both theta (to 162.2 ± 18.0% of control, n=25 slices, p<0.001, **Fig 4.3Ai, B, C**) and gamma (to 159.5 ± 12.4% of control, n=25 slices, p<0.001, **Fig 4.3Aii, B, C**) oscillations.

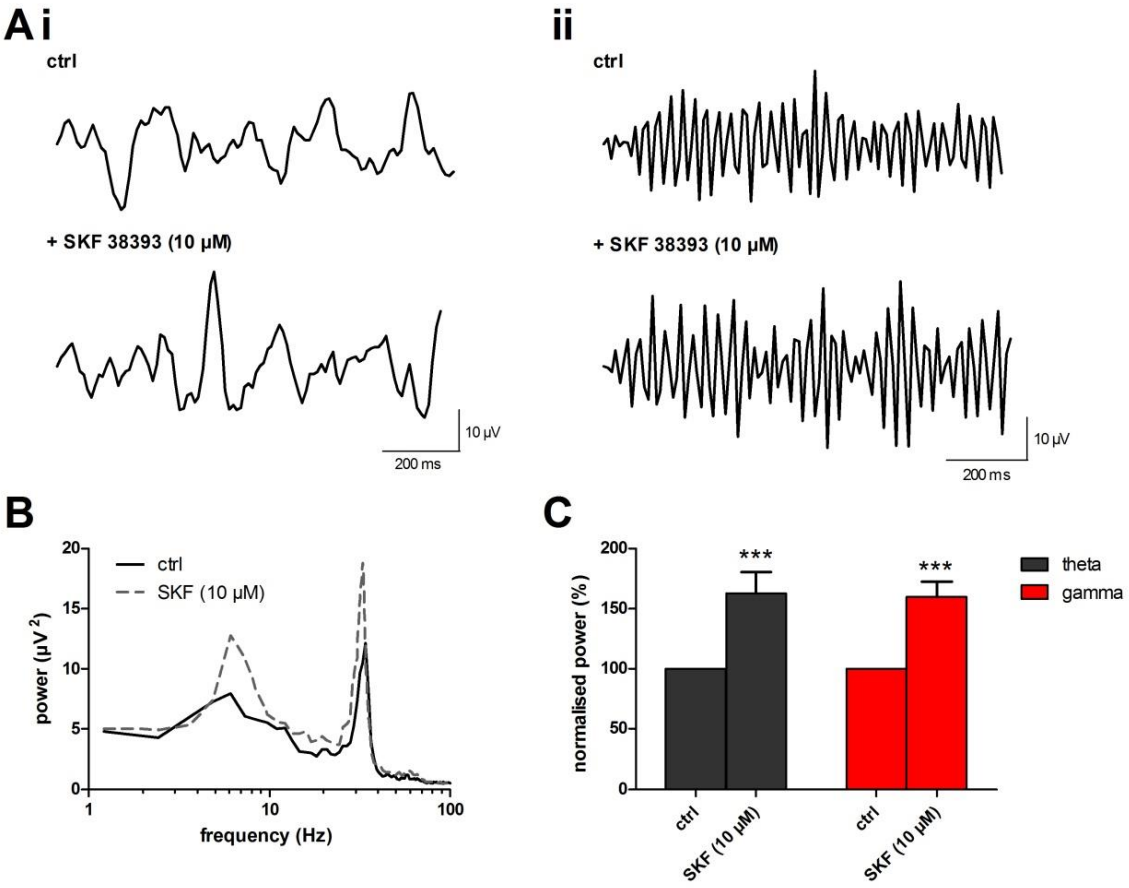


**Figure 4.3 D1-like receptor agonist SKF 38393 significantly increases both theta and gamma oscillations in LV of M1 (A)** Band-passed raw data of (i) theta and (ii) gamma oscillations after induction with CCh and KA (ctrl) and after drug application. **(B)** Typical power spectra demonstrating peak responses before (solid line) and after application of 10 µM SKF 38393 (SKF, dashed line). **(C)** Peak power changes of theta (grey bars) and gamma (red bars) oscillations normalised to control. ***, p<0.001

Surprisingly, application of the D1-like receptor antagonist SCH 23390 (SCH; 2 µM) also resulted in the significant increase of both oscillations in M1 (theta: to 179.6 ± 26.2% of control, n=10 slices, p<0.01; gamma: 157.7 ± 25.3% of control, n=10 slices, p<0.05; **Fig 4.4**).

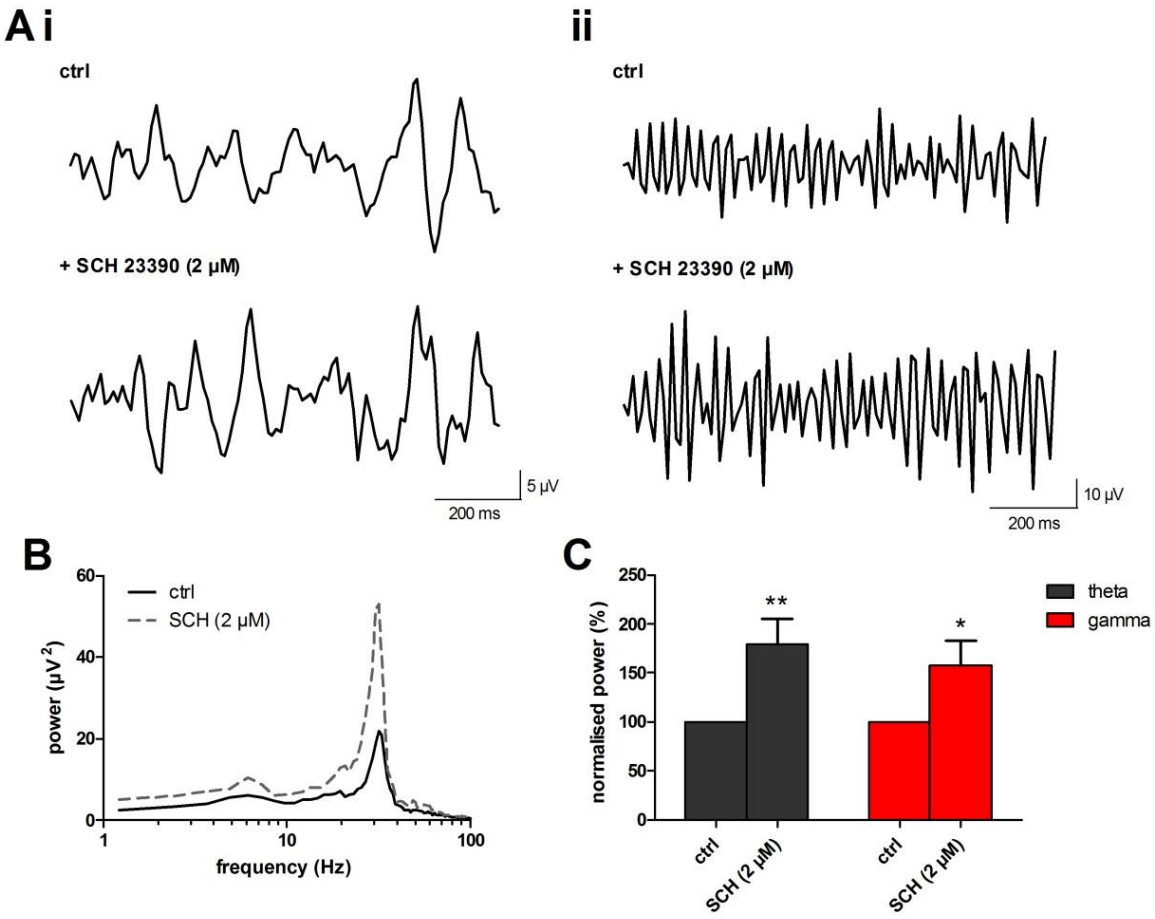


**Figure 4.4 D1-like receptor antagonist SCH 23390 significantly increases the power of both theta and gamma oscillations in LV of M1 (A)** Band-passed raw data of (i) theta and (ii) gamma oscillations after induction with CCh and KA (ctrl) and after drug application. **(B)** Typical power spectra demonstrating peak responses before (solid line) and after application of 2 µM SCH 23390 (dashed line). **(C)** Peak power changes of theta (grey bars) and gamma (red bars) oscillations normalised to control. **, $p<0.01$, *, $p<0.05$.

*4.2.1.3 D2-like receptor pharmacology*

To determine the possible contribution of D2-like receptors in the modulation of network oscillations in M1, we used the D2-like receptor agonist quinpirole (10 µM). This resulted in the significant increase in the power of both theta (to 149.0 ± 13.8% of control, n=9 slices, p<0.01, **Fig 4.5Ai, B, C**) and gamma oscillations (to 133.9 ± 12.3% of control, n=9 slices, p<0.05, **Fig 4.5Aii, B, C**).

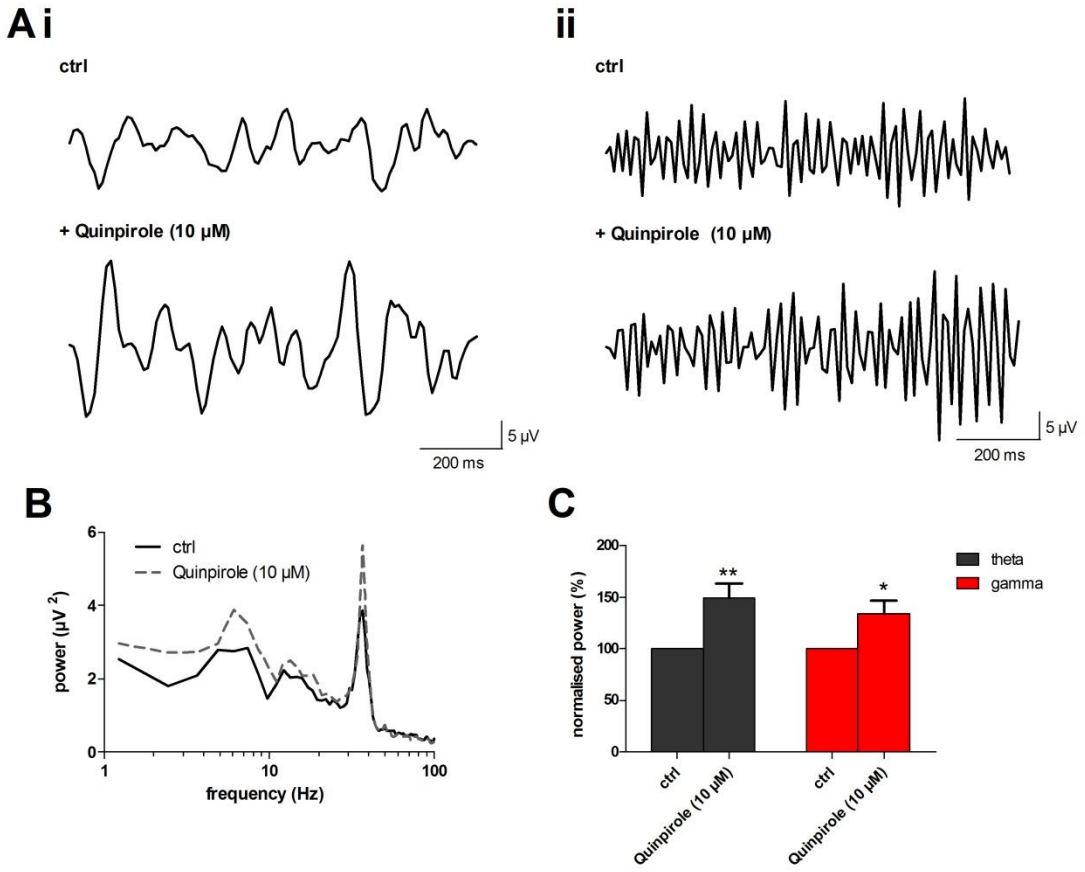


**Figure 4.5 D2-like receptor agonist quinpirole significantly increases both theta and gamma oscillations in LV of M1 (A)** Band-passed raw data of (i) theta and (ii) gamma oscillations after induction with CCh and KA (ctrl) and after drug application. **(B)** Typical power spectra demonstrating peak responses before (solid line) and after application of 10 µM quinpirole (dashed line). **(C)** Peak power changes of theta (grey bars) and gamma (red bars) oscillations normalised to control. **, p<0.01, *, p<0.05.

The application of the D2-like receptor antagonist sulpiride (10 µM) also resulted in the significant increase of theta oscillations (to 126.3 ± 9.0% of control, n=9 slices, p<0.01, **Fig 4.6Ai, B, C**), with no significant change in gamma oscillatory power (to 113.3 ± 6.5% of control, n=9 slices, ns, **Fig 4.6Aii, B, C**).

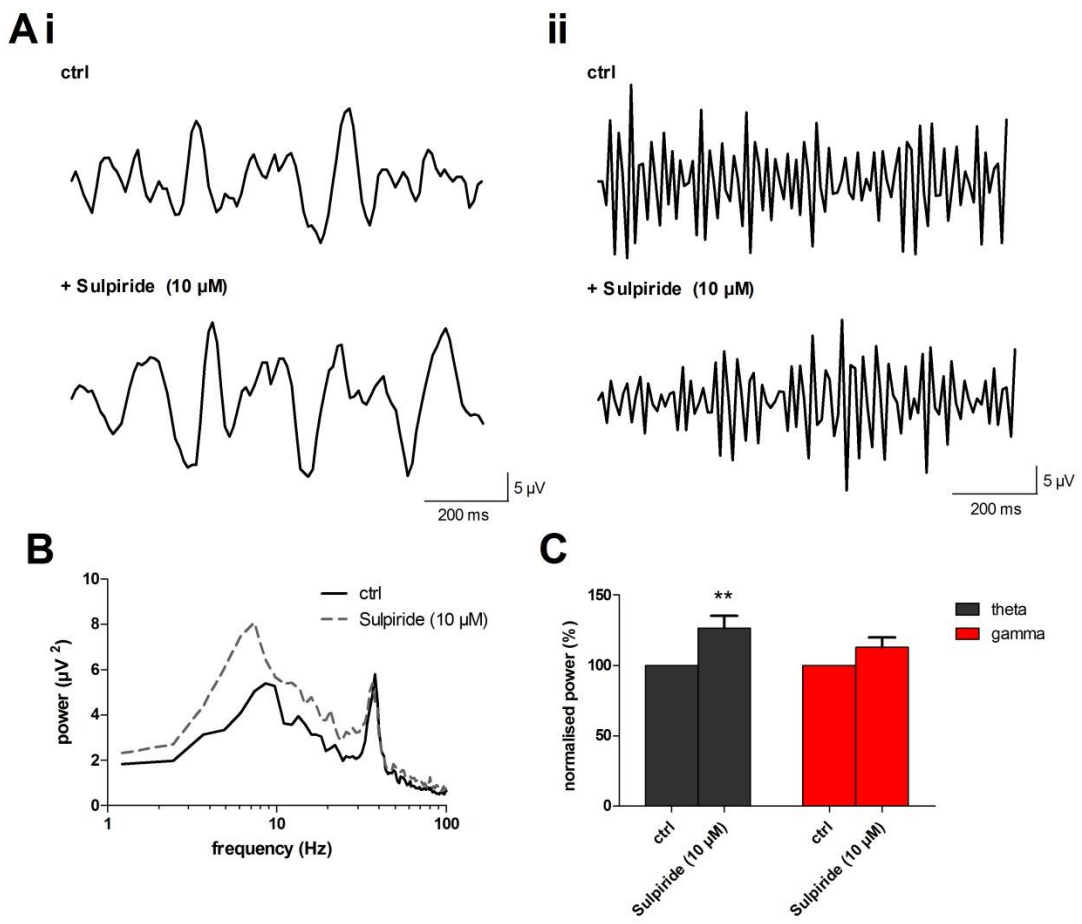


**Figure 4.6 D2-like receptor antagonist sulpiride significantly increases theta but not gamma oscillations in LV of M1 (A)** Band-passed raw data of (i) theta and (ii) gamma oscillations after induction with CCh and KA (ctrl) and after drug application. **(B)** Typical power spectra demonstrating peak responses before (solid line) and after application of 10 µM sulpiride (dashed line). **(C)** Peak power changes of theta (grey bars) and gamma (red bars) oscillations normalised to control. **, $p<0.01$.

### 4.2.2 Dopaminergic pharmacology in 6-OHDA lesioned rats

Using the toxin 6-OHDA we modelled the movement deficits seen in PD and investigated changes in the dopaminergic modulation of oscillations generated in M1, using the same protocol to induce oscillations (5 µM CCh and 150 nM KA), in 280-350 g animals. We performed unilateral lesions of rodent MFB in the left (ipsilateral) hemisphere, which allowed us to use the right (contralateral) hemisphere as a control. In order to account for any potential inter-hemispheric changes which could occur from lesioning, we also performed experiments in age-matched control (AMC) animals. Animals were tested for motor deficits after a post-surgical period of at least two weeks using the stepping test (see methods section 2.2.2.1).

Those animals which displayed deficits in contralateral step adjustment (forehand: 0.45 ± 0.14 steps, $p<0.001$; backhand: 7.56 ± 1.02 steps, $p<0.001$; n=21 animals) compared to ipsilateral step adjustment (forehand: 18.19 ± 0.80 steps; backhand: 21.76 ± 0.75 steps; n=21 animals) were considered successfully lesioned (see **Fig 4.7**). Animals displaying equally high step adjustment in both ipsilateral and contralateral limbs were rejected.

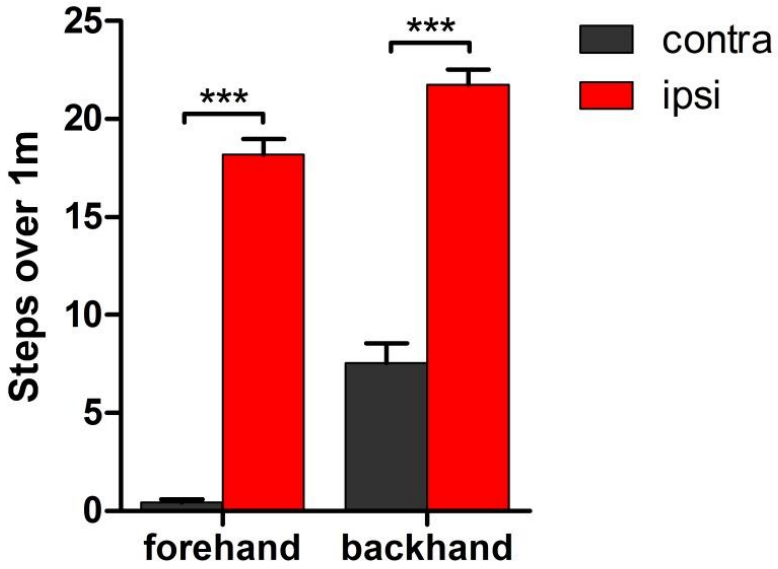


**Figure 4.7 Pooled mean results of stepping test** Mean stepping tests from 6-OHDA lesioned animals for contralateral (contra, grey bars) and ipsilateral (ipsi, red bars) forelimbs in both the forehand and backhand directions. ***, $p<0.001$.

In order to compare the spectral profile of the oscillations generated in AMC, ipsilateral and contralateral slices (following CCh and KA application), baseline power spectra recordings were normalised to the highest value, pooled and averaged (**Fig 4.8**). Overall we observed no significant difference between theta peak frequencies (AMC: 6.04 ± 0.21 Hz, n=68 slices; ipsilateral: 6.38 ± 0.24 Hz, n=51 slices; contralateral: 6.78 ± 0.27 Hz, n=35 slices). Also, there were no significant differences observed in the power of theta oscillations (AMC: 10.97 ± 1.02 $\mu V^2$, n=68 slices; ipsilateral: 9.97 ± 1.00 $\mu V^2$, n=51 slices; contralateral: 9.45 ± 1.20 $\mu V^2$, n=35 slices). When we compared gamma oscillatory peak frequencies in each condition, we again observed no significant differences (AMC: 34.21 ± 0.35 Hz, n=68 slices; ipsilateral: 33.73 ± 0.46 Hz, n=51 slices, contralateral: 33.69 ± 0.60 Hz, n=35 slices) and no differences in the power of gamma oscillations (AMC: 11.06 ± 1.54 $\mu V^2$, n=68 slices; ipsilateral: 11.11 ± 1.82 $\mu V^2$, n=51 slices; contralateral: 9.89 ± 1.65 $\mu V^2$, n=35 slices).

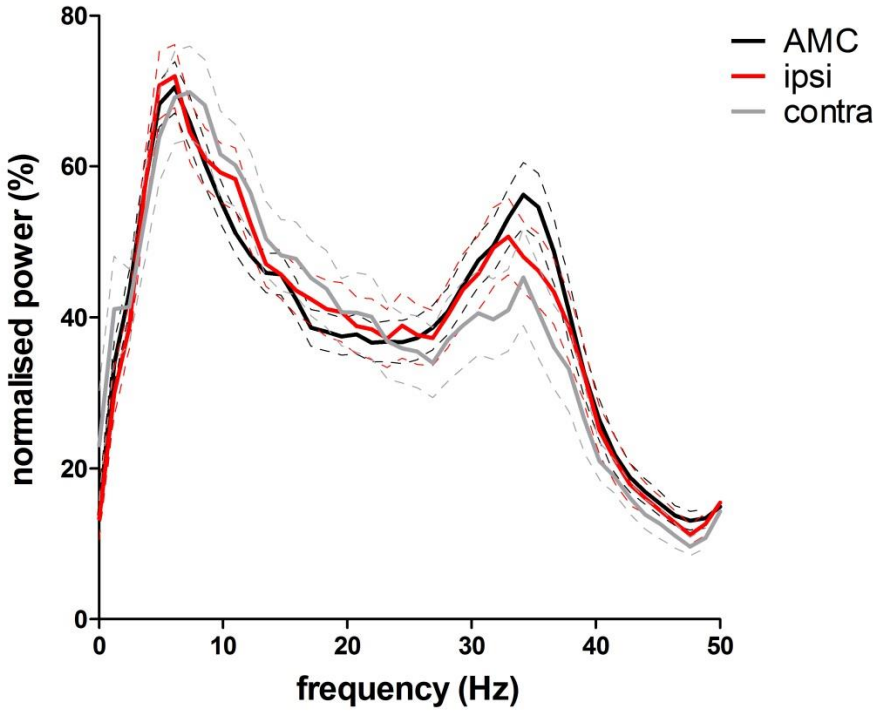


**Figure 4.8 Normalised power spectra of AMC, ipsilateral and contralateral generated oscillations in LV of M1** Normalised power spectra of recordings from AMC animals (black line) compared to 6-OHDA animals in ipsilateral (red line) and contralateral (grey line) hemispheres.

*4.2.2.1 General DA receptor activation*

Following the application of DA (30 µM) to slices from AMC animals we observed no significant changes to oscillatory power in both theta (to 130.2 ± 15.6% of control, n=11 slices, ns, **Fig 4.9Ai, B, C**) and gamma oscillations (to 113.3 ± 18.4% of control, n=11 slices, ns, **Fig 4.9Aii, B, C**).

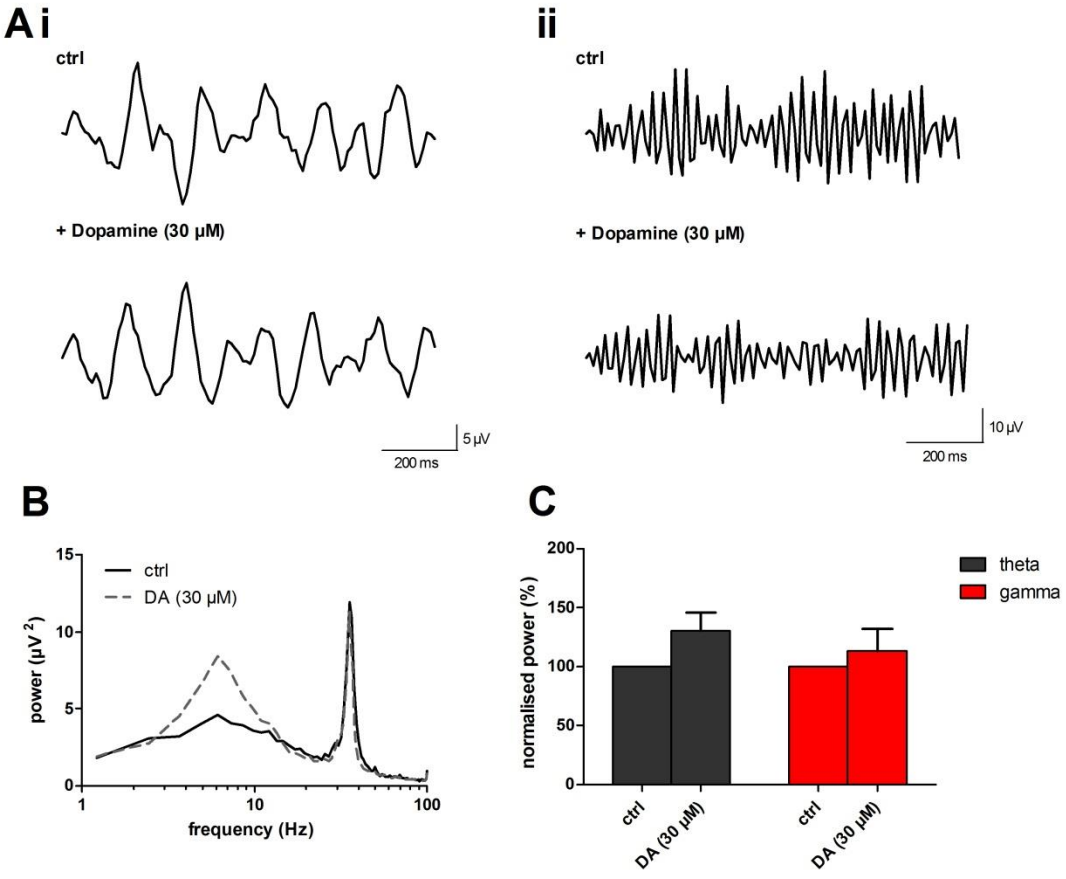


**Figure 4.9 Application of DA (30 µM) to AMC slices results in no significant differences to oscillations in LV of M1 (A)** Band-passed raw data of (i) theta and (ii) gamma oscillations after induction with CCh and KA (ctrl) and after drug application. **(B)** Typical power spectra demonstrating peak responses before (solid line) and after application of 30 µM dopamine (DA, dashed line). **(C)** Peak power changes of theta (grey bars) and gamma (red bars) oscillations normalised to control.

However, in ipsilateral slices of 6-OHDA lesioned animals, on the re-introduction of DA, we observed a significant increase in theta oscillatory power (to 154.2 ± 19.5% of control, n=10 slices, $p<0.01$) and a significant decrease in gamma oscillatory power (82.0 ± 5.8% of control, n=10 slices, $p<0.05$, **Fig 4.10A, C**). Application of DA to contralateral slices resulted in no significant changes to oscillatory power (theta: 131.1 ± 27.2% of control, n=6 slices, ns; gamma: 88.9 ± 11.0% of control, n=6 slices, ns; **Fig 4.10B, C**). Power

analysis of this experiment revealed that the approximate 12.2% difference in normalised power that we observed in **Fig 4.10C** in the contralateral hemisphere only had a 20% power value. This suggests that we only had a 20% chance to observe a statistically significant difference of that magnitude. However in the ipsilateral hemisphere, our significant difference of approximately 18% normalised power change, is deemed to be 75% powered. Giving us a 75% chance of observing a true effect in our experiment.

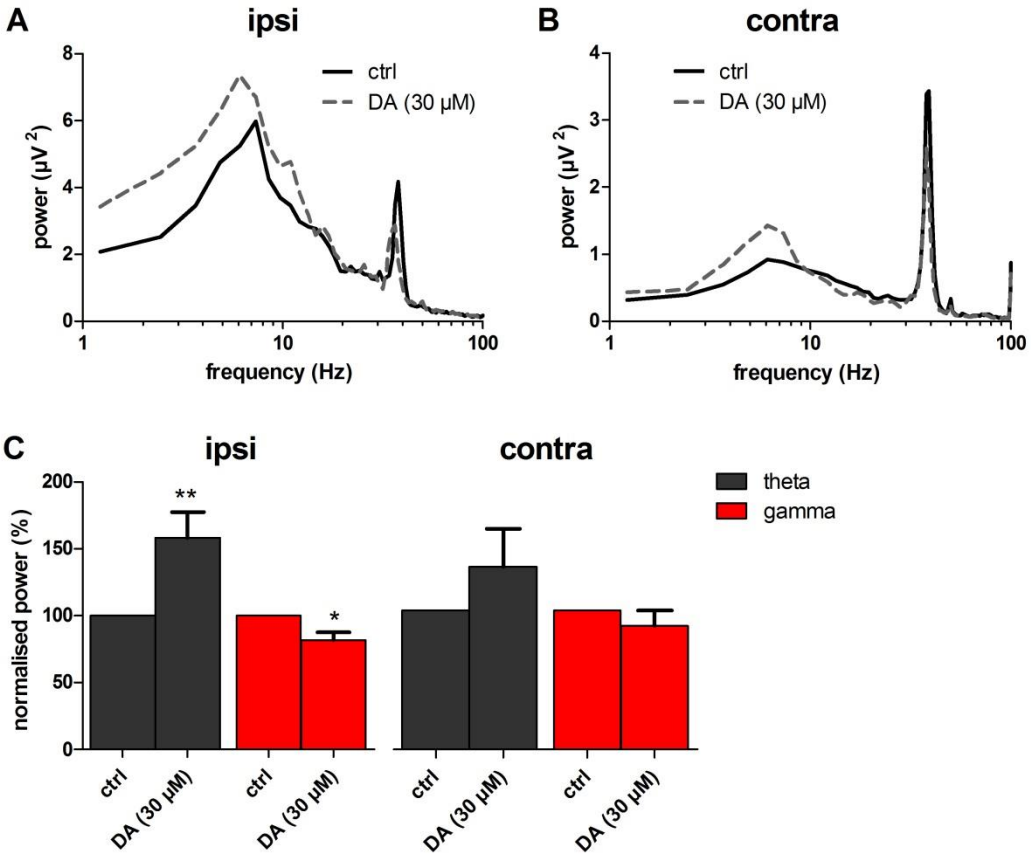


**Figure 4.10 Application of DA (30 µM) to ipsilateral and contralateral hemispheres of 6-OHDA lesioned animals (A)** Typical power spectra demonstrating peak responses before (solid line) and after application of 30 µM dopamine (DA, dashed line) in ipsilateral hemisphere. **(B)** Typical power spectra demonstrating peak responses before (solid line) and after application of 30 µM dopamine (DA, dashed line) in contralateral hemisphere **(C)** Peak power changes of theta (grey bars) and gamma (red bars) oscillations normalised to control in ipsilateral and contralateral hemispheres. ipsi - ipsilateral, contra - contralateral. **, $p<0.01$, *, $p<0.05$.

Amphetamine (AMPH) induces the release of DA from pre-synaptic dopaminergic neuronal terminals through the displacement of vesicular DA (Besson et al., 1969). However, in contrast to the lack of effect of DA in AMC's we observed that application of AMPH (20 µM) resulted in the significant increase in theta oscillatory power (150.7 ± 16.2% of control, n=13 slices, p<0.01, **Fig 4.11Ai, B, C**), as well as a significant decrease in gamma oscillatory power (67.2 ± 7.8% of control, n=13 slices, p<0.01, **Fig 4.11Aii, B, C**).

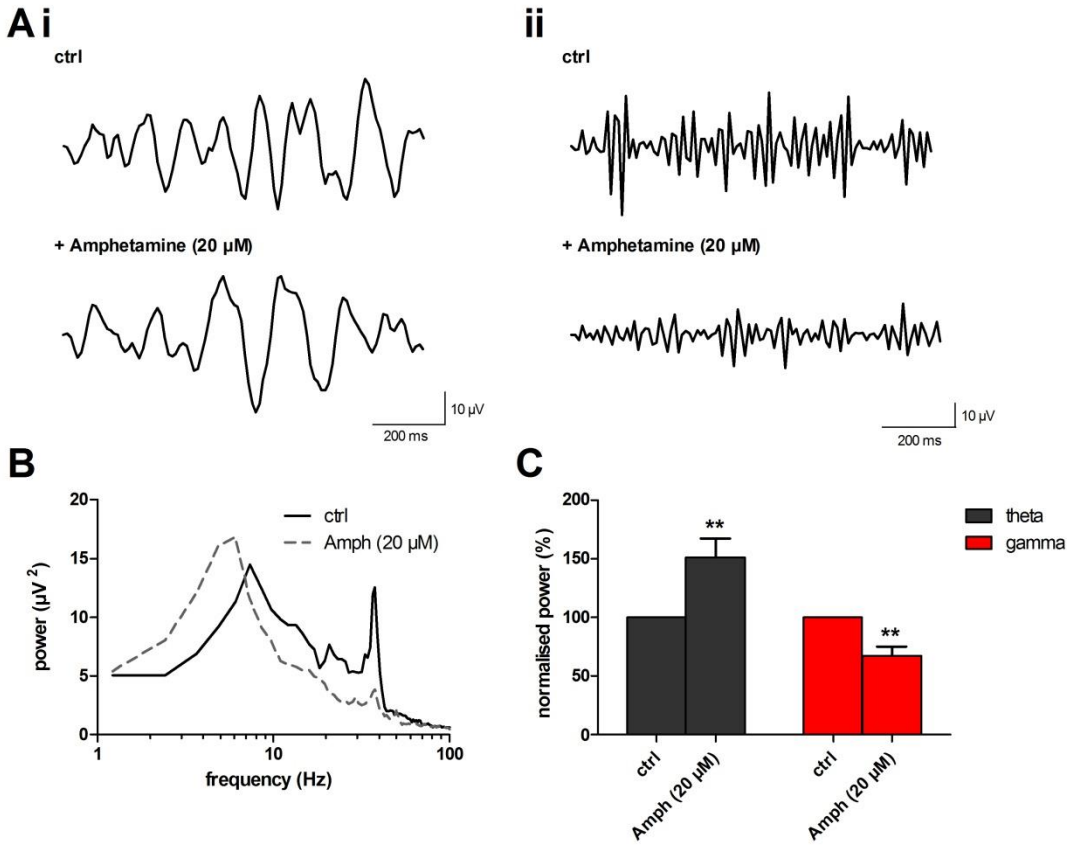


**Figure 4.11 Amphetamine (20 µM) has opposing effects on theta and gamma oscillations in LV of M1 in AMC (A)** Band-passed raw data of (i) theta and (ii) gamma oscillations after induction with CCh and KA (ctrl) and after drug application. **(B)** Typical power spectra demonstrating peak responses before (solid line) and after application of 20 µM amphetamine (Amph, dashed line). **(C)** Peak power changes of theta (grey bars) and gamma (red bars) oscillations normalised to control. **, p<0.01.

When AMPH (20 µM) was applied to ipsilateral, dopamine-depleted, slices we observed a significant increase in theta oscillations (to 159.1 ± 11.7% of control, n=9 slices, p<0.01) with no significant change in gamma oscillatory power (84.9 ± 15.4% of control, n=8 slices, ns, **Fig 4.12A, C**). Power analysis of the gamma oscillatory change suggests that this experiment only provided a 10% chance to see a true effect, however to have a 75% chance to see a true effect we would have had to observe a 40% change in normalised power. In contrast, AMPH applied to contralateral slices caused no significant changes to theta oscillatory power (134.1 ± 18.2% of control, n=8 slices, ns) but a significant decrease in gamma oscillations (55.7 ± 8.6% of control, n=8 slices, p<0.01, **Fig 4.12B, C**).

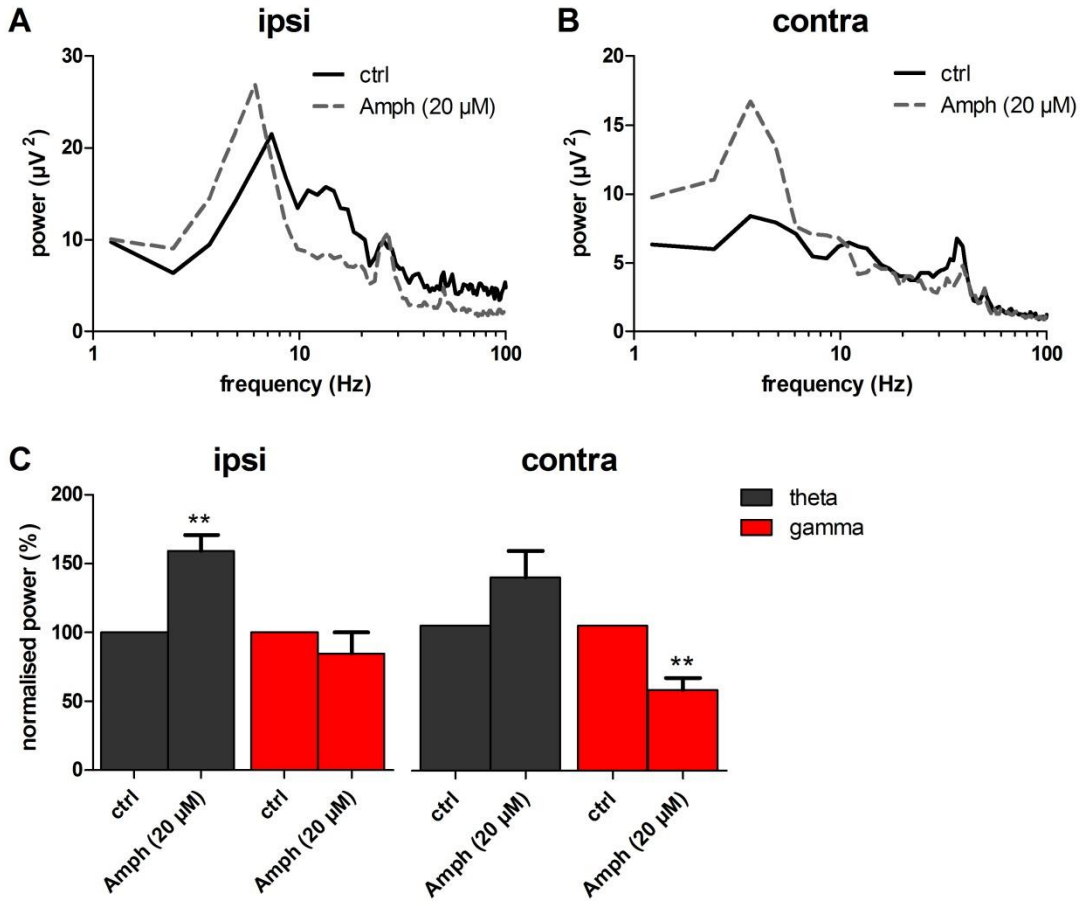


**Figure 4.12 Application of amphetamine (20 µM) to 6-OHDA lesioned slices of M1 results in a differential response between hemispheres (A)** Typical power spectra demonstrating peak responses before (solid line) and after application of 20 µM amphetamine (Amph, dashed line) in ipsilateral hemisphere. **(B)** Typical power spectra demonstrating peak responses before (solid line) and after application of 20 µM amphetamine (Amph, dashed line) in contralateral hemisphere **(C)** Peak power changes of theta (grey bars) and gamma (red bars) oscillations normalised to control in ipsilateral and contralateral hemispheres. Ipsi = ipsilateral, Contra = contralateral. **, p<0.01.

*4.2.2.2 D1-like receptor pharmacology*

To determine the possible contribution of D1-like receptors in modulation of network oscillations in M1 in older animals (290-310 g), we again applied the D1-like receptor agonist SKF (10 µM). In AMC animals, the oscillatory power of both theta and gamma oscillations was increased (theta: 130.1 ± 8.2% of control, n=13 slices, p<0.01; **Fig 4.13Ai, B, C**; gamma: 134.2 ± 9.2% of control, n=13 slices, p<0.01; **Fig 4.13Aii, B, C**). These changes were similar to those observed in young animals (50-100 g).

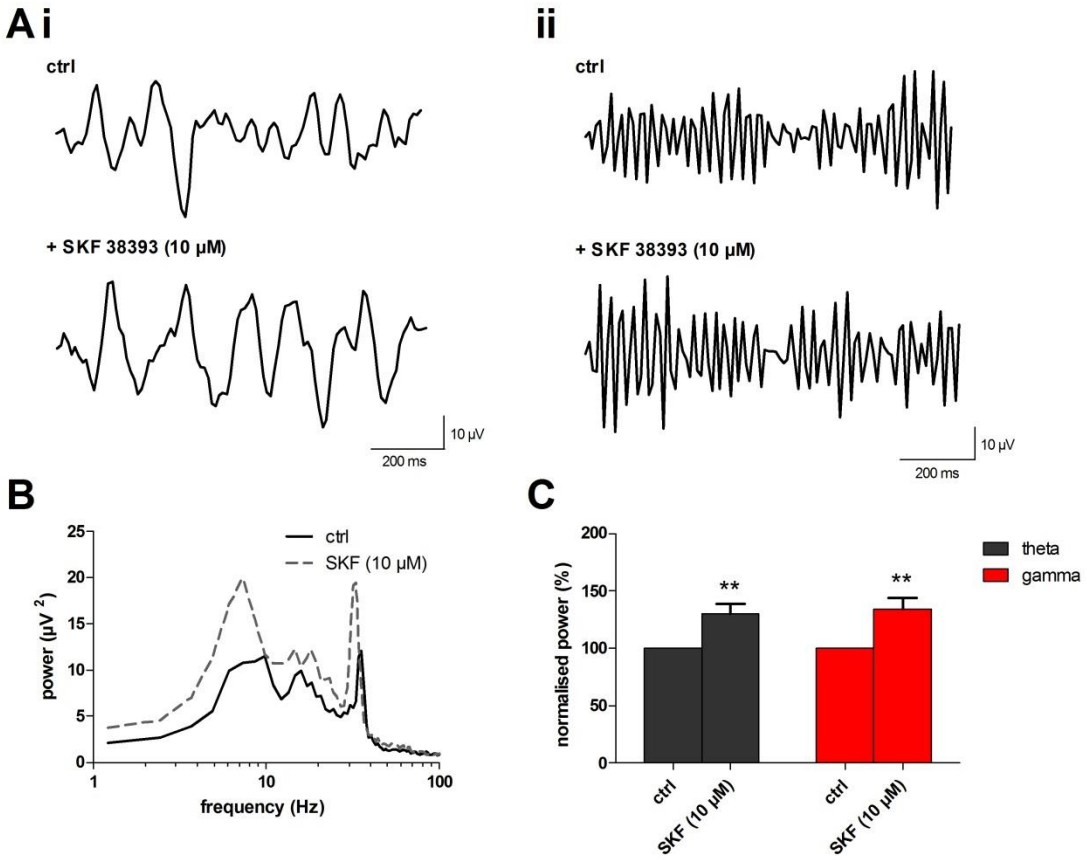


**Figure 4.13 Application of D1-like agonist SKF 38393 (10 µM) results in increases to both oscillations in LV of M1 (A)** Band-passed raw data of (i) theta and (ii) gamma oscillations after induction with CCh and KA (ctrl) and after drug application. **(B)** Typical power spectra demonstrating peak responses before (solid line) and after application of 10 µM SKF (dashed line). **(C)** Peak power changes of theta (grey bars) and gamma (red bars) oscillations normalised to control. **, p<0.01.

Upon application of SKF (10 µM) to slices from lesioned animals we observed significant increases to oscillatory power in the ipsilateral hemisphere, of both theta (to 133.5 ± 11.4% of control, n=16 slices, p<0.05) and gamma (to 161.8 ± 17.0 of control, n=16 slices, p<0.01, **Fig 4.14A, C**) oscillations. Similar increases in theta oscillatory power were observed upon application of SKF to contralateral slices (to 145.3 ± 16.0% of control, n=10 slices, p<0.05) and to gamma oscillatory power (to 260.7 ± 72.0% of control, n=10 slices, p<0.01, **Fig 4.14B, C**).

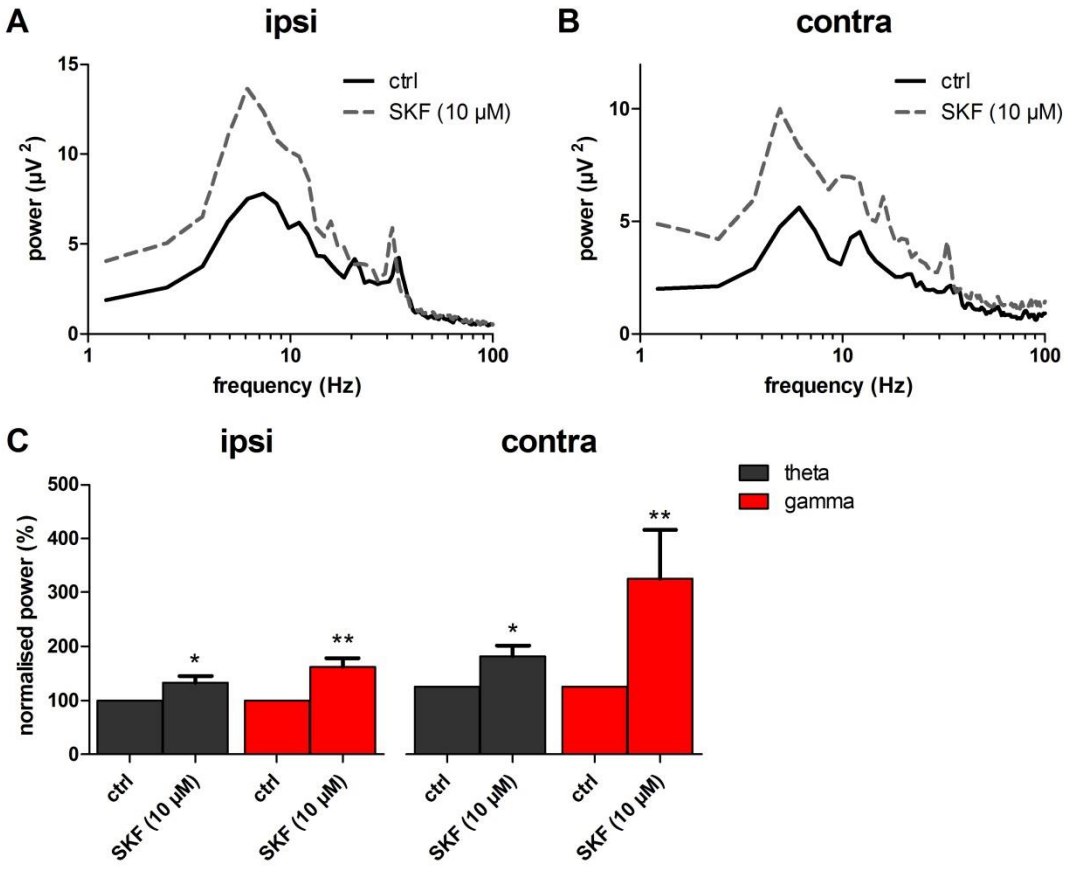


**Figure 4.14 Application of D1-like agonist SKF 38393 (10 µM) to 6-OHDA lesioned slices increased the power of all oscillations (A)** Typical power spectra demonstrating peak responses before (solid line) and after application of 10 µM SKF (dashed line) in ipsilateral hemisphere. **(B)** Typical power spectra demonstrating peak responses before (solid line) and after application of 10 µM SKF (dashed line) in contralateral hemisphere **(C)** Peak power changes of theta (grey bars) and gamma (red bars) oscillations normalised to control in ipsilateral and contralateral hemispheres. Ipsi = ipsilateral, Contra = contralateral. **, p<0.01, *, p<0.05.

However, application of the D1-like antagonist SCH (2 µM) resulted in no changes to the power of either theta or gamma oscillations in AMC animals (theta: to 109.7 ± 7.4% of control, n=11 slices, ns; gamma: 125.0 ± 15.1% of control, n=11 slices, ns; **Fig 4.15**).

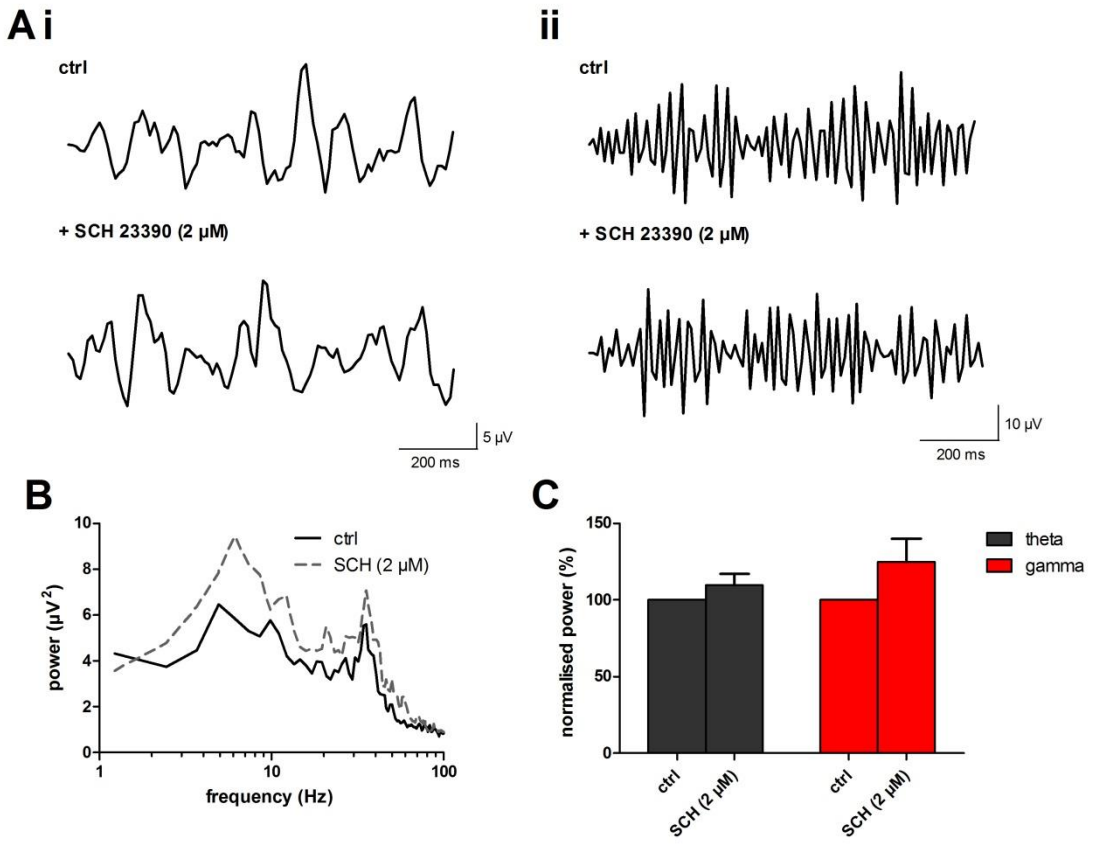


**Figure 4.15 Application of D1-like antagonist SCH 23390 (2 µM) to slices from AMC results in no significant changes to oscillatory power (A)** Band-passed raw data of (i) theta and (ii) gamma oscillations after induction with CCh and KA (ctrl) and after drug application. **(B)** Typical power spectra demonstrating peak responses before (solid line) and after application of 2 µM SCH (dashed line). **(C)** Peak power changes of theta (grey bars) and gamma (red bars) oscillations normalised to control.

Application of SCH (2 µM) to ipsilateral dopamine-depleted slices, caused no significant changes to theta (113.8 ± 7.5% of control, n=13 slices, ns, **Fig 4.16A, C**) or gamma (158.4 ± 26.0% of control, n=13 slices, ns, **Fig 4.16A, C**) oscillatory power. However, application of SCH (2 µM) significantly increased theta (153.5 ± 19.3% of control, n=9 slices, p<0.01, **Fig 4.16B, C**), and gamma (142.1 ± 13.9% of control, n=9 slices, p<0.01, **Fig 4.16B, C**) oscillatory power in contralateral slices.

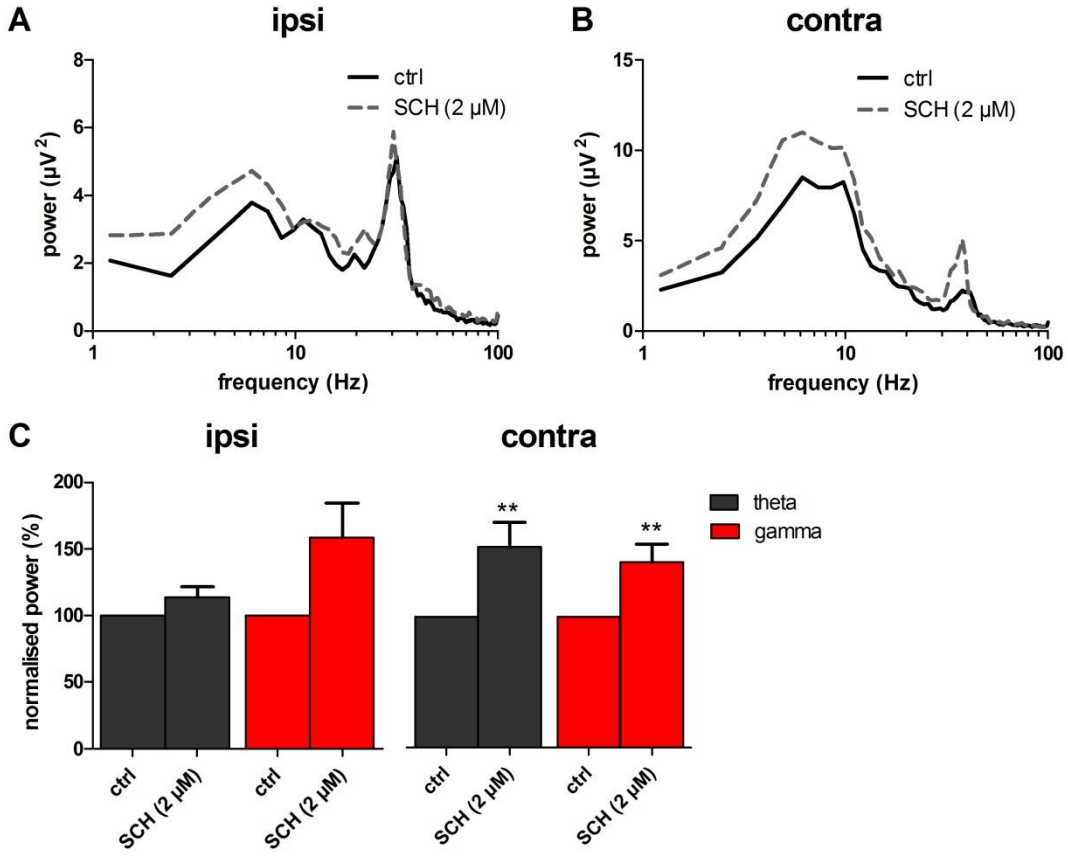


**Figure 4.16 Application of D1-like antagonist SCH 23390 (2 µM) to 6-OHDA lesioned slices has differential effects on theta and gamma oscillations (A)** Typical power spectra demonstrating peak responses before (solid line) and after application of 2 µM SCH (dashed line) in ipsilateral hemisphere. **(B)** Typical power spectra demonstrating peak responses before (solid line) and after application of 2 µM SCH (dashed line) in contralateral hemisphere **(C)** Peak power changes of theta (grey bars) and gamma (red bars) oscillations normalised to control in ipsilateral and contralateral hemispheres. ipsi - ipsilateral, contra - contralateral. **, p<0.01.

*4.2.2.3 D2-like receptor pharmacology*

Application of the D2-like receptor agonist quinpirole (10 µM) in slices from AMC animals resulted in significantly increased power of both theta (to 127.8 ± 6.7% of control, n=12 slices, p<0.01, **Fig 4.17Ai, B, C**) and gamma oscillations (to 183.5 ± 40.3%, n=12 slices, p<0.05, **Fig 4.17Aii, B, C**).

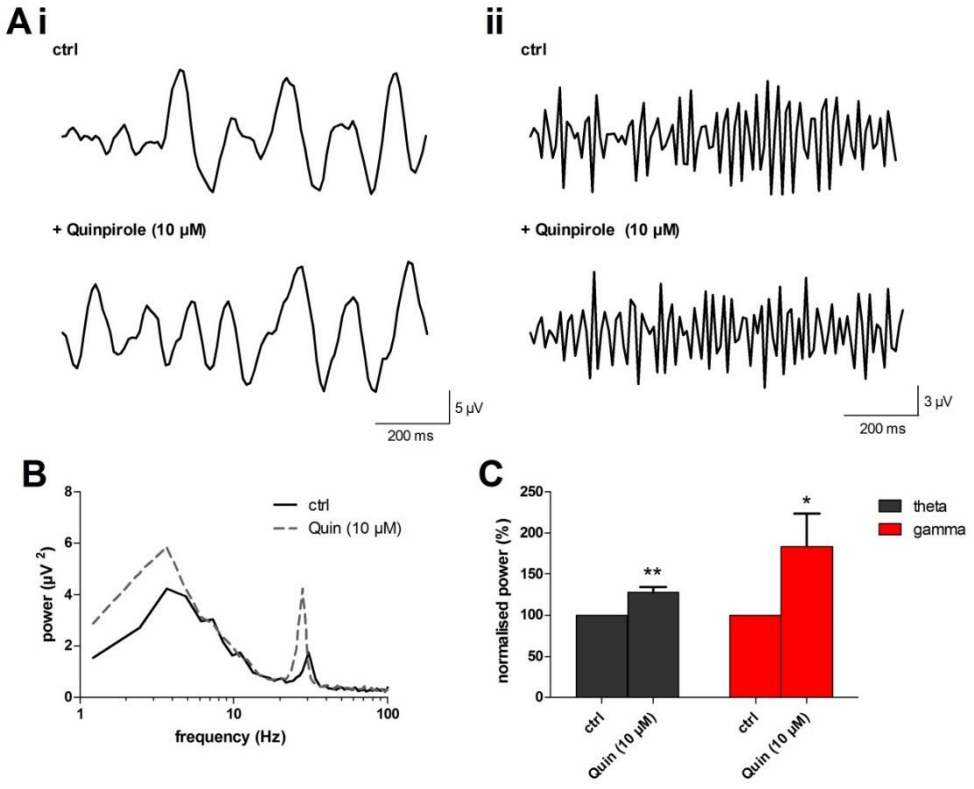


**Figure 4.17 The D2-like agonist quinpirole (10 µM) results in increased oscillations in AMC slices of LV in M1 (A)** Band-passed raw data of (i) theta and (ii) gamma oscillations after induction with CCh and KA (ctrl) and after drug application. **(B)** Typical power spectra demonstrating peak responses before (solid line) and after application of 10 µM quinpirole (Quin, dashed line). **(C)** Peak power changes of theta (grey bars) and gamma (red bars) oscillations normalised to control. **, p<0.01, *, p<0.05.

Application of quinpirole to ipsilateral DA-depleted slices significantly increased theta oscillatory power (to 140.9 ± 12.6% of control, n=14 slices, p<0.01). In contrast however, gamma oscillatory power showed no significant difference from control (to 98.9 ± 7.4% of control, n=15 slices, ns, **Fig 4.18A, C**). Application of quinpirole to contralateral slices resulted in no significant change to theta oscillations (to 124.8 ± 15.7% of control, n=7 slices, ns) while gamma oscillatory power was significantly increased (to 152.5 ± 19.4% of control, n=7 slices, p<0.05, **Fig 4.18B, C**). A comparison between ipsilateral and contralateral changes in the power of gamma oscillations demonstrated that these were significantly different (p<0.05).

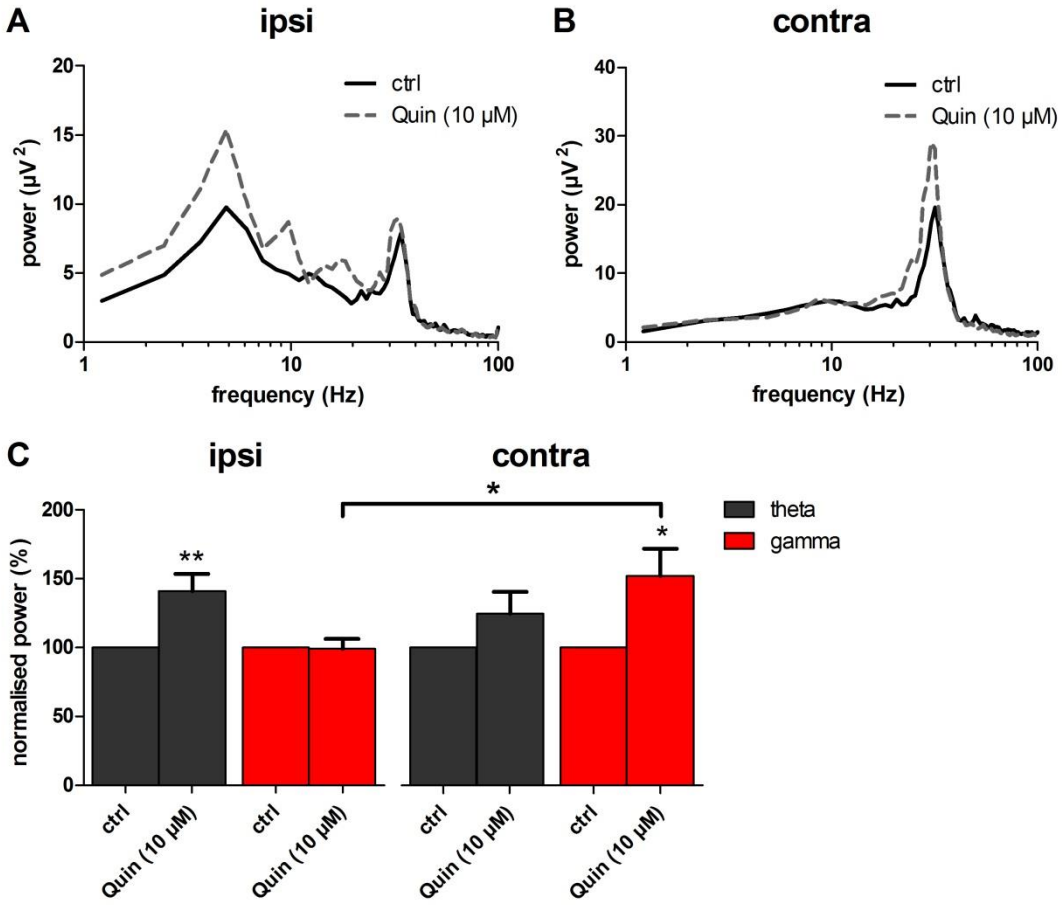


**Figure 4.18 Quinpirole (10 µM) showed differential effects on the power of theta and gamma oscillations in layer V of M1 from 6-OHDA animals between hemispheres (A)** Typical power spectra demonstrating peak responses before (solid line) and after application of 10 µM quinpirole (Quin, dashed line) in ipsilateral hemisphere. **(B)** Typical power spectra demonstrating peak responses before (solid line) and after application of 10 µM quinpirole (Quin, dashed line) in contralateral hemisphere **(C)** Peak power changes of theta (grey bars) and gamma (red bars) oscillations normalised to control in ipsilateral and contralateral hemispheres. Ipsi = ipsilateral, Contra = contralateral. **, $p<0.01$, *, $p<0.05$.

To complete our investigation into the D2-like receptors, we used the D2-like antagonist sulpiride. When sulpiride (10 µM) was applied to slices from AMC animals we observed significant increases in power to both the theta (to 118.3 ± 6.4% of control, n=7 slices, p<0.05) and gamma oscillations (to 118.8 ± 5.0% of control, n=7 slices, p<0.05, **Fig 4.19**), which was different to what was observed previously in the young (50-100 g) control animals.

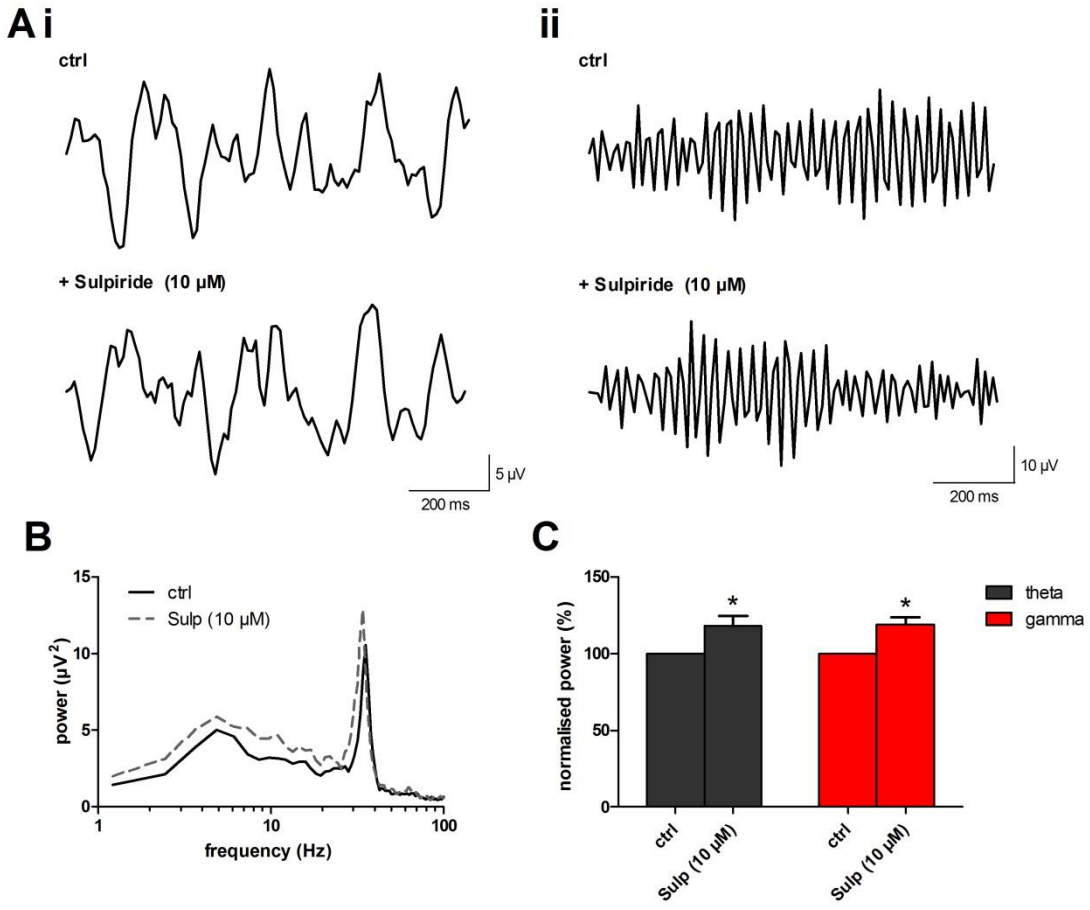


**Figure 4.19 D2-like antagonist sulpiride (10 µM) increases the power of theta and gamma oscillations in LV of M1 in AMC animals (A)** Band-passed raw data of (i) theta and (ii) gamma oscillations after induction with CCh and KA (ctrl) and after drug application. **(B)** Typical power spectra demonstrating peak responses before (solid line) and after application of 10 µM sulpiride (Sulp, dashed line). **(C)** Peak power changes of theta (grey bars) and gamma (red bars) oscillations normalised to control. *, p<0.05.

However, when applied to ipsilateral slices from DA-depleted animals sulpiride was without effect on theta oscillatory power (to 122.1 ± 10.55 of control, n=10 slices, ns) but caused a significant increase in gamma power (to 133.8 ± 13.8% of control, n=10 slices, p<0.05, **Fig 4.20A, C**). In contralateral slices, application of sulpiride resulted in a significant increase in theta (to 162.8 ± 20.2% of control, n=6 slices, p<0.05,) and gamma (to 208.6 ± 44.2% of control, n=6 slices, p<0.05, **Fig 4.20B, C**) oscillatory power.

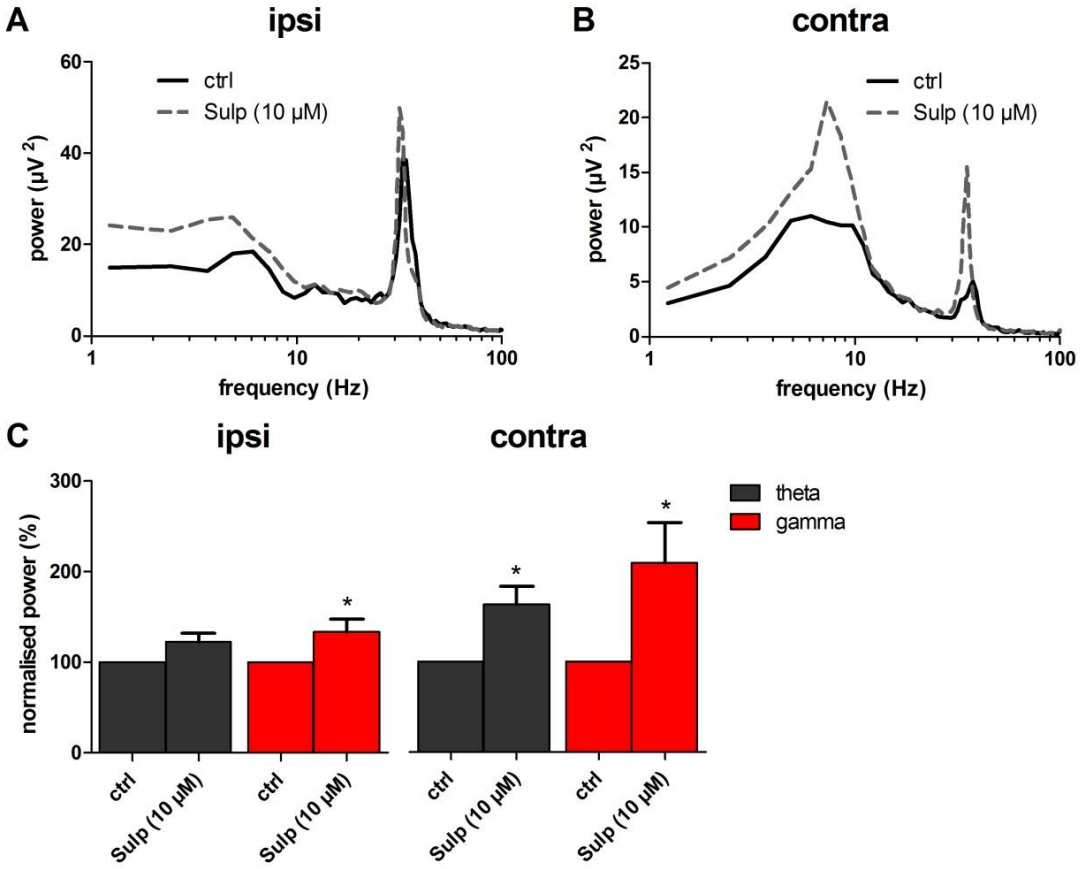


**Figure 4.20 In 6-OHDA lesioned rats, sulpiride (10 µM) increases the power of contralateral oscillations and only gamma oscillations in ipsilateral slices (A)** Typical power spectra demonstrating peak responses before (solid line) and after application of 10 µM sulpiride (Sulp, dashed line) in ipsilateral hemisphere. **(B)** Typical power spectra demonstrating peak responses before (solid line) and after application of 10 µM sulpiride (Sulp, dashed line) in contralateral hemisphere **(C)** Peak power changes of theta (grey bars) and gamma (red bars) oscillations normalised to control in ipsilateral and contralateral hemispheres. Ipsi = ipsilateral, Contra = contralateral. *, p<0.05.

## 4.3 Discussion

In this chapter we have pharmacologically characterised the dopaminergic modulation of both theta and gamma oscillatory power in the M1 network in DA-intact and DA-depleted slices. Initially, no overall effect was observed on DA application in DA-intact slices obtained from young animals (50-100 g), although, in general, application of D1-like and D2-like receptor agonists as well as the antagonists increased both theta and gamma oscillatory power. These results are difficult to reconcile unless one postulates differing DA concentrations from slice to slice and propose the possibility other non-specific receptor-mediated effects such activity at $\alpha_1$-adrenergic receptors (see Ozkan et al., 2016).

In slices obtained from older animals (290-310 g), DA application significantly decreased gamma oscillatory power in DA-depleted (ipsilateral) slices, an effect not observed in contralateral slices or those obtained from DA-intact AMC animals. Furthermore, AMPH only decreased gamma power in DA-intact slices (contralateral and AMC), as expected if DA (or noradrenaline or 5-HT) was being released from intact terminals. Application of DA, apomorphine or amphetamine all showed a trend to, or significant increases in, theta oscillatory power. Interestingly, quinpirole consistently increased both theta and gamma power in AMC and contralateral slices, whereas gamma power was not affected in ipsilateral DA-depleted slices.

Overall, these data suggest that DA and its receptors mediate a series of complex interactions which affect the power of theta and gamma oscillations in M1.

### 4.3.1 Dopamine-depletion on oscillatory profiles

We had hypothesised that the ipsilateral DA-depleted hemisphere and contralateral DA-intact hemisphere would show contrasting oscillatory profiles. However, no significant differences were observed between the control frequency and power of the theta and gamma oscillations. It is possible that the contralateral hemisphere does exhibit some DA-depletion and this is affecting the profile. However, when we assessed activity in slices from AMC animals, they also showed a similar profile. Therefore no changes in the frequency or power of theta or gamma oscillations and no evidence of enhanced activity in the beta frequency range was observed as a result of DA-depletion.

It is generally accepted that DA depletion leads to exaggerated beta oscillations in patients (Brown et al., 2001; Brown and Williams, 2005) and in animal models of PD (Nini et al., 1995; Sharott et al., 2005; Hammond et al., 2007; Mallet et al., 2008a; Mallet et al., 2008b) (see section 1.3.2.1). Therefore it appears that M1 can support the local generation of oscillations in the reduced slice preparation, but that DA-depletion cannot generate pathological oscillations like those observed *in vivo*. However, we do know that stimulation of M1 can reduce pathological oscillations (Pagni et al., 2003; Drouot et al., 2004; Lefaucheur et al., 2004), which suggests a critical role of M1 in the modulation and control of information flow throughout the intact cortico-BG network.

### 4.3.2 Dopamine receptors on neuronal activity

Research on DA signalling and modulation of neuronal activity has concentrated on the pre-frontal cortex (PFC), which receives direct dopaminergic modulation from midbrain DA neurons of the VTA (for review see Seamans, 2010 and Tritsch and Sabatini, 2012). However, the literature regarding individual DA receptors and their specific effects is inconsistent.

#### *4.3.2.1 General effects of DA application*

A study by Seamans et al. (2001a) outlined the contrasting role of the D1-like and D2-like receptors on pyramidal neurons in PFC. They demonstrated that after the application of DA, there was a time-dependent modulation of IPSC amplitude over a period of 50 mins. They found that the initial (<20 min) response to DA was mediated by D2-like receptors, resulting in a decrease in IPSC amplitude and therefore an increase in the excitability of pyramidal neurons recorded. In contrast, 20-50 mins after DA application they observed an increase in IPSC amplitude, above original baseline levels, mediated via D1-like receptors, which increased inhibition of pyramidal neurons to reduce excitability (Seamans et al., 2001a). Furthermore, the activation of both D1-like and D2-like receptors in striatum had opposing effects on GABA release (Harsing and Zigmond, 1997). This demonstrates not only the possibility of competing D1-like and D2-like receptor mediated effects but also the importance of overlapping or competing time-dependent effects. Our experiments last 40 mins from point of drug application. Therefore, our analysis of the effect of DA could be hindered by the point of cross-over between D2-like and D1-like receptor dominance, if indeed we are observing these effects in our slices. This could potentially be a reason why we do not observe a consistent response of DA in our slices. Alternatively, the inconsistent response to applied DA could be due to variable concentrations of DA

present between slices such that only those exhibiting low ambient levels of DA respond to DA application.

In addition, recent studies have suggested the involvement of $\alpha_{1/2}$-adrenergic receptors in DA receptor mediated responses. A study by Yang et al. (2014) found that a DA-induced membrane hyperpolarisation was mediated by adrenergic receptors. Furthermore, it has been shown in PFC that D1 receptors and adrenergic receptors can co-localise in the dendrites of neurons, potentially resulting in the generation of heterodimeric receptor complexes that have altered signalling and activation properties (Prinster et al., 2005; Rashid et al., 2007; Gonzalez et al., 2012; Rebois et al., 2012; Mitrano et al., 2014).

In a concomitant but separate study in our laboratory, using slices from young animals (50-100 g), Ozkan et al. (2016) found that application of DA resulted in a small but significant decrease in gamma oscillatory power. However, SKF and QUIN application both resulted in significant power increases (as in this study). Application of the α1-adrenergic agonist phenylephrine (10 µM) mimicked the effect of DA and the α1-adrenergic antagonist prazosin (10 µM) blocked the effect of DA, indicating an interaction between the dopaminergic and adrenergic system. Therefore, it is possible that these DA-α1 receptor complexes are present within M1 and could be contributing to the variable results we have observed in slices obtained from young animals (50-100 g).

#### *4.3.2.2 DA application significantly decreases gamma oscillatory power in DA-depleted slices*

We observed a significant decrease in gamma oscillatory power in DA-depleted ipsilateral slices, associated with DA application. Presumably the action of applied DA is masked by the levels of DA already present in DA-intact slices. Overall, there are a number of pre- and post-synaptic mechanisms by which DA receptor activation could affect the excitability of both pyramidal cells and interneurons involved in the generation of network activity.

DA has been shown to induce membrane depolarisation and increase the excitability of pyramidal neurons in PFC through the enhanced activity of slowly-inactivating $Na^+$ currents, an increase in the conductance of NMDA channels and the attenuation of slow-inactivating $K^+$ currents (Yang and Seamans, 1996; Durstewitz et al., 2000; Henze et al., 2000; Durstewitz and Seamans, 2002). Furthermore, D1-like receptor activation increases EPSC amplitude by $Ca^{2+}$ modulation and protein kinase A (PKA) signalling (Gonzalez-

Islas and Hablitz, 2003), an effect also observed in striatum (Calabresi et al., 1992; Cepeda et al., 2001; Tang et al., 2001).

DA also inhibits the activity of the FS-interneuronal network (Weiss et al., 2003; Ikegaya et al., 2004). D1 and D2-like receptor activation has been shown to reduce the amplitude of IPSCs on FS-interneurons (Zaitsev et al., 2007; Towers and Hestrin, 2008) through presynaptic reduction of GABA release (Harsing and Zigmond, 1997; Cooper and Stanford, 2001; Momiyama and Koga, 2001). However, there are reports that activation of D1-like receptors has been shown to increase IPSC amplitude and frequency (Harsing and Zigmond, 1997; Seamans et al., 2001b; Trantham-Davidson et al., 2004).

In summary, DA is generally believed to increase the excitability of pyramidal cells but reduce inhibition in the inhibitory network, both of which could result in a loss of synchronous network activity.

#### *4.3.2.3 AMPH decreases gamma oscillations in DA-intact slices*

AMPH induces the release of DA from intact pre-synaptic DA terminals by the active exchange of DA (Chiueh and Moore, 1975; Jones et al., 1998; Mair and Kauer, 2007). In our experiments, AMPH only decreased gamma in DA-intact slices (contralateral and AMC) and had no effect in DA-depleted (ipsilateral) slices. This would be expected if AMPH was acting to release DA from an extensive population of intact terminals. Although we have assumed DA depletion, through behavioural testing of animals prior to obtaining brain slices, we have not directly confirmed the loss of DA terminals by, for example, histological studies. However, the AMPH results presented do endorse the assumption that our slices are extensively DA-depleted.

AMPH has also been shown to release noradrenaline, 5-HT and ACh as well as DA (Raiteri et al., 1975; Mandel et al., 1994). Therefore, we cannot be certain that the effects observed in DA-intact slices are solely due to action of DA on DA receptors.

#### *4.3.2.4 Application of DA, apomorphine or amphetamine increases theta oscillatory power*

Theta oscillations are suggested to be the result of synchronous intrinsic membrane potentials in the hippocampus and cortex (Bland et al., 1988; Leung and Yim, 1991; Konopacki et al., 1992b; Bland and Colom, 1993; Bland et al., 2002). Theta oscillations in our slices showed a propensity to increase in power in the presence of DA, AMPH or APO

as would be expected if DA acts to increase membrane excitability and increase sub-threshold membrane potentials.

Injection of AMPH into the VTA *in vivo* has been shown to elicit theta oscillations, presumably via the induction of DA release (Orzel-Gryglewska et al., 2013) and more recent work in the PFC has suggested that in patients and animal models of PD, theta oscillatory power is attenuated (Parker et al., 2015). However, past studies have also shown that neocortical and hippocampal theta in rodents was not affected by the loss of DA (Whishaw et al., 1978) while Weiss et al. (2003) reported that intrinsic membrane potentials at theta frequency in slices of rodent hippocampus were not altered by the application of DA.

Interestingly, while we did see a significant increase in the power of theta oscillations with the application of apomorphine, we did not see the same effect with dopamine application. As apomorphine is a broad agonist of dopamine receptors, the same as dopamine, we would have expected to see similar results from both. It is possible that when we are applying dopamine it is becoming oxidised, reducing the activation of the receptors, or the rate of uptake of dopamine via DA reuptake transporters and mechanisms is reducing the effective dopamine response we observed in the network. We also have to be aware of the potential for non-specific effects of apomorphine on non-dopamine receptors, such as its antagonistic activity at 5-HT and α-adrenergic receptors (Millan et al., 2002; LeWitt, 2004). Therefore it is possible that these differences and non-specific effects are what result in the differential responses we observed in these studies.

The use of amphetamine in the DA-depleted/intact and AMC slices also appeared to result in a reduction of theta oscillation frequency. This change appeared to be consistent across the AMC and lesioned slices and was still within the frequency band analysed for changes in theta oscillatory power. It is possible that this effect is a result of the increased power than amphetamine produced in the theta oscillations, due to an increased contributory network involved in the oscillation, which may result in reduced oscillation frequency. Though, the changes in frequency could also be due to changes in receptor activation that may alter the decay time kinetics of receptors responsible for the timing of the theta oscillation. The final possibility is that these are simply natural changes that the slices have undergone over the course of the experiment. Regardless, without further experiments to assess whether the changes we have observed are due to the specific action on a particular DA receptor, using amphetamine in combination with different DA-

receptor antagonists, the full impact of amphetamine on network dynamics cannot be fully understood.

#### *4.3.2.5 D2-like mediated increase in gamma power is lost in DA-depleted slices*

We have observed significant increases in the power of our theta and gamma oscillations after activation of D2-like receptors by their specific agonist quinpirole in young (50-100 g) and old (290-310 g) DA-intact slices. However, the increase in gamma power was not seen in DA-depleted (ipsilateral) slices. D2-like receptors are known to be located pre-synaptically on dopaminergic fibres, acting as feedback auto-receptors to inhibit the release of DA (Aghajanian and Bunney, 1977; Carlson et al., 1987; Lacey et al., 1987). Therefore this result is easily explained by the loss of DA innervation to M1 during the lesioning process. In contrast, theta oscillations in our slices also showed increases in oscillatory power after the application of quinpirole, even in the DA-depleted slices suggesting that the postsynaptic D2-like receptors are still present in M1 after lesioning and can modulate intrinsic membrane potentials involved in theta generation.

#### *4.3.2.6 Age-related effects*

Between the young animals (50-100 g) and AMC older (290-310 g) animals, there are some noticeable differences in the response of the theta and gamma oscillations to the application of different dopaminergic drugs.

A brief observation is that the magnitude of any changes observed in response to drug application is reduced in the AMC slices, as well as the level of significance of such changes. Additionally, the response of both theta and gamma oscillations to SCH 23390 in the older animals is lost. This is a surprising result, as you would usually expect to see no differences in what we consider to be “control” animals. However, there are many different changes that occur in the brain throughout maturity, which could have some impact on the networks that generate these oscillations (Kolb et al., 1998). These changes that occur between the different ages could be attributable to the consolidation of the neuronal networks present in the rodents from young to old.

Alternatively, there are limitations to using older animals in *in vitro* work. Older animals, by virtue of them being larger, are more difficult to anaesthetise quickly and prepare slices from in comparison to younger animals. Therefore, this could result in unforeseen neuronal death in the networks which is not present in slices prepared from younger animals. This may explain the reduced response with the application of the drugs, as there is a less connected network which mediates the oscillations to manipulate with

drugs. The lack of significant change in the oscillations of older slices with the application of SCH 23390 could also be explained through these limitations. As well this could be due to the unequal health of older slices or due to the less abundant network present in the slice.

#### *4.3.2.7 Limitations*

These studies have outlined some of the basic responses of our oscillations in M1 in both the DA-intact and DA-depleted slices. However, while these can inform us about the potential impact of DA-depletion upon the networks present in M1 and the relative contributions and changes that the network may be undertaking in PD; there are several limitations to this study which must be considered.

In the use of the specific D1-like receptor agonist SKF 38393 and antagonist SCH 23390, we observed that these both resulted in increased oscillatory power in our young (50-100 g) and older (250-310 g) animals. These could be considered the main effects of the drugs specifically at D1-like receptors. However, SKF 38393 is known to be only a partial agonist at D1-like receptors, which means that it competes for the activation site with the endogenous ligand. While this means it is still an agonist at these sites, the activation rate could overall be lower than it would be with the actual ligand present. Thus, SKF 38393 could only be having a partial agonistic effect on our oscillations, which may result in the responses we have observed. This potential mixed response by the SKF 38393 could be mitigated through the use of other agonists in order to clarify the response we observed. Furthermore, SCH 23390 is also believed to act as an agonist at 5-$HT_{1C+2C}$ receptors, shown previously in cloned human receptors (Millan et al., 2001). Therefore, without additional experiments using a specific antagonist of D1-like receptors it possible that the effects we observed in our experiments are actually mediated by non-specific actions at other receptors.

Furthermore, the effects of the D1-like and D2-like receptor antagonists (SCH 23390 and sulpiride) on oscillations from the ipsilateral hemispheres of 6-OHDA lesioned animals are potentially difficult to reconcile. We would have expected to see no change in the power of our theta and gamma oscillations when blocking the dopamine receptors in ipsilateral slices, as we would not expect there to be dopamine present activating these receptors to begin with. It is possible that there are dopamine terminals, from sources other than the MFB such as the VTA, which may be innervating M1 networks. Alternatively, we have to assume that there will be some remaining dopamine terminals or fibres which were damaged during the slicing procedure. It is possible that dopamine released from these

damaged terminals into the surrounding tissue may be resulting in the activation of dopamine receptors in the network. Additionally, as we sliced and stored our brain slices from ipsilateral and contralateral hemispheres in the same interface chamber, there is the possibility that DA from the intact hemisphere could have become mixed into the solution and activated receptors in the depleted hemisphere.

In order to avoid these potential issues in the future, brain slices could be stored in separate chambers prior to experiments being performed. Likewise, multiple antagonists and agonists of the different dopamine receptors could be utilised in order to control for the effects of non-specific drugs. Future studies would also benefit from performing immunohistochemistry staining for TH+ neurons and DA reuptake transporters in order to verify the presence or loss of DA neurons in M1. This would not only help in confirming our lesioning but also would allow greater comparisons between amount of loss and oscillatory power or pharmacological changes.

## 4.4 Conclusions

In this chapter we have demonstrated that DA modulation of M1 has complex and sometimes variable effects on CCh and KA induced theta and gamma oscillations in M1. Although we have observed differences in the modulation of oscillations in slices obtained from young (50-100 g) animals and older (290-310 g) AMC and lesioned animals, a number of key conclusions can be made (an overall summary is in **table 4.1**). These include DA-depleted slice-specific decreases in gamma oscillatory power after DA application and loss of decreased gamma power after AMPH application. Additionally, the effect of D2-like receptor activation is lost in lesioned slices, consistent with the pre-synaptic action of D2-like receptors in reducing DA release from intact fibres. Finally DA increases in theta oscillatory power were most probably due to the enhancement of intrinsic subthreshold oscillations.

Furthermore, in contrary to previous studies of PD *in vivo*, we did not observe the emergence of pathological oscillatory activity in M1, suggesting the importance of an intact cortico-BG network in their generation. In order to further examine the changes that individual D1-like and D2-like receptors undergo between these slice conditions, we could use immunofluorescence or immunohistochemistry to identify the locations of the receptors in the slices or on particular cell types. Furthermore, the involvement of the different dopamine receptors on specific neuronal types could further be examined

through the use of fluorescent sensors sensitive to $Ca^{2+}$ changes, as an indicator of activity. This could begin to demonstrate the relative involvement or lack of involvement that different cells in the network demonstrate in relation to dopaminergic signalling. If we could begin to understand the role that dopaminergic signalling plays in network oscillations in control animals, we could begin to investigate the individual role that different DA receptors have in signalling in PD. This could be through similar experiments or could involve different genetic KO's of receptors, on either a global or targeted scale. For instance, targeted knock out of the D2-like receptor of a wild type animal may start to explain why we do not see a response to D2-like receptor activation in the lesioned animals.

| Drug | | N (slice) | Theta power | Gamma power |
|---|---|---|---|---|
| **Young (50-100 g)** | | | | |
| **Dopamine** | **30 µM** | 9 | - | - |
| **Apomorphine** | **20 µM** | 15 | ↑↑↑ | - |
| **SKF38393** | **10 µM** | 25 | ↑↑↑ | ↑↑↑ |
| **SCH 23390** | **2 µM** | 10 | ↑↑ | ↑ |
| **Quinpirole** | **10 µM** | 9 | ↑↑ | ↑ |
| **Sulpiride** | **10 µM** | 9 | ↑↑ | - |
| **AMC (280-310 g)** | | | | |
| **Dopamine** | **30 µM** | 11 | - | - |
| **Amphetamine** | **20 µM** | 13 | ↑↑ | ↓↓ |
| **SKF38393** | **10 µM** | 13 | ↑↑ | ↑↑ |
| **SCH 23390** | **2 µM** | 11 | - | - |
| **Quinpirole** | **10 µM** | 12 | ↑↑ | ↑ |
| **Sulpiride** | **10 µM** | 7 | ↑ | ↑ |
| **Ipsilateral hemispheres (280-310 g)** | | | | |
| **Dopamine** | **30 µM** | 10 | ↑↑ | ↓ |
| **Amphetamine** | **20 µM** | 9 | ↑↑ | - |
| **SKF38393** | **10 µM** | 16 | ↑ | ↑↑ |
| **SCH 23390** | **2 µM** | 13 | - | - |
| **Quinpirole** | **10 µM** | 14 | ↑↑ | - |
| **Sulpiride** | **10 µM** | 10 | - | ↑ |
| **Contralateral hemispheres (280-310 g)** | | | | |
| **Dopamine** | **30 µM** | 6 | - | - |
| **Amphetamine** | **20 µM** | 8 | - | ↓↓ |
| **SKF38393** | **10 µM** | 10 | ↑ | ↑↑ |
| **SCH 23390** | **2 µM** | 9 | ↑↑ | ↑↑ |
| **Quinpirole** | **10 µM** | 7 | - | ↑ |
| **Sulpiride** | **10 µM** | 6 | ↑ | ↑ |

**Table 4.1 Summary table of drugs used to pharmacologically characterise theta and gamma oscillations.** Listed are names of individual drugs, the N's per experiment, the changes to oscillatory power for theta and gamma oscillations.

# Chapter 5 *In vivo* oscillations in M1 of 6-OHDA lesioned animals

## 5.1 Introduction

*In vivo,* beta oscillations (12-25 Hz) have been associated with a resting or idling state, consisting of pre-movement preparation or anticipation (Cheyne et al., 2008; Tzagarakis et al., 2010), and may also have a role in maintaining posture or tonic contraction (Baker et al., 1997; Jenkinson and Brown, 2011). During movement execution, beta oscillations undergo several changes in power in M1. Event-related desynchronisation (ERD) precedes movement and is associated with a decrease in beta oscillatory power (Crone et al., 1998; Pfurtscheller et al., 2003; Jurkiewicz et al., 2006). During movement, brief bursts of gamma oscillations (30-80 Hz) can be observed which are thought to be involved with the actual processing of the movement (Pfurtscheller et al., 1993; Brown et al., 1998; Crone et al., 1998; Cheyne et al., 2008). Post-movement beta rebound (PMBR) follows upon the completion of movement, with a resynchronisation of beta oscillatory power which may represent inhibition of M1 (Salmelin et al., 1995; Jurkiewicz et al., 2006). These dynamic changes in M1 oscillations demonstrate very specific roles in movement for beta and gamma oscillations.

The loss of dopamine (DA) fibres from the SNc results in the excessive synchronisation of beta frequency oscillations throughout the cortico-BG network (Wichmann and DeLong, 1999; Brown et al., 2001; Bevan et al., 2002; Brown, 2003; Brown and Williams, 2005; Mallet et al., 2008b; Brazhnik et al., 2012). Exaggerated beta oscillations are thought to contribute to the hypokinetic symptoms experienced by PD patients, such as bradykinesia and rigidity (Chen et al., 2007). It remains a matter of debate as to whether the reduction in beta is directly related to the improvement in motor ability.

The primary treatment for PD is the administration of the DA precursor L-DOPA, which replenishes DA levels after undergoing conversion in catecholaminergic terminals. Administration of L-DOPA induces a concurrent reduction in pathological beta oscillations present in the cortico-BG network and improvement in the motor symptoms of PD in patients (Brown et al., 2001; Kuhn et al., 2006). However, one in five patients with Parkinson's fails to respond to DA replacement therapy which becomes progressively less effective and leads to wearing off effects, periods of 'freezing' and unpredictable movements as well as sickness, low blood pressure, hallucinations and confusion. Furthermore, late-stage cognitive decline associated with PD is not improved by dopaminergic therapies. Therefore, drug targets other than those which affect the DA system are urgently required (Davie, 2008; Kalia and Lang, 2015).

Zolpidem is commonly used as a sedative and is a non-benzodiazepine modulator of $GABA_A$ receptors, specific for those that contain the $\alpha_1$-subunit. Recent work *in vivo* has also demonstrated that sub-sedative doses of zolpidem (in the nM range) can reduce presumed pathological activity and improve deficits observed in vegetative states and stroke (Clauss and Nel, 2006; Brefel-Courbon et al., 2007; Hall et al., 2010). In PD patients studies have further demonstrated that sub-sedative doses of zolpidem *in vivo* can improve motor symptoms and at the same time desynchronise pathological beta oscillations in M1 (Hall et al., 2014). In PD patients specifically, improvements in movement ability were correlated with a balancing of beta oscillatory power between hemispheres (interhemispheric ratio). The excessive beta oscillatory power in the DA-depleted hemisphere is reduced, as the beta oscillatory power DA-intact hemisphere is increased (Hall et al., 2014).

In this chapter we have used the 6-OHDA unilateral rodent model of PD to evaluate the long-term effects of the lesion on motor behaviour, the oscillatory profile in each layer of M1 and compared how the oscillatory power is altered after L-DOPA and zolpidem application.

## 5.2 Results

### 5.2.1 Evaluation of 6-OHDA lesions

Unilateral 6-OHDA lesions of male Sprague-Dawley rats (280-320 g) were performed (see 2.2.1.1). Following surgery, animals were allowed to recover for 2 weeks, after which the success of the lesion was assessed using rotations in a rotometer (Ungerstedt, 1971), and during locomotor activity (LMA) in an open field (Cools et al., 1990), as well as the adjusting step test (Olsson et al., 1995).

#### *5.2.1.1 The rotometer test*

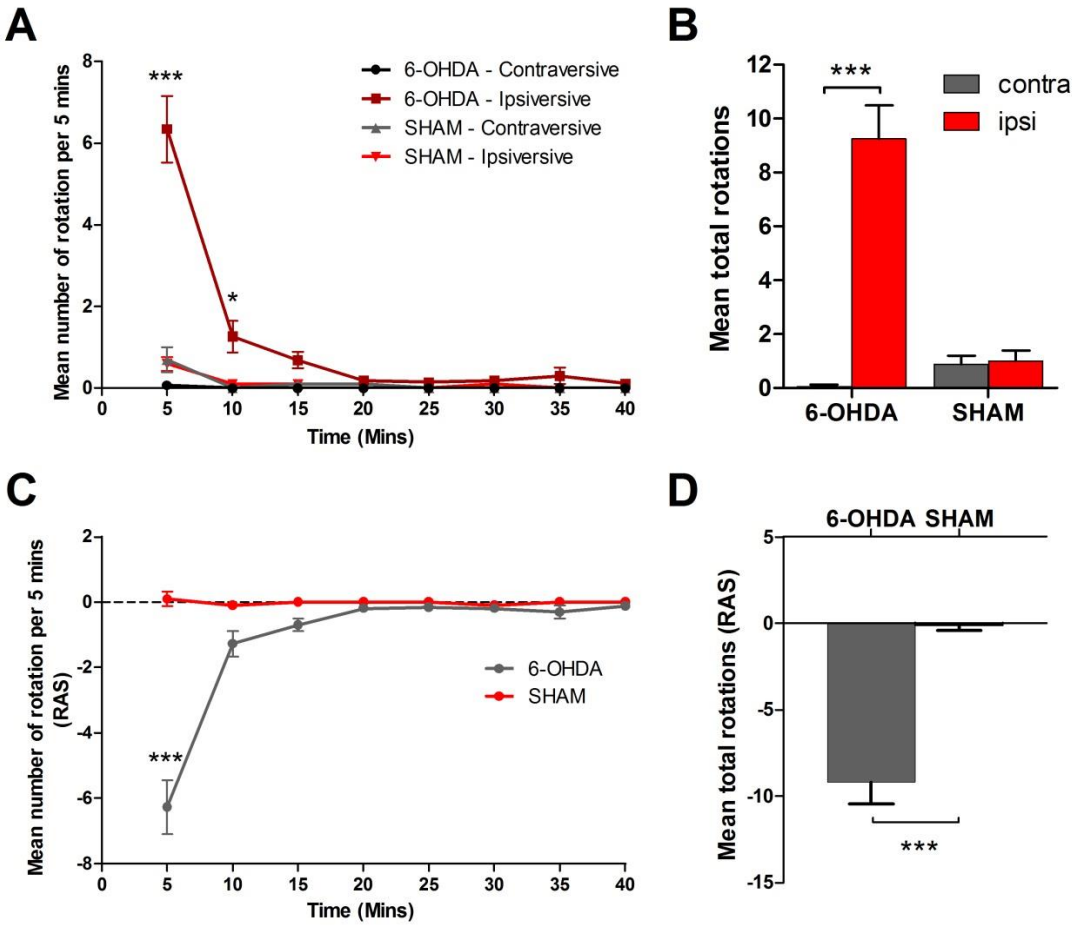


**Figure 5.1 Rotometer testing demonstrated significant differences between the lesioned and sham animals. (A)** Mean rotations per 5 min epoch in contraversive (black and grey and ipsiversive (dark red and light red) directions in 6-OHDA (black and dark red) and SHAM (grey and light red) animals. **(B)** Bar graph showing mean total rotations for 40 mins in each direction (contraversive, grey; ipsiversive, red) for each condition group. **(C)** Mean rotations per each 5 min epoch for each condition (6-OHDA, grey; SHAM, red) shown as the rotational asymmetry score (RAS). **(D)** Bar graph showing mean RAS for total 40 mins in each condition (6-OHDA, grey; SHAM, red). ***, p<0.001, *, p<0.05.

Rotometer tests are usually accompanied by a pharmacological prompt (apomorphine or amphetamine) to induce robust rotations (Ungerstedt, 1971; Creese et al., 1976; Perese et al., 1989). However, to prevent any possible conflicts with later pharmacological experiments, only basal non-drug induced rotations were used. Animals were assessed individually over a period of 40 mins and data grouped into 5 min epochs. Data was presented as full $360^{o}$ rotations in contraversive (clockwise towards the non-lesioned hemisphere) and ipsiversive (counter-clockwise towards the lesioned hemisphere) directions. The results may make it appear that animals do not move greatly after the first 10-15 min epochs but this is usual for animals investigating their surroundings and subsequently resting. Mean total rotations for the whole 40 min period demonstrate that there are clear differences present between the lesioned and non-lesioned groups even when averaged.

In the first 5 min epoch, lesioned animals (6-OHDA) showed a significant bias towards ipsiversive rotations (6.35 ± 0.81 rotations, n=26 animals, **Fig 5.1A**), compared to 6-OHDA contraversive rotations and sham animals in both directions ($p<0.001$). This was also demonstrated in the 10 min epoch (1.27 ± 0.39 rotations, n=26 animals, $p<0.05$, **Fig 5.1A**). In pooled data from all epochs (**Fig 5.1B**), lesioned animals demonstrated a clear preference for ipsiversive compared to contraversive rotations (9.27 ± 1.23 rotations, n=26 animals, $p<0.001$, **Fig 5.1B**) while sham animals demonstrated no significant preference in either direction of rotation (contraversive: 0.90 ± 0.31 rotations, n=10 animals, ns; ipsiversive: 1.00 ± 0.39 rotations, n=10 animals, ns; **Fig 5.1B**). On calculating the rotational asymmetry score (RAS), lesioned animals were significantly different in the initial 5 min epoch (-6.27 ± 0.83 RAS, n=26 animals, $p<0.001$, **Fig 5.1C**) and when pooled the RAS's for lesioned animals (-9.19 ± 1.25 RAS, n=26 animals, $p<0.001$, **Fig 5.1D**) were significantly different compared to sham animals (-0.10 ± 0.99 RAS, n=10 animals, **Fig 5.1D**). One 6-OHDA animal was excluded from electrophysiological experiments as their RAS was similar to sham animals, indicating an inadequate lesion.

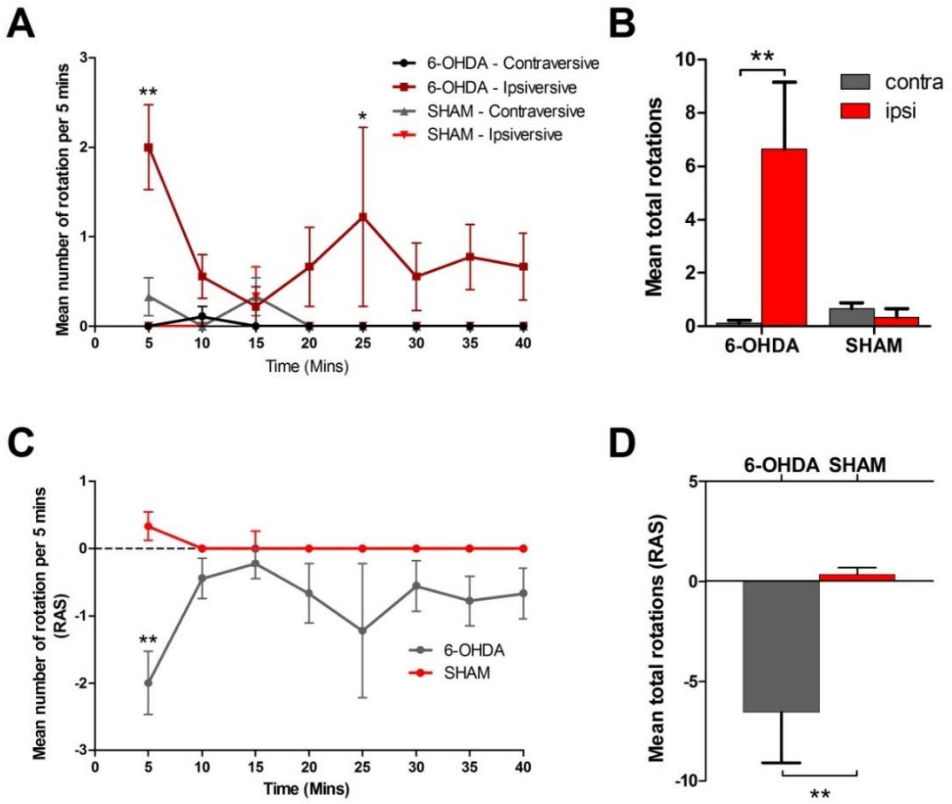


**Figure 5.2 Long-term rotometer testing demonstrated lesions persisted after 22 weeks. (A)** Mean rotations per each 5 min epoch in each direction (contraversive, black and grey; ipsiversive, dark red and light red) in both conditions (6-OHDA, black and dark red; SHAM, grey and light red). **(B)** Bar graph showing mean total rotations for the total 40 mins in each direction (contraversive, grey; ipsiversive, red) for each condition group. **(C)** Mean rotations per each 5 min epoch for each condition (6-OHDA, grey; SHAM, red) shown as the rotational asymmetry score (RAS). **(D)** Bar graph showing mean RAS for total 40 mins in each condition (6-OHDA, grey; SHAM, red). **, p<0.01, *, p<0.05.

After 22 weeks lesioned animals continued to show a significant bias toward ipsiversive rotations over contraversive rotations in the 5 min (2.00 ± 0.47 rotations, n=9 animals, p<0.001, **Fig 5.2A**) and 25 min (1.22 ± 1.00 rotations, n=9 animals, p<0.05, **Fig 5.2A**) epochs. Pooled data from all epochs showed that ipsiversive rotations (6.67 ± 2.49 rotations, n=9 animals, p<0.01, **Fig 5.2B**) were significantly different to contraversive rotations (0.11 ± 0.11 rotations, n=9 animals, ns) and to sham animals in both directions (ipsiversive: 0.33 ± 0.33 rotations, n=6 animals, ns; contraversive: 0.67 ± 0.21 rotations, n=6 animals, ns, **Fig 5.2B**). Using RAS, lesioned animals exhibited significant directional bias during the first 5 min epoch (-2.00 ± 0.47 RAS, n=9 animals, p<0.01, **Fig 5.2C**) compared to sham lesioned animals (0.33 ± 0.21 RAS, n=6 animals) and pooled RAS scores were also significantly different for lesioned animals compared to sham animals (lesioned: -6.56 ± 2.51 RAS, n=9 animals; sham: +0.33 ± 0.33 RAS, n=6 animals; p<0.01, **Fig 5.2D**).

*5.2.1.2 Locomotor activity (LMA) test*

The LMA test was used to test rotational activity in an open field (Cools et al., 1990). The Ethovision XT (Noldus, Netherlands) software recorded basal movement over a period of 40 min and calculated the number of rotations in both contraversive and ipsiversive directions, where a turn greater than 90$^{o}$ was counted as one rotation (based on a 2-point head-centre analysis).

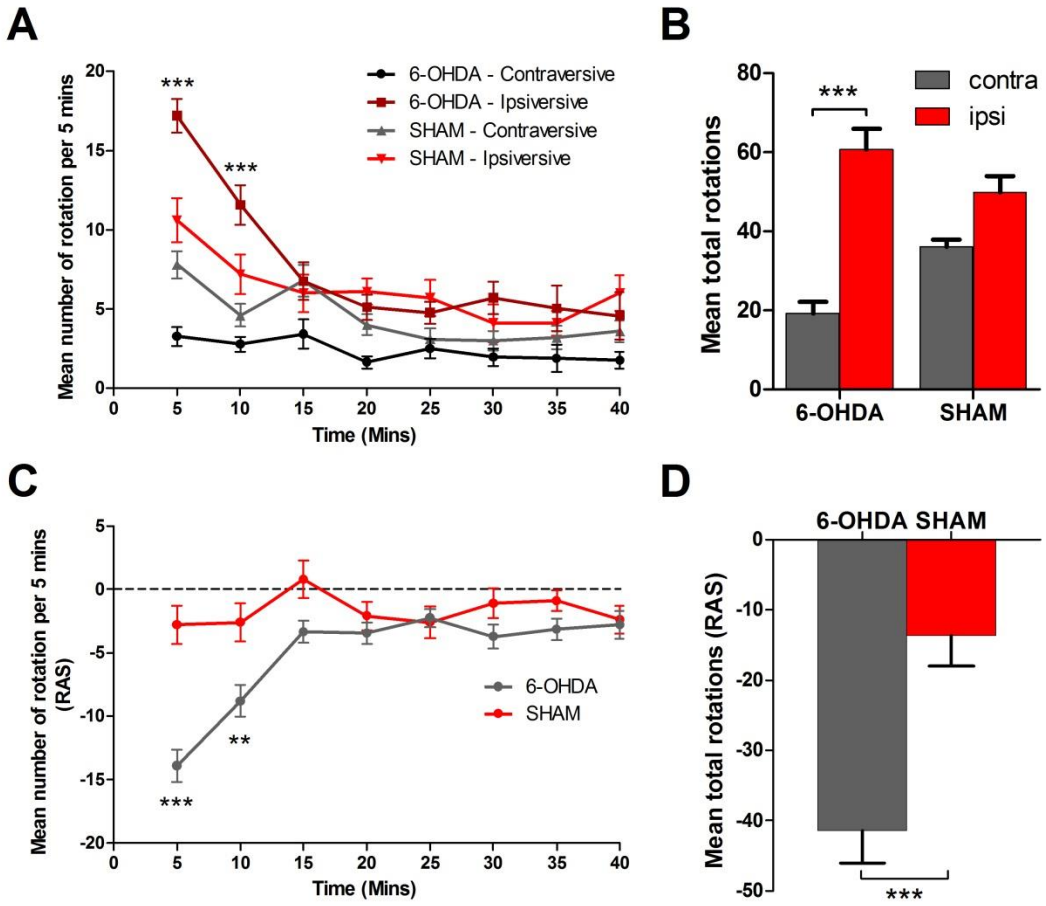


**Figure 5.3 LMA testing demonstrated differences between the lesioned and sham animals.** **(A)** Mean rotations per each 5 min epoch in each direction (contraversive, black and grey; ipsiversive, dark red and light red) in both conditions (6-OHDA, black and dark red; SHAM, grey and light red). **(B)** Bar graph showing mean total rotations for the 40 mins period in each direction (contraversive, grey; ipsiversive, red) for each condition group. **(C)** Mean rotations per each 5 min epoch for each condition (6-OHDA, grey; SHAM, red) shown as the rotational asymmetry score (RAS). **(D)** Bar graph showing mean RAS for total 40 mins in each condition (6-OHDA, grey; SHAM, red). ***, p<0.001, **, p<0.01, *, p<0.05.

In the initial 5 and 10 min epochs, lesioned animals had a significantly higher number of ipsiversive rotations (5 min: 17.19 ± 1.05, n=26 animals; 10 min: 11.58 ± 1.25, n=26 animals, **Fig 5.3A**) compared to contraversive rotations (5 min: 3.27 ± 0.60, n=26 animals, p<0.001; 10 min: 2.77 ± 0.47, n=26 animals, p<0.001, **Fig 5.3A**). Sham lesioned animals

had no significant bias towards either contraversive or ipsiversive direction. On pooling all epochs lesioned animals demonstrated significant bias towards ipsiversive rotations (60.73 ± 5.21, n=26 animals, p<0.001, **Fig 5.3B**) rather than contraversive rotations (19.23 ± 2.90, n=26 animals, **Fig 5.3B**). Sham lesioned animals had no significant bias towards either the ipsiversive rotations (49.80 ± 4.16, n=10 animals, ns, **Fig 5.3B**) or contraversive rotations (36.10 ± 1.72, n=10 animals, **Fig 5.3B**).

Using RAS, lesioned animals exhibited significant directional bias during the 5 and 10 min epochs (5 min: -13.92 ± 1.28, p<0.001; 10 min: -8.81 ± 1.27, p<0.01; n=26 animals, **Fig 5.3C**), compared to sham lesioned animals (5 min: -2.80 ± 1.52; 10 min: -2.60 ± 1.51; n=10 animals, **Fig 5.3C**). On pooling all RAS data, lesioned animals exhibited significant directional bias (-41.50 ± 4.52, n=26 animals, p<0.001, **Fig 5.3D**) compared to sham animals (-13.70 ± 4.27, n=10 animals, **Fig 5.3D**). The LMA results from the presumed non-lesioned animal identified in the rotometer test were consistent with sham animals.

*5.2.1.3 Adjusting step test*

The adjusting step test was developed by Olsson et al. (1995) to test forelimb akinesia in rat PD models (see methods section 2.2.2.1), a low score indicating a successful lesion.

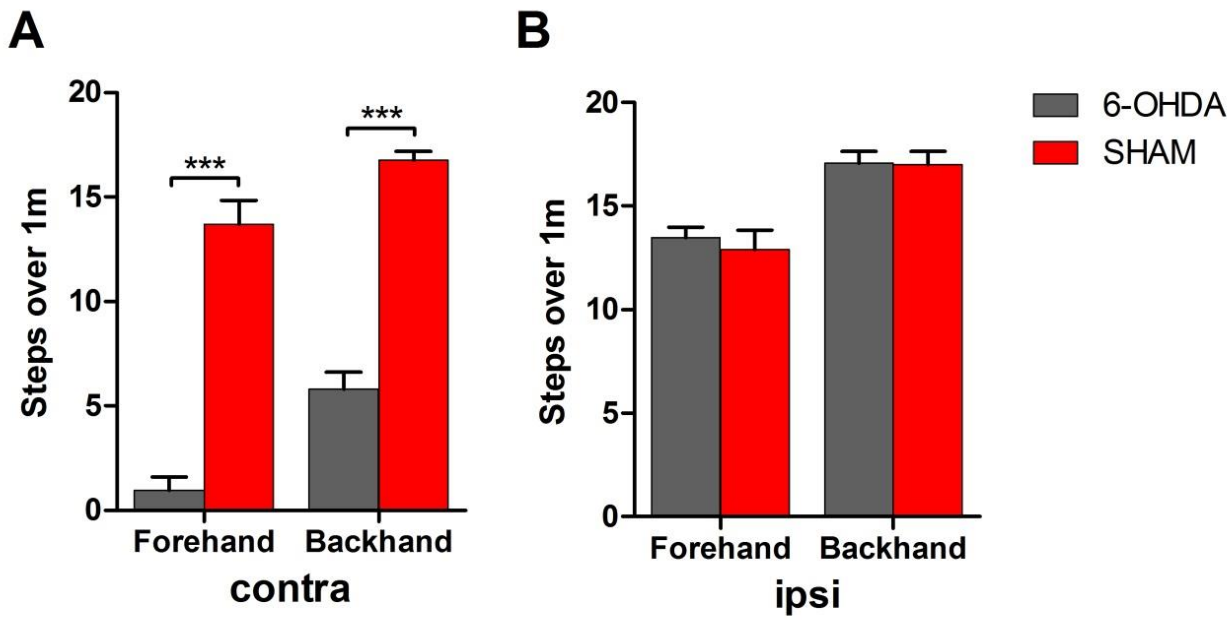


**Figure 5.4 Adjusting step test identified significant forelimb bias in the 6-OHDA lesioned rats. (A)** Bar graph showing mean total number of steps over a 1m space when assessing the contralateral paw in both the forehand and backhand directions. **(B)** Bar graph showing mean total number of steps over a 1m space when assessing the ipsilateral paw in both the forehand and backhand directions. Grey bars, 6-OHDA lesioned. Red bars, SHAM lesioned.

In contralateral limbs (the side of body controlled by the lesioned hemisphere), lesioned animals performed significantly less adjustment steps than sham animals (**Fig 5.4A**). There was a significant difference in both the forehand (6-OHDA: 0.96 ± 0.65 steps, n=26 animals; SHAM: 13.70 ± 1.13 steps, n=10 animals; p<0.001, **Fig 5.4A**) and the backhand (6-OHDA: 5.80 ± 0.82 steps, n=26 animals; SHAM: 16.75 ± 0.44 steps, n=10 animals; p<0.001, **Fig 5.4A**) directions. In comparison, ipsilateral limbs (the side of body controlled by the non-lesioned hemisphere, **Fig 5.4B**) were not significantly different between lesioned and sham animals. No difference was seen in either the forehand (6-OHDA: 13.46 ± 0.51 steps, n=26 animals; SHAM: 12.88 ± 0.95 steps, n=10 animals; ns, **Fig 5.4B**) or backhand (6-OHDA: 17.06 ± 0.56 steps, n=26 animals; SHAM: 16.98 ± 0.65 steps, n=10 animals; ns, **Fig 5.4B**) directions. Once again, the one presumed unsuccessfully lesioned animal was easily identified, as the number of adjusting steps was consistent with sham animals.

### 5.2.2 Frequency profile of 6-OHDA lesions

#### *5.2.2.1 Depth recordings*

We bilaterally implanted depth electrodes to investigate the oscillatory profile through the different cortical layers of M1. This data is based off of experiments in one lesioned animal.

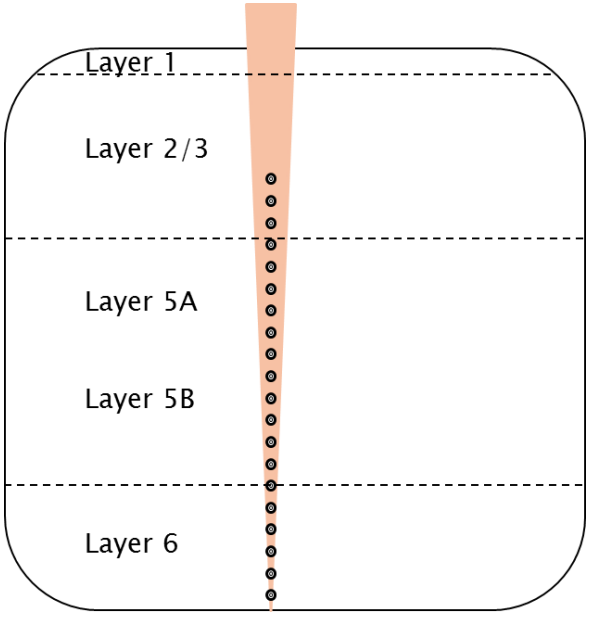


**Figure 5.5 Approximation of depth electrode positioning within M1.** Approximate position of depth electrode in M1, based upon surgical co-ordinates and size of depth electrode. Orange bar, depth implant. Grey circles, LFP channel recording points.

Each depth electrode consisted of 16 channels. Although no histology was undertaken, by reference to surgical co-ordinates it was estimated that channel 1 was located in central part of LII/III with channel 16 located at the bottom edge of LVI (**Fig 5.5**). Recordings of

baseline activity from a 6-OHDA lesioned animals demonstrated distinct differences between the ipsilateral (lesioned **Fig 5.6Ai**) and contralateral (non-lesioned **Fig 5.6Aii**) hemispheres. FFT analysis of 30 s of data recorded in channel 10, believed to be in mid-layer V, from the ipsilateral hemisphere revealed peaks at a frequency of 32.17 Hz (power: 2.24 x $10^{-10}$ V) and 6.89 Hz (power: 1.43 x $10^{-10}$ V), while recordings from the same location in the contralateral hemisphere displayed a single oscillatory peak at a frequency of 6.89 Hz (power: 1.8 x $10^{-10}$ V) (**Fig 5.6B, C**).

Taking the peak oscillatory power of the 30-40 Hz band from each recording channel in the ipsilateral hemisphere, we plotted the change in power descending through M1 (**Fig 5.7A**). We observed that there were two areas of higher power, in channels 1-4 (superficial LII/III; 1.79 x $10^{-10}$ ± 9.12 x $10^{-12}$ V, n=4 channels) and in channel 10 (LV; 2.24 x $10^{-10}$). Current-source density analysis of 20-45 Hz oscillations revealed a pattern of sources (red) and sinks (blue) in the superficial and deeper layers, in line with the power change observed in **fig 5.7A** (**Fig 5.7B**). No prominent 30-40 Hz oscillation was evident in the contralateral hemisphere (**Fig 5.7Bii**).

CSD plots would ordinarily be expected to demonstrate the phase inversion of the sources and sinks across the layers, however we see no such changes. Additionally, as this is a recording from only a single animal we cannot assume this to be representative of M1 after 6-OHDA lesioning. In order to assess this CSD we need to consider potential problems that may affect this analysis, such as a damaged probe or periodic noise in the recording. The CSD also shows a large smearing effect of the sources and sinks across many of the layers, which may be due to an oscillation of high coherence affecting the analysis. As such, the analysis may not be suitable for this form of recording and may need to be investigated further for any potential problems which could affect the outcome.

While we are approximating the depth of the electrode within M1 and the recordings appear to correspond to the superficial and deep layers. We should be aware of the different sites of oscillation generation across the layers and steps should be taken to verify the positioning of the electrodes before final conclusions can be drawn.

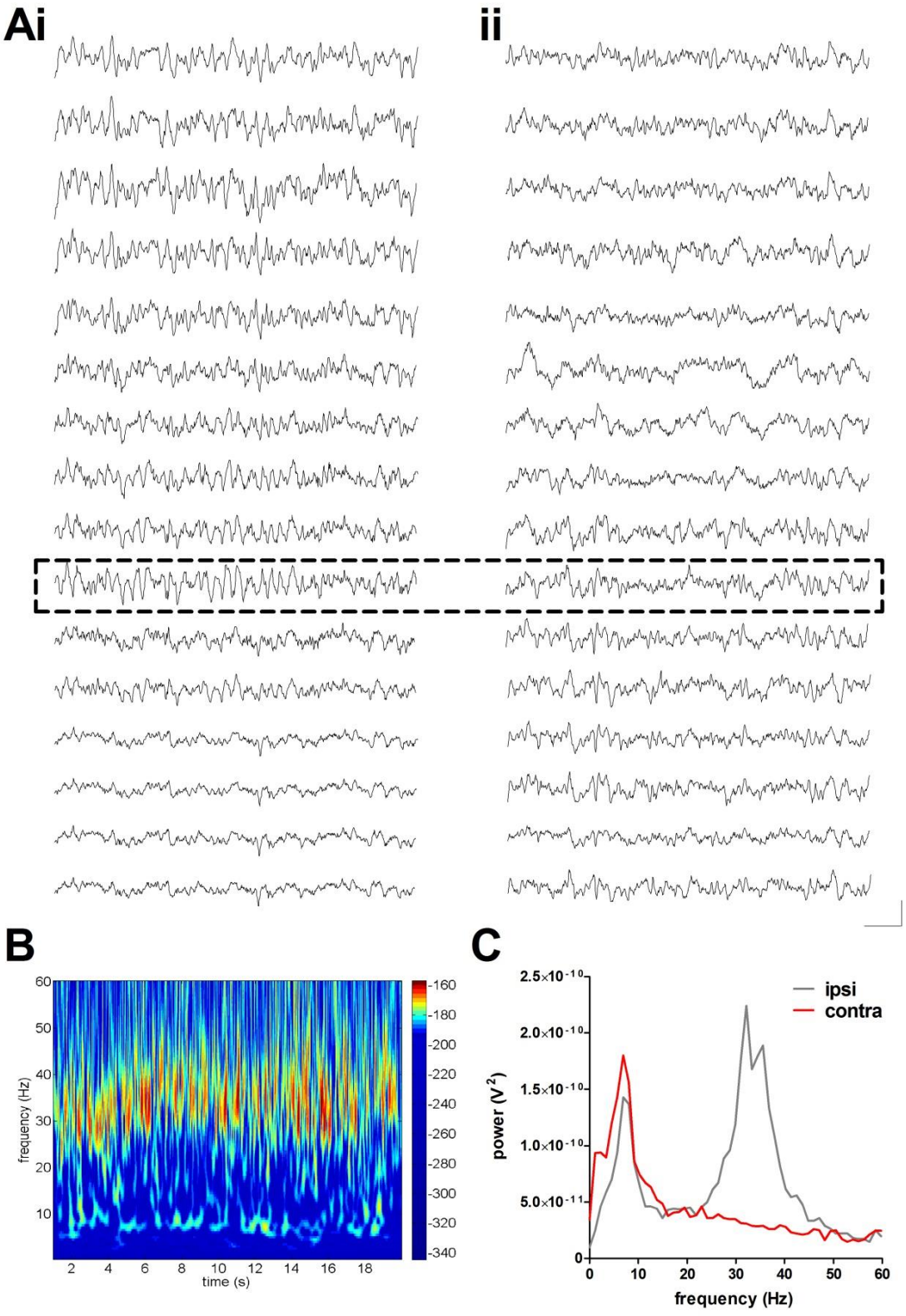


**Figure 5.6 Comparison of depth electrode recordings from contralateral and ipsilateral hemispheres in a 6-OHDA rat. (A)** 1 s of raw data from ipsilateral (i) and contralateral (ii) hemispheres of M1 with representative channel used in further graphs highlighted by box (scale bar: 200 ms x $2.0x10^{-4}$ V). **(B)** Spectrogram of 20 s of data from ipsilateral hemisphere. **(C)** Representative power spectrum showing differences between ipsilateral (grey line) and contralateral (red line) hemispheric recordings.

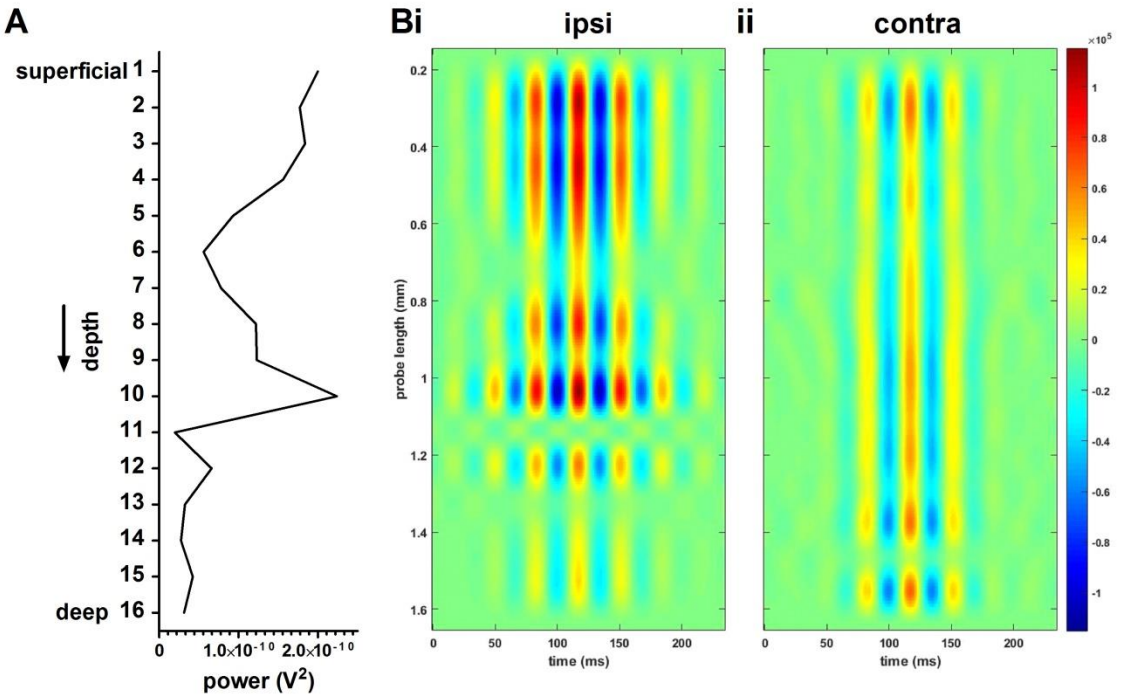


**Figure 5.7 Current-source density analysis demonstrated a 30-40 Hz oscillation originating in the deeper channels of M1. (A)** Graph showing peak power changes in the 30-40 Hz oscillation band descending through M1 cortical layers from superficial to deep. **(B)** CSD analysis graphs in the 20-45 Hz range in the (i) ipsilateral and (ii) contralateral hemisphere, demonstrating sources (red) and sinks (sinks).

### *5.2.2.2 EEG recordings*

6-OHDA and sham lesioned animals were implanted with bilateral EEG electrodes over the frontal cortex and placed inside a 24 h recording system. Data collected during the most active (dark) phase of a rodent diurnal cycle was analysed. Initial baseline recordings from the ipsilateral hemispheres of lesioned animal data revealed two main oscillatory peaks at a frequency of 2.3 ± 0.4 Hz and 30.5 ± 0.2 Hz with power $2.4x10^{-4}$ ± $2.8x10^{-5}$ $\mu V^2$ and $6.9x10^{-5}$ ± $5.3x10^{-6}$ $\mu V^2$ respectively (n=7 animals; **Fig 5.8A**). The contralateral hemispheres of lesioned animals displayed a single peak at a frequency of 2.4 ± 0.4 Hz and power $1.9x10^{-4}$ ± $2.7x10^{-5}$ $\mu V^2$ (n=7 animals; **Fig 5.8A**) as did sham animals (ipsi: 2.6 ± 0.5 Hz, $2.1x10^{-4}$ ± $1.9x10^{-5}$ $\mu V^2$; contra: 2.2 ± 0.3 Hz, $2.1x10^{-5}$ ± $3.1x10^{-5}$ $\mu V^2$; n=3 animals; **Fig 5.8B**).

Pooling all baseline data from 6-OHDA and sham animals, we identified that the peak in the 30-40 Hz band was consistently significantly greater in power ($p<0.001$) in the ipsilateral hemisphere's of 6-OHDA animals (30.53 ± 0.07 Hz, $6.41x10^{-5}$ ± $1.66x10^{-6}$ $\mu V^2$, n=51 baseline recordings) compared to ipsilateral hemispheres of sham lesioned animals (30.26 ± 0.05 Hz, $4.88x10^{-5}$ ± $9.99x10^{-6}$ $\mu V^2$, n=43 baseline recordings).

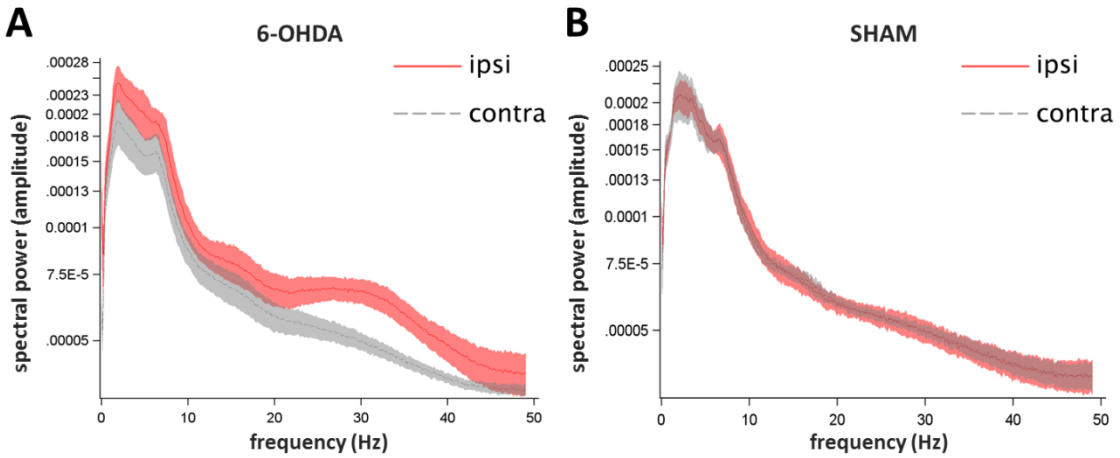


**Figure 5.8 Power spectra of 6-OHDA and sham lesioned animals' baseline recordings demonstrates differences between ipsilateral hemispheres in 6-OHDA animals.** Pooled power spectra demonstrating ipsilateral (ipsi, red line) and contralateral (contra, grey line) differences in oscillatory profiles between **(A)** 6-OHDA lesioned and **(B)** sham lesioned animals.

### 5.2.3 L-DOPA and zolpidem in depth electrode recordings

All depth electrode recordings outlined in this section were obtained from a single animal leaving a minimum of two days between experiments to ensure full clearance of the previous drug. The animal was connected to depth electrode recording equipment, placed in an open field environment and left to habituate for at least 20 mins.

*5.2.3.1 L-DOPA vehicle (glucose 5%)*

Initially the animal was dosed with vehicle (glucose 5% i/p). We observed no changes in ipsilateral oscillatory power in the 30-40 Hz band relative to contralateral hemisphere peak power for the whole 90 min experimental period (ns, **Fig 5.9B**).

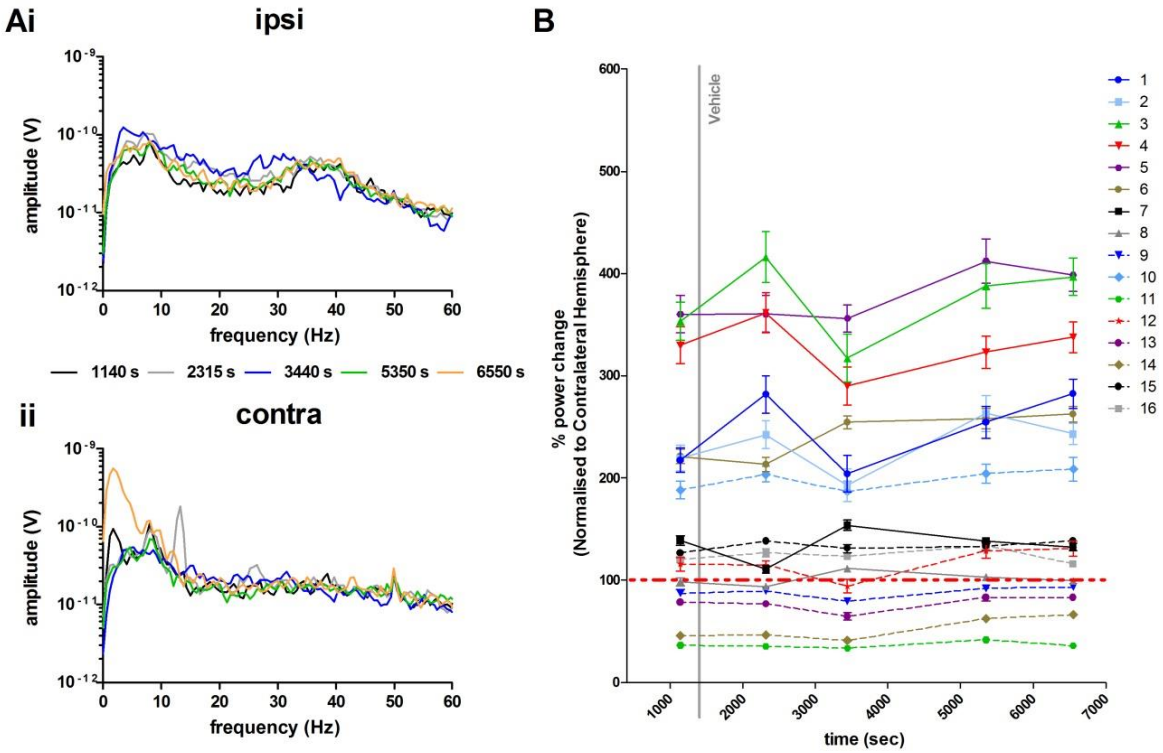


**Figure 5.9 Administration of vehicle (glucose 5%) results in no changes to 30-40 Hz oscillations (A)** Representative power spectra demonstrating oscillatory peaks of two corresponding channels in (i) ipsilateral (ipsi) and (ii) contralateral (contra) hemispheres over time (s). **(B)** Line graph demonstrating changes in power of ipsilateral hemisphere normalised to contralateral hemisphere. Each pair of corresponding channels from either hemisphere labelled 1-16 in descending depth. Grey vertical line notifies the time at which vehicle was administered.

*5.2.3.2 L-DOPA (6 mg/kg)*

We investigated oscillatory peak changes in a 6-OHDA lesioned animal (n=1 animal) in an open field before and after the administration of the DA precursor L-DOPA (6 mg/kg i/p). L-DOPA was co-administered with benserazide (15 mg/kg i/p), a DOPA decarboxylase inhibitor, in order to prevent enzymatic degradation of L-DOPA in the peripheral system.

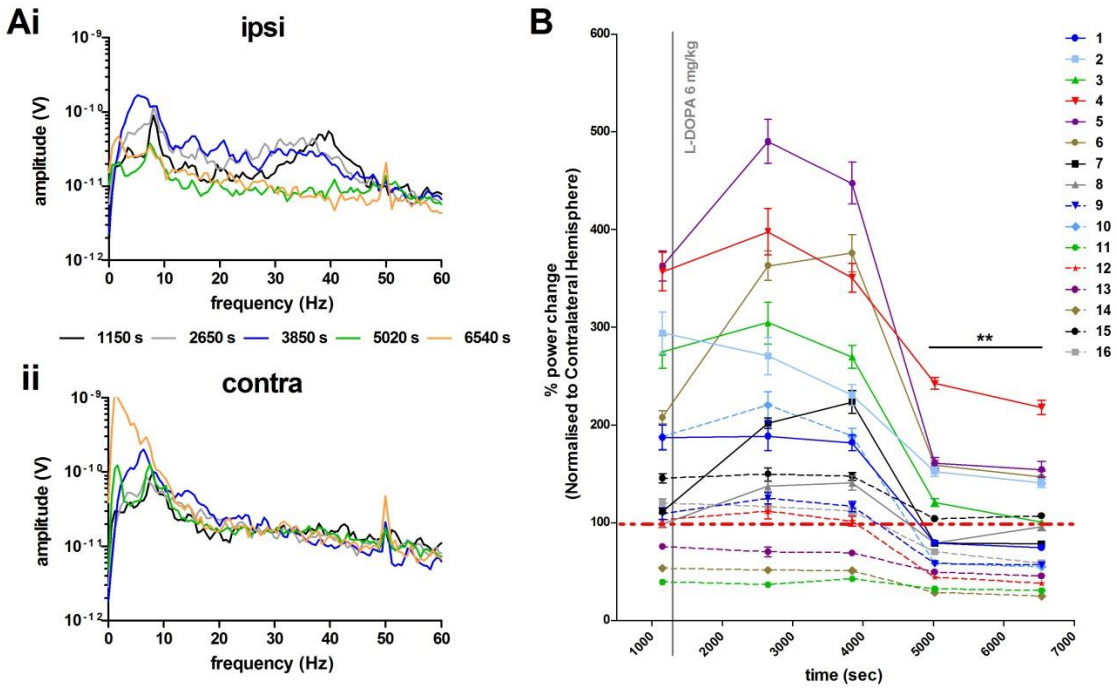


**Figure 5.10 Administration of L-DOPA decreases the power of ipsilateral 30-40 Hz oscillations. (A)** Representative power spectra demonstrating changes in oscillatory peaks of two corresponding channels in (i) ipsilateral and (ii) contralateral hemispheres over time (s). **(B)** Line graph demonstrating changes in power of ipsilateral hemisphere normalised to contralateral hemisphere. Each pair of corresponding channels from either hemisphere labelled 1-16 in descending depth. Grey vertical line notifies the time at which L-DOPA was administered. Black bar signifies significance with respect to control power pre-L-DOPA administration. ** p<0.01.

Following L-DOPA administration we observed significant reductions in ipsilateral hemisphere 30-40 Hz oscillatory peak power relative to contralateral hemisphere peak power from the time period 3850 s to 5020 s (95.64 ± 19.0 % pooled change of n=16 channels, p<0.01 for 10 channels in comparison to control time point (not including channels 11, 13 and 14, **Fig 5.10B**), which persisted to the end of the experiment (total 90 mins).

*5.2.3.3 Zolpidem (0.3 mg/kg)*

Previous work has investigated the use of low-doses of zolpidem to improve PD symptoms and reduce pathological oscillations in patients (Hall et al., 2010; Hall et al., 2014) and *in vitro* (Prokic et al., 2015). We aimed to show whether this could be replicated using the 6-OHDA model, using a dose of zolpidem of 0.3 mg/kg.

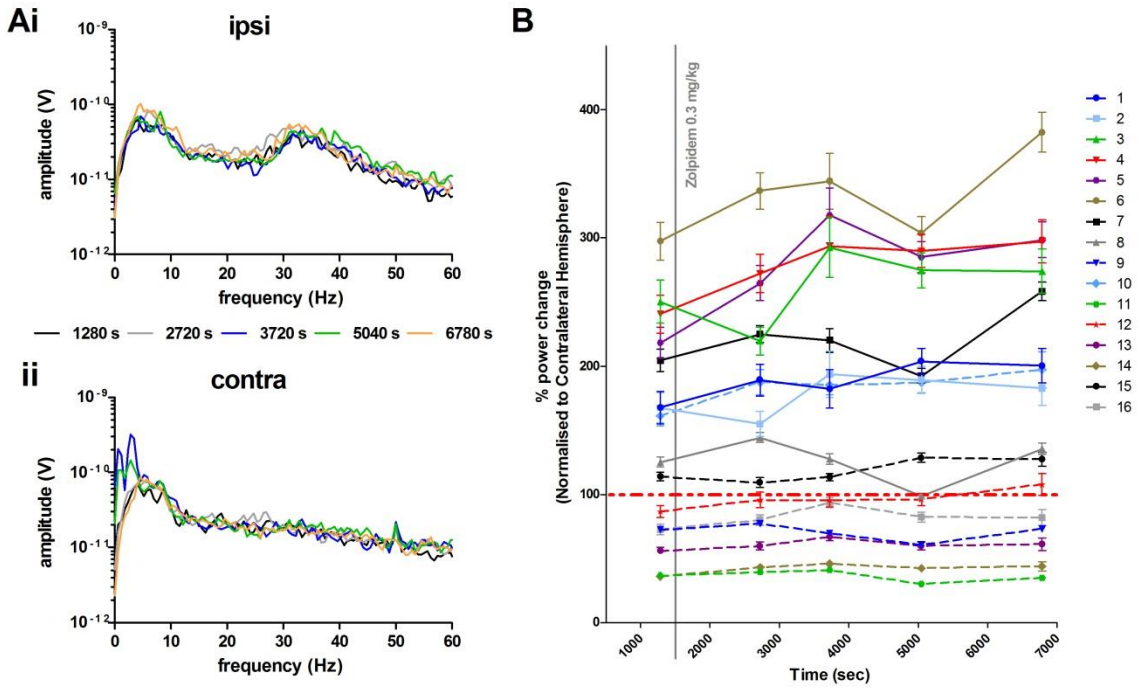


**Figure 5.11 Administration of zolpidem (0.3 mg/kg) does not result in a significant change in the power of the ipsilateral hemisphere relative to the contralateral hemisphere. (A)** Representative power spectra demonstrating changing oscillatory peaks of two corresponding channels in (i) ipsilateral (ipsi) and (ii) contralateral (contra) hemispheres over time (s). **(B)** Line graph demonstrating changes in power of ipsilateral hemisphere normalised to contralateral hemisphere. Each pair of corresponding channels from either hemisphere labelled 1-16 in descending depth. Grey vertical line notifies the time at which zolpidem was administered.

After recording baseline activity for 20 mins, zolpidem was administered orally and the animal placed back into open field chamber for a further 90 mins. No significant change in oscillatory power was observed in any channel (1-16), in either ipsilateral or contralateral hemisphere (ns, n=16 channels, **Fig 5.11**).

### 5.2.4 L-DOPA and zolpidem in EEG recordings

No animals were dosed with the same drug twice and drugs order was randomised. Data from the whole pre- and post-dosing period was collected using the EEG continuous recording system. 30 min epochs of data from pre- (BL) and post-dosing was analysed using cumulative power analysis of band-pass filtered 30-40 Hz oscillations, designed to correspond to the abnormal peaks observed in the FFT analysis.

#### *5.2.4.1 L-DOPA (6 mg/kg)*

6-OHDA and sham animals were administered both L-DOPA (6 mg/kg i/p) and vehicle (glucose 5% i/p). L-DOPA was co-administered with the peripheral DOPA decarboxylase inhibitor with benserazide (15 mg/kg i/p).

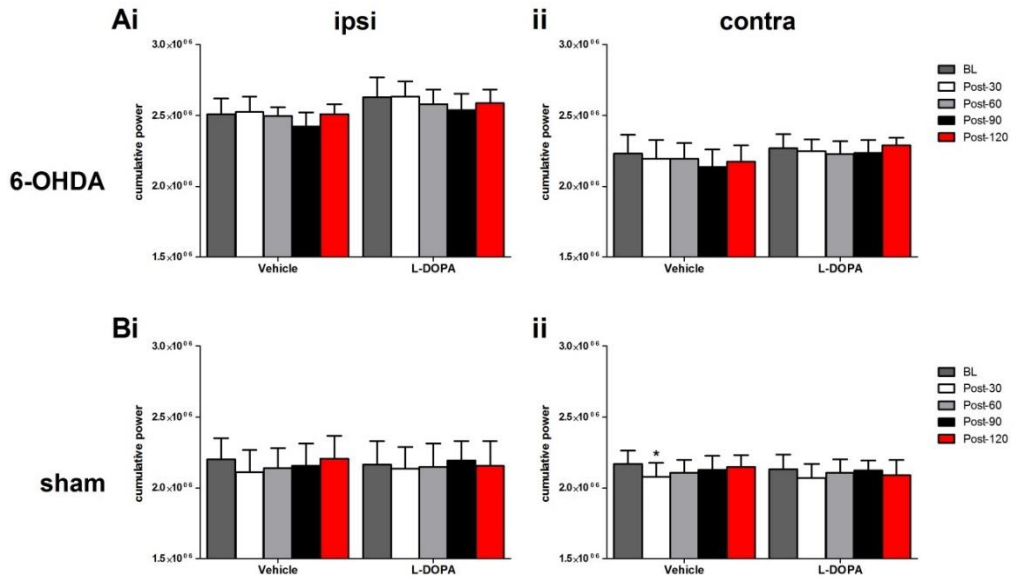


**Figure 5.12 Cumulative power graphs of 30-40 Hz oscillations with L-DOPA showed no significant effects on 6-OHDA or sham animals.** Graphs demonstrating changes in cumulative power over time in (i) ipsilateral (ipsi) and (ii) contralateral (contra) hemispheres. Data presented as total cumulative power from baseline (BL) condition up to 120 min post dosing (Post-120) in **(A)** 6-OHDA and **(B)** sham animals.*, p<0.05

In 6-OHDA animals no changes in cumulative power were observed in response to L-DOPA (n=7 animals) or vehicle (n=6 animals), in either ipsilateral or contralateral hemispheres over the entire 120 mins recording period (ns, **Fig 5.12A**). In sham animals, a significant decrease in cumulative power in vehicle after 30 mins (post-30) compared to BL in the contralateral hemisphere (to 95.70 ± 0.66% of BL, p<0.05, n=5 animals; **Fig 5.12Bii**) was observed. No other significant differences were observed (L-DOPA: n=5 animals; vehicle: n=5 animals; ns, **Fig 5.12B**).

Previous MEG recordings from M1 in patients with Parkinson's had revealed that the motor improvements afforded by zolpidem were directly correlated with the balancing of beta oscillatory power between hemispheres (interhemispheric ratio, Hall et al., 2014). Here, we attempted to replicate these finding in the 6-OHDA lesioned animal. However, following dosing with L-DOPA in either 6-OHDA (**Fig 5.13A**) or sham (**Fig 5.13B**) animals we observed no significant changes in the inter-hemispheric power ratio.

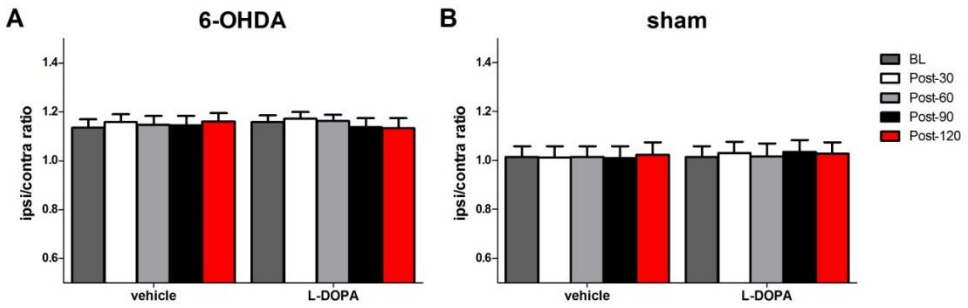


**Figure 5.13 Ipsilateral/contralateral ratios after L-DOPA and vehicle dosing demonstrate no significant differences.** Graphs demonstrating the ratio between ipsilateral and contralateral hemispheres in each drug condition in **(A)** 6-OHDA and **(B)** sham animals.

Nevertheless, when 30-40 Hz cumulative power is averaged across all time points (**Fig 5.14A**), it was significantly higher in the ipsilateral hemispheres of 6-OHDA animals ($2.49 \times 10^6 \pm 4.18 \times 10^4$, n=24 baseline recordings) than contralateral hemispheres ($2.17 \times 10^6 \pm 5.68 \times 10^4$, n=24 baseline recordings, $p<0.001$, **Fig 5.14A**) and both the ipsilateral ($2.15 \times 10^6 \pm 7.15 \times 10^4$, n=20 baseline recordings) and contralateral ($2.11 \times 10^6 \pm 4.37 \times 10^4$, n=20 baseline recordings; **Fig 5.14A**) hemispheres of sham animals. In addition, the averaged interhemispheric ratio of the 30-40 Hz oscillations were significantly higher in 6-OHDA lesioned animals (1.15 ± 0.01 ratio, n=24 baseline recordings, **Fig 5.14B**) compared to sham animals (1.02 ± 0.02 ratio, n=20 baseline recordings, $p<0.001$, **Fig 5.14B**).

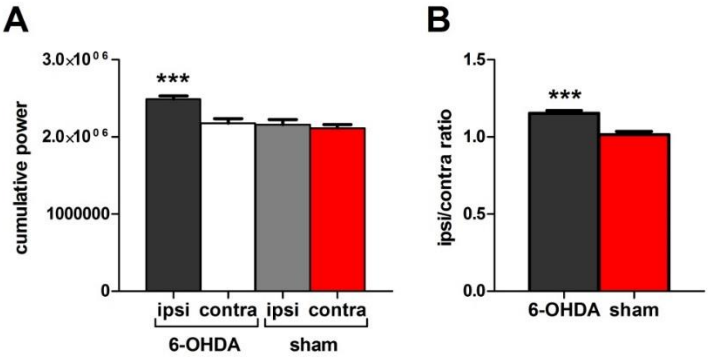


**Figure 5.14 Average cumulative power and inter-hemispheric ratio of 30-40 Hz oscillations in post-vehicle dosing demonstrates significantly higher power in 6-OHDA ipsilateral hemispheres. (A)** Bar graph demonstrating average post-dosing cumulative power in 6-OHDA ipsilateral (dark grey) and contralateral (white) hemispheres, and sham ipsilateral (light grey) and contralateral (red) hemispheres. **(B)** Bar graph demonstrating average interhemispheric ratio post-dosing. ***, p<0.001.

### *5.2.4.2 Zolpidem (0.3 and 1 mg/kg)*

6-OHDA and sham animals were orally administered zolpidem (0.3 and 1 mg/kg) and vehicle (methylcellulose 0.25%), leaving a minimum of seven days between experiments to ensure full clearance of the previous drug.

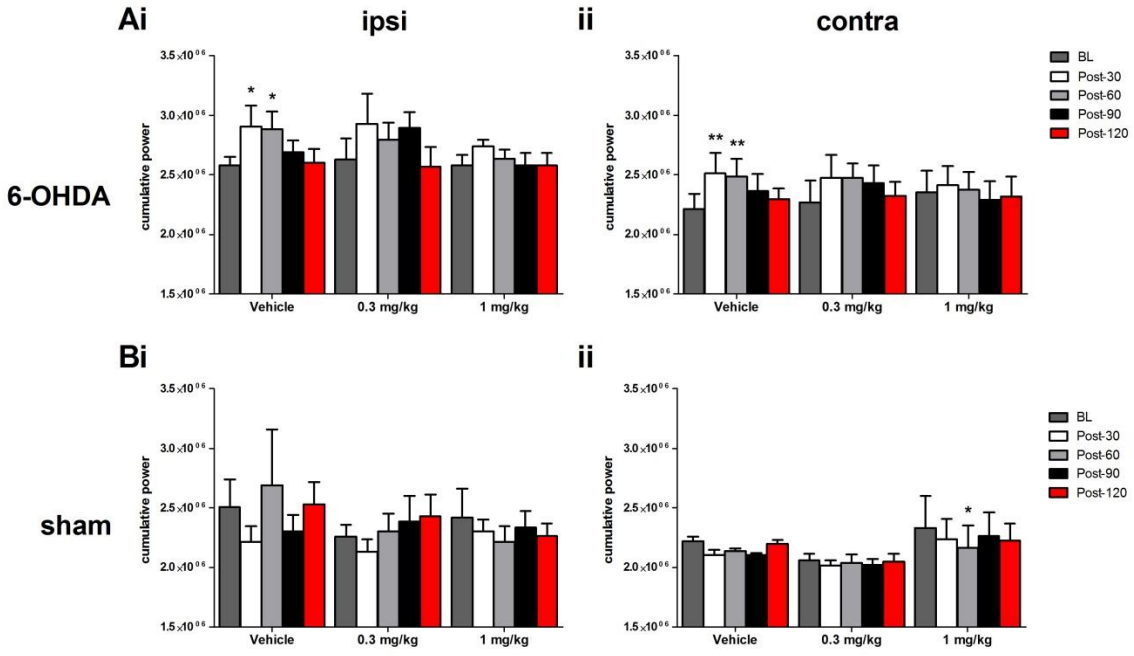


**Figure 5.15 Cumulative power graphs of 30-40 Hz oscillations with 0.3 and 1 mg/kg zolpidem showed no significant effect on 6-OHDA or sham animals.** Graphs demonstrating changes in cumulative power over time in (i) ipsilateral (ipsi) and (ii) contralateral (contra) hemispheres. Data presented as total cumulative power from baseline (BL) condition up to 120 min post dosing (Post-120) in **(A)** 6-OHDA and **(B)** sham animals. **, p<0.01, *, p<0.05.

In 6-OHDA lesioned animals, no significant changes in the cumulative power were observed following administration of 0.3 mg/kg or 1 mg/kg zolpidem in either ipsilateral or contralateral hemispheres (**Fig 5.15Ai and ii**). However, after dosing with vehicle significant increases to cumulative power were observed in the 30 and 60 minute epochs in both ipsilateral (30: by 13.19 ± 7.80%, n=6 animals, $p<0.05$; 60: by 12.30 ± 6.65%, n=6 animals, $p<0.05$; **Fig 5.15Ai**) and contralateral (30: by 14.11 ± 6.67 %, n=7 animals, $p<0.01$; 60: by 13.18 ± 5.91%, n=7 animals, $p<0.01$) hemispheres (**Fig 5.15Aii**)

Sham animals displayed no significant change in cumulative power on administration of vehicle in both ipsilateral (n=3 animals) and contralateral (n=2 animals) hemispheres. Similarly no changes were observed in either ipsilateral (n=4 animals) and contralateral (n=3 animals) hemisphere on administration of zolpidem at 0.3 or 1 mg/kg **(Fig 5.15B)**. However, note the one outlier which shows significant difference in cumulative power, 60 mins post-dosing of 1 mg/kg zolpidem ($p<0.05$; **Fig 5.15Bii**).

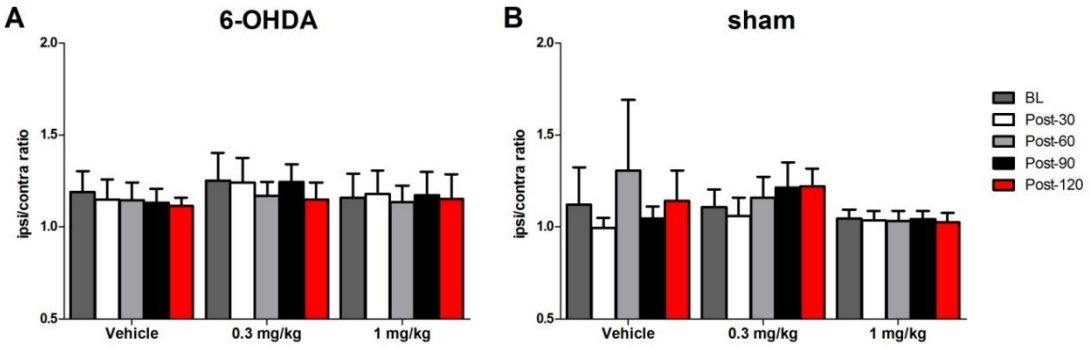


**Figure 5.16 Ipsilateral/contralateral ratios after 0.3 and 1 mg/kg zolpidem and vehicle dosing demonstrate no significant differences.** Graphs demonstrating the ratio between ipsilateral and contralateral hemispheres in each drug condition in **(A)** 6-OHDA and **(B)** sham animals.

Once again, following dosing with zolpidem at 0.3 or 1 mg/kg in either 6-OHDA (**Fig 5.16A**) or sham (**Fig 5.16B**) animals, we observed no significant changes in the inter-hemispheric power ratio. However, as observed previously, the cumulative power in the ipsilateral hemispheres of 6-OHDA animals ($2.77 \times 10^6 \pm 7.09 \times 10^4$, n=24 baseline recordings) was significantly higher than contralateral hemisphere ($2.41 \times 10^6 \pm 6.85 \times 10^4$, $p<0.01$, n=28 baseline recordings) and both the ipsilateral ($2.44 \times 10^6 \pm 1.28 \times 10^5$, $p<0.05$, n=12 baseline recordings) and contralateral ($2.14 \times 10^6 \pm 1.80 \times 10^4$, $p<0.001$, n=8 baseline recordings, **Fig 5.17A**) hemispheres of sham animals. However, in this cohort there was no significant difference observed between the average interhemispheric ratios of 6-OHDA (1.14 ± 0.04 ratio, n=24 baseline recordings, **Fig 5.17B**) and sham (1.12 ± 0.09 ratio, n=8 baseline recordings, **Fig 5.17B**) animals.

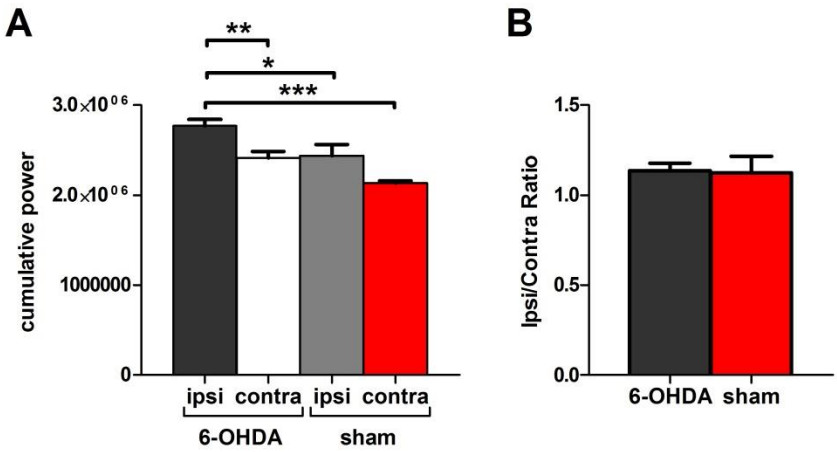


**Figure 5.17 Average cumulative power and interhemispheric ratio of 30-40 Hz oscillations in post-vehicle dosing demonstrates significantly higher power in 6-OHDA ipsilateral hemispheres but no difference in interhemispheric ratio (A)** Bar graph demonstrating average post-dosing cumulative power in 6-OHDA ipsilateral (dark grey) and contralateral (white) hemispheres, and sham ipsilateral (light grey) and contralateral (red) hemispheres. **(B)** Bar graph demonstrating average interhemispheric ratio post-dosing.

## 5.3 Discussion

In this chapter we have investigated the oscillatory activity of M1 *in vivo* using the 6-OHDA model of PD. The success of the lesion protocol was assessed in each animal using the rotometer, the LMA and the adjusting step test. Further testing at 22 weeks post-surgery indicated the long-term stability of the lesions. Using depth electrode and EEG recordings, oscillatory activity in the 2-10 Hz range was found in the ipsilateral and contralateral hemispheres of both lesioned and sham animals. However, only in the ipsilateral hemisphere of DA-depleted animals did we detect a 30-40 Hz oscillatory peak, which was localised to LII/III and LV of M1. In EEG recordings, this was observed as a significant increase in the interhemispheric ratio in lesioned animals.

Using depth electrode recordings the ipsilateral 30-40 Hz oscillation (but not 2-10 Hz oscillation) was reduced by the administration of L-DOPA (6 mg/kg) with associated change in interhemispheric ratio. However, administration of zolpidem (0.3 mg/kg), which previously reduced abnormal beta oscillatory activity *in vivo* and *in vitro* resulting in the rebalancing of interhemispheric beta power (Hall et al., 2014; Prokic et al., 2015), was without effect.

### 5.3.1 Testing 6-OHDA lesions

#### *5.3.1.1 Short-term testing*

During rotometer and LMA testing, amphetamine or apomorphine are usually administered to induce robust rotations in a pre-hypothesised direction. In this study we were able to observe pronounced basal rotational activity in lesioned animals (but not sham animals) without the use of drugs. These tests were both performed over a period of 40 mins, which produced clear differences in activity at the start compared to the end of the testing period. The increased activity in the initial 5 and 10 min epochs can be explained by the initial exploratory behaviour that animals perform when placed into a novel environment. After this period, the animals tended to relax (and often enter a resting/sleep state), resulting in a reduction in the amount of movement registered. This is clearest in the lesioned animals who demonstrate robust rotations in a particular direction. However, this is not to say that the sham animals do not move or explore in the rotometers or the LMA environment. Further experiments could set a lower threshold in terms of rotational degrees (which was set at $360^{o}$ in rotometer testing and $90^{o}$ in LMA testing) to count as one rotation. If a higher resolution of what counted as a single rotation

were used then the results would be clearer in the actual movement performed by the sham animals, but as there should be no bias in these animals they would still demonstrate a roughly equal RAS. However, a higher resolution of rotational accuracy in the lesioned animals should only relay a greater number of movements in the pre-hypothesised direction. While this information may be useful for a greater understanding of the rotational behaviour demonstrated in the lesioned animals, it would not necessarily inform us as clearly as to the success or failure of the lesioning surgery.

The success of lesion experiments was further confirmed using the adjusting step test, which measures rodent forelimb akinesia (Olsson et al., 1995). This was a method used previously in testing 6-OHDA lesions in our *in vitro* experiments (see chapter 4). Using this test, scores for limbs contralateral to the lesioned hemisphere were significantly reduced compared to ipsilateral limbs, which was consistent with their rotometer and LMA scores.

#### *5.3.1.2 Long-term testing*

Rodents who have undergone 6-OHDA lesioning do not begin to exhibit movement deficits until 80-90% of dopamine cells are lost (Bernheimer et al., 1973; Orr et al., 1986). Indeed, 2-5 weeks post-lesion is thought to correspond to a time when the pathophysiological state has likely stabilised at a maximum level (Pan and Walters, 1988; Vila et al., 2000). Following this, compensatory mechanisms which attempt to normalise striatal activity through increased DA synthesis and release (Nisenbaum et al., 1986; Robinson and Whishaw, 1988; Zigmond et al., 1990), may contribute to a partial functional recovery at 12 to 16 weeks (Schwarting and Huston, 1996). However, other studies have demonstrated that there are still significant reductions in nigral cell counts and tyrosine hydroxylase reactivity at 16 weeks (Sauer and Oertel, 1994).

As our electrophysiological studies commenced 10-12 weeks post-lesion, we decided to re-assess the rotational ability of the remaining animals at 22 weeks. We found that while the number of rotations was reduced from the original testing, lesioned animals' still demonstrated significant directional bias compared to sham animals. Whilst this could be attributed to compensation though DA-related mechanisms, other studies have suggested that decreases in movement deficits may be related to animals learning to cope with and adapt to their impairments, with the actual physiological changes still intact (Morgan et al., 1983; Schwarting and Huston, 1996). Therefore, as our animals continued to demonstrate significantly altered movement deficits 22 weeks post-lesion, we believed our lesions and results to be without significant compensatory mechanisms.

### 5.3.2 *In vivo* oscillatory profile

In both depth electrode and EEG recordings, we observed abnormal oscillatory activity in the 30-40 Hz range in our 6-OHDA animals. This was specific to ipsilateral hemispheres of lesioned animals and was not observed in sham animals. Whilst abnormal oscillatory activity is readily observed in BG structures in PD animal models (Brown and Marsden, 1998; Sharott et al., 2005; Mallet et al., 2008a; Mallet et al., 2008b) and in PD patients (Brown et al., 2001; Bevan et al., 2002; Brown, 2003; Brown and Williams, 2005; Kuhn et al., 2006; Chen et al., 2007; Hammond et al., 2007), the frequency of activity commonly found is within in the beta range (12-25 Hz). However, the observation of a higher frequency range is not without precedence and maybe related to recordings made during different behavioural states. During rest or inactivity, beta oscillations in the 12-25 Hz range are commonly observed, but during alertness and activity oscillations in this range are reduced and 25-40 Hz oscillations dominate (Avila et al., 2010; Brazhnik et al., 2014). As our recordings took place in home cages or an open field arena where rodents were able to move freely, and depth recordings were made during the dispensing of food pellets to promote activity, the higher oscillatory frequency range may be expected.

CSD analysis of depth electrode recordings predominantly localised the 30-40 Hz oscillations to LV of M1, although oscillations were also detected in LII/III. Similar results had been reported previously in *in vitro* studies of M1, where beta (see Yamawaki et al., 2008) and gamma (see chapter 3) oscillations have been localised to LV and are believed to be due to the predominance of large pyramidal Betz cells (Rivara et al., 2003). This has also been observed in somatosensory cortex (S2), where pharmacologically similar *in vitro* beta oscillations were observed in LV (Roopun et al., 2006). However, care should be taken when interpreting the CSD analysis in **Fig 5.7B**. While the periodicity of the sources and sinks demonstrated across this graph does suggest an oscillatory pattern at ~30-35 Hz, in line with the FFT generated, the fact that there is no phase inversion across the channel sites is somewhat suspect. It is possible that there is a high level of coherence of the oscillation across the layers which results in the smearing pattern of the sources and sinks at each channel. However, it is also possible that there was a problem with the probe or even with the CSD computation that was been performed, resulting in a potentially inaccurate CSD response. As a result, we should consider other methods of validating the depth of the probe, via immunohistochemistry in order to observe the probe tract. Furthermore, in order to understand which cortical layers the oscillations are being generated from, we could perform the same experiments with multiple N numbers and validated probe telemetry. Alternatively we could utilise *in vivo* recordings under

anaesthesia in order to record oscillations from a stable setup and reduce the potential for technical problems associated with an awake recording set up.

In the M1-BG, enhanced oscillatory activity within the 4-6 Hz range correlates with tremor in PD patients (Volkmann et al., 1996; Timmermann et al., 2003; Pollok et al., 2004; Timmermann and Florin, 2012). However, in this study, oscillatory peaks in the 2-8 Hz range were also seen in both the ipsilateral and contralateral hemispheres of both 6-OHDA and sham animals consistent with previous studies which described oscillations in the <10 Hz range between DA-depleted and DA-intact animals (Brazhnik et al., 2012).

### 5.3.3 L-DOPA

In depth electrode recordings, L-DOPA decreased the power of the abnormal 30-40 Hz oscillations in ipsilateral M1 after 30-40 mins. This reduction was not observed during the administration of the vehicle over the same time period. These results are consistent with previous reports of L-DOPA reducing 8-30 Hz oscillations in the BG, restoring the network to a pro-kinetic state (Kuhn et al., 2006; Delaville et al., 2014). Additionally, in 6-OHDA lesioned animals, Brazhnik et al. (2014) observed that L-DOPA administration resulted in improvements in motor ability and a reduction in SNr oscillatory power in the ipsilateral hemisphere with no change in the contralateral hemisphere. The same study also demonstrated that L-DOPA reduced the interhemispheric oscillatory ratio to normal (Brazhnik et al., 2014). These observations are consistent with our results and the previous results from the lab where improvements in symptoms were consistent with a balancing of the interhemispheric power in PD patients (Hall et al., 2014).

However, the administration of L-DOPA in our EEG recordings resulted in no change to the power of 30-40 Hz oscillations in ipsilateral hemispheres. This was surprising, considering the significant response seen in the depth electrode recordings. However, it is possible that this is due to the inability to isolate active periods from periods of rest or sleep. While this was also a potential issue with the depth electrode studies, in these experiments, rodents were encouraged to remain active by the dispensing of food pellets.

Furthermore, depth electrodes record activity from networks which are local to each recording channel and therefore have excellent spatial resolution, an attribute which is lost in EEG recording. Previous studies have shown that while L-DOPA and DA agonists reduce abnormal oscillations in M1 of 6-OHDA animals (Brazhnik et al., 2012; Delaville et al., 2015) they have no effect on 30-40 Hz oscillations observed in PFC (Delaville et al.,

2015). Therefore, our negative results could also be due to the recording of activity from networks, other than M1, which are insensitive to L-DOPA.

### 5.3.4 Low-dose zolpidem

Low-dose zolpidem (10 nM) reduces CCh and KA induced beta *in vitro* (Prokic et al., 2015). In addition, sub-sedative doses of zolpidem (0.05 mg/kg) have been shown to reduce pathological beta oscillatory activity in ipsilateral M1 in PD patient's *in vivo* which is accompanied by a decrease in interhemispheric ratio that is directly correlated with an improvement in symptoms (Hall et al., 2014). In this study we attempted to recreate these experiments in the 6-OHDA lesioned animals in both depth electrode and EEG recordings.

However, on administration of 0.3 mg/kg (depth) and 0.3 and 1 mg/kg (EEG) of zolpidem we observed no significant changes in oscillatory power and no change in the hemispheric ratio. Whilst this result was surprising these doses may miss the effective therapeutic window. The 0.3 mg/kg dose was calculated using animal equivalent dose (AED) to take into account body surface area differences between animals and humans (Nair and Jacob, 2016) (rat factor - 6.2). However, this calculation does not take body weight or differences in metabolism into account which may alter the effective dose.

In patient studies higher doses of zolpidem led to a 'beta buzz' and sedation while in *in vitro* studies, there was a clear difference in the response to 10 nM and 30 nM zolpidem, with only the lower concentration resulting in the desynchronising effect on the beta oscillations, with the latter exaggerating their activity (Prokic et al., 2015). Thus, the dosing regime is critical and any deviation from therapeutic range may produce a very different result. Further studies would therefore incorporate a much lower dosing protocol or use a range of doses to develop a dose response, thus providing a greater idea as to the useful therapeutic dose for our studies, as well as the level at which sedative effects begin to occur.

In our experiments, we identified an abnormal oscillation in the 30-40 Hz range which is in the same range as the oscillations elicited *in vitro*. Whilst this frequency range has been recorded previously *in vivo* (Avila et al., 2010; Brazhnik et al., 2014; Delaville et al., 2014), it is different to the frequency of oscillations that recorded by Hall et al. (2014) and Prokic et al. (2015). Therefore it is possible that the activity arises from distinct neuronal

networks which are differentially modulated by zolpidem. This suggestion is supported by the effect of zolpidem *in vitro* (see chapter 3).

### 5.3.5 Limitations

Having observed the abnormal oscillatory behaviour in both the depth and EEG experiments, there are some limitations to these experiments which should be considered when evaluating these results.

The depth probe experiments utilised a sugar pellet dropping into the arena every 20 seconds, in order to incite the animal to move and remain active during the experiments. However, this approach could be refined to improve the resolution of these experiments. For instance, as the animal is moving and eating at irregular times (even though the pellet drop is regular) it is impossible without video tracking and gated movement to attribute a particular oscillatory period to a particular movement or behaviour. Improving this with a specifically timed movement plan or maze paradigm would improve the variables we would be able to measure in this experiment. In particular, as we were looking at movement before and after a drug condition, a paradigm which has specifically gated and controlled movement would perhaps have yielded a greater resolution to the recordings. Alternatively, using a camera to record the movements, tracked in time to the oscillations would allow specific behaviours and their corresponding oscillatory profile to be attributed and considered independently. Additionally, previous experiments have utilised either a method of determining movement and rest periods or used anaesthetised animals, in order to improve beta signal resolution (Sharott et al., 2005; Mallet et al., 2008a; Mallet et al., 2008b). In order to bring this research more into line with the previous literature on this subject, future experiments could focus more on using these approaches to record beta oscillations. This may help to give a clearer view of these abnormal oscillations, with regard to previously completed work.

Further consideration when interpreting these results has to be given with regard to the total experimental period. Although we have shown that there was no recovery of the lesioned state in the 6-OHDA lesioned animals over the course of the experiments, we have not considered any age-related effects in our experiments. As we demonstrated in the previous chapter (chapter 4), there are some minor differences in the response of the oscillatory networks in M1 to different dopaminergic drugs. While this could be due to not enough N numbers to provide a consistent result or differences in the health of older slices compared to younger ones, it is possible there are age-related physiological effects

occurring. The experiments performed in this chapter took place in animals which ranged from 300-600 g over the experimental period. However, the majority of brain development and maturation would have already taken place prior to this period, when the animals were 50-100 g (Kolb et al., 1998; Wagner et al., 2000). Future experiments could use 2 or more cohorts of animals at different ages to determine whether there are any differences to the impact of 6-OHDA lesioning dependent on the age of the rodents involved. These could be tested pharmacologically using different dopaminergic drugs, in an attempt to replicate the experimental results observed *in vitro*. The use of immunohistochemistry or genetic fluorescence labelling in these experiments could also help to determine any differences in dendritic branching or number and type of cells current expressed at these age groups. This could provide new information relating to the *in vitro* results in chapter 4 and give insight into the effects of dopamine loss in the developing brain.

## 5.4 Conclusion

In this chapter, using the 6-OHDA animal model of PD, we observed prominent abnormal 30-40 Hz oscillations in deep layer V of the ipsilateral M1 which were not seen in contralateral hemisphere or sham animals. Additionally, we observed 2-8 Hz oscillations in both lesioned and sham animals. A long-term study demonstrated that both the motor deficits and 30-40 Hz oscillations were stable over a period of 22 weeks. Abnormal oscillations were sensitive to L-DOPA which led to a decrease in interhemispheric ratio. However, this result was not replicated with zolpidem which has previously been shown to reduce pathological beta and rebalance the interhemispheric ratio in PD patients (Hall et al., 2014; Prokic et al., 2015). Further experiments, as explained previously, could help to elucidate the exact nature of the abnormal oscillations observed in M1 through the use of gated or specific movement paradigms. These would not only allow us to separate the different beta and gamma phases of movement that take place throughout the cortico-basal ganglia circuits, but also allow us to observe the differences in these phases with respect to the 6-OHDA lesion, and whether L-DOPA and zolpidem have similar or different effects on these phases.

# Chapter 6 General Discussion and Future Experiments

The main aim of this thesis was to provide a mechanistic understanding of oscillatory behaviour in M1 and how they were altered in the DA-depleted state. We obtained M1 slices in vitro, maintaining viability through the use of specific neuroprotectants, to investigate the pharmacology of simultaneously elicited theta and gamma oscillations (chapter 3). We next investigated how DA-depletion, as a result of 6-OHDA lesioning to model unilateral Parkinson's disease (PD), affected these oscillations *in vitro* (chapter 4). Finally, we sought to investigate the oscillations in M1 as a result of 6-OHDA lesions *in vivo* and the effects of L-DOPA and low-dose zolpidem (chapter 5).

The main question explored in chapter 3 was how these theta and gamma oscillations observed in M1 *in vitro* differed from previously seen beta oscillations (Yamawaki et al., 2008). Simultaneous theta and gamma oscillations were induced in LV of M1 using reduced concentrations of CCh and KA, which were both essential for the generation of these oscillations. Using cross-correlation we determined that these oscillations had distinct laminar origins within the slices, theta was prominent in more superficial layer LVa, whilst gamma oscillations were localised in deeper LVb. Repeating the experiments using a multi-electrode array would provide further information regarding the flow of information through the layers of M1 (and S1) as well as evidence for local oscillatory networks between the superficial and deep layers.

A significant portion of simultaneously recorded theta and gamma oscillations demonstrated phase-amplitude coupling, which has previously only been assessed *in vivo* (Bragin et al., 1995). Further analysis may provide more information on the interaction of theta and gamma in PAC, in addition to the pharmacological results already observed in chapter 3. This could focus on how the strength of PAC between theta and gamma oscillations in M1 changes with respect to the amplitude of the individual oscillations. This could be achieved by using the already collected pharmacological data and further analysing the changes in theta and gamma power using overlapping epochs over the time of the whole experiment, thus obtaining an understanding of any changes in both the pre- and post-drug conditions. If these changes were then compared to alterations in the modulation index over time, we could observe how changes in the individual phase and amplitude components contributed to the PAC observed. By performing this for different drug conditions where we see different power shifts in each of the theta and gamma oscillation, we may be able to observe how PAC changes as selective parts of the network are enhanced or diminished.

A pharmacological dissection of theta and gamma oscillatory networks indicated that gap junctions and cholinergic receptors were essential for the generation of both oscillations. However, AMPA and $GABA_A$ receptors were necessary for gamma but not theta oscillatory activity, suggesting that theta is generated via a non-synaptically coupled network of intrinsic generators. In contrast, the sensitivity of gamma oscillations to the block of AMPA and the lack of block by low-dose zolpidem (10 nM), distinguishes them from previously seen beta oscillations in M1 (Yamawaki et al., 2008) and suggests that these gamma oscillations are similar to persistent synaptically generated oscillations found in the hippocampus and entorhinal cortex (Fisahn et al., 1998; Traub et al., 2000; Cunningham et al., 2003).

In the cortico-BG network, DA-depletion results in the emergence of exaggerated beta oscillations (Magill et al., 2001; Bevan et al., 2002; Brown, 2003; Mallet et al., 2008a; Mallet et al., 2008b). Previous studies *in vivo* have shown that stimulation of M1 can reduce the power of these oscillations, suggesting that this area has an important role in their control or indeed their generation (Pagni et al., 2003; Drouot et al., 2004; Lefaucheur et al., 2004). Following unilateral 6-OHDA lesions we obtained slices of DA-depleted M1 and applied CCh and KA to elicit simultaneous theta and gamma oscillations. However, we found the frequency and power of theta and gamma oscillations in ipsilateral slices to be no different to that observed in contralateral slices or in slices obtained from AMC. This suggests that either the network responsible for the generation of these oscillations was unaffected by DA-depletion or that the complete cortico-BG network is required for the generation of pathological oscillations in the DA-depleted state. Further studies could repeat these experiments 22 weeks post-surgery (a timeframe tested in chapter 5), to determine whether long-term plastic and adaptive changes alter the oscillatory profile in M1 *in vitro*.

Despite not seeing alterations in power or frequency, the influence of DA on the network was found to be altered after DA-depletion. Application of DA significantly reduced gamma oscillatory power and significant power increases elicited by D2-like receptor activation were lost in DA-depleted slices. This suggests that in our study, DA-depletion may be changing network components such as receptor complement or efficacy but that this is not being directly expressed as a change in oscillatory frequency or power. These potential findings could be combined in future experiments, in order to further understand the role that DA plays in M1. The use of immunohistochemistry or high resolution fluorescence microscopy to localise the different DA receptors to specific cell types and layers in M1 would be useful to compare their expression and localisation in the control and 6-OHDA

lesioned states. These studies could then be followed up with knock-out models of different DA receptors to investigate their individual involvement in oscillations. Alternatively, if particular receptor subtypes have their expression altered in the lesion model, they could be targeted or reintroduced specifically on particular cell types to investigate how the loss of DA changes receptor expression in the cortico-basal ganglia circuit, and therefore how this affects oscillatory activity. This would help us understand the role of different receptor types in M1 and how these could be manipulated or selectively activated in the brain to treat PD or other dopamine-related disorders.

There were also some distinctive pharmacological results when using dopaminergic drugs, such as the selective increase in theta oscillatory power in sulpiride with no effect on gamma oscillatory power. This could also be subject to the analysis of PAC strength over time, in order to observe the specific changes in theta and gamma oscillatory power on the modulation index. Looking at changes to theta and gamma oscillatory power in relation to PAC in the DA-depleted slices, may reveal differences in how the networks are able to couple together in the absence of DA signalling.

Following 6-OHDA lesion surgery, rotometer, locomotor activity (LMA) and adjusting step tests were carried out. These tests indicated that the lesions were successful and remained stable throughout the experimental period up to at least 22 weeks post-lesion. Using both *in vivo* depth electrode and EEG recordings, we observed an abnormal 30-40 Hz oscillation which was specific to the DA-depleted ipsilateral hemisphere of 6-OHDA animals. An oscillatory peak in the 2-8 Hz range was also observed in ipsilateral and contralateral hemispheres of lesioned animals, as well as sham animals. The abnormal 30-40 Hz oscillations were a faster frequency than beta oscillations (12-25 Hz) seen previously *in vivo* in M1 (Mallet et al., 2008b) but were similar to oscillations observed in previous studies of 6-OHDA lesioned animals during active states (Delaville et al., 2014). We utilised CSD analysis, which suggested that these oscillations might be localised to the superficial (II/III) and deep layers (V) of M1. Application of L-DOPA reduced the power of abnormal 30-40 Hz oscillations and restored inter-hemispheric parity. This demonstrated that 30-40 Hz oscillations could be pharmacologically altered in a similar way to abnormal oscillations previously seen in PD patients (Brown et al., 2001; Kuhn et al., 2006) and 6-OHDA lesioned animals (Delaville et al., 2014).

Finally, we investigated the effect of zolpidem using both depth electrode and EEG recordings in 6-OHDA animals. However, in contrast to the results from a study in PD patients, where low-dose zolpidem was found to reduce exaggerated beta oscillations

(Hall et al., 2014), application of zolpidem did not result in significant changes to abnormal oscillatory activity. Whilst this may be due to differences in the dose of zolpidem being administered, it may also indicate that the abnormal 30-40 Hz oscillations recorded in lesioned animals are pharmacologically distinct from the pathological beta oscillations observed in PD patients. Further experiments using different doses of zolpidem may be necessary in order to define the therapeutic window in 6-OHDA lesioned animals, as well as further experimental paradigms designed to isolate the individual oscillatory components that relate to movement in M1. For instance the use of a maze to hold animals in a stationary position and have pre-defined points at which movement would be occurring, would allow greater resolution of movement and stationary periods. Alternatively, performing these same experiments and drug exposures on anaesthetized animals would provide greater comparisons to be drawn to previous studies in the literature.

Future experiments should focus on the expansion of chapter 3 through a greater understanding of the discrete networks individually generating the theta and gamma oscillations in M1 and how these networks interact to generate the phase-amplitude coupling we have observed. Additionally, a greater understanding of any changes to DA receptor expression or localisation in M1 in the control and 6-OHDA lesioned states would aid in understanding changes that occur in PD.

The comprehensive pharmacological analysis of our theta and gamma oscillations, described in chapter 3, suggests that the modulation of $GABA_A$ receptors plays an important role in the generation and modulation of both oscillations. However, as shown in other brain areas, such as the hippocampus (Klausberger et al., 2003; Somogyi et al., 2014), there are many different populations of interneurons that contribute to oscillations and form synaptic connections with multiple cells types at both synaptic and extrasynaptic locations. Understanding the relative involvement and contribution these different interneuronal subtypes have on network oscillations in M1 would provide a better understanding of how these oscillations can be affected both in PD and other disorders, as well as how oscillations contribute to movement and other physiological processes. In order to investigate the involvement of different interneuronal subtypes, further experiments could utilise $Ca^{2+}$ imaging using a fluorescent indicator, which if it was targeted to specific neuronal cell types could indicate the timing and relative contribution of these neurons to oscillations if recordings were paired with LFPs. Alternatively, using genetic knock-outs or lox-cre conditional knock-outs to different cell types, we could also observe how networks adapt to the loss or specific involvement of these neurons in the

generation of theta and gamma oscillations. This could also be achieved through the use of optogenetics, whereby different genetically targeted and incorporated ion channels that are sensitive to light could be used to artificially activate or silence individual neuronal populations. Combining multiple sensitive receptors, which respond to different wavelengths of light, would allow for more complex and specific control of the different excitatory and inhibitory populations that contribute to oscillations. This would also allow the manipulation of these networks *in vivo*, whereby the involvement of the different neuronal networks and cellular subtypes could be silenced or activated to investigate the role of these cells in behavioural tests. Additionally, oscillations could be targeted and manipulated pharmacologically using DREADDs (designer receptors exclusively activated by designer drugs), which are human-made synthetic receptors that are known to only be activated by a single synthetically made drug. If these were genetically targeted to different neuronal types, then the involvement of these cells could be manipulated during oscillatory activity with absolute certainty that there are no unknown non-specific effects of these drugs on other receptors or untargeted cell types. The use of any of these experimental techniques would be invaluable in beginning to separate the different interneuronal types involved in our oscillations. Furthermore, manipulation of the networks involved would aid in our understanding of how the theta and gamma oscillations interact and couple together both *in vitro* and *in vivo*.

These studies could also be expanded to investigate other brain areas *in vitro*, as the whole of the cortico-basal ganglia network is involved in movement and dysfunction in PD, not just M1. There have been investigations into the use of slice orientations that maintain the cortico-basal ganglia hyperdirect connections (Bosch et al., 2012), as well as those that maintain the cortico-thalamic connections (Smeal et al., 2007). If these were utilised, using the improved solutions for slice preparation that we have used in this thesis, it is possible that we could investigate the oscillatory activity in M1 and the basal ganglia nuclei. This may provide a much more physiological view of network oscillations in these brain areas, as the connections which are present *in vivo* would be maintained. This would be beneficial, not only for analysis of control oscillations or coherence analysis between the cortex and basal ganglia, but also for understanding oscillations generated in the 6-OHDA lesion model of PD. Understanding how oscillations throughout the cortico-basal ganglia circuit are affected by the loss of DA would allow greater comparisons between these circuits *in vitro* and the changes observed in PD patients, and may even generate the characteristic beta oscillatory pathology we did not observe in isolated M1 slices.

Overall, if we could determine the neuronal network machinery which underlies 12-25 Hz and 30-40 Hz oscillations observed both *in vitro* and *in vivo*, we could begin to isolate the changes that result in PD pathology. These could lead to a better understanding of this disease and guide the advancement of future treatments, aimed as targeting the pathological network activity and underlying symptoms in PD.

# References

Adrian ED (1942) Olfactory reactions in the brain of the hedgehog. Journal of Physiology 100:459-473.

Aghajanian GK, Bunney BS (1977) Pharmacological characterization of dopamine "autoreceptors" by microiontophoretic single-cell recording studies. Advances in Biochemical Psychopharmacology 16:433-438.

Aizman O, Brismar H, Uhlen P, Zettergren E, Levey AI, Forssberg H, Greengard P, Aperia A (2000) Anatomical and physiological evidence for D-1 and D-2 dopamine receptor colocalization in neostriatal neurons. Nature Neuroscience 3:226-230.

Albin RL, Young AB, Penney JB (1989) The functional-anatomy of basal ganglia disorders. Trends in Neurosciences 12:366-375.

Amador M, Dani J (1991) MK-801 inhibition of nicotinic acetylcholine receptor channels. Synapse 215:207-215.

Amtage F, Henschel K, Schelter B, Vesper J, Timmer J, Luecking CH, Hellwig B (2008) Tremor-correlated neuronal activity in the subthalamic nucleus of Parkinsonian patients. Neuroscience Letters 442:195-199.

Aronstam RS, Narayanan L, Wenger DA (1982) Ketamine inhibition of ligand binding to cholinergic receptors and ion channels. European Journal of Pharmacology 78:367-370.

Avila I, Parr-Brownlie LC, Brazhnik E, Castaneda E, Bergstrom DA, Walters JR (2010) Beta frequency synchronization in basal ganglia output during rest and walk in a hemiparkinsonian rat. Experimental Neurology 221:307-319.

Awenowicz PW, Porter LL (2002) Local application of dopamine inhibits pyramidal tract neuron activity in the rodent motor cortex. Journal of Neurophysiology 88:3439-3451.

Aziz TZ, Peggs D, Sambrook MA, Crossman AR (1991) Lesion of the subthalamic nucleus for the alleviation of 1-methyl-4-phenyl-1,2,3,6-tetrahydropyridine (MPTP)-induced parkinsonism in the primate. Movement Disorders 6:288-292.

Baker SN, Olivier E, Lemon RN (1997) Coherent oscillations in monkey motor cortex and hand muscle EMG show task-dependent modulation. Journal of Physiology 501:225-241.

Bandrowski AE, Huguenard JR, Prince DA (2003) Baseline glutamate levels affect group I and II mGluRs in layer V pyramidal neurons of rat sensorimotor cortex. Journal of Neurophysiology 89:1308-1316.

Barnard EA, Skolnick P, Olsen RW, Mohler H, Sieghart W, Biggio G, Braestrup C, Bateson AN, Langer SZ (1998) International Union of Pharmacology. XV. Subtypes of gamma-aminobutyric acid A receptors: classification on the basis of subunit structure and receptor function. Pharmacological Reviews 50:291-313.

Bartos M, Vida I, Frotscher M, Meyer A, Monyer H, Geiger JRP, Jonas P (2002) Fast synaptic inhibition promotes synchronized gamma oscillations in hippocampal interneuron networks. Proceedings of the National Academy of Sciences of the United States of America 99:13222-13227.

Beckstead MJ, Grandy DK, Wickman K, Williams JT (2004) Vesicular dopamine release elicits an inhibitory postsynaptic current in midbrain dopamine neurons. Neuron 42:939-946.

Bergman H, Wichmann T, Delong MR (1990) Reversal of experimental Parkinsonism by lesions of the subthalamic nucleus. Science 249:1436-1438.

Bergman H, Wichmann T, Karmon B, DeLong MR (1994) The primate subthalamic nucleus. II. Neuronal activity in the MPTP model of parkinsonism. Journal of Neurophysiology 72:507-520.

Bernheimer H, Birkmayer W, Hornykiewicz O, Jellinger K, Seitelberger F (1973) Brain dopamine and the syndromes of Parkinson and Huntington. Clinical, morphological and neurochemical correlations. Journal of the Neurological Sciences 20:415-455.

Besson MJ, Chermay A, Feltz P, Glowinski J (1969) Release of newly synthesized dopamine from dopamine containing terminals in the striatum of the rat. Proceedings of the National Academy of Sciences of the United States of America 62:741-748.

Bettler B, Tiao JYH (2006) Molecular diversity, trafficking and subcellular localization of GABAB receptors. Pharmacology and Therapeutics 110:533-543.

Bettler B, Kaupmann K, Mosbacher J, Gassmann M (2004) Molecular structure and physiological functions of GABA B receptors. Physiological Reviews 84:835-867.

Bevan MD, Magill PJ, Terman D, Bolam JP, Wilson CJ (2002) Move to the rhythm: oscillations in the subthalamic nucleus-external globus pallidus network. Trends in Neurosciences 25:525-531.

Bibbig A, Traub RD, Whittington MA (2002) Long-range synchronization of gamma and beta oscillations and the plasticity of excitatory and inhibitory synapses: A network model. Journal of Neurophysiology 88:1634-1654.

Binkofski F, Fink GR, Geyer S, Buccino G, Gruber O, Shah NJ, Taylor JG, Seitz RJ, Zilles K, Freund HJ (2002) Neural activity in human primary motor cortex areas 4a and 4p is modulated differentially by attention to action. Journal of Neurophysiology 88:514-519.

Bland BH (1986) The physiology and pharmacology of hippocampal-formation theta rhythms. Progress in Neurobiology 26:1-54.

Bland BH, Colom LV (1993) Extrinsic and intrinsic-properties underlying oscillation and synchrony in limbic cortex. Progress in Neurobiology 41:157-208.

Bland BH, Oddie SD (2001) Theta band oscillation and synchrony in the hippocampal formation and associated structures: the case for its role in sensorimotor integration. Behavioural Brain Research 127:119-136.

Bland BH, Konopacki J, Dyck RH (2002) Relationship between membrane potential oscillations and rhythmic discharges in identified hippocampal theta-related cells. Journal of Neurophysiology 88:3046-3066.

Bland BH, Colom LV, Konopacki J, Roth SH (1988) Intracellular records of carbachol-induced theta rhythm in hippocampal slices. Brain Research 447:364-368.

Blum D, Torch S, Lambeng N, Nissou MF, Benabid AL, Sadoul R, Verna JM (2001) Molecular pathways involved in the neurotoxicity of 6-OHDA, dopamine and MPTP: contribution to the apoptotic theory in Parkinson's disease. Progress in Neurobiology 65:135-172.

Bocian R, Posłuszny A, Kowalczyk T, Gołebiewski H, Konopacki J (2009) The effect of carbenoxolone on hippocampal formation theta rhythm in rats: In vitro and in vivo approaches. Brain Research Bulletin 78:290-298.

Bolam JP, Smith Y (1992) The striatum and the globus-pallidus send convergent synaptic inputs onto single cells in the entopeduncular nucleus of the rat - a double anterograde labeling study combined with postembedding immunocytochemistry for GABA. Journal of Comparative Neurology 321:456-476.

Borroto-Escuela DO, Pintsuk J, Schäfer T, Friedland K, Ferraro L, Tanganelli S, Liu F, Fuxe K (2016) Multiple D2 heteroreceptor complexes: new targets for treatment of schizophrenia. Therapeutic Advances in Psychopharmacology:1-18.

Bosch C, Mailly P, Degos B, Deniau JM, Venance L (2012) Preservation of the hyperdirect pathway of basal ganglia in a rodent brain slice. Neuroscience 215:31-41.

Boyce S, Kelly E, Reavill C, Jenner P, Marsden CD (1984) Repeated administration of N-methyl-4-phenyl-1,2,3,6-tetrahydropyridine to rats is not toxic to striatal dopamine neurons. Biochemical Pharmacology 33:1747-1752.

Braak H, Del Tredici K, Rub U, de Vos RAI, Steur E, Braak E (2003) Staging of brain pathology related to sporadic Parkinson's disease. Neurobiology of Aging 24:197-211.

Bragin A, Jando G, Nadasdy Z, Hetke J, Wise K, Buzsaki G (1995) Gamma (40-100-Hz) oscillation in the hippocampus of the behaving rat. Journal of Neuroscience 15:47-60.

Brazhnik E, Novikov N, McCoy AJ, Cruz AV, Walters JR (2014) Functional correlates of exaggerated oscillatory activity in basal ganglia output in hemiparkinsonian rats. Experimental Neurology 261:563-577.

Brazhnik E, Cruz AV, Avila I, Wahba MI, Novikov N, Ilieva NM, McCoy AJ, Gerber C, Walters JR (2012) State-dependent spike and local field synchronization between motor cortex and substantia nigra in hemiparkinsonian rats. Journal of Neuroscience 32:7869-7880.

Breese GR, Traylor TD (1971) Depletion of brain noradrenaline and dopamine by 6-hydroxydopamine. British Journal of Pharmacology 42:88-99.

Brefel-Courbon C, Payoux P, Ory F, Sommet A, Slaoui T, Raboyeau G, Lemesle B, Puel M, Montastruc JL, Demonet JF, Cardebat D (2007) Clinical and imaging evidence of zolpidem effect in hypoxic encephalopathy. Annals of Neurology 62:102-105.

Brittain J-S, Brown P (2014) Oscillations and the basal ganglia: Motor control and beyond. Neuroimage 85:637-647.

Brittain J-S, Sharott A, Brown P (2014) The highs and lows of beta activity in cortico-basal ganglia loops. European Journal of Neuroscience 39:1951-1959.

Brown P (2003) Oscillatory nature of human basal ganglia activity: relationship to the pathophysiology of Parkinson's disease. Movement Disorders 18:357-363.

Brown P, Marsden CD (1998) What do the basal ganglia do? Lancet 351:1801-1804.

Brown P, Williams D (2005) Basal ganglia local field potential activity: Character and functional significance in the human. Clinical Neurophysiology 116:2510-2519.

Brown P, Salenius S, Rothwell JC, Hari R (1998) Cortical correlate of the piper rhythm in humans. Journal of Neurophysiology 80:2911-2917.

Brown P, Oliviero A, Mazzone P, Insola A, Tonali P, Di Lazzaro V (2001) Dopamine dependency of oscillations between subthalamic nucleus and pallidum in Parkinson's disease. Journal of Neuroscience 21:1033-1038.

Bueeler H (2009) Impaired mitochondrial dynamics and function in the pathogenesis of Parkinson's disease. Experimental Neurology 218:235-246.

Buhl EH, Tamas G, Fisahn A (1998) Cholinergic activation and tonic excitation induce persistent gamma oscillations in mouse somatosensory cortex in vitro. Journal of Physiology 513:117-126.

Buzsaki G (2002) Theta oscillations in the hippocampus. Neuron 33:325-340.

Buzsaki G, Draguhn A (2004) Neuronal oscillations in cortical networks. Science 304:1926-1929.

Buzsaki G, Wang X-J (2012) Mechanisms of gamma oscillations. Annual Review of Neuroscience 35:203-225.

Buzsaki G, Anastassiou CA, Koch C (2012) The origin of extracellular fields and currents - EEG, ECoG, LFP and spikes. Nature Reviews Neuroscience 13:407-420.

Cacucci F, Lever C, Wills TJ, Burgess N, O'Keefe J (2004) Theta-modulated place-by-direction cells in the hippocampal formation in the rat. Journal of Neuroscience 24:8265-8277.

Calabresi P, Maj R, Pisani A, Mercuri NB, Bernardi G (1992) Long-term synaptic depression in the striatum - physiological and pharmacological characterization. Journal of Neuroscience 12:4224-4233.

Calabresi P, Di Filippo M, Ghiglieri V, Tambasco N, Picconi B (2010) Levodopa-induced dyskinesias in patients with Parkinson's disease: filling the bench-to-bedside gap. Lancet Neurology 9:1106-1117.

Canolty RT, Knight R (2010) The functional role of cross-frequncy coupling. Trends in Cognitive Sciences 14:506-515.

Canolty RT, Edwards E, Dalal SS, Soltani M, Nagarajan SS, Kirsch HE, Berger MS, Barbaro NM, Knight RT (2006) High gamma power is phase-locked to theta oscillations in human neocortex. Science 313:1626-1628.

Cantero JL, Atienza M, Stickgold R, Kahana MJ, Madsen JR, Kocsis B (2003) Sleep-dependent theta oscillations in the human hippocampus and neocortex. Journal of Neuroscience 23:10897-10903.

Cardin JA, Carlen M, Meletis K, Knoblich U, Zhang F, Deisseroth K, Tsai LH, Moore CI (2009) Driving fast-spiking cells induces gamma rhythm and controls sensory responses. Nature 459:663-U663.

Carlson JH, Bergstrom DA, Weick BG, Walters JR (1987) Neurophysiological investigation of effects of the D-1 agonist SKF-38393 on tonic activity of substantia-nigra dopamine neurons. Synapse 1:411-416.

Cassidy M, Mazzone P, Oliviero A, Insola A, Tonali P, Di Lazzaro V, Brown P (2002) Movement-related changes in synchronization in the human basal ganglia. Brain 125:1235-1246.

Castro-Alamancos MA (2013) The motor cortex: a network tuned to 7-14 Hz. Frontiers in Neural Circuits 7:1-7.

Cepeda C, Hurst RS, Altemus KL, Flores-Hernandez J, Calvert CR, Jokel ES, Grandy DK, Low MJ, Rubinstein M, Ariano MA, Levine MS (2001) Facilitated glutamatergic transmission in the striatum of D-2 dopamine receptor-deficient mice. Journal of Neurophysiology 85:659-670.

Chen CC, Litvak V, Gilbertson T, Kuhn A, Lu CS, Lee ST, Tsai CH, Tisch S, Limousin P, Hariz M, Brown P (2007) Excessive synchronization of basal ganglia neurons at 20 Hz slows movement in Parkinson's disease. Experimental Neurology 205:214-221.

Chevalier G, Deniau JM (1990) Disinhibition as a basic process in the expression of striatal functions. Trends in Neurosciences 13:277-280.

Cheyne D, Bells S, Ferrari P, Gaetz W, Bostan AC (2008) Self-paced movements induce high-frequency gamma oscillations in primary motor cortex. Neuroimage 42:332-342.

Chiueh CC, Moore KE (1975) D-amphetamine-induced release of newly synthesized and stores dopamine from caudate-nucleus invivo. Journal of Pharmacology and Experimental Therapeutics 192:642-653.

Chiueh CC, Markey SP, Burns RS, Johannessen JN, Pert A, Kopin IJ (1984) Neurochemical and behavioral effects of systemic and intranigral administration of N-methyl-4-phenyl-1,2,3,6-tetrahydropyridine in the rat. European Journal of Pharmacology 100:189-194.

Cho RH, Segawa S, Okamoto K, Mizuno A, Kaneko T (2004) Intracellularly labeled pyramidal neurons in the cortical areas projecting to the spinal cord - II. Intra- and juxta-columnar projection of pyramidal neurons to corticospinal neurons. Neuroscience Research 50:395-410.

Chrobak JJ, Buzsaki G (1998) Gamma oscillations in the entorhinal cortex of the freely behaving rat. Journal of Neuroscience 18:388-398.

Chu ZG, Galarreta M, Hestrin S (2003) Synaptic interactions of late-spiking neocortical neurons in layer 1. Journal of Neuroscience 23:96-102.

Clarke PB, Reuben M (1995) Inhibition by dizocilpine (MK-801) of striatal dopamine release induced by MPTP and MPP+: possible action at the dopamine transporter. British Journal of Pharmacology 114:315-322.

Clauss R, Nel W (2006) Drug induced arousal from the permanent vegetative state. Neurorehabilitation 21:23-28.

Cobb SR, Bulters DO, Davies CH (2000) Coincident activation of mGluRs and mAChRs imposes theta frequency patterning on synchronised network activity in the hippocampal CA3 region. Neuropharmacology 39:1933-1942.

Colom LV, Nassif-Caudarella S, Dickson CT, Smythe JW, Bland BH (1991) In vivo intrahippocampal microinfusion of carbachol and bicuculline induces theta-like oscillations in the septally deafferented hippocampus. Hippocampus 1:381-390.

Connors BW (2012) Tales of a Dirty Drug: Carbenoxolone, Gap Junctions, and Seizures. Epilepsy Currents 12:66-68.

Cools AR, Brachten R, Heeren D, Willemen A, Ellenbroek B (1990) Search after neurobiological profile of individual-specific features of wistar rats. Brain Research Bulletin 24:49-69.

Cooper AJ, Stanford IM (2001) Dopamine D2 receptor mediated presynaptic inhibition of striatopallidal GABA(A) IPSCs in vitro. Neuropharmacology 41.

Cosgrove KE, Meriney SD, Barrionuevo G (2011) High affinity group III mGluRs regulate mossy fiber input to CA3 interneurons. Hippocampus 21:1302-1317.

Cossart R, Esclapez M, Hirsch JC, Bernard C, Ben-Ari Y (1998) GluR5 kainate receptor activation in interneurons increases tonic inhibition of pyramidal cells. Nature Neuroscience 1:470-478.

Costa E, Guidotti A (1985) Endogenous ligands for benzodiazepine recognition sites. Biochemical Pharmacology 34:3399-3403.

Couve A, Calver AR, Fairfax B, Moss SJ, Pangalos MN (2004) Unravelling the unusual signalling properties of the GABA B receptor. Biochemical Pharmacology 68:1527-1536.

Creese I, Burt DR, Snyder SH (1976) Dopamine receptor binding predicts clinical and pharmacological potencies of antischizophrenic drugs. Science 192:481-483.

Crestani F, Martin JR, Mohler H, Rudolph U (2000) Mechanism of action of the hypnotic zolpidem in vivo. British Journal of Pharmacology 131:1251-1254.

Crone NE, Miglioretti DL, Gordon B, Lesser RP (1998) Functional mapping of human sensorimotor cortex with electrocorticographic spectral analysis - II. Event-related synchronization in the gamma band. Brain 121:2301-2315.

Csicsvari J, Jamieson B, Wise KD, Buzsáki G (2003) Mechanisms of gamma oscillations in the hippocampus of the behaving rat. Neuron 37:311-322.

Cunningham MO, Davies CH, Buhl EH, Kopell N, Whittington MA (2003) Gamma oscillations induced by kainate receptor activation in the entorhinal cortex in vitro. Journal of Neuroscience 23:9761-9769.

Cunningham MO, Whittington MA, Bibbig A, Roopun A, LeBeau FEN, Vogt A, Monyer H, Buhl EH, Traub RD (2004) A role for fast rhythmic bursting neurons in cortical gamma oscillations in vitro. Proceedings of the National Academy of Sciences of the United States of America 101:7152-7157.

Davie CA (2008) A review of Parkinson's disease. British Medical Bulletin 86:109-127.

Dawson TM, Gehlert DR, McCabe RT, Barnett A, Wamsley JK (1986) D-1 dopamine receptors in the rat-brain - a quantitative autoradiographic analysis. Journal of Neuroscience 6:2352-2365.

de Lau LML, Breteler MMB (2006) Epidemiology of Parkinson's disease. Lancet Neurology 5:525-535.

Deans MR, Gibson JR, Sellitto C, Connors BW, Paul DL (2001) Synchronous activity of inhibitory networks in neocortex requires electrical synapses containing Connexin36. Neuron 31:477-485.

Delaville C, McCoy AJ, Gerber CM, Cruz AV, Walters JR (2015) Subthalamic nucleus activity in the awake hemiparkinsonian rat: relationships with motor and cognitive networks. Journal of Neuroscience 35:6918-6930.

Delaville C, Cruz AV, McCoy AJ, Brazhnik E, Avila I, Novikov N, Walters JR (2014) Oscillatory activity in basal ganglia and motor cortex in an awake behaving rodent model of Parkinson's disease. Basal Ganglia 3:221-227.

Delong MR (1990) Primate models of movement-disorders of basal ganglia origin. Trends in Neurosciences 13:281-285.

Deng P-Y, Xiao Z, Lei S (2010) Distinct modes of modulation of GABAergic transmission by Group I metabotropic glutamate receptors in rat entorhinal cortex. Hippocampus 20:980-993.

Desai MA, Conn PJ (1991) Excitatory effects of ACPD receptor activation in the hippocampus are mediated by direct effects on pyramidal cells and blockade of synaptic inhibition. Journal of Neurophysiology 66:40-52.

Desai MA, McBain CJ, Kauer JA, Conn PJ (1994) Metabotropic glutamate receptor-induced disinhibition is mediated by reduced transmission at excitatory synapses onto interneurons and inhibitory synapses onto pyramidal cells. Neuroscience Letters 181:78-82.

Dickson CT, Biella G, de Curtis M (2000) Evidence for spatial modules mediated by temporal synchronization of carbachol-induced gamma rhythm in medial entorhinal cortex. Journal of Neuroscience 20:7846-7854.

Donoghue JP, Wise SP (1982) The motor cortex of the rat - cytoarchitecture and microstimulation mapping. Journal of Comparative Neurology 212:76-88.

Donoghue JP, Sanes JN, Hatsopoulos NG, Gaal G (1998) Neural discharge and local field potential oscillations in primate motor cortex during voluntary movements. Journal of Neurophysiology 79:159-173.

Drouot X, Oshino S, Jarraya B, Besret L, Kishima H, Remy P, Dauguet J, Lefaucheur JP, Dolle F, Conde F, Bottlaender M, Peschanski M, Keravel Y, Hantraye P, Palfi S (2004) Functional recovery in a primate model of Parkinson's disease following motor cortex stimulation. Neuron 44:769-778.

Durstewitz D, Seamans JK (2002) The computational role of dopamine D1 receptors in working memory. Neural Networks 15:561-572.

Durstewitz D, Seamans JK, Sejnowski TJ (2000) Dopamine-mediated stabilization of delay-period activity in a network model of prefrontal cortex. Journal of Neurophysiology 83:1733-1750.

Eccles JC (1981) Physiology of motor control in man. Applied Neurophysiology 44:5-15.

Eckhorn R (1994) Oscillatory and nonoscillatory synchronizations in the visual cortex and their possible roles in associations of visual features. Progress in Brain Research 102:405-426.

Eeckman FH, Freeman WJ (1990) Correlations between unit firing and EEG int he rat olfactory system. Brain Research 528:238-244.

Eghbali M, Curmi JP, Birnir B, Gage PW (1997) Hippocampal GABA(A) channel conductance increased by diazepam. Nature 388:71-75.

Ehringer H, Hornykiewicz O (1960) Distribution of noradrenaline and dopamine (3-hydroxytyramine) in the human brain and their behavior in diseases of the extrapyramidal system. Klinische Wochenschrift 38:1236-1239.

Ellren K, Lehmann A (1989) Calcium dependency of N-methyl-D-aspartate toxicity in slices from the immature rat hippocampus. Neuroscience 32:371-379.

Elul R (1971) The genesis of the EEG. International Review of Neurobiology 15:227-272.

Engel AK, Fries P (2010) Beta-band oscillations - signalling the status quo? Current Opinion in Neurobiology 20:156-165.

Engel AK, Fries P, Singer W (2001) Dynamic predictions: Oscillations and synchrony in top-down processing. Nature Reviews Neuroscience 2:704-716.

Enjalbert A, Bockaert J (1983) Pharmacological characterization of the D2-dopamine receptor negatively coupled with adenylate-cyclase in rat anterior-pituitary. Molecular Pharmacology 23:576-584.

Ermentrout GB, Kopell N (1998) Fine structure of neural spiking and synchronization in the presence of conduction delays. Proceedings of the National Academy of Sciences of the United States of America 95:1259-1264.

Errington AC, Di Giovanni G, Crunelli V, Cope DW (2011) MGluR control of interneuron output regulates feedforward tonic GABA(A) inhibition in the visual thalamus. Journal of Neuroscience 31:8669-8680.

Eusebio A, Chen CC, Lu CS, Lee ST, Tsai CH, Limousin P, Hariz M, Brown P (2008) Effects of low-frequency stimulation of the subthalamic nucleus on movement in Parkinson's disease. Experimental Neurology 209:125-130.

Fabbrini G, Brotchie JM, Grandas F, Nomoto M, Goetz CG (2007) Levodopa-induced dyskinesias. Movement Disorders 22:1379-1389.

Farrant M, Nusser Z (2005) Variations on an inhibitory theme: Phasic and tonic activation of GABA(A) receptors. Nature Reviews Neuroscience 6:215-229.

Farzampour Z, Reimer RJ, Huguenard J (2015) Endozepines. In: Advances in Pharmacology, pp 147-164.

Faulkner HJ, Traub RD, Whittington MA (1998) Disruption of synchronous gamma oscillations in the rat hippocampal slice: A common mechanism of anaesthetic drug action. British Journal of Pharmacology 125:483-492.

Fearnley JM, Lees AJ (1991) Aging and Parkinsons-disease - substantia-nigra regional selectivity. Brain 114:2283-2301.

Ferezou I, Haiss F, Gentet LJ, Aronoff R, Weber B, Petersen CCH (2007) Spatiotemporal dynamics of cortical sensorimotor integration in behaving mice. Neuron 56:907-923.

Filion M, Tremblay L (1991) Abnormal spoontanueous activity of globus-pallidus neurons in monkeys with MPTP-induced Parkinsonism. Brain Research 547:142-151.

Fisahn A, Pike FG, Buhl EH, Paulsen O (1998) Cholinergic induction of network oscillations at 40 Hz in the hippocampus in vitro. Nature 394:186-189.

Fisahn A, Contractor A, Traub RD, Buhl EH, Heinemann SF, McBain CJ (2004) Distinct roles for the kainate receptor subunits GluR5 and GluR6 in kainate-induced hippocampal gamma oscillations. Journal of Neuroscience 24:9658-9668.

Fisahn A, Yamada M, Duttaroy A, Gan JW, Deng CX, McBain CJ, Wess J (2002) Muscarinic induction of hippocampal gamma oscillations requires coupling of the M1 receptor to two mixed cation currents. Neuron 33:615-624.

Fitzgerald PB, Fountain S, Daskalakis ZJ (2006) A comprehensive review of the effects of rTMS on motor cortical excitability and inhibition. Clinical Neurophysiology 117:2584-2596.

Forno LS, Langston JW, Delanney LE, Irwin I, Ricaurte GA (1986) Locus-ceruleus lesions and eosinophilic inclusions in MPTP-treated monkeys. Annals of Neurology 20:449-455.

Freeman WJ (1978) Spatial properties of an EEG event in olfactory-bulb and cortex. Electroencephalography and Clinical Neurophysiology 44:586-605.

Freund TF, Antal M (1988) GABA-containing neurons in the septum control inhibitory interneurons in the hippocampus. Nature 336:170-173.

Friedman E, Jin LQ, Cai GP, Hollon TR, Drago J, Sibley DR, Wang HY (1997) D-1-like dopaminergic activation of phosphoinositide hydrolysis is independent of D-1A dopamine receptors: Evidence from D-1A knockout mice. Molecular Pharmacology 51:6-11.

Fries P (2005) A mechanism for cognitive dynamics: neuronal communication through neuronal coherence. Trends in Cognitive Sciences 9:474-480.

Fuchs EC, Doheny H, Faulkner H, Caputi A, Traub RD, Bibbig A, Kopell N, Whittington MA, Monyer H (2001) Genetically altered AMPA-type glutamate receptor kinetics in interneurons disrupt long-range synchrony of gamma oscillation. Proceedings of the National Academy of Sciences of the United States of America 98:3571-3576.

Fuchs EC, Zivkovic AR, Cunningham MO, Middleton S, LeBeau FEN, Bannerman DM, Rozov A, Whittington MA, Traub RD, Rawlins JNP, Monyer H (2007) Recruitment of parvalbumin-positive interneurons determines hippocampal function and associated behavior. Neuron 53:591-604.

Gabbott PLA, Somogyi P (1986) Quantitative distribution of GABA-immunoreactive neurons in the visual-cortex (area 17) of the cat. Experimental Brain Research 61:323-331.

Gage PW (1992) Activation and modulation of neuronal K+ channels by GABA. Trends in Neurosciences 15:46-51.

Galarreta M, Hestrin S (1999) A network of fast-spiking cells in the neocortex connected by electrical synapses. Nature 402:72-75.

Gancher ST, Nutt JG, Woodward WR (1987) Peripheral pharmacokinetics of levodopa in untreated, stable, and fluctuating Parkinsonian-patients. Neurology 37:940-944.

Garcia L, D'Alessandro G, Fernagut PO, Bioulac B, Hammond C (2005) Impact of high-frequency stimulation parameters on the pattern of discharge of subthalamic neurons. Journal of Neurophysiology 94:3662-3669.

Garcia-Cabezas MA, Barbas H (2014) Area 4 has layer IV in adult primates. European Journal of Neuroscience 39:1824-1834.

Gaspar P, Bloch B, Lemoine C (1995) D1 and D2 receptor gene expression in the rat frontal cortex: Cellular localization in different classes of efferent neurons. European Journal of Neuroscience 7:1050-1063.

Gauthier J, Parent M, Levesque M, Parent A (1999) The axonal arborization of single nigrostriatal neurons in rats. Brain Research 834:228-232.

Gerfen CR, Surmeier DJ (2011) Modulation of Striatal Projection Systems by Dopamine. Annual Review of Neuroscience, Vol 34 34:441-466.

Gerfen CR, Engber TM, Mahan LC, Susel Z, Chase TN, Monsma FJ, Sibley DR (1990) D1 and D2 dopamine receptor regulated gene-expression of striatonigral and striatopallidal neurons. Science 250:1429-1432.

German DC, Dubach M, Askari S, Speciale SG, Bowden DM (1988) 1-methyl-4-phenyl-1,2,3,6-tetra-hydropyridine-induced Parkinsonian syndrome in macaca-fasicularis - which midbrain dopaminergic-neurons are lost? Neuroscience 24:161-174.

Gertler TS, Chan CS, Surmeier DJ (2008) Dichotomous Anatomical Properties of Adult Striatal Medium Spiny Neurons. Journal of Neuroscience 28:10814-10824.

Giannicola G, Marceglia S, Rossi L, Mrakic-Sposta S, Rampini P, Tamma F, Cogiamanian F, Barbieri S, Priori A (2010) The effects of levodopa and ongoing deep brain stimulation on subthalamic beta oscillations in Parkinson's disease. Experimental Neurology 226:120-127.

Gibson JR, Beierlein M, Connors BW (1999) Two networks of electrically coupled inhibitory neurons in neocortex. Nature 402:75-79.

Gillies MJ, Traub RD, LeBeau FEN, Davies CH, Gloveli T, Buhl EH, Whittington MA (2002) A model of atropine-resistant theta oscillations in rat hippocampal area CA1. Journal of Physiology 543:779-793.

Glaze D (1990) Drug effects. In: Current practice of clinical electroencephalography (Daly D, Pedley T, eds), pp 489-512: Raven Press, New York.

Golebiewski H, Eckersdorf B, Konopacki J (1993) Muscarinic (M1) mediation of hippocampal spontaneous theta rhythm in freely moving cats. Neuroreport 4:1323-1326.

Golebiewski H, Eckersdorf B, Konopacki J (2006) Electrical coupling underlies theta rhythm in freely moving cats. European Journal of Neuroscience 24:1759-1770.

Gonchar Y, Burkhalter A (1999) Differential subcellular localization of forward and feedback interareal inputs to parvalbumin expressing GABAergic neurons in rat visual cortex. Journal of Comparative Neurology 406:346-360.

Gonzalez S, Moreno-Delgado D, Moreno E, Perez-Capote K, Franco R, Mallol J, Cortes A, Casado V, Lluis C, Ortiz J, Ferre S, Canela E, McCormick PJ (2012) Circadian-related heteromerization of adrenergic and dopamine D-4 receptors modulates melatonin synthesis and release in the pineal gland. PLOS Biology 10.

Gonzalez-Islas C, Hablitz JJ (2003) Dopamine enhances EPSCs in layer II-III pyramidal neurons in rat prefrontal cortex. Journal of Neuroscience 23:867-875.

Goto S, Hirano A, Matsumoto S (1989) Subdivisional involvement of nigrostriatal loop in idiopathic Parkinsons-disease and striatonigral degeneration. Annals of Neurology 26:766-770.

Gradinaru V, Mogri M, Thompson KR, Henderson JM, Deisseroth K (2009) Optical deconstruction of Parkinsonian neural circuitry. Science 324:354-359.

Gray CM (1994) Synchronous oscillations in neuronal systems: mechanisms and functions. Journal of Computational Neuroscience 1:11-38.

Gray CM, Singer W (1989) Stimulus-specific neuronal oscillations in orientation columns of cat visual cortex. Proceedings of the National Academy of Sciences of the United States of America 86:1698-1702.

Gray CM, Konig P, Engel AK, Singer W (1989) Oscillatory responses in cat visual-cortex exhibit inter-columnar synchronization which reflects global stimulus properties. Nature 338:334-337.

Green JD, Arduini AA (1954) Hippocampal electrical activity in arousal. Journal of Neurophysiology 17:533-557.

Greengard P (2001) The neurobiology of slow synaptic transmission. Science 294:1024-1030.

Griffiths MJD, Messent M, Macallister RJ, Evans TW (1993) Aminoguanidine selectively inhibits inducible nitric-oxide synthase. British Journal of Pharmacology 110:963-968.

Grunze HC, Rainnie DG, Hasselmo ME, Barkai E, Hearn EF, McCarley RW, Greene RW (1996) NMDA-dependent modulation of CA1 local circuit inhibition. Journal of Neuroscience 16:2034-2043.

Gulyas AI, Seress L, Toth K, Acsady L, Antal M, Freund TF (1991) Septal GABAergic neurons innervate inhibitory interneurons in the hippocampus of the macaque monkey. Neuroscience 41:381-390.

Haber SN, Fudge JL, McFarland NR (2000) Striatonigrostriatal pathways in primates form an ascending spiral from the shell to the dorsolateral striatum. Journal of Neuroscience 20:2369-2382.

Hajos N, Palhalmi J, Mann EO, Nemeth B, Paulsen O, Freund TF (2004) Spike timing of distinct types of GABAergic interneuron during hippocampal gamma oscillations in vitro. Journal of Neuroscience 24:9127-9137.

Hajos N, Katona I, Naiem SS, Mackie K, Ledent C, Mody I, Freund TF (2000) Cannabinoids inhibit hippocampal GABAergic transmission and network oscillations. European Journal of Neuroscience 12:3239-3249.

Hakami T, Jones NC, Tolmacheva EA, Gaudias J, Chaumont J, Salzberg M, O'Brien TJ, Pinault D (2009) NMDA receptor hypofunction leads to generalized and persistent aberrant gamma oscillations independent of hyperlocomotion and the state of consciousness. PLOS One 4.

Halje P, Tamte M, Richter U, Mohammed M, Cenci MA, Petersson P (2012) Levodopa-induced dyskinesia is strongly associated with resonant cortical oscillations. Journal of Neuroscience 32:16541-16551.

Hall SD, Yamawaki N, Fisher AE, Clauss RP, Woodhall GL, Stanford IM (2010) GABA(A) alpha-1 subunit mediated desynchronization of elevated low frequency oscillations alleviates specific dysfunction in stroke - A case report. Clinical Neurophysiology 121:549-555.

Hall SD, Stanford IM, Yamawaki N, McAllister CJ, Ronnqvist KC, Woodhall GL, Furlong PL (2011) The role of GABAergic modulation in motor function related neuronal network activity. Neuroimage 56:1506-1510.

Hall SD, Prokic EJ, McAllister CJ, Ronnqvist KC, Williams AC, Yamawaki N, Witton C, Woodhall GL, Stanford IM (2014) GABA-mediated changes in inter-hemispheric beta frequency activity in early-stage Parkinson's disease. Neuroscience 281:68-76.

Halliwell JV, Adams PR (1982) Voltage-clamp analysis of muscarinic excitation in hippocampal-neurons. Brain Research 250:71-92.

Hamada I, Delong MR (1992) Excitotoxic acid lesions of the primate subthalamic nucleus result in reduced pallidal neuronal activity during active holding. Journal of Neurophysiology 68:1859-1866.

Hammond C, Bergman H, Brown P (2007) Pathological synchronization in Parkinson's disease: networks, models and treatments. Trends in Neurosciences 30:357-364.

Harsing LG, Zigmond MJ (1997) Influence of dopamine on GABA release in striatum: Evidence for D-1-D-2 interactions and non-synaptic influences. Neuroscience 77:419-429.

Hasselmo ME, Hay J, Ilyn M, Gorchetchnikov A (2002) Neuromodulation, theta rhythm and rat spatial navigation. Neural Networks 15:689-707.

Hastings TG, Zigmond MJ (1994) Identification of catechol-protein conjugates in neostriatal slices incubated with [3H]dopamine - impact of ascorbic-acid and glutathione. Journal of Neurochemistry 63:1126-1132.

Hastings TG, Lewis DA, Zigmond MJ (1996) Role of oxidation in the neurotoxic effects of intrastriatal dopamine injections. Proceedings of the National Academy of Sciences of the United States of America 93:1956-1961.

Heikkila R, Cohen G (1971) Inhibition of biogenic amine uptake by hydrogen peroxide - mechanism for toxic effects of 6-hydroxydopamine. Science 172:1257-1258.

Heikkila R, Cohen G (1972a) Further studies on generation of hydrogen-peroxide by 6-hydroxydopamine - potentiation by ascorbic-acid. Molecular Pharmacology 8:241-248.

Heikkila RE, Cohen G (1972b) In-vivo generation of hydrogen-peroxide from 6-hydroxydopamine. Experientia 28:1197-1198.

Heistek TS, Jaap Timmerman A, Spijker S, Brussaard AB, Mansvelder HD (2010) GABAergic synapse properties may explain genetic variation in hippocampal network oscillations in mice. Frontiers in Cellular Neuroscience 4:18.

Henze DA, Gonzalez-Burgos GR, Urban NN, Lewis DA, Barrionuevo G (2000) Dopamine increases excitability of pyramidal neurons in primate prefrontal cortex. Journal of Neurophysiology 84:2799-2809.

Hikosaka O, Takikawa Y, Kawagoe R (2000) Role of the basal ganglia in the control of purposive saccadic eye movements. Physiological Reviews 80:953-978.

Hirsch E, Graybiel AM, Agid YA (1988) Melanized dopaminergic-neurons are differentially susceptible to degeneration in Parkinsons-disease. Nature 334:345-348.

Hohlefeld FU, Ehlen F, Tiedt HO, Krugel LK, Horn A, Kuhn AA, Curio G, Klostermann F, Nikulin VV (2015) Correlation between cortical and subcortical neural dynamics on multiple time scales in Parkinson's disease. Neuroscience 298:145-160.

Hormuzdi SG, Pais I, LeBeau FEN, Towers SK, Rozov A, Buhl EH, Whittington MA, Monyer H (2001) Impaired electrical signaling disrupts gamma frequency oscillations in connexin 36-deficient mice. Neuron 31:487-495.

Hosp JA, Molina-Luna K, Hertler B, Atiemo CO, Luft AR (2009) Dopaminergic modulation of motor maps in rat motor cortex: an in vivo study. Neuroscience 159:692-700.

Hughes AJ, Daniel SE, Kilford L, Lees AJ (1992) Accuracy of clinical diagnosis of idiopathic Parkinson's disease: a clinico-pathological study of 100 cases. Journal of Neurology Neurosurgery and Psychiatry 55:181-184.

Huntley GW, Morrison JH, Prikhozhan A, Sealfon SC (1992) Localization of multiple dopamine receptor subtype messenger-RNAs in human and monkey motor cortex and striatum. Molecular Brain Research 15:181-188.

Hutchison WD, Lozano AM, Tasker RR, Lang AE, Dostrovsky JO (1997) Identification and characterization of neurons with tremor-frequency activity in human globus pallidus. Experimental Brain Research 113:557-563.

Hyman JM, Zilli EA, Paley AM, Hasselmo ME (2005) Medial prefrontal cortex cells show dynamic modulation with the hippocampal theta rhythm dependent on behavior. Hippocampus 15:739-749.

Igarashi J, Isomura Y, Arai K, Harukuni R, Fukai T (2013) A theta-gamma oscillation code for neuronal coordination during motor behavior. Journal of Neuroscience 33:18515-18530.

Ikegaya Y, Aaron G, Cossart R, Aronov D, Lampl I, Ferster D, Yuste R (2004) Synfire chains and cortical songs: Temporal modules of cortical activity. Science 304:559-564.

Iravani MM, Muscat R, Kruk ZL (1999) MK-801 interaction with the 5-HT transporter: A real-time study in brain slices using fast cyclic voltammetry. Synapse 32:212-224.

Iserhot C, Gebhardt C, Schmitz D, Heinemann U (2004) Glutamate transporters and metabotropic receptors regulate excitatory neurotransmission in the medial entorhinal cortex of the rat. Brain Research 1027:151-160.

Jagadeesh B, Gray CM, Ferster D (1992) Visually evoked oscillations of membrane potential in cells of cat visual cortex. Science 257:552-554.

Jakel RJ, Maragos WF (2000) Neuronal cell death in Huntington's disease: a potential role for dopamine. Trends in Neurosciences 23:239-245.

Jasper H, Penfield W (1949) Electrocorticograms in man: effect of voluntary movement upon the electrical activity of the precentral gyrus. Archiv für Psychiatrie und Nervenkrankheiten 183:163-174.

Jenkinson N, Brown P (2011) New insights into the relationship between dopamine, beta oscillations and motor function. Trends in Neurosciences 34:611-618.

Jenner P (2008) Molecular mechanisms of L-DOPA-induced dyskinesia. Nature Reviews Neuroscience 9:665-677.

Jensen O, Colgin LL (2007) Cross-frequency coupling between neuronal oscillations. Trends in Cognitive Sciences 11:267-269.

Jensen O, Kaiser J, Lachaux J-P (2007) Human gamma-frequency oscillations associated with attention and memory. Trends in Neurosciences 30:317-324.

Jones MW, Wilson MA (2005) Theta rhythms coordinate hippocampal-prefrontal interactions in a spatial memory task. PLOS Biology 3:2187-2199.

Jones SR, Gainetdinov RR, Wightman RM, Caron MG (1998) Mechanisms of amphetamine action revealed in mice lacking the dopamine transporter. Journal of Neuroscience 18:1979-1986.

Jurkiewicz MT, Gaetz WC, Bostan AC, Cheyne D (2006) Post-movement beta rebound is generated in motor cortex: Evidence from neuromagnetic recordings. Neuroimage 32:1281-1289.

Kalia LV, Lang AE (2015) Parkinson's disease. The Lancet 386:896-912.

Karoum F, Chrapusta SJ, Egan MF, Wyatt RJ (1993) Absence of 6-hydroxydopamine in the rat-brain after treatment with stimulants and other dopaminergic agents - a mass fragmentographic study. Journal of Neurochemistry 61:1369-1375.

Kawaguchi Y (1995) Physiological subgroups of nonpyramidal cells with specific morphological-characteristics in layer II/III of rat frontal-cortex. Journal of Neuroscience 15:2638-2655.

Kebabian JW, Greengard P (1971) Dopamine-sensitive adenyl cyclase - possible role in synaptic transmission. Science 174:1346-&.

Kebabian JW, Calne DB (1979) Multiple receptors for dopamine. Nature 277:93-96.

Keber U, Klietz M, Carlsson T, Oertel WH, Weihe E, Schafer MKH, Hoglinger GU, Depboylu C (2015) Striatal tyrosine hydroxylase-positive neurons are associated with L-DOPA-induced dyskinesia in hemiparkinsonian mice. Neuroscience 298:302-317.

Kempster PA, Frankel JP, Bovingdon M, Webster R, Lees AJ, Stern GM (1989) Levodopa peripheral pharmacokinetics and duration of motor response in Parkinsons-disease. Journal of Neurology Neurosurgery and Psychiatry 52:718-723.

Kerner JA, Standaert DG, Penney JB, Young AB, Landwehrmeyer GB (1997) Expression of group one metabotropic glutamate receptor subunit mRNAs in neurochemically identified neurons in the rat neostriatum, neocortex, and hippocampus. Molecular Brain Research 48:259-269.

Khedr EM, Farweez HM, Islam H (2003) Therapeutic effect of repetitive transcranial magnetic stimulation on motor function in Parkinson's disease patients. European Journal of Neurology 10:567-572.

Kim J, Matney CJ, Blankenship A, Hestrin S, Brown SP (2014) Layer 6 Corticothalamic Neurons Activate a Cortical Output Layer, Layer 5a. Journal of Neuroscience 34:9656-9664.

Kita H, Kitai ST (1994) The morphology of globus-pallidus projection neurons in the rat - an intracellular staining study. Brain Research 636:308-319.

Kita H, Chang HT, Kitai ST (1983) The morphology of intracellularly labeled rat subthalamic neurons - a light microscopic analysis. Journal of Comparative Neurology 215:245-257.

Klausberger T, Magill PJ, Marton LF, Roberts JDB, Cobden PM, Buzsaki G, Somogyi P (2003) Brain-state- and cell-type-specific firing of hippocampal interneurons in vivo. Nature 421:844-848.

Kohrs R, Durieux ME (1998) Ketamine - teaching an old drug new tricks. Anesthesia and Analgesia 87:1186-1193.

Kolb B, Forgie M, Gibb R, Gorny G, Rowntree S (1998) Age, experience and the changing brain. Neuroscience and Biobehavioral Reviews 22:143-159.

Konopacki J, Golebiewski H (1992) Theta-rhythms in the rat medial entorhinal cortex invitro - evidence for involvement of muscarinic receptors. Neuroscience Letters 141:93-96.

Konopacki J, Golebiewski H (1993) Theta-like activity in hippocampal-formation slices - cholinergic-GABAergic interaction. Neuroreport 4:963-966.

Konopacki J, Golebiewski H, Eckersdorf B (1992a) Carbachol-induced theta-like activity in entorhinal cortex slices. Brain Research 572:76-80.

Konopacki J, Kowalczyk T, Golebiewski H (2004) Electrical coupling underlies theta oscillations recorded in hippocampal formation slices. Brain Research 1019:270-274.

Konopacki J, Maciver MB, Bland BH, Roth SH (1987) Carbachol-induced EEG theta-activity in hippocampal brain-slices. Brain Research 405:196-198.

Konopacki J, Bland BH, Colom LV, Oddie SD (1992b) In vivo intracellular correlates of hippocampal-formation theta-on and theta-off cells. Brain Research 586:247-255.

Konopacki J, Golebiewski H, Eckersdorf B, Blaszczyk M, Grabowski R (1997) Theta-like activity in hippocampal formation slices: the effect of strong disinhibition of GABA(A) and GABA(B) receptors. Brain Research 775:91-98.

Kopell N, Ermentrout GB, Whittington MA, Traub RD (2000) Gamma rhythms and beta rhythms have different synchronization properties. Proceedings of the National Academy of Sciences of the United States of America 97:1867-1872.

Korotkova T, Fuchs EC, Ponomarenko A, von Engelhardt J, Monyer H (2010) NMDA receptor ablation on parvalbumin-positive interneurons impairs hippocampal synchrony, spatial representations, and working Memory. Neuron 68:557-569.

Krack P, Fraix V, Mendes A, Benabid AL, Pollak P (2002) Postoperative management of subthalamic nucleus stimulation for Parkinson's disease. Movement Disorders 17:S188-S197.

Kramer MA, Eden UT (2013) Assessment of cross-frequency coupling with confidence using generalized linear models. Journal of Neuroscience Methods 220:64-74.

Kramis R, Vanderwolf CH, Bland BH (1975) 2 types of hippocampal rhythmical slow activity in both rabbit and rat - relations to behavior and effects of atropine, diethyl-ether, urethane, and pentobarbital. Experimental Neurology 49:58-85.

Kreisman NR, Olson JE (2003) Taurine enhances volume regulation in hippocampal slices swollen osmotically. Neuroscience 120:635-642.

Kuhn AA, Kupsch A, Schneider GH, Brown P (2006) Reduction in subthalamic 8-35 Hz oscillatory activity correlates with clinical improvement in Parkinson's disease. European Journal of Neuroscience 23:1956-1960.

Kuhn AA, Williams D, Kupsch A, Limousin P, Hariz M, Schneider GH, Yarrow K, Brown P (2004) Event-related beta desynchronization in human subthalamic nucleus correlates with motor performance. Brain 127:735-746.

Kwan HC, Mackay WA, Murphy JT, Wong YC (1978) Spatial-organization of precentral cortex in awake primates. II. motor outputs. Journal of Neurophysiology 41:1120-1131.

Lacey MG, Mercuri NB, North RA (1987) Dopamine acts on D2 receptors to increase potassium conductance in neurons of the rat substantia-nigra zona compacta. Journal of Physiology 392:397-416.

Lakatos P, Karmos G, Mehta AD, Ulbert I, Schroeder CE (2008) Entrainment of neuronal oscillations as a mechanism of attentional selection. Science 320:110-113.

Lakatos P, Shah AS, Knuth KH, Ulbert I, Karmos G, Schroeder CE (2005) An oscillatory hierarchy controlling neuronal excitability and stimulus processing in the auditory cortex. Journal of Neurophysiology 94:1904-1911.

Lassek AM (1940) The human pyramidal tract: II. a numerical investigation of the betz cells of the motor area. Archives of Neurology & Psychiatry 44:718.

Lavreysen H, Dautzenberg FM (2008) Therapeutic potential of group III metabotropic glutamate receptors. Current Medicinal Chemistry 15:671-684.

Lefaucheur JP, Drouot X, Von Raison F, Menard-Lefaucheur I, Cesaro P, Nguyen JP (2004) Improvement of motor performance and modulation of cortical excitability by repetitive transcranial magnetic stimulation of the motor cortex in Parkinson's disease. Clinical Neurophysiology 115:2530-2541.

LeMoine C, Gaspar P (1998) Subpopulations of cortical GABAergic interneurons differ by their expression of D1 and D2 dopamine receptor subtypes. Molecular Brain Research 58:231-236.

Leung LS (2011) Field potential generation and current source density analysis. In: Electrophysiological Recording Techniques (Vertes PR, Stackman Jr WR, eds), pp 1-25. Totowa, NJ: Humana Press.

Leung LWS (1982) Non-linear feedback model of neuronal populations in hippocampal CA1 region. Journal of Neurophysiology 47:845-868.

Leung LWS, Yim CYC (1991) Intrinsic membrane-potential oscillations in hippocampal-neurons invitro. Brain Research 553:261-274.

LeWitt PA (2004) Subcutaneously administered apomorphine - Pharmacokinetics and metabolism. Neurology 62:S8-S11.

Lidow MS, Goldmanrakic PS, Gallager DW, Rakic P (1991) Distribution of dopaminergic receptors in the primate cerebral-cortex - quantitative autoradiographic analysis using [3H]raclopride, [3H]spiperone and [3H]SCH23390. Neuroscience 40:657-671.

Lidow MS, Goldmanrakic PS, Gallager DW, Geschwind DH, Rakic P (1989) Distribution of major neurotransmitter receptors in the motor and somatosensory cortex of the rhesus-monkey. Neuroscience 32:609-627.

Lindvall O, Bjorklund A (1979) Dopaminergic innervation of the globus pallidus by collaterals from the nigrostriatal pathway. Brain Research 172:169-173.

Lisman JE, Otmakhova NA (2001) Storage, recall, and novelty detection of sequences by the hippocampus: Elaborating on the SOCRATIC model to account for normal and aberrant effects of dopamine. Hippocampus 11:551-568.

Liu T, Petrof I, Sherman SM (2014) Modulatory effects of activation of metabotropic glutamate receptors on GABAergic circuits in the mouse cortex. Journal of Neurophysiology 111:2287-2297.

Logothetis NK (2003) The underpinnings of the BOLD functional magnetic resonance imaging signal. The Journal of Neuroscience 23:3963-3971.

Lopez-Bendito G, Shigemoto R, Kulik A, Paulsen O, Fairen A, Lujan R (2002) Expression and distribution of metabotropic GABA receptor subtypes GABA(B)R1 and GABA(B)R2 during rat neocortical development. European Journal of Neuroscience 15:1766-1778.

Lopez-Bendito G, Shigemoto R, Kulik A, Vida I, Fairen A, Lujan R (2004) Distribution of metabotropic GABA receptor Subunits GABA(B1a/b) and GABA(B2) in the rat hippocampus during prenatal and postnatal development. Hippocampus 14:836-848.

Lorente de No R (1947) Analysis of the distribution of the action currents of nerve in volume conductors. Studies from the Rockefeller institute for medical research Reprints Rockefeller Institute for Medical Research 132:384-477.

Lucas-Meunier E, Fossier P, Baux G, Amar M (2003) Cholinergic modulation of the cortical neuronal network. Pflugers Archiv: European Journal of Physiology 446:17-29.

Lukatch HS, MacIver MB (1997) Physiology, pharmacology, and topography of cholinergic neocortical oscillations in vitro. Journal of Neurophysiology 77:2427-2445.

Luo H, Poeppel D (2007) Phase patterns of neuronal responses reliably discriminate speech in human auditory cortex. Neuron 54:1001-1010.

Luscher C, Jan LY, Stoffel M, Malenka RC, Nicoll RA (1997) G protein-coupled inwardly rectifying K+ channels (GIRKs) mediate postsynaptic but not presynaptic transmitter actions in hippocampal neurons. Neuron 19:687-695.

Macdonald RL, Barker JL (1979) Anticonvulsant and anesthetic barbiturates: different postsynaptic actions in cultured mammalian neurons. Neurology 29:432-447.

MacIver MB, Harris DP, Konopacki J, Roth SH, Bland BH (1986) Carbachol induced rhythmical slow wave activity recorded from dentate granule neurons in vitro. Proceedings of the Western Pharmacology Society 29:159-161.

MacVicar BA, Tse FW (1989) Local neuronal circuitry underlying cholinergic rhythmical slow activity in CA3 area of rat hippocampal slices. The Journal of physiology 417:197-212.

Magill PJ, Bolam JP, Bevan MD (2000) Relationship of activity in the subthalamic nucleus-globus pallidus network to cortical electroencephalogram. Journal of Neuroscience 20:820-833.

Magill PJ, Bolam JP, Bevan MD (2001) Dopamine regulates the impact of the cerebral cortex on the subthalamic nucleus-globus pallidus network. Neuroscience 106:313-330.

Mair RD, Kauer JA (2007) Amphetamine depresses excitatory synaptic transmission at prefrontal cortical layer V synapses. Neuropharmacology 52:193-199.

Mallet N, Pogosyan A, Marton LF, Bolam JP, Brown P, Magill PJ (2008a) Parkinsonian beta oscillations in the external globus pallidus and their relationship with subthalamic nucleus activity. Journal of Neuroscience 28:14245-14258.

Mallet N, Pogosyan A, Sharott A, Csicsvari J, Bolam JP, Brown P, Magill PJ (2008b) Disrupted dopamine transmission and the emergence of exaggerated beta oscillations in subthalamic nucleus and cerebral cortex. Journal of Neuroscience 28:4795-4806.

Mandel RJ, Leanza G, Nilsson OG, Rosengren E (1994) Amphetamine induces excess release of striatal acetylcholine in-vivo that is independent of nigrostriatal dopamine. Brain Research 653:57-65.

Mao TY, Kusefoglu D, Hooks BM, Huber D, Petreanu L, Svoboda K (2011) Long-range neuronal circuits underlying the interaction between sensory and motor Cortex. Neuron 72:111-123.

Marceglia S, Foffani G, Bianchi AM, Baselli G, Tamma F, Egidi M, Priori A (2006) Dopamine-dependent non-linear correlation between subthalamic rhythms in Parkinson's disease. Journal of Physiology 571:579-591.

Martin DC, Watkins CA, Adams RJ, Nason LA (1988) Anesthetic effects on 5-hydroxytryptamine uptake by rat brain synaptosomes. Brain Research 455:360-365.

Martin LJ, Blackstone CD, Levey AI, Huganir RL, Price DL (1993) AMPA glutamate receptor subunits are differentially distributed in rat-brain. Neuroscience 53:327-358.

McBain CJ, Freund TE, Mody I (1999) Glutamatergic synapses onto hippocampal interneurons: precision timing without lasting plasticity. Trends in Neurosciences 22:228-235.

McGeorge AJ, Faull RLM (1989) The organization of the projection from the cerebral cortex to the striatum in the rat. Neuroscience 29:503-537.

McNally JM, McCarley RW, McKenna JT, Yanagawa Y, Brown RE (2011) Complex receptor mediation of acute ketamine application on in vitro gamma oscillations in mouse prefrontal cortex: Modeling gamma band oscillation abnormalities in schizophrenia. Neuroscience 199:51-63.

Millan MJ, Newman-Tancredi A, Quentric Y, Cussac D (2001) The '' selective'' dopamine D-1 receptor antagonist, SCH23390, is a potent and high efficacy agonist at cloned human serotonin(2C) receptors. Psychopharmacology 156:58-62.

Millan MJ, Maiofiss L, Cussac D, Audinot V, Boutin JA, Newman-Tancredi A (2002) Differential actions of antiparkinson agents at multiple classes of monoaminergic receptor. I. A multivariate analysis of the binding profiles of 14 drugs at 21 native and cloned human receptor subtypes. Journal of Pharmacology and Experimental Therapeutics 303:791-804.

Miller WC, DeLong MR (1987) Altered tonic activity of neurons in the globus pallidus and subthalamic nucleus in the primate MPTP model of parkinsonism. In: The Basal Ganglia II: Structure and Function—Current Concepts (Carpenter MB, Jayaraman A, eds), pp 415-427. Boston, MA: Springer US.

Miller WC, Delong MR (1988) Parkinsonian symptomatology - an anatomical and physiological analysis. Annals of the New York Academy of Sciences 515:287-302.

Mink JW (1996) The basal ganglia: Focused selection and inhibition of competing motor programs. Progress in Neurobiology 50:381-425.

Mink JW (2006) Neurobiology of basal ganglia and Tourette syndrome: basal ganglia circuits and thalamocortical outputs. Advances in Neurology 99:89-98.

Mink JW, Thach WT (1993) Basal ganglia intrinsic circuits and their role in behavior. Current Opinion in Neurobiology 3:950-957.

Missale C, Nash SRS, Robinson SW, Jaber M, Caron MG (1998) Dopamine receptors: from structure to function. Physiological Reviews 78:189-225.

Mitrano DA, Pare JF, Smith Y, Weinshenker D (2014) D1-dopamine and alpha 1-adrenergic receptors co-localize in dendrites of the rat prefrontal cortex. Neuroscience 258:90-100.

Mitsi V, Zachariou V (2016) Modulation of pain, nociception, and analgesia by the brain reward center. Neuroscience:10.1016/j.neuroscience.2016.1005.1017.

Mitzdorf U (1985) Current source-density method and application in cat cerebral cortex: investigation of evoked potentials and EEG phenomena. Physiological Reviews 65:37-100.

Modebadze T (2014) Neuronal network dynamics during epileptogenesis in the medial temporal lobe. In: School of Life and Health Science, p 249. Birmingham: Aston University.

Molnar Z, Cheung AFP (2006) Towards the classification of subpopulations of layer V pyramidal projection neurons. Neuroscience Research 55:105-115.

Momiyama T, Koga E (2001) Dopamine D-2-like receptors selectively block N-type Ca2+ channels to reduce GABA release onto rat striatal cholinergic interneurones. Journal of Physiology 533:479-492.

Monakow KH, Akert K, Kunzle H (1978) Projections of the precentral motor cortex and other cortical areas of the frontal lobe to the subthalamic nucleus in the monkey. Experimental Brain Research 33:395-403.

Montoya CP, Sainsbury RS (1985) The effects of entorhinal cortex lesions on type-1 and type-2 theta. Physiology and Behavior 35:121-126.

Morgan S, Huston JP, Pritzel M (1983) Effects of reducing sensory-motor feedback on the appearance of crossed nigro-thalamic projections and recovery from turning induced by unilateral substantia nigra lesions. Brain Research Bulletin 11:721-727.

Mormann F, Fell J, Axmacher N, Weber B, Lehnertz K, Elger CE, Fernández G (2005) Phase/amplitude reset and theta-gamma interaction in the human medial temporal lobe during a continuous word recognition memory task. Hippocampus 15:890-900.

Moro E, Esselink RJA, Xie J, Hommel M, Benabid AL, Pollak P (2002) The impact on Parkinson's disease of electrical parameter settings in STN stimulation. Neurology 59:706-713.

Murthy VN, Fetz EE (1992) Coherent 25- to 35-Hz oscillations in the sensorimotor cortex of awake behaving monkeys. Proceedings of the National Academy of Sciences of the United States of America 89:5670-5674.

Murthy VN, Fetz EE (1996) Oscillatory activity in sensorimotor cortex of awake monkeys: Synchronization of local field potentials and relation to behavior. Journal of Neurophysiology 76:3949-3967.

Muthukumaraswamy SD (2010) Functional Properties of Human Primary Motor Cortex Gamma Oscillations. Journal of Neurophysiology 104:2873-2885.

Nair AB, Jacob S (2016) A simple practice guide for dose conversion between animals and human. Journal of Basic and Clinical Pharmacy 7:27-31.

Nambu A, Tokuno H, Takada M (2002) Functional significance of the cortico-subthalamo-pallidal 'hyperdirect' pathway. Neuroscience Research 43:111-117.

Nambu A, Tokuno H, Hamada I, Kita H, Imanishi M, Akazawa T, Ikeuchi Y, Hasegawa N (2000) Excitatory cortical inputs to pallidal neurons via the subthalamic nucleus in the monkey. Journal of Neurophysiology 84:289-300.

Narabayashi H (1982) Surgical approach to tremor. Movement Disorders: Butterworths International Medical Reviews: Neurology 2:292-299.

Newberry NR, Nicoll RA (1984) Direct hyperpolarizing action of baclofen on hippocampal pyramidal cells. Nature 308:450-452.

Neymotin SA, Hilscher MM, Moulin TC, Skolnick Y, Lazarewicz MT, Lytton WW (2013) Ih tunes theta/gamma oscillations and cross-frequency coupling in an in silico CA3 model. PLOS one 8.

Nguyen QT, Kleinfeld D (2005) Positive feedback in a brainstem tactile sensorimotor loop. Neuron 45:447-457.

Nini A, Feingold A, Slovin H, Bergman H (1995) Neurons in the globus-pallidus do not show correlated activity in the normal monkey, but phase-locked oscillations appear in the MPTP model of Parkinsonism. Journal of Neurophysiology 74:1800-1805.

Nisenbaum ES, Stricker EM, Zigmond MJ, Berger TW (1986) Long-term effects of dopamine-depleting brain-lesions on spontaneous activity of type-II striatal neurons - relation to behavioral recovery. Brain Research 398:221-230.

Noyce AJ, Bestwick JP, Silveira-Moriyama L, Hawkes CH, Giovannoni G, Lees AJ, Schrag A (2012) Meta-analysis of early nonmotor features and risk factors for Parkinson's disease. Annals of Neurology 72:893-901.

Nudo RJ, Jenkins WM, Merzenich MM, Prejean T, Grenda R (1992) Neurophysiological correlates of hand preference in primary motor cortex of adult squirrel-monkeys. Journal of Neuroscience 12:2918-2947.

O'Keefe J (1976) Place units in hippocampus of freely moving rat. Experimental Neurology 51:78-109.

O'Keefe J, Recce ML (1993) Phase relationship between hippocampal place units and the EEG theta-rhythm. Hippocampus 3:317-330.

Obeso JA, Rodriguez-Oroz MC, Blesa FJ, Guridi J (2006) The globus pallidus pars externa and Parkinson's disease. Ready for prime time? Experimental Neurology 202:1-7.

Olsson M, Nikkhah G, Bentlage C, Björklund A (1995) Forelimb akinesia in the rat Parkinson model: differential effects of dopamine agonists and nigral transplants as assessed by a new stepping test. Journal of Neuroscience 15:3863-3875.

Onslow ACE, Jones MW, Bogacz R (2014) A canonical circuit for generating phase-amplitude coupling. PLOS one 9:e102591.

Orr WB, Gardiner TW, Stricker EM, Zigmond MJ, Berger TW (1986) Short-term effects of dopamine-depleting brain lesions on spontaneous activity of striatal neurons: Relation to local dopamine concentration and behavior. Brain Research 376:20-28.

Orzel-Gryglewska J, Kusmierczak M, Matulewicz P, Jurkowlaniec E (2013) Dopaminergic transmission in the midbrain ventral tegmental area in the induction of hippocampal theta rhythm. Brain Research 1510:63-77.

Ozkan M, Johnson NW, Woodhall GL, Stanford IM (2016) Differential effects of dopamine on simultaneous recorded theta and beta oscillatory activity in primary motor cortex (M1) in vitro. In: 10th FENS Forum of Neuroscience 2016, p B085. Copenhagen, Denmark: FENS.

Pagni C, Zeme S, Zenga F (2003) Further experience with extradural motor cortex stimulation for treatment of advanced Parkinson's disease: Report of 3 new cases. Journal of Neurosurgical Sciences 47:189.

Pakhotin PI, Pakhotina ID, Andreev AA (1997) Functional stability of hippocampal slices after treatment with cyclooxygenase inhibitors. Neuroreport 8:1755-1759.

Palmer LM, Schulz JM, Murphy SC, Ledergerber D, Murayama M, Larkum ME (2012) The cellular basis of GABAB-mediated interhemispheric inhibition. Science 335:989-993.

Pan HS, Walters JR (1988) Unilateral lesion of the nigrostriatal pathway decreases the firing rate and alters the firing pattern of globus pallidus neurons in the rat. Synapse 2:650-656.

Parent A, Levesque M, Parent M (2001) A re-evaluation of the current model of the basal ganglia. Parkinsonism & Related Disorders 7:193-198.

Parent A, Sato F, Wu Y, Gauthier J, Levesque M, Parent M (2000) Organization of the basal ganglia: the importance of axonal collateralization. Trends in Neurosciences 23:S20-S27.

Parker KL, Chen K-H, Kingyon JR, Cavanagh JF, Narayanan NS (2015) Medial frontal similar to 4-Hz activity in humans and rodents is attenuated in PD patients and in rodents with cortical dopamine depletion. Journal of Neurophysiology 114:1310-1320.

Paxinos G, Watson C (1998) The Rat Brain in Stereotaxic Coordinates: Academic Press.

Penfield W, Boldrey E (1937) Somatic motor and sensory representation in the cerebral cortex of man as studied by electrical stimulation. Brain 60:389-443.

Perese DA, Ulman J, Viola J, Ewing SE, Bankiewicz KS (1989) A 6-hydroxydopamine-induced selective Parkinsonian rat model. Brain Research 494:285-293.

Petsche H, Stumpf C, Gogolak G (1962) [The significance of the rabbit's septum as a relay station between the midbrain and the hippocampus. I. The control of hippocampus arousal activity by the septum cells]. Electroencephalography and Clinical Neurophysiology 14:202-211.

Pettersen KH, Devor A, Ulbert I, Dale AM, Einevoll GT (2006) Current-source density estimation based on inversion of electrostatic forward solution: Effects of finite extent of neuronal activity and conductivity discontinuities. Journal of Neuroscience Methods 154:116-133.

Pfurtscheller G, Berghold A (1989) Patterns of cortical activation during planning of voluntary movement. Electroencephalography and Clinical Neurophysiology 72:250-258.

Pfurtscheller G, Neuper C (1992) Simultaneous EEG 10-Hz desynchronization and 40-Hz synchronization during finger movements. Neuroreport 3:1057-1060.

Pfurtscheller G, Neuper C, Kalcher J (1993) 40-Hz oscillations during motor behaviour in man. Neuroscience Letters 164:179-182.

Pfurtscheller G, Graimann B, Huggins JE, Levine SP, Schuh LA (2003) Spatiotemporal patterns of beta desynchronization and gamma synchronization in corticographic data during self-paced movement. Clinical Neurophysiology 114:1226-1236.

Pinault D (2008) N-methyl d-aspartate receptor antagonists ketarnine and MK-801 induce wake-related aberrant,gamma oscillations in the rat neocortex. Biological Psychiatry 63:730-735.

Pollok B, Gross J, Dirks M, Timmermann L, Schnitzler A (2004) The cerebral oscillatory network of voluntary tremor. Journal of Physiology 554:871-878.

Polymeropoulos MH, Lavedan C, Leroy E, Ide SE, Dehejia A, Dutra A, Pike B, Root H, Rubenstein J, Boyer R, Stenroos ES, Chandrasekharappa S, Athanassiadou A, Papapetropoulos T, Johnson WG, Lazzarini AM, Duvoisin RC, DiIorio G, Golbe LI, Nussbaum RL (1997) Mutation in the alpha-synuclein gene identified in families with Parkinson's disease. Science 276:2045-2047.

Porter CC, Totaro JA, Stone CA (1963) Effect of 6-hydroxydopamine and some other compounds on the concentration of norepinephrine in the hearts of mice. The Journal of Pharmacology and Experimental Therapeutics 140:308-316.

Porter CC, Totaro JA, Burcin A (1965) The relationship between radioactivity and norepinephrine concentrations in the brains and hearts of mice following administration of labeled methyldopa or 6-hydroxydopamine. The Journal of Pharmacology and Experimental Therapeutics 150:17-22.

Porter LL, Sakamoto K (1988) Organization and synaptic relationships of the projection from the primary sensory to the primary motor cortex in the cat. Journal of Comparative Neurology 271:387-396.

Postuma RB, Aarsland D, Barone P, Burn DJ, Hawkes CH, Oertel W, Ziemssen T (2012) Identifying prodromal Parkinson's disease: Pre-Motor disorders in Parkinson's disease. Movement Disorders 27:617-626.

Price CJ, Karayannis T, Pal BZ, Capogna M (2005) Group II and III mGluRs-mediated presynaptic inhibition of EPSCs recorded from hippocampal interneurons of CAI stratum lacunosum moleculare. Neuropharmacology 49:45-56.

Prinster SC, Hague C, Hall RA (2005) Heterodimerization of G protein-coupled receptors: Specificity and functional significance. Pharmacological Reviews 57:289-298.

Proctor PH (2008) Uric acid and neuroprotection. Stroke 39:E126-E126.

Prokic EJ (2011) Modulation of neuronal network activity in the primary motor cortex. In: School of Life and Health Sciences, p 216. Birmingham: Aston University.

Prokic EJ, Weston C, Yamawaki N, Hall SD, Jones RSG, Stanford IM, Ladds G, Woodhall GL (2015) Cortical oscillatory dynamics and benzodiazepine-site modulation of tonic inhibition in fast spiking interneurons. Neuropharmacology 95:192-205.

Pérez-Garci E, Gassmann M, Bettler B, Larkum ME (2006) The GABAB1b isoform mediates long-lasting inhibition of dendritic Ca2+ spikes in layer 5 somatosensory pyramidal neurons. Neuron 50:603-616.

Quilichini P, Sirota A, Buzsaki G (2010) Intrinsic circuit organization and theta-gamma oscillation dynamics in the entorhinal cortex of the rat. Journal of Neuroscience 30:11128-11142.

Raiteri M, Bertollini A, Angelini F, Levi G (1975) D-amphetamine as a releaser of reuptake inhibitor of biogenic-amines in synaptosomes. European Journal of Pharmacology 34:189-195.

Rashid AJ, O'Dowd BF, Verma V, George SR (2007) Neuronal, Gq/11-coupled dopamine receptors: an uncharted role for dopamine. Trends in Pharmacological Sciences 28:551-555.

Raz A, Vaadia E, Bergman H (2000) Firing patterns and correlations of spontaneous discharge of pallidal neurons in the normal and the tremulous 1-methyl-4-phenyl-1,2,3,6-tetrahydropyridine vervet model of parkinsonism. Journal of Neuroscience 20:8559-8571.

Rebois RV, Maki K, Meeks JA, Fishman PH, Hebert TE, Northup JK (2012) D-2-like dopamine and p-adrenergic receptors forma signaling complex that integrates G(s)- and G(i)-mediated regulation of adenylyl cyclase. Cellular Signalling 24:2051-2060.

Rice ME (2000) Ascorbate regulation and its neuroprotective role in the brain. Trends in Neuroscience 23:209-216.

Rivara CB, Sherwood CC, Bouras C, Hof PR (2003) Stereologic characterization and spatial distribution patterns of Betz cells in the human primary motor cortex. The Anatomical Record Part A, Discoveries in Molecular, Cellular and Evolutionary Biology 270:137-151.

Robinson TE, Whishaw IQ (1988) Normalization of extracellular dopamine in striatum following recovery from a partial unilateral 6-OHDA lesion of the substantia nigra: a microdialysis study in freely moving rats. Brain Research 450:209-224.

Rogers CJ, Twyman RE, Macdonald RL (1994) Benzodiazepine and beta-carboline regulation of single GABAA receptor channels of mouse spinal neurones in culture. Journal of Physiology 475:69-82.

Roopun AK, Cunningham MO, Racca C, Alter K, Traub RD, Whittington MA (2008) Region-specific changes in gamma and beta2 rhythms in NMDA receptor dysfunction models of schizophrenia. Schizophrenia Bulletin 34:962-973.

Roopun AK, Middleton SJ, Cunningham MO, LeBeau FEN, Bibbig A, Whittington MA, Traub RD (2006) A beta2-frequency (20-30 Hz) oscillation in nonsynaptic networks of somatosensory cortex. Proceedings of the National Academy of Sciences of the United States of America 103:15646-15650.

Sahgal A, Andrews JS, Biggins JA, Candy JM, Edwardson JA, Keith AB, Turner JD, Wright C (1984) 1-methyl-4-phenyl-1,2,3,6-tetrahydropyridine (MPTP) affects locomotor activity without producing a nigrostriatal lesion in the rat. Neuroscience Letters 48:179-184.

Sakamoto T, Arissian K, Asanuma H (1989) Functional-role of the sensory cortex in learning motor-skills in cats. Brain Research 503:258-264.

Saleh M, Reimer J, Penn R, Ojakangas CL, Hatsopoulos NG (2010) Fast and Slow Oscillations in Human Primary Motor Cortex Predict Oncoming Behaviorally Relevant Cues. Neuron 65:461-471.

Salmelin R, Hamalainen M, Kajola M, Hari R (1995) Functional segregation of movement-related rhythmic activity in the human brain. Neuroimage 2:237-243.

Sanes JN, Donoghue JP (1997) Static and dynamic organization of motor cortex. Brain Plasticity 73:277-296.

Sanes JN, Donoghue JP (2000) Plasticity and primary motor cortex. Annual Review of Neuroscience 23:393-415.

Sato F, Lavallee P, Levesque M, Parent A (2000) Single-axon tracing study of neurons of the external segment of the globus pallidus in primate. Journal of Comparative Neurology 417:17-31.

Sauer H, Oertel WH (1994) Progressive degeneration of nigrostriatal dopamine neurons following intrastriatal terminal lesions with 6-hydroxydopamine: a combined retrograde tracing and immunocytochemical study in the rat. Neuroscience 59:401-415.

Scanziani M (2000) GABA spillover activates postsynaptic GABA(B) receptors to control rhythmic hippocampal activity. Neuron 25:673-681.

Schapira AHV (2009) Neurobiology and treatment of Parkinson's disease. Trends in Pharmacological Sciences 30:41-47.

Schroeder CE, Wilson DA, Radman T, Scharfman H, Lakatos P (2010) Dynamics of active sensing and perceptual selection. Current Opinion in Neurobiology 20:172-176.

Schultz W (1998) Predictive reward signal of dopamine neurons. Journal of Neurophysiology 80:1-27.

Schwarting RKW, Huston JP (1996) The unilateral 6-hydroxydopamine lesion model in behavioral brain research. Analysis of functional deficits, recovery and treatments. Progress in Neurobiology 50:275-331.

Seamans JK, Robbins TW (2010) Dopamine modulation of the prefrontal cortex and cognitive function. In: The Dopamine Receptors, 2nd Edition Edition (Neve KA, ed), pp 373-398. New York, USA: Humana Press.

Seamans JK, Gorelova N, Durstewitz D, Yang CR (2001a) Bidirectional dopamine modulation of GABAergic inhibition in prefrontal cortical pyramidal neurons. Journal of Neuroscience 21:3628-3638.

Seamans JK, Durstewitz D, Christie BR, Stevens CF, Sejnowski TJ (2001b) Dopamine D1/D5 receptor modulation of excitatory synaptic inputs to layer V prefrontal cortex neurons. Proceedings of the National Academy of Sciences of the United States of America 98:301-306.

Seeman P, Vantol HHM (1994) Dopamine-receptor pharmacology. Trends in Pharmacological Sciences 15:264-270.

Segal M, Barker JL (1984) Rat hippocampal neurons in culture: voltage-clamp analysis of inhibitory synaptic connections. Journal of Neurophysiology 52:469-487.

Selby G (1967) Stereotactic surgery for the relief of Parkinson's disease. 1. A critical review. Journal of the Neurological Sciences 5:315-342.

Semyanov A, Kullmann DM (2000) Modulation of GABAergic signaling among interneurons by metabotropic glutamate receptors. Neuron 25:663-672.

Semyanov A, Kullmann DM (2001) Kainate receptor-dependent axonal depolarization and action potential initiation in interneurons. Nature Neuroscience 4:718-723.

Seniuk NA, Tatton WG, Greenwood CE (1990) Dose-dependent destruction of the coeruleus-cortical and nigtal-striatal projections by MPTP. Brain Research 527:7-20.

Shannon CE (1949) Communication in the presence of noise. Proceedings of the IRE 37:10-21.

Sharott A, Magill PJ, Harnack D, Kupsch A, Meissner W, Brown P (2005) Dopamine depletion increases the power and coherence of beta-oscillations in the cerebral cortex and subthalamic nucleus of the awake rat. European Journal of Neuroscience 21:1413-1422.

Shipp S (2005) The importance of being agranular: a comparative account of visual and motor cortex. Philosophical Transactions of the Royal Society of London Series B, Biological Sciences 360:797-814.

Shipp S (2007) Structure and function of the cerebral cortex. Current Biology 17:R443-R449.

Siapas AG, Lubenov EV, Wilson MA (2005) Prefrontal phase locking to hippocampal theta oscillations. Neuron 46:141-151.

Singer W, Gray CM (1995) Visual feature integration and the temporal correlation hypothesis. Annual Review of Neuroscience 18:555-586.

Sirota A, Montgomery S, Fujisawa S, Isomura Y, Zugaro M, Buzsaki G (2008) Entrainment of neocortical neurons and gamma oscillations by the hippocampal theta rhythm. Neuron 60:683-697.

Smeal RM, Gaspar RC, Keefe KA, Wilcox KS (2007) A rat brain slice preparation for characterizing both thalamostriatal and corticostriatal afferents. Journal of Neuroscience Methods 159:224-235.

Smith DJ, Bouchal RL, DeSanctis CA, Monroe PJ, Amedro JB, Perrotti JM, Crisp T (1987) Properties of the interaction between ketamine and opiate binding sites in vivo and in vitro. Neuropharmacology 26:1253-1260.

Smith Y, Bolam JP (1989) Neurons of the substantia nigra reticulata receive a dense GABA-containing input from the globus pallidus in the rat. Brain Research 493:160-167.

Smythe JW, Colom LV, Bland BH (1992) The extrinsic modulation of hippocampal-theta depends on the coactivation of cholinergic and GABAergic medial septal inputs. Neuroscience and Biobehavioral Reviews 16:289-308.

Snyder SH, Taylor KM, Coyle JT, Meyerhof Jl (1970) Role of brain dopamine in behavioral regulation and the actions of psychotropic drugs. American Journal of Psychiatry 127:199-207.

Somogyi P, Katona L, Klausberger T, Lasztoczi B, Viney TJ (2014) Temporal redistribution of inhibition over neuronal subcellular domains underlies state-dependent rhythmic change of excitability in the hippocampus. Philosophical Transactions of the Royal Society of London Series B, Biological Sciences 369:11.

Spano PF, Govoni S, Trabucchi M (1978) Studies on the pharmacological properties of dopamine receptors in various areas of the central nervous system. Advances in Biochemical Psychopharmacology 19:155-165.

Stoney SD, Thompson WD, Asanuma H (1968) Excitation of pyramidal tract cells by intracortical microstimulation: effective extent of stimulating current. Journal of Neurophysiology 31:659.

Sun M, Zhao Y, Gu Y, Xu C (2010) Neuroprotective actions of aminoguanidine involve reduced the activation of calpain and caspase-3 in a rat model of stroke. Neurochemistry International 56:634-641.

Sutton AC, Yu WJ, Calos ME, Smith AB, Ramirez-Zamora A, Molho ES, Pilitsis JG, Brotchie JM, Shin DS (2012) Deep brain stimulation of the substantia nigra pars reticulata improves forelimb akinesia in the hemiparkinsonian rat. Journal of Neurophysiology:363-374.

Svennilson E, Torvik A, Lowe R, Leksell L (1960) Treatment of parkinsonism by stereotatic thermolesions in the pallidal region. A clinical evaluation of 81 cases. Acta Psychiatrica Scandinavica 35:358-377.

Swanson JM, Kinsbourne M, Nigg J, Lanphear B, Stefanatos GA, Volkow N, Taylor E, Casey BJ, Castellanos FX, Wadhwa PD (2007) Etiologic subtypes of attention-deficit/hyperactivity disorder: Brain imaging, molecular genetic and environmental factors and the dopamine hypothesis. Neuropsychology Review 17:39-59.

Tang KC, Low MJ, Grandy DK, Lovinger DM (2001) Dopamine-dependent synaptic plasticity in striatum during in vivo development. Proceedings of the National Academy of Sciences of the United States of America 98:1255-1260.

Taverna FA, Cameron BR, Hampson DL, Wang LY, Macdonald JF (1994) Sensitivity of AMPA receptors to pentobarbital. European Journal of Pharmacology-Molecular Pharmacology Section 267:R3-R5.

Tian H, Zhang GY, Li HC, Zhang QG (2003) Antioxidant NAC and AMPA/KA receptor antagonist DNQX inhibited JNK3 activation following global ischemia in rat hippocampus. Neuroscience Research 46:191-197.

Timmermann L, Florin E (2012) Parkinson's disease and pathological oscillatory activity: Is the beta band the bad guy? - New lessons learned from low-frequency deep brain stimulation. Experimental Neurology 233:123-125.

Timmermann L, Gross J, Dirks M, Volkmann J, Freund HJ, Schnitzler A (2003) The cerebral oscillatory network of parkinsonian resting tremor. Brain 126:199-212.

Tokuno H, Nambu A (2000) Organization of nonprimary motor cortical inputs on pyramidal and nonpyramidal tract neurons of primary motor cortex: An electrophysiological study in the macaque monkey. Cerebral Cortex 10:58-68.

Tort ABL, Komorowski R, Eichenbaum H, Kopell N (2010) Measuring phase-amplitude coupling between neuronal oscillations of different frequencies. Journal of Neurophysiology 104:1195-1210.

Tort ABL, Rotstein HG, Dugladze T, Gloveli T, Kopell NJ (2007) On the formation of gamma-coherent cell assemblies by oriens lacunosum-moleculare interneurons in the hippocampus. Proceedings of the National Academy of Sciences of the United States of America 104:13490-13495.

Tort ABL, Kramer MA, Thorn C, Gibson DJ, Kubota Y, Graybiel AM, Kopell NJ (2008) Dynamic cross-frequency couplings of local field potential oscillations in rat striatum and hippocampus during performance of a T-maze task. Proceedings of the National Academy of Sciences of the United States of America 105:20517-20522.

Towers SK, Hestrin S (2008) D(1)-like dopamine receptor activation modulates GABAergic inhibition but not electrical coupling between neocortical fast-spiking interneurons. Journal of Neuroscience 28:2633-2641.

Towers SK, Lebeau FEN, Gloveli T, Traub RD, Whittington MA, Buhl EH (2002) Fast network oscillations in the rat dentate gyrus in vitro. Journal of Neurophysiology 87:1165-1168.

Trantham-Davidson H, Neely LC, Lavin A, Seamans JK (2004) Mechanisms underlying differential D1 versus D2 dopamine receptor regulation of inhibition in prefrontal cortex. Journal of Neuroscience 24:10652-10659.

Traub RD, Whittington MA, Stanford IM, Jefferys JGR (1996a) A mechanism for generation of long-range synchronous fast oscillations in the cortex. Nature 383:621-624.

Traub RD, Whittington MA, Colling SB, Buzsaki G, Jefferys JGR (1996b) Analysis of gamma rhythms in the rat hippocampus in vitro and in vivo. Journal of Physiology 493:471-484.

Traub RD, Whittington MA, Buhl EH, Jefferys JGR, Faulkner HJ (1999) On the mechanism of the gamma ->beta frequency shift in neuronal oscillations induced in rat hippocampal slices by tetanic stimulation. Journal of Neuroscience 19:1088-1105.

Traub RD, Bibbig A, LeBeau FEN, Buhl EH, Whittington MA (2004) Cellular mechanisms of neuronal population oscillations in the hippocampus in vitro. Annual Review of Neuroscience 27:247-278.

Traub RD, Bibbig A, LeBeau FEN, Cunningham MO, Whittington MA (2005) Persistent gamma oscillations in superficial layers of rat auditory neocortex: experiment and model. Journal of Physiology 562:3-8.

Traub RD, Bibbig A, Fisahn A, LeBeau FEN, Whittington MA, Buhl EH (2000) A model of gamma-frequency network oscillations induced in the rat CA3 region by carbachol in vitro. European Journal of Neuroscience 12:4093-4106.

Traub RD, Cunningham MO, Gloveli T, LeBeau FEN, Bibbig A, Buhl EH, Whittington MA (2003) GABA-enhanced collective behavior in neuronal axons underlies persistent gamma-frequency oscillations. Proceedings of the National Academy of Sciences of the United States of America 100:11047-11052.

Tritsch NX, Sabatini BL (2012) Dopaminergic modulation of synaptic transmission in cortex and striatum. Neuron 76:33-50.

Tutak E, Satar M, Zorludemir S, Erdogan S, Yapicioglu H, Narli N (2005) Neuroprotective effects of indomethacin and aminoguanidine in the newborn rats with hypoxic-ischemic cerebral injury. Neurochemical Research 30:937-942.

Tyszkiewicz JP, Gu Z, Wang X, Cai X, Yan Z (2004) Group II metabotropic glutamate receptors enhance NMDA receptor currents via a protein kinase C-dependent mechanism in pyramidal neurones of rat prefrontal cortex. Journal of Physiology 554:765-777.

Tzagarakis C, Ince NF, Leuthold AC, Pellizzer G (2010) Beta-band activity during motor planning reflects response uncertainty. Journal of Neuroscience 30:11270-11277.

Ueta Y, Otsuka T, Morishima M, Ushimaru M, Kawaguchi Y (2014) Multiple layer 5 pyramidal cell subtypes relay cortical feedback from secondary to primary motor areas in rats. Cerebral Cortex 24:2362-2376.

Ungerstedt U (1968) 6-Hydroxy-dopamine induced degeneration of central monoamine neurons. European Journal of Pharmacology 5:107-110.

Ungerstedt U (1971) Postsynaptic supersensitivity after 6-hydroxy-dopamine induced degeneration of the nigro-striatal dopamine system. Acta Physiologica Scandinavica Supplementum 367:69-93.

Ungerstedt U, Arbuthnott GW (1970) Quantitative recording of rotational behavior in rats after 6-hydroxy-dopamine lesions of the nigrostriatal dopamine system. Brain Research 24:485-493.

Valjent E, Bertran-Gonzalez J, Herve D, Fisone G, Girault JA (2009) Looking BAC at striatal signaling: cell-specific analysis in new transgenic mice. Trends in Neurosciences 32:538-547.

Vanbrederode JFM, Spain WJ (1995) Differences in inhibitory synaptic input between layer-II-III and layer-V neurons of the cat neocortex. Journal of Neurophysiology 74:1149-1166.

Vanderwolf CH (1969) Hippocampal electrical activity and voluntary movement in the rat. Electroencephalography and Clinical Neurophysiology 26:407-417.

Vanderwolf CH (1971) Limbic-diencephalic mechanisms of voluntary movement. Psychological Review 78:83-113.

Vanderwolf CH (1975) Neocortical and hippocampal activation in relation to behavior - effects of atropine, eserine, phenothiazines, and amphetamine. Journal of Comparative and Physiological Psychology 88:300-323.

Varma N, Carlson GC, Ledent C, Alger BE (2001) Metabotropic glutamate receptors drive the endocannabinoid system in hippocampus. Journal of Neuroscience 21:art. no.-RC188.

Vila M, Perier C, Feger J, Yelnik J, Faucheux B, Ruberg M, Raisman-Vozari R, Agid Y, Hirsch EC (2000) Evolution of changes in neuronal activity in the subthalamic nucleus of rats with unilateral lesion of the substantia nigra assessed by metabolic and electrophysiological measurements. European Journal of Neuroscience 12:337-344.

Vinogradova OS (1995) Expression, control, and probable functional-significance of the neuronal theta-rhythm. Progress in Neurobiology 45:523-583.

Vitrac C, Péron S, Frappé I, Fernagut P-O, Jaber M, Gaillard A, Benoit-Marand M (2014) Dopamine control of pyramidal neuron activity in the primary motor cortex via D2 receptors. Frontiers in Neural Circuits 8:13.

Volkmann J, Joliot M, Mogilner A, Ioannides AA, Lado F, Fazzini E, Ribary U, Llinas R (1996) Central motor loop oscillations in parkinsonian resting tremor revealed by magnetoencephalography. Neurology 46:1359-1370.

von Nicolai C, Engler G, Sharott A, Engel AK, Moll CK, Siegel M (2014) Corticostriatal coordination through coherent phase-amplitude coupling. Journal of Neuroscience 34:5938-5948.

von Stein A, Sarnthein J (2000) Different frequencies for different scales of cortical integration: from local gamma to long range alpha/theta synchronization. International Journal of Psychophysiology 38:301-313.

Wagner AP, Schmoll H, Badan I, Platt D, Kessler C (2000) Brain plasticity: to what extent do aged animals retain the capacity to coordinate gene activity in response to acute challenges. Experimental Gerontology 35:1211-1227.

Walter BL, Vitek JL (2004) Surgical treatment for Parkinson's disease. Lancet Neurology 3:719-728.

Walter WG, Dovey VJ (1944) Electro-encephalography in cases of sub-cortical tumour. Journal of Neurology, Neurosurgery, and Psychiatry 7:57-65.

Wang HS, McKinnon D (1995) Potassium currents in rat prevertebral and paravertebral sympathetic neurons - control of firing properties. Journal of Physiology 485:319-335.

Wang XJ, Rinzel J (1993) Spindle rhythmicity in the reticularis thalami nucleus: synchronization among mutually inhibitory neurons. Neuroscience 53:899-904.

Wang XJ, Buzsaki G (1996) Gamma oscillation by synaptic inhibition in a hippocampal interneuronal network model. Journal of Neuroscience 16:6402-6413.

Weintraub D (2008) Dopamine and Impulse Control Disorders in Parkinson's Disease. Annals of Neurology 64:S93-S100.

Weiss T, Veh RW, Heinemann U (2003) Dopamine depresses cholinergic oscillatory network activity in rat hippocampus. European Journal of Neuroscience 18:2573-2580.

Whishaw IQ, Robinson TE, Schallert T, Deryck M, Ramirez VD (1978) Electrical-activity of the hippocampus and neocortex in rats depleted of brain dopamine and norepinephrine - relations to behavior and effects of atropine. Experimental Neurology 62:748-767.

White JA, Chow CC, Ritt J, Soto-Trevino C, Kopell N (1998) Synchronization and oscillatory dynamics in heterogeneous, mutually inhibited neurons. Journal of Computational Neuroscience 5:5-16.

Whittemore ER, Yang W, Drewe JA, Woodward RM (1996) Pharmacology of the human gamma-aminobutyric acid A receptor alpha 4 subunit expressed in Xenopus laevis oocytes. Molecular Pharmacology 50:1364-1375.

Whittington MA, Traub RD, Jefferys JGR (1995) Synchronized oscillations in interneuron networks driven by metabotropic glutamate-receptor activation. Nature 373:612-615.

Whittington MA, Jefferys JGR, Traub RD (1996) Effects of intravenous anaesthetic agents on fast inhibitory oscillations in the rat hippocampus in vitro. British Journal of Pharmacology 118:1977-1986.

Whittington MA, Traub RD, Faulkner HJ, Stanford IM, Jefferys JGR (1997) Recurrent excitatory postsynaptic potentials induced by synchronized fast cortical oscillations. Proceedings of the National Academy of Sciences of the United States of America 94:12198-12203.

Whittington MA, Traub RD, Faulkner HJ, Jefferys JGR, Chettiar K (1998) Morphine disrupts long-range synchrony of gamma oscillations in hippocampal slices. Proceedings of the National Academy of Sciences of the United States of America 95:5807-5811.

Whittington MA, Traub RD, Kopell N, Ermentrout B, Buhl EH (2000) Inhibition-based rhythms: experimental and mathematical observations on network dynamics. International Journal of Psychophysiology 38:315-336.

Wichmann T, DeLong MR (1999) Neurobiology - Oscillations in the basal ganglia. Nature 400:621-622.

Wichmann T, Soares J (2006) Neuronal firing before and after burst discharges in the monkey basal ganglia is predictably patterned in the normal state and altered in parkinsonism. Journal of Neurophysiology 95:2120-2133.

Wichmann T, Dostrovsky JO (2011) Pathological basal ganglia activity in movement disorders. Neuroscience 198:232-244.

Wichmann T, DeLong MR, Guridi J, Obeso JA (2011) Milestones in research on the pathophysiology of Parkinson's disease. Movement Disorders 26:1032-1041.

Willard AM, Bouchard RS, Gittis AH (2015) Differential degradation of motor deficits during gradual dopamine depletion with 6-hydroxydopamine in mice. Neuroscience 301:254-267.

Williams D, Tijssen M, van Bruggen G, Bosch A, Insola A, Di Lazzaro V, Mazzone P, Oliviero A, Quartarone A, Speelman H, Brown P (2002) Dopamine-dependent changes in the functional connectivity between basal ganglia and cerebral cortex in humans. Brain 125:1558-1569.

Wilson CJ, Bevan MD (2011) Intrinsic dynamics and synaptic inputs control the activity patterns of subthalamic nucleus neurons in health and in Parkinson's disease. Neuroscience 198:54-68.

Wilson CJ, Beverlin B, 2nd, Netoff T (2011) Chaotic desynchronization as the therapeutic mechanism of deep brain stimulation. Frontiers in Systems Neuroscience 5:50.

Winson J (1974) Patterns of hippocampal theta rhythm in freely moving rat. Electroencephalography and Clinical Neurophysiology 36:291-301.

Winson J (1978) Loss of hippocampal theta rhythm results in spatial memory deficit in rat. Science 201:160-163.

Wright RA, Arnold MB, Wheeler WJ, Ornstein PL, Schoepp DD (2000) Binding of H-3 (2S,1 ' S,2 ' S)-2-(9-xanthylmethyl)-2-(2 '-carboxycycloprophyl) glycine ( H-3 LY341495) to cell membranes expressing recombinant human group III metabotropic glutamate receptor subtypes. Naunyn-Schmiedebergs Archives of Pharmacology 362:546-554.

Wu AD, Fregni F, Simon DK, Deblieck C, Pascual-Leone A (2008) Noninvasive brain stimulation for Parkinson's disease and dystonia. Neurotherapeutics 5:345-361.

Wulff P, Ponomarenko AA, Bartos M, Korotkova TM, Fuchs EC, Bähner F, Both M, Tort ABL, Kopell NJ, Wisden W, Monyer H (2009) Hippocampal theta rhythm and its coupling with gamma oscillations require fast inhibition onto parvalbumin-positive interneurons. Proceedings of the National Academy of Sciences of the United States of America 106:3561-3566.

Yamawaki N, Shepherd GMG (2015) Synaptic circuit organization of motor corticothalamic neurons. Journal of Neuroscience 35:2293-2307.

Yamawaki N, Stanford IM, Hall SD, Woodhall GL (2008) Pharmacologically induced and stimulus evoked rhythmic neuronal oscillatory activity in the primary motor cortex in vitro. Neuroscience 151:386-395.

Yamawaki N, Magill PJ, Woodhall GL, Hall SD, Stanford IM (2012) Frequency selectivity and dopamine-dependence of plasticity at glutmatergic synapses in the subthalamic nucleus. Neuroscience 203:1-11.

Yamawaki N, Borges K, Suter BA, Harris KD, Shepherd GM (2014) A genuine layer 4 in motor cortex with prototypical synaptic circuit connectivity. Elife 3:e05422.

Yang CR, Seamans JK (1996) Dopamine D1 receptor actions in layers V-VI rat prefrontal cortex neurons in vitro: Modulation of dendritic-somatic signal integration. Journal of Neuroscience 16:1922-1935.

Yang N, Zhang K-Y, Wang F-F, Hu Z-A, Zhang J (2014) Dopamine inhibits neurons from the rat dorsal subcoeruleus nucleus through the activation of alpha(2)-adrenergic receptors. Neuroscience Letters 559:61-66.

Yuan H, Sarre S, Ebinger G, Michotte Y (2005) Histological, behavioural and neurochemical evaluation of medial forebrain bundle and striatal 6-OHDA lesions as rat models of Parkinson's disease. Journal of Neuroscience Methods 144:35-45.

Zaitsev AV, Povysheva NV, Lewis DA, Krimer LS (2007) P/Q-type, but not N-type, calcium channels mediate GABA release from fast-spiking interneurons to pyramidal cells in rat prefrontal cortex. Journal of Neurophysiology 97:3567-3573.

Zhou FM, Hablitz JJ (1996) Morphological properties of intracellularly labeled layer I neurons in rat neocortex. Journal of Comparative Neurology 376:198-213.

Zigmond MJ, Abercrombie ED, Berger TW, Grace AA, Stricker EM (1990) Compensations after lesions of central dopaminergic-neurons - some clinical and basic implications. Trends in Neurosciences 13:290-296.

Zuo L, Motherwell MS (2013) The impact of reactive oxygen species and genetic mitochondrial mutations in Parkinson's disease. Gene 532:18-23.